Seismic Response Control of Integral Abutment Bridge using Sleeved Piles

Thesis Submitted in Partial Fulfilment of the Requirement

for the Degree of

DOCTOR OF PHILOSOPHY

By

Atop Lego

Department of Civil Engineering
Indian Institute of Technology, Guwahati
Guwahati-781039, Assam, India

September 2018

Candidate's Declaration

I do hereby declare that the present work presented in the thesis entitled "**Seismic Response Control of Integral Abutment Bridge using Sleeved Piles**" in partial fulfilment of the requirement for the award of the degree of Doctor of Philosophy is an authentic record of my own work carried out in Department of Civil Engineering at Indian Institute of Technology (IIT) Guwahati. The work has been carried out under supervision Prof. Anjan Dutta and Prof. Sajal Kanti Deb.

The content presented in this thesis has not been submitted by me for award of any other degree of this or any other Institute.

Atop Lego

This is to certify that the above statement made by the candidate is correct to best of our knowledge.

Dr. Anjan Dutta
Professor
Department of Civil Engineering
Indian Institute of Technology,
Guwahati
Guwahati-781039
India

Dr. Sajal Kanti Deb
Professor
Department of Civil Engineering
Indian Institute of Technology,
Guwahati
Guwahati-781039
India

Acknowledgement

This thesis is the outcome of studies carried out in Department of Civil Engineering at Indian Institute of Technology (IIT) Guwahati. First and foremost, I would like to express my sincere gratitude to my supervisors Prof. Anjan Dutta and Prof. Sajal Kanti Deb. It was an honour to work with them throughout the duration of my course and this thesis wouldn't have been possible without their continuous support, expert guidance, and constant encouragement.

I would also like to thank the members of my Doctoral Committee, Dr. K.S.R.K. Murthy, Dr. Kaustubh Dasgupta and Dr. Arindam Dey for their valuable observation, inputs and suggestions during the course of my research.

I am also extremely thankful to the other faculty members of the Department of Civil of Civil Engineering, IIT Guwahati, who encouraged me in this endeavour.

I am grateful to the Public Works Department, Government of Arunachal Pradesh, for facilitating the completion of my study.

Lastly, I would like to thank my family members for their moral support.

Atop Lego

Table of Contents

Abstract

Integral abutment bridges (IAB) are constructed without any deck joints with abutment and pier. In a single span construction, the deck is cast integrally with abutment. In the case of a multi-span construction, the intermediate support to the deck is provided either by flexible pier with deck integrated monolithically with the pier or by rigid pier with a bearing on it supporting the deck. This practice is a significant deviation from the conventional method of bridge construction which employs deck joints at the location of pier and abutment for the release of stresses caused by the expansion and contraction of the deck due to thermal variation and vehicular action. However, in the case of IAB, the construction of the deck without joint introduces secondary stress due to thermal variation, which are required to be considered in the design. Despite this, the popularity of integral abutment bridge is recorded to be growing. This is because of the fact that the distress caused by the malfunctioning of bearing and joints along with associated damage to the components of the bridges with conventional bridge are experienced to be more than the distress caused by secondary stresses. The IAB also has an advantage over conventional bridge type as it avoids the requirement of frequent maintenance of bearing and deck joints, unseating of deck and damage of bearing during seismic excitation. Further, the redundant frame configuration of integral abutment bridge greatly improves the performance of the bridge under seismic excitation.

Considering the inherent redundancy of the bridge, IAB is preferred for adoption in construction of bridges in areas classified under high seismic risk zone. Review of literature indicates insufficient information in the seismic behavior of the integral abutment bridge with soil structure interaction to frame a detailed procedure for

seismic design and implementation of integral abutment. To adopt integral abutment bridge in areas of high seismic risk zone, a holistic study on the seismic behavior of integral abutment bridge with simulation of soil condition is required to be undertaken. Further, strategies for additional improvement in seismic performance of the bridge under seismic excitation is also required to be explored for implementation in the construction of the bridge in highly important roads and railway corridor.

With an objective for adopting a suitable method for modelling of soil pile interaction and abutment backfill interaction, the background literature on formulation of the existing approaches is studied in detail. Amongst the existing approaches available, the method which are simple to implement in modelling of soil structure interaction of integral abutment bridge but simulate the soil behavior without loss of accuracy are selected. The modelling of tip bearing interaction of pile using load settlement $Q - z$ curve, shaft skin frictional force interaction using load transfer $t - z$ curve and lateral pile soil interaction using load displacement $p - y$ curves are found to be adequate to account for the soil pile interaction in IAB. For precise evaluation of seismic response of the bridge, the far field soil reaction is also incorporated in the modelling of the pile soil interaction. The abutment backfill interaction is modelled using the hyperbolic relation between the abutment wall movement towards backfill and passive resistance mobilized.

The finite element modelling of an existing sample bridge considered for study is carried out by modelling the steel concrete composited deck using grillage model, while the pier, pier cap and piles are modelled using beam element. The abutments and the pile caps are modelled using thick shell element. Nonlinear analyses are carried out for observing the response of the bridge, where soil as well as the

structural components may undergo yielding. Nonlinear plastic hinges are modelled for concrete pier and piles using results from the moment curvature analysis of the section. To identify the effect of incorporation of far field soil element in the modelling of soil pile interaction, two categories of models are developed by varying the modelling in the soil pile interaction. In the first category, the soil pile interaction is modelled using soil spring modelled by $p-y$ curve, only representing the nonlinear behavior of soil near the pile. In the second category, the far field soil element is attached in series to the soil spring modelled by $p-y$ curve to simulate the radiation damping and elastic response of soil in the vicinity of the pile but away from zone of nonlinear behavior. The modal analyses of both the models indicate that the incorporation of far field element in the modelling of soil pile interaction make IAB more flexible. Nonlinear time history analyses of both the models using ground motions compatible to design response spectrum were also carried out. The second category of model results in higher displacement and higher seismic forces in the piles supporting the pier due to the incorporation of far field soil reaction in the modelling of soil pile interaction. The drift of the pier is also observed to have increased in second category model of IAB. The precise evaluation of seismic design forces in IAB thus require detailed modelling of soil pile interaction incorporating far field soil reaction.

The analysis of IAB under cyclic thermal loading for a variation of $\pm 17^0$ C temperature of deck considered for the site is found to induce displacement in abutment which is much lesser than that of theoretically computed value of deck expansion. The forces induced in piles and abutments are also observed to be within the elastic capacity. Hence, the cyclic strain induced in the pier, abutment and piles

are expected to be within elastic limit and not susceptible to low cycle fatigue due to cyclic thermal deformation.

To explore the strategy for improving the performance of IAB under seismic excitation, sleeved pile foundation is proposed. Sleeved piles are designed and introduced to the foundation of abutment and pier. The provision of sleeved pile increases the flexibility of the IAB lengthening the vibration period of the bridge thereby reducing the seismic forces in pier. The nonlinear time history analyses of the IAB with and without sleeved pile using ground motion compatible with design response spectrum indicate improvement of seismic performance of bridge with sleeved pile. The sleeved pile is observed to be a feasible arrangement for improvement of seismic performance of IAB. Further, the provision of sleeved pile is also found to improve the thermal response of IAB.

The seismic capacity of IAB with and without sleeved pile is also assessed using incremental dynamic analysis (IDA). The IDA is a method for thorough evaluation of the seismic performance of a structure. The IDA results are presented in the form of intensity measure (IM) *vs* damage measure (DM). The IAB models with and without sleeved pile are subjected to a suite of 20 ground motions, scaling each to a different intensity (IM) to force the model all the way from elastic response to collapse. The response of IAB to each scaled ground motion in the form of drift of pier (DM) are extracted from every step of the analysis and IDA curves are developed for all the ground motions considered. The IDA curves are summarized to obtain the median seismic demand of the IAB. The seismic capacity of the bridge is estimated by interpolating the IDA curves using Ramberg-Osgood (R-O) equation using the median values of initial slope of IDA curve, critical IM, critical value of engineering demand parameter. The estimated median capacity of the

bridge through interpolation using R-O equation indicates that the IAB with sleeved pile is having reasonably higher capacity than IAB without sleeved pile. The median seismic demand for the various damage states observed from the summarized value of IDA indicates a higher demand various damage states for the IAB with sleeved pile implying a higher seismic capacity.

The seismic vulnerability of the IAB with and without sleeved pile is compared by developing an analytical fragility curve. The different damage states such as yielding, cover spalling and bar buckling are assigned a quantitative value in the form of drift of pier, estimated using moment curvature analysis of section as well as using the empirical equations developed from the experiment on bridge column data set. Probabilistic median seismic demand is estimated from the summarized IDA results taking the value of IM from the corresponding $DM_{50\%}$ at different damage state. The fragility curve developed for different damage states for IAB with and without sleeved pile displays that the IAB with sleeved pile is less vulnerable as compared to that of IAB without sleeved pile.

List of Figures

List of Tables

Notations

Symbol	Meaning
A	= empirical adjustment factor cyclic and static lateral load of soil
A_c	= empirical factor for lateral static loading on pile
A_d	= area of concrete deck
A_{sg}	= area of steel girder
A_{DBE}	= ground acceleration of design base earthquake
A_m	= peak ground acceleration
A_p	= area of pile tip
A_r	= area of rod/cylinder
A_s	= area of steel tube pile section
a	= dimensionless parameters in expression of horizontal stiffness of sleeved pile
a'	= dimensionless parameters in expression of length of sleeved length sleeved pile
a_s	= surface area of the pile
b	= diameter of pile
c	= cohesion of soil
c_a	= cohesion between the pile and clay
c_d	= dashpot coefficient
c_m	= material damping coefficient
c_r	= radiation damping coefficient
c_x	= total damping coefficient of pile

D = diameter of pile/overall depth of section

D_{DBE} = design basis drift of pile

D_{max} = maximum drift of pile

D_p = diameter of pile

D_s = average diameter of steel tube sleeved pile

D_{sa} = external diameter of steel tube sleeved pile in abutment

D_{sp} = external diameter of steel tube sleeved pile in pier

d = displacement of abutment top

d' = depth of extreme compression fiber to centre of the compression rebar

d_{sp} = internal diameter of steel tube sleeved pile

E_d = modulus of elasticity of concrete deck

EDP = engineering demand parameter

EDP_c = critical value of EDP

E_g = modulus of elasticity of the steel girder

E_p = modulus elasticity of the pile

E_s = modulus elasticity of the soil

E_t = tangent modulus of soil

E_{ti} = initial tangent modulus of soil

E_{tf} = final tangent modulus of soil

F_a = total active force

F_n = force acting normal to side face of passive wedge

F_s = force acting along the side face of the passive wedge

F_p = total passive force

f = frequency of excitation

f_c' = expected concrete strength

f_{bc} = combined axial and bending stress in sleeved pile

f_s = unit frictional forces on pile shaft

F_{di} = effective horizontal stress factor for downward load

F_{pt} = total resistance of soil to pile deflection

F_ϕ = force acting on the sliding bottom face of passive wedge

H = height of pile / abutment

IM = intensity measure

IM_c = critical intensity measure that occurs at the onset of large EDP

IM = median intensity measure for chosen damage state

I_p = moment of inertial of the pile section

I_{sa} = moment of inertial steel tube sleeved pile in abutment

I_{sa_cal} = calculated moment of inertial steel tube sleeved pile in abutment

I_{sp} = moment of inertial steel tube sleeved pile in pier

J = empirical constant for lateral resistance of clay

K = dimensionless modulus number

K_e = initial slop of IDA curve in proportionate range

k = modulus of reaction of soil

K_0 = coefficient of earth pressure at rest

K_a = coefficient of active earth pressure

k_{ap} = horizontal stiffness of sleeved pile in abutment

k_L = lateral stiffness of pile

K_{max} = initial slop of load deflection curve for passive pressure

K_p = coefficient of passive earth pressure

k_{pp} = horizontal stiffness of sleeved pile in pier

k_{pl} = constant for plastic hinge length

k_s = lateral stiffness of soil/support spring in force per unit length

k_{sec} = secant stiffness of pile

K^* = overall passive wall reaction coefficient

k_{xx} = translational stiffness of soil in x axis

$k_{x\emptyset}$ = rotational stiffness of soil about x axis

k_1 = initial stiffness coefficient of soil

$k_{\emptyset\emptyset}$ = rotational stiffness of soil in $x - z$ plane

L = length of bridge

L_0 = length of pile in the zone of negligible frictional resistance

L = length of bridge

L_c = length of column from critical point to the point of contraflexure

L_e = effective length of pile in which the frictional forces of the pile are effective

L_{eq} = equivalent free-standing length of pile

L_f = depth of fixity of pile below ground level

L_i = length of pile up to depth "i"

L_{SP} = Length of strain penetration

L_u = length of pile above ground level

l = free standing length of sleeved pile

l_e = effective length of sleeved pile

l_p = length of sleeved pile in pier foundation

l_a = length of sleeved pile in abutment foundation

M = moment in pile

M_{abut} = mass of deck on abutment

M_{pier} = mass of deck on pier

M_{Edseis} = Seismic design moment

M_{seisx} = Seismic moment due to seismic force in x direction

M_{seisy} = Seismic moment due to seismic force in y direction

M_t = total mass on the top of the sleeved pile

n = dimensionless modulus exponent

n_h = coefficient of variation of subgrade modulus or rate of increase of soil modulus with depth (force/length^3)

N_c = dimensionless bearing capacity of clayed soil

N_q = dimensionless bearing capacity factor for sand

p = soil reaction per unit length of pile

P_c = effective vertical stress on soil at depth "$L_0 + 20D$"

P_E = Euler's buckling load

P_e = axial load on section

P_i = effective vertical stress in soil at depth "i"

p_p = passive pressure

P_p = passive pressure resistance

p_s = perimeter of pile shaft

P_u = ultimate lateral resistance of soil

P_{uc1} = ultimate lateral resistance of clay near ground surface

P_{uc2} = ultimate lateral resistance of clay at depth below ground surface

P_{ud} = ultimate lateral resistance of soil at depth below the ground surface

P_{us} = ultimate resistance of soil near the ground surface

P_{ult} = maximum passive pressure resistance

P_x = axial load acting on the end cross section of pile

Q = axial load on pile

Q_f = frictional resisting capacity of pile to axial load

Q_p = tip bearing capacity of pile

Q_u = ultimate bearing capacity of pile

R_f = failure ratio

r_0 = radius of pile

r_m = mass adjustment factor

r_p = ratio of axial load on pile to Euler's buckling load

r_{stiff} = ratio of horizontal stiffness of abutment piles to horizontal stiffness of pier piles

S_C = median estimate of capacity

S_d = median estimate of demand

S_{max} = maximum shear force in the steel tube pile

S_{pa} = spectral acceleration in design response spectrum

T = characteristic length of pile embedded in ground

t = frictional resistance mobilized with the movement of pile

t_{cal} = calculated thickness of sleeved pile

t_{max} = maximum frictional resistance mobilized at depth under consideration

t_{sp} = wall thickness of sleeved pile in pier

t_s = wall thickness of steel tube pile

V = velocity of wave along a cross section

V_p = P-waves velocity

V_s = S-waves velocity

X = depth of pile below ground level

x = ordinate point on the pile along its depth below ground level

X_R = depth at which the value of N_p becomes equal to 9

y = lateral deflection of pile

y_c = deflection of pile at lateral load equal to the one half of the ultimate lateral resistance

z = depth below the ground level along the pile length / movement of pile in vertical direction

z_c = critical value of movement of pile required to mobilize t_{max}

α_c = stress block parameter of the concrete

α_d = coefficient of thermal expansion of the concrete deck materials

α_g = coefficient of thermal expansion of steel girder

α_s = horizontal dispersion angle of passive wedge width

α_t = coefficient of thermal expansion of deck materials

β = angle between the vertical plane of pile and failure surface

β_c = stress block parameter of concrete

β_{cD} = dispersion of capacity

$\beta_{D|IM}$ = dispersion of demand about its median conditioned upon IM

β_s = hysteretic damping coefficient of soil

γ = unit weight of soil

ΔL = incremental length of pile

ΔL_b = increment in bridge length due the thermal variation

ΔT = rise or fall in bridge temperature

δ = coefficient of lateral stiffness of pile

δ_i = frictional angle between pile and soil at depth "i"

ϵ = strain in soil

ϵ_c = strain of soil at one half of the maximum stress on laboratory

ϕ = internal angle of friction of soil

ϕ_{y1} = curvature at first yield

ϕ_y = yield curvature

κ = reduction factor for shearing resistance along the face of the pile

ν = Poisson's ratio of soil

ρ = mass density of rod materials

ρ_s = mass density of soil

ρ_t = volumetric ratio of longitudinal reinforcement

σ = stress at the soil

σ_0' = effective overburden pressure on soil at a depth in question

σ_v = vertical stress on the soil at depth in question

σ_x = effective overburden stress on the soil at ordinate x below ground level

σ_1 = major principal stress

σ_3 = minor principal stress

ω = frequency of excitation

ω_p = target frequency of vibration of the bridge with sleeved pile

Chapter 1

Introduction

1.1 Background

The Integral Abutment Bridge (IAB) is designed without any movable deck joints at the pier or at abutment. They are either single span or multiple span with their superstructure cast integrally with the abutment. However, in the case of a multiple span IAB, the superstructure is supported either on a flexible pier with the deck integrated to the pier or on a rigid pier with a bearing supporting the deck. The rigid connection between the superstructure and substructure enables the bridge to accommodate the deformation due the thermal load, breaking load and seismic load exerted on the bridge superstructures in the substructure and surrounding soil. The abutment of the IAB is usually supported on a single row of piles driven vertically and restrained laterally by backfill. As per the record (Burke, 2009), Ohio Department of Transportation (DOT), USA was the first state to routinely eliminate deck joints at the abutment. This was accomplished by constructing a continuous reinforced concrete slab bridge with the embankment and stub type abutment supported on flexible piles in lieu of the movable joint and wall type abutment. During 1946 the maximum span limit of the integral abutment bridge as per Ohio DOT was 53.3 m.

The practice of construction of IAB is a significant departure from the conventional method of bridge construction which employs deck joints at the location of piers and abutment with bearings supporting the deck. In conventional bridges, the secondary stress caused by expansion and contraction of the deck due to thermal variations and settlement of piers and abutment are released through the deck joint and movement through the bearing supports. Therefore, the bridge components are

designed considering the response to the primary load on the bridge. However, in the case of IAB, single or multiple span superstructures are constructed without a deck joint and it is likely that the continuity achieved by such a construction will introduce secondary stress on the superstructure due to thermal variation and settlement of the substructure. The justification for adopting a construction like IAB is based on the growing awareness that for a single or multiple-span bridge of moderate length, the distresses caused by the malfunctioning of bearings and joint along with its associated damage to components of bridge at piers and abutment are higher than that by secondary stress. Continuous maintenance of the joints and bearings are also required to ensure that they perform the intended function considered in the design of the bridge. A typical image of an integral abutment bridge is shown in Fig. 1.1.

Fig. 1.1 Integral Abutment Bridge (Addington Forks Underpass, Canada)

Based on the results of the continual assessment of integral abutment bridges, it has been found that this bridge type performs well even without regular maintenance,

an issue associated with conventional bridges. This improved performance of the integral abutment bridge has led to the acceptance of this particular type by bridge designers and bridge owners worldwide. As per the records of survey conducted by Federal Highway Administration (FHWA) and Constructed Facilities Center (CFC), (Petro and Maruri, 2005) 8900 integral abutment bridges were built since 1995. The total number of integral abutment bridges in the records of the survey, up to the year 2005, is 13,000 (Petro and Maruri, 2005). This indicates the rapid acceptance and increase in the adoption of integral abutment bridges in USA. Similarly, in New England, over 130 new integral abutment bridges have been constructed in the last 20 years (Petro and Maruri, 2005). In India, some integral bridges have been built recently under Delhi Metro Railway (Kumar, 2008).

1.2 Types of Integral Abutment Bridge

Broadly, there are three types of integral bridges in practice. The main characteristic of the bridge distinguishing the three types lies with the connection detailing method of the deck with the abutment. The suitability of each type is decided by considering the bridge alignment and type of founding strata. The detailing process also varies based on the specification and practice adopted by various design institutions, but the basic structural responses by the bridge to primary and secondary forces remain the same. The three types of integral bridges are: full integral, semi-integral and deck extension. The detailing practice commonly adopted for each type is discussed (Weakley, 2005).

1.2.1 Full Integral Abutment Bridge

The full integral abutment bridge (IAB) is the bridge structure where the bridge girder and deck are directly connected to the substructure by casting into a concrete abutment wall which is connected to a single row of pile supporting the abutment,

as shown in Fig. 1.2. During thermal expansion and contraction, the superstructure and substructure move together into and away from the backfill. In order to relieve the stress induced in the pile by expansion and contraction of deck, Virginia Department of Transportation (VDOT) also adopts a hinge detailing between the pile cap and integral abutment wall as shown in Fig. 1.2 (b) (Weakley, 2005)..

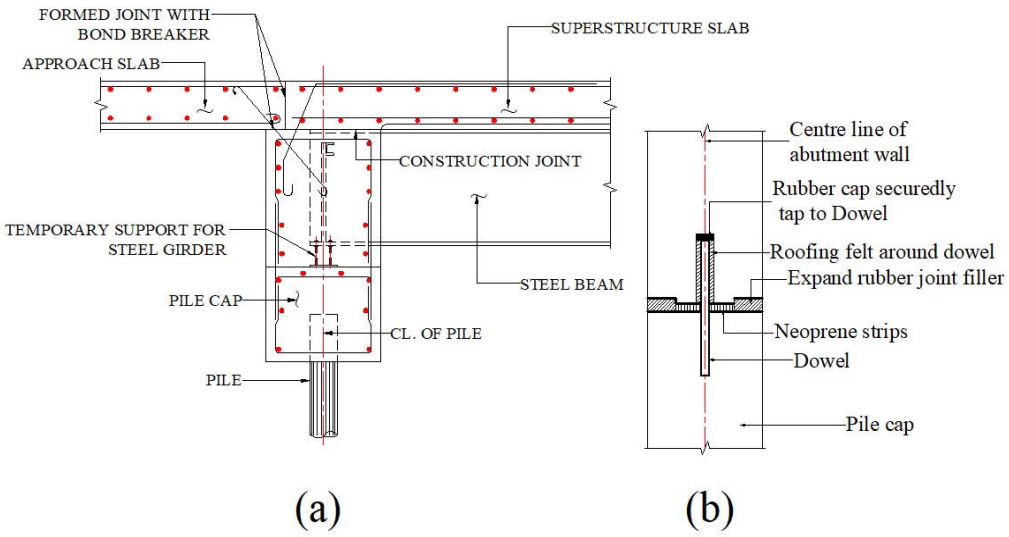

Fig.1.2 Full IAB (a) with Steel girder superstructure (b) Hinge detailing of VDOT

The hinge consists of dowels, with strips of high durometer neoprene attached on either side, installed along the centre line of the integral abutment and through which the vertical load is transmitted (Weakley, 2005). The bridges designed as fully integrated are supported commonly on vertically driven single row of H-piles for increasing the flexibility of the foundation to accommodate thermal expansion and contraction of the deck. The inherent flexibility of the H-piles allow them to endure constant combined axial and flexural strains induced by the cyclic thermal expansion and contraction of the deck.

1.2.2 Semi-Integral Bridge

The semi-integral bridge (SIAB) is similar to the full integral bridge constructed without movable deck joints with the exception that the concrete abutment wall is not rigidly connected to the substructure as shown in Fig 1.3.

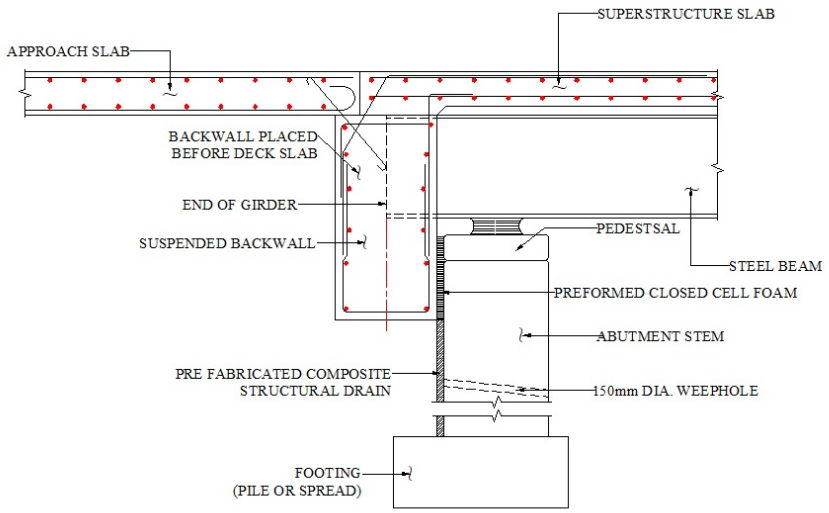

Fig.1.3 Semi-integral bridge

The superstructure moves longitudinally, independent of the abutment. Hence, the abutment can be supported on a rigid foundation. The backwall portion of the substructure is suspended by directly connecting it to the superstructure. The beam rests on a bearing on a stationary abutment stem. The integral back wall overlaps the abutment and overhangs slightly. A small gap is provided between the integral back wall and the substructure to allow it to move freely in the longitudinal direction to accommodate the expansion and contraction of the deck and thereby releasing the secondary stresses. The backwall and the approach slab move in and away from the backfill during thermal expansion and contraction. In the case of a multi-span SIAB, the longitudinal and lateral stability of the superstructure under lateral forces

is commonly achieved by adopting fixed intermediate pier supports for the superstructure. In the case of single span SIAB, specific design and arrangement are required to provide stability to the superstructure. The Semi integral bridge is the second preferred type of integral bridge as per VDOT (Weakley,2005). This bridge type is observed to be not as economical as that of IAB, but adaptable to varying field conditions.

1.2.3 Deck Extension

Deck Extension is the third type of integral bridge. The deck extension is essentially a cross between a conventional bridge and a semi-integral bridge as shown in Fig. 1.4. Though the substructure does have a back wall, the girders are not embedded in concrete end diaphragm. The deck slab overlaps the back wall, resulting in the elimination of the joint in the deck. The deck slab is extended across the tip of the shortened back wall. The girder expands and contracts under thermal variation thereby no secondary stress is induced in the substructure.

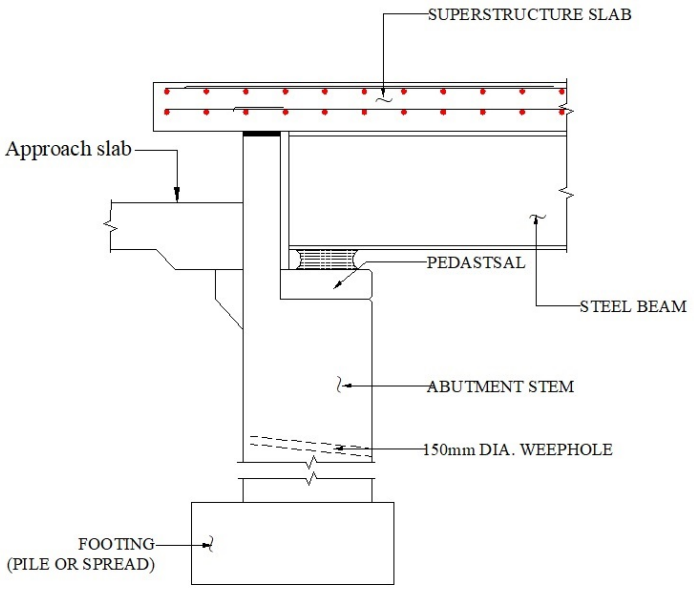

Fig. 1.4 Deck Extension

The deck extension is used when neither the IAB nor the SIAB types meet the condition of a particular site of a bridge. Usually such a situation arises, if the length or skew of the bridge exceeds the maximum values specified by the relevant guidelines.

1.3 Merits of Integral Abutment Bridge

In the usual practice of design and construction of traditional highway bridges, the expansion joints, roller supports, and other structural releases are provided to permit thermal expansion, contraction, creep and shrinkage without inducing any stress on the abutment and pier. The deck joints of different types, including various types of neoprene seals and finger joints are provided at the joint of the girder on abutment and pier. However, all joint types have been observed to be prone to leakage and allow water containing road salt to drain into the underlying components of the superstructure like superstructure beams, bearings, abutment wall cap and pier cap (Mistry, 2005). The leakage of a joint acts as a source for corrosion of steel girders and steel bearings as shown in Fig 1.5.

Fig. 1.5 Rusting of bearing joint in conventional bridge type

Due to the rusting of bearing from leakage, maintenance or replacement is required to allow the release of stress by enabling free movement of the bearing as designed, which is also costly. The rusting of bearings also has a cascading effect by damaging other connected structural elements by inducing stresses not considered in the original design process, when they are unable to move as they were designed. Similarly, as shown in Fig. 1.6, the bridge deck joints get frequently damaged as the joints are subjected to continuous wear and heavy impact from the repeated live loads as well as from constant expansion and contraction caused by temperature changes, creep and shrinkages. The joints are sometimes subjected to impact loading that can exceed their design capacity, leading to breakage of weaker joints. The broken joints become a traffic hazard and a liability for the owner. Thus, the movable joints in the deck entail constant repair and replacement thereby increasing the cost of maintenance.

Fig. 1.6 Damage to the expansion deck joint in a conventional bridge type.

The different types of such distresses in bearings and joints result in the reduction of the life of the structure. Because of the underlying problems of installing, maintaining and repairing of deck joints and bearings, the elimination of the deck joints and associated bearings have been found to be more beneficial and designers have chosen to relinquish the control on secondary stresses, primarily to achieve a simpler and more cost-effective bridge. The elimination of the deck joint also provides greater overall integrity and durability. This has led to the wide acceptance of the *Integral Abutment Bridge or Jointless Bridge*.

Apart from the elimination of the joint leakage, which has a destructive effect on the performance and maintenance of the bridge, the following additional advantages can be derived by adopting the IAB:

- Redundant frame configuration of IAB improves seismic performance of the bridge.
- In case of multi-span IAB with rigid pier supporting the bridge deck on bearing, longitudinal forces applied on the bridge deck are shared by two abutments and backfill soil at both ends. Therefore, the piers are not required to be designed for longitudinal seismic force applied along the axis of the bridge and the design of pier becomes more economical.
- In IAB, longitudinal displacement due to horizontal forces from earth pressure, live load and seismic excitation is restrained by both abutment and backfill and also, the longitudinal earth pressure due to backfill is balanced at each end due to the continuity of the deck. Therefore, a single row of vertical pile foundation is required to support the abutment, in contrast to the requirement in a conventional bridge, which consists of two or more rows of both vertical and battered piles to counter vertical as well as horizontal loads.

In addition to the above, there are also numerous advantages like, speedier construction of the foundation as only a single row of piles are driven for abutment foundations, lower cost of maintenance and improvement of riding quality. The IAB has consistently performed better during seismic events as compared to the conventional jointed bridge. The failure of a bridge due to unseating of the superstructure from the bearing and damage to the bearing under seismic force is directly avoided in the integral abutment bridge. Because of these numerous merits in IAB, VDOT consider the IAB as the first choice for construction of a new bridge (Weakley, 2005).

1.4 Problem Identification

In areas classified as high seismic zones, the integral abutment bridges are expected to outperform the conventional seat type abutment bridges during a seismic event owing to its increased redundancy, avoidance of bearings, and restraint provided by the backfill to the longitudinal displacement of bridge under seismic excitation, as outlined in the previous section. However, there are no exhaustive guidelines for seismic design of IAB. The information on seismic behavior of integral abutment bridges with soil structure interaction are also insufficient to draw a detailed procedure for the seismic design of IAB and implementation at site. To adopt IAB in the construction of bridges for highways and railways in high seismic risk areas, with the confidence of superior performance under seismic excitation, a holistic study on seismic behavior of IAB with simulation of various soil condition is essential. Furthermore, it may also be observed the the conventional design with isolation of bridge superstructure for upgrading its performance under seismic event is not feasible. Hence, it is important to identify a different strategy to enhance the seismic performance of IAB under seismic excitation for its implementation in the

construction of bridges in highly important roads and railway transportation corridor.

1.5 Objective of Present Study

The objective of the present study is to examine the seismic behavior of IAB supported on concrete pile. The IAB may be constructed in different types of founding soil, in the areas classified to be under high seismic risk. Therefore, it is essential to accurately simulate the seismic behavior of IAB in different types of soil in the foundation for proper assessment of design forces in each component. This is proposed to be done by carrying out a critical review of available literature on the modelling of soil structure interaction of IAB and to carry out analysis to evaluate the dynamic characteristics of IAB. A feasible design strategy to further upgrade the seismic performance of IAB under seismic excitation is also intended. Hence, the major objectives of the study considered are:

1. To carry out studies on different existing approaches for the modelling of soil pile interaction and abutment backfill interaction and adopt suitable methods for the development of three-dimensional finite element model of IAB considering soil pile and abutment backfill interaction and analyze to understand the dynamic characteristics of IAB.
2. To study the effect of incorporation of far field soil reaction modelling for precise evaluation of dynamic characteristics of IAB and its implication in the estimation of design forces.
3. To study the forces induced in concrete pile, abutment and pier of IAB due to expansion and contraction of deck under thermal variation and its effect on the allowable length of the bridge.

4. To study the feasibility of adopting sleeved pile for seismic response control of IAB.
5. To recommend a simple and implementable design procedure for sleeved pile.
6. To carry out comparative study on evaluation of seismic capacity of bridge without and with sleeved pile through incremental dynamic analysis and seismic vulnerability assessment using fragility analysis.

1.6. Scope of Study

The scope of the present study is limited to carry out numerical investigation on three-dimensional model of IAB founded in different types of soil for exploring the dynamic characteristics under seismic excitation. The design of sleeved pile for adoption in bridge foundation for seismic response control is also covered under this study. The comparative study on evaluation of bridge model with and without sleeved pile is carried out by incremental dynamic analysis and fragility analysis of the bridge. The detailed scopes are given as follows:

- To carry out three-dimensional finite element modelling of existing IAB using finite element software SAP 2000 (Version 18) which takes into account the soil pile interaction based on $p-y$ curve, $t-z$ curve, $Q-z$ curves and abutment backfill interaction based on a hyperbolic relation between the wall movement and backfill pressure mobilized.
- To carry out modelling of soil pile interaction modelling of IAB by considering five different type of founding soil and to study the effects of soil type on the dynamic characteristics of IAB under seismic excitation and loading due to thermal variation.

- To incorporate far field soil reaction element in the modelling of soil pile interaction to evaluate its influence on the dynamic characteristics and seismic response of IAB. The far field soil reaction element would be included in series with the near field model.
- To design sleeved pile foundation for IAB and study its effectiveness in the seismic response control of bridge.
- To evaluate the seismic capacity of IAB with and without sleeved pile using IDA and develop analytical fragility curves for comparative assessment of their seismic vulnerability.

1.7. Outline of Thesis

In this study the numerical investigation of seismic behavior of IAB with soil structure interaction is studied. The numerical investigation on feasibility of sleeved pile in seismic response control of the bridge is also carried out. The thesis of this study is arranged in seven Chapters:

Chapter 1 provides the overview of the configuration of IAB and the advantage of adopting the bridge. The identified problems and the objective of the present study are also presented in this chapter.

Chapter 2 provides the review of literature on the current state-of-the-art practices in the modelling of soil pile interaction in foundation and abutment backfill interaction of IAB. Brief review on literature of finite element modelling and analysis of IAB subjected to thermal load and seismic excitation are also presented in this chapter. In addition, this chapter also contains the review of literature related to adoption of sleeved pile in foundation of civil structures and improved seismic performance of structures. Furthermore, review of incremental dynamic analysis

and fragility analysis of bridges for seismic risk assessment are also presented in this chapter.

Chapter 3 presents different existing approaches for modelling of soil pile interaction for piles in both sand and clay, based on the standard literature and previous research. The basis of selection of method for the modelling of soil pile interaction adopted in this study is presented in this chapter with comparative analysis of existing methods from the point of view of practicability in a design office with reasonable accuracy.

Chapter 4 presents the development of a three-dimensional finite element model of an IAB. It also includes the detailed modelling of nonlinear soil pile interaction effect for piles in sand and clay. The nonlinear abutment backfill interaction modelling and its effects on thermal and seismic behavior of the bridge is also highlighted in this chapter. In addition, this chapter also explore the significances of inclusion of far field soil element in dynamic characteristics of IAB along with its implication in the design of bridges.

Chapter 5 describes the introduction of sleeved pile in the foundation of IAB and the results of numerical studies on its effectiveness on the seismic response control of the bridge.

Chapter 6 describes the incremental dynamic analysis and development of analytical fragility curves of the bridge with and without sleeved pile and comparative evaluation of seismic capacity and vulnerability of the bridge under seismic excitation.

Chapter 7 summarizes the observation of the present study with important conclusion. It also indicates areas of possible further studies in this field.

Appendix A presents the step by step procedure for the design of sleeved pile for implementation in a bridge foundation.

Chapter 2

Literature Review

2.1 Introduction:

The IAB has a rigid connection between the girder of the superstructure and the abutment of the bridge. In the case of multi-span IAB the decks are either integrated with the flexible pier or supported on the rigid piers with bearings. The abutments are generally supported on pile foundation to enhance the flexibility of the bridge along the axis of bridge. However, spread footings are also adopted for short span IAB. Due to these types of structural configuration, the IAB responds to external load as a single structural unit in which all the components accommodate the deformation caused by the external load. Therefore, the combined effect of primary load like dead load, live load, breaking load, seismic load and secondary loads due to thermal expansion/contraction are required to be taken into account in the design of the bridge. In order to understand the important aspect of the state-of-the-art practice in modelling, analysis and design of IAB, the review of the relevant literatures available on integral abutment bridge have been carried out under the following sections:

1. Foundation types adopted for integral abutment bridge.
2. Finite element modelling and analysis of IAB under thermal load.
3. Finite element modelling and analysis of IAB under seismic excitation.
4. Maximum permissible length of integral abutment bridge.
5. Sleeved piles for structures.
6. Incremental dynamic analysis.
7. Fragility function and development of fragility curve of bridge.

In addition, accounting for the soil structure interaction is very important in analysis and design of IAB as all the deformation induced by external load are transferred to soil due to integral connection of deck with abutment and pier. The soil pile interaction and the abutment backfill interaction significantly influence the response of the bridge under the action of seismic excitation and thermal load. Therefore, a detailed study on the strategies of modelling of soil structure interaction for IAB is carried out in a separate chapter 3.

2.2 Foundation in Integral Abutment Bridge

Pile foundations are generally the most popular type of foundation, for integral abutment bridge. Dunker and Liu (2007), indicated that most of the states in USA adopt H-piles for the foundation of IAB. It is also mentioned that some of the states permit use of precast concrete and prestressed concrete piles. For relatively short span bridges, stiffer foundation such as drilled shaft and spread footing have also been adopted in USA. Some states in USA orient weak axis of bending of the H-piles along the axis of bridge while others orient the strong axis of H-pile along the axis of bridge. The justification of orientation of weak axis of bending along bridge axis has been that only the tip of the flanges will yield under large bending stress, leaving basic core of the pile to carry load. The other justification for the orienting strong axis of bending along the bridge axis has been that the H-piles will have better capacity to resist flange buckling if the piles are oriented along strong axis of bending. White ll et al. (2007) observed that pile foundation is not always required in the European practices in construction of IAB, contradicting many US practices in general. In U.K. the spread footing has been observed to be the preferred foundation for IAB because it is felt that the bridge and approach pavement will settle equally and further, the spread footing will restrain the movement of deck due

to thermal variation. However, White ll et al. (2007) also observed that although spread footing is preferred in U.K., other European countries adopt pile foundation for the integral abutment bridge in which the concrete filled tube pile is most commonly adopted. The design philosophy varies leading to varying selection of foundation types as some countries strive to make the pile stiff to resist the stresses induced from the abutment translation and rotation while some others choose slender piles in an attempt to lessen the impact of piles on the overall structures. To lessen the impact of abutment translation and rotation, sleeves around the pile has also been adopted in England, Ireland and Sweden to avoid the restraining effect of the soil.

2. 3 Finite Element Modelling and Thermal Analysis of IAB

In the service life of IAB, the deck of the bridge, expands with the rise in temperature and contracts with the fall of temperature. This expansion and contraction of the superstructure induces cyclic deflection and stress in the abutment, piers integrated with the deck and piles supporting abutment and pier. The effective temperature of the bridge governs the overall longitudinal movement of the bridge superstructure (Oesterli and Volz, 2005). AASHTO LRFD Bridge Design Specification (2012) recommended effective temperature for estimation of thermal load for concrete girder with concrete slab bridge and also for steel girder with concrete slab bridges separately, depending on the location of the bridge. IRC: 6 (2014), the standard specification and code of practice for road bridges published by Indian Road Congress also recommended the effective maximum and minimum temperature for computation of thermal load on bridges located in different parts of India.

In order to simulate the response of IAB subjected to thermal expansion and contraction load, the 2D and 3D mathematical model of the bridge simulating the behavior of prototype bridge is required to be developed. Yang et al. (1985) created a model of IAB by modelling deck using beam element with equivalent properties of deck and pile using beam column element. The model of pile included lateral and vertical soil springs along the depth of the pile for idealization of soil surrounding the pile. In the analyses, two different categories of pile were considered; one without predrilled oversized hole and one with predrilled oversize hole of length 1.2 to 3.0m from the top portion of the pile. The model was subjected to axial load and thermal deflection. From the results of analyses, it was observed that the ultimate load carrying capacity of the pile installed in the oversized predrilled hole was observed to be higher than that of pile installed without predrilled hole under a specified lateral displacement. This was because the piles installed in predrilled oversized holes was more flexible and thus accommodating the thermal displacement.

Faraji et al. (2001) studied the thermal response of three span integral abutment bridge of total length 45.73 m by developing the finite element model of the bridge. The deck of the bridge consisting of concrete deck slab and steel girder was modelled using plate element and beam element respectively. The plate element representing the concrete deck slab and the beam element representing the girder was connected with rigid link element to ensure strain compatibility and shear transfer between the deck and girder. The abutment wall of the bridge was modelled using plate element while the pier, drilled shaft and H piles was modelled using beam element. Nonlinear $(p - y)$ spring was used in the modelling of soil pile interaction. The abutment backfill interaction was modelled by using relation

between the wall deflection and passive resistance mobilized as proposed by Clough and Duncan (1991). The model of IAB was analyzed under thermal variation of $+44.40^0$C. The displacement of the abutment of the bridge under thermal expansion was recorded as 11mm. With the dense backfill behind the abutment, the moment in piles was reduced by a factor of two regardless of the stiffness of the soil adjacent to the pile.

Dicleli and Albhasi (2003), used the 2-D frame model of a six-span IAB of a total length of 120m for thermal load analysis of the bridge. The steel concrete composite deck of the bridge was modelled as beam element by transforming the stiffness properties in terms of concrete slab. The abutment was modelled as elastic beam element and the pile was modelled as beam element with nonlinear hinge. The pile soil interaction and abutment backfill interaction was modelled using truss element with bilinear axial hinge at its end. The model was analyzed with cyclic thermal loading. From the results of parametric analysis, it was observed that the displacement capacity of the bridge increases with increase in the flexural capacity of the pile. The displacement of abutment was also observed to be more in the contraction of deck than in expansion. Further, the moment in the abutment increases proportional to the increase in subgrade reaction modulus of the sand surrounding the pile. This was attributed to the larger lateral resistance of the soil system at the bottom of the abutment as the top moves with the thermal expansion of deck.

Fannema et al. (2005) developed two and three-dimensional model of a three-span integral abutment bridge having unequal height of abutment where the shorter abutment was supported on spread footing and the taller abutment was supported on the H-piles. The deck was modelled with beam element with equivalent

properties of prestressed girder and deck slab. The abutment and H-pile supporting the abutment was modelled using beam element. The soil pile interaction was modelled with multilinear $p - y$ curve. The model was analyzed with thermal variation of $\pm 40^0$ C. The theoretical values of response evaluated was observed and compared with the field observation of the instrumented bridge. It was found that the magnitude of moment in pile derived from the field data was different from that obtained from the numerical model. This difference was attributed to the limited field data and difference between actual and idealized bridge temperature and soil stiffness. Measured of the displacement of the abutment under the contraction of deck at -17^0C was 4.80mm at the top of abutment against theoretical contraction of 20 mm.

Civijan et al. (2007) carried out parametric studies on a three span IAB having a total length of 82.30 m subjected to thermal cyclic loading. The deck system consisted of concrete slab on steel girder. The bridge had two piers of drilled shaft with elastomeric bearing support for the superstructure. The abutment of the bridge was supported on H piles. The 2-D finite element model of the bridge was developed using GT STRUDL (2002), where the deck of the bridge was modelled with beam element with transformed properties of beam. The pile supporting the abutment was modelled with beam element. The pile soil interaction was modelled with $p - y$ curve as recommended in API (2007). The nonlinear abutment backfill interaction was modelled by adopting the passive resistance-displacement relation proposed by Clough and Duncan (1991). The model was analyzed for thermal load for rise of temperature by 40^0 C and contraction for fall of 55^0 C. It was observed that rotation of abutment about the base occurred when the bridge expanded and therefore, the deflection at the base of the abutment was controlled predominantly

by backfill condition. The rotation of abutment was observed to be predominantly higher during the contraction.

Kim and Laman (2010) used beam element for modelling of girder and abutment. The pile was modelled with transformed nonlinear lateral spring and nonlinear rotational springs using Lpile software. The model of IAB developed was analyzed under thermal load. Sinusoidal variation of thermal load was taken from the annual mean temperature of the actual data at site. Based on the study, the following observations were made: (a) the girder axial force and girder central moment were significantly influenced by thermal expansion coefficient and bridge length, (b) the girder axial force and girder central moment increased with the increase in the pile soil stiffness and (c) the short abutment resulted in higher lateral force than tall abutment, when pile soil stiffness was higher.

2.4 Finite Element Modelling and Seismic Analysis of IAB

The detailed study on seismic performance of IAB is intended since the bridge type is expected to give a improved performance in an earthquake scenario as compared to a conventional bridge. The literatures on the bridge type suggested that the inherent increase in redundancy derived from the configuration of IAB is expected to redistribute the forces and perform better under the action of seismic excitation.

Goel (1997) investigated the vibration characteristics of IAB at 101/Painter Street Overpass, USA, which has a total length of 80.772 m using the motion recorded during actual earthquake events. The bridge is composed of two unequal spans of 36.271 m and 44.501 m. The superstructure consists of a continuous reinforced concrete multicell box girder supported at ends with integral abutment. The east abutment is monolithic with superstructure supported by 14 numbers of concrete

friction piles. However, the west abutment contains a thermal expansion joint between the abutment wall and pile cap supported by 16 numbers of concrete piles. In the course of the investigation, it was affirmed that the bridge with the integral abutment may experience nonlinear behavior, because of the nonlinearity in the abutment soil pile system even though the other superstructure components remains elastic. The identified properties from the investigations were the vibration period, mode shape and damping ratio of the bridge. The identified period of the bridge indicated that the transverse period of the bridge derived from the motions of the bridge during the strong earthquake shaking phase was two times longer than those derived from the motions recorded during the earthquake shaking of lower level. This led to the observation that the transverse period of integral abutment bridge depends to a large degree on the level of shaking. The damping ratio in first transverse mode of the bridge was observed to be approximately in the range of 6-12%. It was also observed that during the strong shaking phase of a relatively larger earthquake, the damping ratio increased from 8.5% to 12.1%. This increase in damping was attributed to the softening of abutment-soil pile system due to nonlinear soil behavior during the strong shaking phase of earthquake and was associated with longer period of bridge. Thus, it was shown that the vibration properties like period and damping are affected significantly by abutment flexibility. However, it was shown that the period lengthened, and damping increased for the sample bridge with the increase in flexibility of abutment, but the increased period did not affect the lateral design force for the bridge. This was due to the fact that the increased period was in the zone of constant pseudo acceleration in design spectrum. On the other hand, it was further shown that deformation demand on the column in the central bent would increase significantly due to

elongation of period. This was attributed to the fact that although increased period is in the zone of constant acceleration the spectral displacement increases with increase in time period which led to increase in the column forces.

Spyrakos and Loannidis (2003) studied modal and seismic analysis of the post-tensioned IAB supported on abutment wall with a hinge near its base on spread footing. A hinge connection was provided in the interface of abutment wall and foundation to reduce the load on the foundation. The bridge was modelled as frame element and the abutment soil and foundation soil interaction was modelled using spring element with stiffness calculated using linear elastic half space theory. A general form of abutment-wall backfills stiffness equation that considers the passive resistance of soil was adopted in the study to estimate the longitudinal stiffness of the end wall and the transverse stiffness of the wing wall. Modal analysis was carried out on the numerically simulated frame model and it was observed that influence of foundation soil interaction on the response characteristics were more significant on higher modes than at lower modes. The first mode shape of the bridge was observed to be translation mode in vertical direction and the second mode shape was observed to be translation model along bridge axis. Hence, the second mode was observed to be the most significant contributor in the seismic response of the bridge. Analyses with and without backfill were done for comparison and it was indicated that the inclusion of backfill effect significantly influences the seismic response of bridge and changes the first and second mode shape.

Kumar (2008) performed seismic analysis of five span continuous bridge with integral abutment. The total length and width of the bridge was 130 m and 12 m respectively. The superstructures consisted of four cast-in-situ R.C.C girders with deck slab. The deck slab was modelled with shell element and the girder was

modelled with frame element. The abutment of 1000 mm thickness was modelled with shell element. The piers and piles were modelled using beam element. The pile soil interaction was modelled with $p-y$ curve, $t-z$ curve and $Q-z$ curve as recommended in API (2007). Linear elastic, Nonlinear Static (Pushover) and nonlinear dynamic analyses was carried out using the model developed. The results of nonlinear dynamic analysis and pushover analysis based on modal distribution pattern of forces in longitudinal direction indicated that pushover analysis overestimated displacement of abutment by 33% and base shear by 23% as compared to that of nonlinear dynamic analysis. It was also found that pushover analysis with modal distribution pattern of force overestimated displacement by 40% and underestimated base shear by 100% in transverse direction. The uniform force distribution gave conservative estimate of base shear by about 10% but it underestimated the displacement by 60%.

Farahani et al. (2010) modelled two span IAB with steel concrete composite deck considered for seismic analysis using shell element for deck, abutment wall and pile cap and beam element for girder, pier and bent cap. To account for the composite action of the superstructure, rigid link elements were used to connect deck and girder elements. The hyperbolic relation for force displacement relation proposed by Samsabadi et al. (2007) was used in the modelling of abutment backfill interaction. The H-piles supporting the abutment and pier were modelled with beam element. Nonlinear soil spring of *p-y* curve for clay as per API (2007) was adopted in the modelling of pile soil interaction. To assess the effect of soil type around the piles and degree of compaction of backfill behind the abutment, the analysis was focused on longitudinal mode. It was observed that the dominant longitudinal frequency increased by 19% for IAB in medium clay when backfill behind

abutment was changed from loosely compacted sand to densely compacted sand. Similarly, the dominant longitudinal frequency increased by 13% for IAB in hard clay when the backfill behind the abutment was changed from loosely compacted sand to densely compacted sand. These parametric studies clearly indicated that the effect of the backfill in the seismic behavior of the bridge. Further, it was also indicated that under seismic excitation, the maximum displacement of pile along the depth occurs at the joint between the piles and abutment. The model having dense backfill indicated lesser value of displacement as compared to the model having loose backfill.

Monzon et al. (2014) studied the seismic behavior of IAB with steel concrete composite deck girder. A 3-D finite element model of the bridge was developed using ADINA (2008). 3-D brick element with 20 nodes was used for modelling the steel girder, R.C. deck slab and the abutment. The pile was modelled with beam element along with pin support at bottom. Load displacement ($p - y$) curve was used to model soil pile interaction. From modal analysis of the IAB, it was observed that the degree of rigidity of the connection of girder to abutment influence the vibration period of the bridge. Flexible connection induced longer vibration period as compared to that from the rigid connection. The connection flexibility was observed to have significant effect on dynamic characteristics of the IAB. It was also observed that significant changes in overall structural dynamic characteristics was due to soil pile interaction. The mode shape of the IAB was found to change with associated increase in vibration period when fixed based assumption in modelling of abutment base was replaced with soil structure interaction modelling.

2.5 Maximum Length of IAB in Practice

The maximum permissible length of the bridge depends on the allowable displacement of the bridge deck, which is influenced by the flexibility of abutment and pile foundation. Tinsae et al. (1987) indicated that the determination of allowable length of bridge with integral abutment is a complex problem. The safe length of the bridge not only depends on properties of soil and piles but also on the backwall soil model, approach slab etc.

Dicleli and Albhaisi (2003) presented estimation of the displacement capacity of integral abutment bridge supported on H-piles driven in sandy soil. Different possible failure modes were investigated. The first mode was due to low cycle fatigue failure of H-pile. The displacement capacity of the bridge was taken as the displacement of the abutment corresponding to the maximum cyclic curvature of low cycle fatigue failure of H-piles. The second mode was (Dicleli and Albhaisi, 2005) based on the abutment's flexural capacity to resist the moment induced by thermal expansion of the bridge deck and passive resistance mobilized on the backfill. The results of the analysis indicated a limiting length of IAB with concrete deck as 190 m in cold climate and 240 m in moderate climate. The limiting length of IAB with steel composite girder deck was indicated as 100 m in cold climate and 160 m in moderate climate.

Kumar (2008) demonstrated that the pre-drilling of oversized hole in the pile introduced more flexibility and increased the displacement capacity of the bridge. In addition, increase in the main reinforcement of the pile also increased the ductility of the reinforced concrete piles and increased the displacement capacity of the bridge.

Different department of transportation provided guidelines for the design and construction of IAB and prescribed the maximum length for the different bridge types. The recommendation of some allowable maximum length of IAB without consideration of the skew angle is shown in Table 2.1 (Dicleli and Albhaisi, 2003, White et al. 2005, Stoothoft and Conboy, 2005, Weakley, 2005)

Table 2.1 Maximum length of IAB recommended by various design manuals

Department of Transportation	Maximum length of IAB recommended	
	Steel concrete composite deck (m)	Concrete deck (m)
Manie, USA	61	101
Massachusetts, USA	101	180
New Hampshire, USA	91	183
Vermont, USA	101	180
IOWA, USA	121	175
Colorado, USA	195	241
New York, USA	198	198
Virginia, USA	91	152
Illinois, USA	95	125
New Jersey, USA	140	140
Ontario, Canada	100	100
Washington, USA	91	107

2.6 Sleeved Pile for Foundation of Structures

The sleeved pile is adopted for enhancing the flexibility of foundation. Holley et al. (1973) developed the concept of sleeved pile for offshore structures subjected to the action of lateral loading. The concept was aimed to transfer the lateral force acting on the offshore structure into the soil through pile in bending mode without severe restraint to such bending imposed by soil spring. The objective of the concept of sleeved pile was also to achieve bending flexibility of piles to minimize

shear and bending stress. With these objectives, the sleeved pile was configured by isolating the upper portion of the embedded pile from the soil by driving it through a pipe sleeve of larger diameter. The piles designed to transfer vertical load, was accomplished either by end bearing or by skin friction in the region below the sleeve. The lateral load was transferred to the soil below the region of sleeve. The estimation of the ultimate lateral load capacity of the sleeved pile was carried out by assuming that the pile will reach ultimate load with development of hinge at some depth below ground level.

Kaynia and Kausel (1980) developed expression for the dynamic stiffness of sleeved pile for seismic analysis of the sleeved pile in linear viscoelastic soil medium. The sleeved pile was considered as a column within a sleeve of substantially larger diameter filled with concrete up to predesigned depth below ground level.

Raupach et al. (1981) investigated the feasibility for adopting the sleeved pile as flexible foundation for seismic resistant design of building. The expression for horizontal stiffness of the sleeved pile was formulated by idealizing the building supported on sleeved pile as single degree freedom (SDOF) system. Step by step design procedure for the design of steel tube sleeved pile for building was presented.

Boardman et al. (1983) recorded the adoption of sleeved pile in the construction of Union House, New Zealand in 1983. The building was designed to mimimize ductility demand of each member in the superstructure by providing energy dissipators and bracings within the structures. To allow the dissipators to function, the base of the superstructure was required to move freely. This was achieved by the use of long sleeved pile pinned at both ends.

Charless et al. (2001) referred to the use of sleeved pile in the construction of piled foundation of buildings on slope in Hong Kong to restrain the transfer of lateral wind load on the buildings to ground slope through piles in order to avoid destabilization of slope. In construction of the sleeved pile the gap between the pile shaft are filled with compressible material. Polystyrene is most commonly adopted for the purpose.

Khodair and Hassiotis (2005) analyzed for the thermal loading of soil pile system in Scotch Road I-95 IAB in which the corrugated steel sleeved was inserted around H-piles supporting the abutment to enable free movement of pile under thermal expansion and contraction of deck. In the construction process, the piles were installed in pre-augured holes of 0.76m diameter followed by concreting by encasing the pile up to 7.60m (or 60%) of the pile length. Next, the steel corrugated sleeve of diameter 0.6m was inserted and extended to the top of the pile. The gap between the pile and the sleeve was filled with sand to facilitate movement of piles subjected to lateral load transferred from the superstructure. The results of analysis indicated that providing galvanized steel sleeve of 0.60 m diameter filled with sand is sufficient to accommodate the pressure developing as a result of thermal load corresponding to the change in temperature up to 42^0 C. The result of parametric studies also showed that magnitude of axial stresses in the pile decreased as the diameter of sand surrounding the pile was increased.

2.7 Incremental Dynamic Analysis

The evaluation of seismic capacity of IAB carried out using Incremental Dynamic Analysis (IDA). The IDA is a parametric analysis methodology which has recently emerged in several different forms for use in more thorough estimation of structural performance under seismic loads. The IDA involves nonlinear analyses of the

structural model under a suite of ground motion records, each scaled to several intensity levels designed to force the structure all the way from elastic to final global dynamic instability. The primary objective of IDA is to have thorough understanding of range of responses and demands versus range of potential level of ground records, better understanding of structural implications of rare/severe ground motion level, better understanding of change in the nature of structural response with increase in intensity of ground motion and producing estimates for dynamic capacity of global system. Vamvatsikos and Cornell (2002) presented a basis and terminology to unify the existing format of IDA and set up essential background to achieve the objective of IDA which are reproduced for understanding of IDA process as:

1. Scale Factor (SF): Scale factor of scaled accelerogram a_λ is a non-negative scalar λ that produces a_λ when multiplicatively applied to an unscaled (natural) accelerogram time history a_1. The scale factor is the way to characterize the scaled image of the accelerogram.
2. Intensity Measure (IM): The intensity measure of the scaled accelerogram a_λ is a non-negative scalar IM that constitute a function $IM = f_{a1}(\lambda)$, that depends on the unscaled accelerogram a_1 and is monotonically increasing with the scale factor λ. The popular scalable IMs of the ground motion adopted by various researchers in IDA are Peak Ground Accelerogram (PGA), Peak Ground Velocity (PGV) and 5% damped Spectral Acceleration at the structure's first mode.
3. Damage Measure (DM): Damage measure or structural state variable is a non-negative scalar that characterizes the additional response of the structural model to a prescribed seismic loading. The DM is a part of or can be deduced

from the output corresponding to nonlinear dynamic analysis. The possible choice of the DM is maximum base shear, nodes rotation, peak story ductility, peak roof drift etc.

The IDA is also carried out with single or with multi-records of accelerogram. In single record IDA study, a series of dynamic non-linear runs are performed under scaled images of an accelerogram, the IMs of which are ideally selected to cover the whole ranges from elastic to nonlinear and up to collapse of the structure. Multi-records is a collection of single-record IDA of the same structural model under different accelerograms. The IDA curve in respect of single record IDA is a plot of state variable DM recorded in IDA versus one or more IMs that characterizes the applied scaled accelerograms. In respect of multi-records IDA, it is a collection of IDA curves of same structural model under different accelerograms that are all parameterized on the same IMs and DM.

Vamvatsikos and Cornell (2004) further emphasized that the IDA is a promising method for estimation of structural performance under seismic load particularly in estimation of mean annual frequency of exceeding a specified level of structural demand or a certain limit state capacity for performance-based earthquake engineering. The steps in IDA were summarized as: (a) construction of nonlinear model of structure to be analyzed, (b) selection of suite of records for analysis, (c) running the dynamic analysis of structure by scaling the records to a selected level of intensity and (d) generating of IDA curves of the structural response as measures of DM versus IM. In turn these analyses results are interpolated for each record and summarized over all records to estimate the distributed DM for given IM. The final results are conveniently integrated with conventional probabilistic seismic hazard

analysis and hazard curve for calculating the maximum annual frequency of exceeding a certain limit state capacity or a certain demand.

2.7.1 Selection of Ground Motion

In order to carry out single record or multi-records IDA selection of appropriate ground motion are done for use in the analyses. The selection and scaling of the ground motion are important steps in defining the seismic excitation that will be applied to the structure during the structural analysis, and it serves as an interface between seismology and engineering. Shome and Cornell (1999) showed that for a midrise building, 10 to 20 records are enough to provide sufficient accuracy in the estimation of the seismic demand of the building. Vamvatsikos and Conell (2004) selected 20 ground motions for the estimation of wide range of seismic demand of building. Baker and Cornell (2006) considered several selection methods of ground motion for testing effect the ground motion properties such as magnitude (M), distance (R) and epsilon (ϵ), the number of standard deviation by which an observed logarithmic spectral acceleration differs from the mean logarithmic spectral acceleration of a ground motion predicted by attenuation equations on the structural response. It was difficult to ideally match the target distribution of all of these parameters in practice as only finite numbers of recorded ground motions are available. Due to these limitations, four records selection methods were considered in order to investigate the effect of selection strategies on estimated response of structure. The strategies were ; (1) selection of records at random from records library without attempting to match the properties of any specific record, denoted as AR method as it uses arbitrary records, (2) selection of records with magnitude (M), and distance (R) values representative of the site hazard without attempting to match the ϵ value denoted as MR-BR method as it uses M and R based records, (3)

selection of records with ϵ values representative of site hazard without attempting to match magnitude and distance value abbreviated as ϵ-BR method as it uses ϵ-based records and (4) selection of records with spectral shape that match to the conditional mean spectral shape given M, R, and ϵ. This is denoted as CMS-ϵ method as it uses properties of ground motion M, R, and ϵ. The records selected were used as input for nonlinear dynamic analysis of a 7 storeyed reinforced concrete framed building taking observed inter-story drift ratio as structural response of interest for comparison. The ϵ-BR records produced lowest geometric mean response and CMS-ϵ based records also produced approximately the same response as that of ϵ-BR records. The AR and MR-BR method produced slightly higher response. The AR and MR-BR method also gave higher probability of collapse of the building than other ϵ-BR and CMS-ϵ method.

Vamvatsikos and Cornell (2002) also presented hunt and fill algorithm for speeding of IDA. In performing IDA with this algorithm, it ensured that the scaling levels are approximately selected to minimize the number of runs. In the hunt phase, analyses are performed at rapidly increasing level of IM until the numerical non-convergence are accounted signaling global dynamic instability. In the fill phase, additional analyses are performed at the intermediate IM levels sufficiently to bracket the collapse and increase the accuracy of the lower IM. The IDA curve is plotted from IMs and DMs extracted from the nonlinear dynamic analysis corresponding to each record. By interpolation of the IDA results, entire curve is developed without performing additional analysis (Vamvatsikos and Cornell 2004). Having the complete curve available, it is possible to calculate the DM values at the arbitrary level of IMs. Vamvatsikos and Cornell (2004) indicated the need to employ approximate summarization technique that would reduce the data to the

distribution of DM for IM and to the probability of exceeding any specific limit state for the IM.

2.7.2 Definition of Damage States

The capacity of the structure is defined in terms of the damage state of the structure against a corresponding IM. For the case of bridge components, HAZUS-MH MR (2003) gave a qualitative description of four damage states: Slight, Moderate, Extensive and complete with detailed description of damage. These respective qualitative damage states can be described by qualitative damage state in the form of displacement of the components. Dutta and Mander (1998) provided drift limit for bridge columns corresponding to damage state as; Almost no damage, Slight, Moderate, Extensive and collapse as defined in HAZUS (1999). Priestley et al. (2007) recommended different strain limits for different damage states. The strain limit can be converted to drift and rotation by using the appropriate relation between the strain, curvature, hinge length in yielding element. Berry and Eberhard (2007) based on the experiment on bridge columns, calibrated equations for computing damage states like concrete cover spalling, bar buckling and bar fracture in the form of drift ratio, plastic rotation and strain limit for circular bridge columns. The properties of the column including longitudinal and transverse steel ratio, axial load ratio and geometry was considered in the derivation of the empirical equations. Stefanidou and Kappos (2017), presented the damage states of bridge piers in terms of threshold value of limiting curvatures of the pier section for minor/slight damage, moderate damage, major/extensive damage and failure-collapse.

2.8 Fragility function and Development of Fragility Curve of Bridge

Porter et al. (2016) defined fragility function as a mathematical function that expresses the probability that some undesirable event occurs as a function of some measure of environmental excitation. The fragility function also represents the cumulative distribution function of capacity of an asset to resist an undesirable limit state. Further, Elnashai et al. (2015) defined the seismic fragility function as a relationship between the ground shanking, or system demand, and the conditional probability of the same system reaching or exceeding a response limit state. The common form of seismic fragility function is assumed to be lognormal cumulative distribution function. The bridge fragility curves express the probability of bridge components reaching a certain damage state for a given ground motion parameter and play an important role in the overall seismic vulnerability assessment of a transportation network.

Nelson and DesRoches (2006) carried out fragility analysis of the multi-span simply supported (MSSS) highway bridge using component level approach. The methodology considered the contribution of major components of the bridge such as columns, bearings and abutment to overall bridge system fragility. The distribution of the capacity of the components were assumed to be lognormal. The seismic response was evaluated using a suite of synthetic ground motion developed as a part of research in Mid-America. A total of 48 ground motions were selected for the analysis considering different moment magnitudes M_w (5.5, 6.5 and 7.5) and four different hypocenters (10, 20, 50 and 100 km). Four damaged states were considered in determining the capacity of the bridge components monitored as Slight Damage, Moderate Damage, Extensive Damage and Complete Damage.

Responses of eight components of the bridge were monitored during the analyses under each ground motion. The fragility curve of each bridge component was developed assuming that the demand and capacity of the bridge component was lognormally distributed. The estimation of median demand was carried out using the power model as proposed by Cornell el al. (2002). The general vulnerability of the bridge system as a whole was developed by combining the effect of various bridge components.

Kwon and Elnashai (2010) carried out fragility analysis of the highway bridge by selecting 60 ground motions to account for the uncertainty of seismic hazard of the site. The failure of bearings, bent and abutment were considered in the study. The fragility curve was developed for each component monitored in the analysis assuming that the seismic demand and capacity of the component were lognormally distributed. The relationship between seismic intensity and demand was not considered deterministic and a term that accounts for uncertainty was introduced in the power model proposed by Cornell el al. (2002). The fragility curve for each component was combined to develop the fragility curve for the bridge system.

Akbari (2012) carried out fragility analysis of an irregular bridge with different height of pier. The height of bridge pier was 14.0m 7.0m and 21.0m. A total of 60 ground motions in the Los Angeles area developed for the FEMA-SAC (1997) were adopted. The fragility curves for all the piers were developed adopting lognormal cumulative probability function. The fragility curves showed that in the highly irregular bridge the shortest piers were more vulnerable than others because of higher stiffness than the tall piers.

Tehrani and Mitchell (2014) carried out seismic risk assessment of four span bridge using IDA and fragility analysis. Total 39 ground motions were selected for

carrying out nonlinear time history analysis. The ground motions were applied twice, first along the principal direction and again along the direction rotated at 90^0. The damage states considered in the analysis were yielding, concrete cover spalling and bar buckling. The limiting drift ratio for yielding was computed from the limiting compressive strain of concrete as recommended by Priestley et al. (2007). The drift ratio for the concrete cover spalling and bar buckling were computed using the empirical relation proposed by Berry and Eberhard (2007). Assuming that the IDA results were lognormally distributed, the fragility curve was developed using the lognormal cumulative distribution function.

Stefanidou and Kappos (2016) proposed a methodology for the development of the bridge specific fragility curve. The methodology proposed consisted of three distinct steps: (a) defining the capacity threshold for the quantification of component damage and associated uncertainties, (b) demand estimation and uncertainties in demand estimation and (c) Correlation of component fragilities to evaluate system fragility. The first step involved, detailed identification of critical bridge components such as piers, bearing and abutment and a database of pier sections type, varying geometry, materials, reinforcement and loading were documented. The definition of pier limit states threshold for all pier section in database were developed using local EDP by means of section analysis and correlation of materials strains (related to cracks) to local curvature (local damage). Similar definition of limit state threshold values for bearing, abutment and other components considered for monitoring during analysis were developed. Four limit states were considered for pier as minor/slight damage, moderate damage, major or extensive damage and failure-collapse. The threshold values for each limit state was computed in the terms of curvatures from the limiting compressive strain of

concrete or limiting tensile strain of steel reinforcement and ultimately correlating the curvature to the drift of pier. Similarly, the limit state of the elastomeric bearing has been computed based on the limiting shear strain of elastomeric bearing. The second step involved the estimation of seismic demand for the components. In the case of the analysis of a single bridge, evaluation of nonlinear response history using suite of time history was suggested. For analysis of bridge stock, Response Spectrum Analysis (RSA) was suggested using a simplified model of the single bridge by varying the level of earthquake intensity. The displacement developed at the control point of each critical components were to be recorded. The third step involved developing the fragility curve for the component of stock of bridge. The results in terms of displacement demand of the component at control point of each critical component were plotted against the earthquake parameters PGA, termed as primary vulnerability curve. The capacity limit states threshold is determined in terms of PGA using the primary vulnerability curve and definition of the damage in terms of displacement. The fragility curves for every limit state were plotted assuming lognormal distribution. However, in case of single bridge the fragility curves of the components were developed from the results of IDA.

2.9 Concluding Remarks

The literatures pertaining to the state-of-the-art practice for finite element modelling and analysis of IAB subjected to thermal load and seismic excitation are reviewed. Further, literatures on the sleeved pile foundation for structures, incremental dynamic analysis and seismic vunerability assessment are also studied. 2-D finite element frame model of IAB is found to be adequate for analysis of the bridge subjected to thermal loading since the forces induced in IAB by axial expansion and contraction of deck due to thermal variation can be estimated using

the simplified model with sufficient accuracy. The IAB with tall abutment is observed to increase the allowable deflection of abutment resulting in longer allowable length of IAB although the moment in the tall abutment is comparatively higher than that in shorter abutment.

In the finite element model for seismic analysis of IAB, 3-D finite element model is adopted to simulate the behavior of the deck and its effects on seismic forces in substructure. It is observed that the soil pile interaction modelling significantly influence the dynamic characteristics of IAB. The literature on seismic analysis of IAB, considering soil structure interaction is found to be limited and inadequate to frame guidelines for design and implementation of IAB in area classified as high seismic risk zone. Further, literature on dynamic analysis of IAB indicates that the study of dynamic characteristics and response subjected to seismic excitation by IAB, incorporating far field soil reaction modelling of soil pile interaction have not been studied adequately. No literatures on the seismic resistant design of IAB with additional measures for seismic response control leading to enhancement in seismic performance of IAB during seismic event is found in the literature survey.

The concept of sleeved pile for foundation of structure may provide adequate flexibility to structure thereby lengthening the vibration period resulting in an improved seismic performance of the structure. It is observed to be an efficient alternative for seismic response control of structure including IAB. However, no study on use of sleeved pile in seismic response control of IAB is recorded. The flexibility to the foundation provided by sleeved pile may also reduce the thermal stress induced in IAB.

The IDA is observed to be a very exhaustive methodology to estimate thoroughly the capacity of the structure under seismic excitation. It is also observed that the

fragility of bridge is approached components wise. However, in the case of IAB in which the bearings are not provided, the fragility of the bridge system can be represented by the fragility of critical components like pier.

Chapter 3

Soil Structure Interactions Modelling Approach for Integral Abutment Bridge

3.1 Introduction:

In order to obtain meaningful response of integral abutment bridge subjected to seismic excitation and load due to thermal, detailed three-dimensional modelling of the bridge with soil structure interaction in foundation and abutment back fill is required. Goel (1997) observed that under strong shaking, the dynamic properties of the integral bridge were affected by abutment-pile soil system due to nonlinear behavior. Spyrakos and Loannidis (2003) carried out seismic analysis of single span integral abutment bridge with spread footing and noted that the abutment backfill influences the seismic response of bridge significantly. Farahani et al. (2010) observed that the dominant longitudinal frequency of the bridge was increased with the increase in the stiffness of the backfill. Monzon et al. (2014) observed that the direction predominant modes of vibration get modified on consideration of soil structure interaction. Soil structure interaction dramatically influences the seismic response of IAB.

Similarly, various researchers, like Faraji et al. (2001), Dicleli and Albhaisi (2003), Civjan (2007), and Kim and Laman (2010) observed that the soil structure interaction plays a significant role in the response of integral abutment bridge under thermal load. The stiffness of the soil surrounding the pile influences the deflection and forces in pile, abutment and in girder. Based on field monitoring of instrumented IAB Frosch et al. (2005), Fennema et al. (2005), Breña et al (2007) and Kim and Laman (2011) concluded that the stiffness of the soil surrounding the pile and backfill behind the abutment have significant influence on the response of

bridge under thermal variation. Therefore, accounting for the soil structure interaction in the modelling for analysis of IAB is essential for obtaining reasonably accurate design forces.

In this chapter, the state-of-the-art methods of modelling of soil structure interaction for analysis of integral abutment bridges, along with the brief theoretical background, are presented. The soil structure interaction modelling in the IAB involves modelling of soil foundation interactions and abutment backfill interaction. Since the pile foundation is the most commonly adopted foundation in IAB, the soil pile interaction modelling is considered under the present study. The different modelling strategies to account for the tip bearing capacity, resistance to axial movement due to shaft frictional force and lateral resistance of soil to pile deflection that develop in pile foundation are available in literatures. The commonly adopted methods in modelling of soil pile interaction such as load settlement ($Q - z$) curve for modelling the relation between mobilized tip bearing capacity and settlement, load transfer ($t - z$) curve for modelling the relation between the shaft skin frictional forces mobilized and relative movement of pile and soil and load displacement ($p - y$) curve for modelling the relation between the lateral resistance of soil and pile displacement are considered in this study. These said curves are nonlinear in character and represent the soil near the pile which exhibit nonlinear behavior under the action of deformation from pile. The soil in the far field zone from pile which respond to deformation induced by pile in an elastic manner are also considered in the soil pile interaction modelling. This far field soil reaction is modelled with linear spring and dashpot representing the linear response and dissipation energy due to far field soil. Further, for modelling the abutment backfill interaction, the nonlinear relation between the displacement of abutment wall

towards the backfill and passive pressure mobilized by the wall movement is adopted. Based on the comparative analysis of different strategies for modelling different component of soil pile interaction and abutment backfill interaction, the method of modelling which are simpler but can effectively simulate the response of soil under loads from pile are adopted in this study

3.2 Soil Pile Interaction in Axially Loaded pile in Sand

The vertical load on pile is resisted by the combination of tip bearing capacity at the bottom of the piles (Q_p) and resistance due to frictional force mobilized around the perimeter of the pile (Q_f) embedded in soil. The standard relation expressing the axial capacity of the pile is given as

$$Q_u = Q_p + Q_f \tag{3.1}$$

For cohesionless soil (sand) with cohesion $c = 0$, the tip bearing capacity of the pile is computed using the relation proposed by Prakash & Sharma (1990) as

$$Q_p = A_p \times N_q \times \sigma_0' \tag{3.2}$$

The maximum tip bearing capacity Q_{p_max} of the pile is calculated by adopting Equation (3.2), considering the value of the dimensionless bearing capacity factor based the properties of soil supporting the foundation and overburden pressure at the level of the bottom of the pile. However, the soil reaction at the tip of the pile is mobilized with the relative displacement between the soil and pile. Vijayvergiya (1977) studied load movement characteristics of pile which included criteria for skin friction *vs* pile movement and tip bearing *vs* tip movement. It was observed that tip soil resistance continues to increase with the settlement of pile. Considering this phenomenon, the interaction between the tip bearing resistance of pile with the load applied on the pile is modelled using the load settlement curve known as $Q -$

z curve. This curve provides a relation between the settlement of pile and the tip bearing resistance mobilized. API (2007) and Reese et al. (2006) indicated that settlement of 10% of the pile diameter is required for full mobilization of the tip bearing capacity of pile. For the implementation of the tip bearing resistance-pile settlement interaction of pile, the $Q - z$ curve recommended by API (2007) is adopted in this study is shown in Fig. 3.1. This pile tip bearing interaction behaviour as per Fig. 3.1 is represented in numerical model using nonlinear spring attached to the bottom end of the pile.

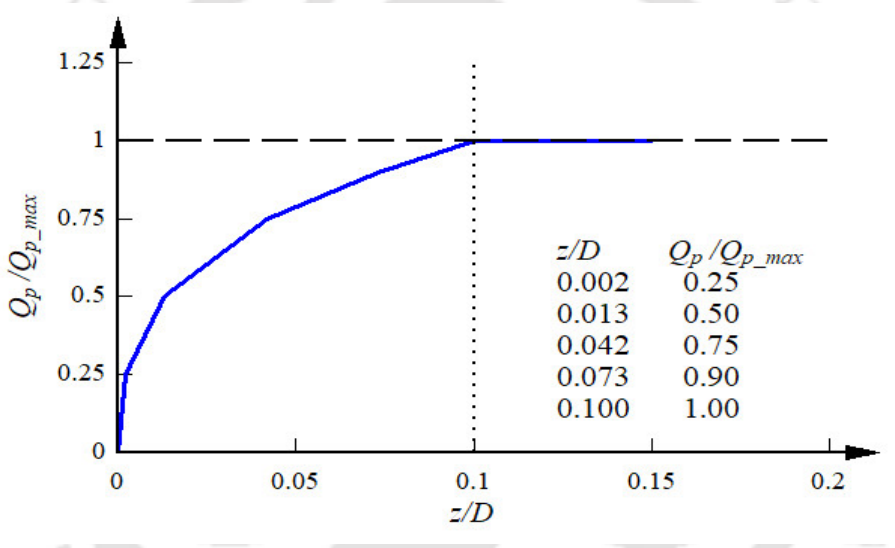

Fig. 3.1 Pile tip load - displacement (Q-z) curve (API 2007)

The other component of resistance contributing to the axial capacity of the pile is the skin frictional resistance of the pile (Q_f) as shown in Equation (3.1). The shaft frictional resistance force mobilised in the length of pile embedded in sandy soil can be expressed as

$$Q_f = p \sum_{L=0}^{L=Le} f_s \Delta L \tag{3.3}$$

For computation of the maximum pile shaft frictional resistance, the variation of shaft frictional force along the depth of the pile is considered as per the recommendation in FEMA- 356 (2000).

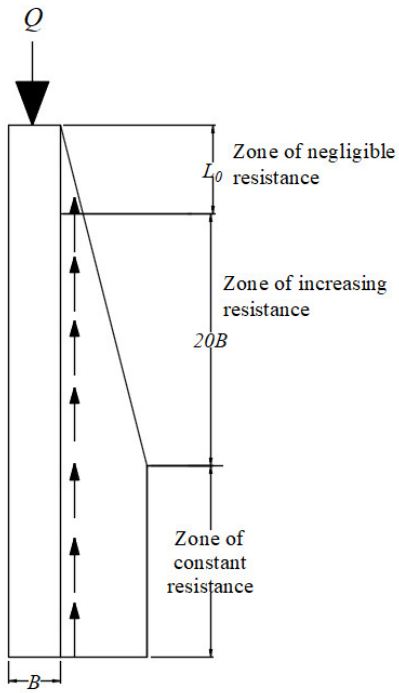

Fig.3.2 Presumptive axial friction capacity of pile (FEMA356, 2000)

In the recommendation of FEMA 356 (2000) (Fig. 3.2), the pile shaft frictional force at the top portion of the pile for an embedded length equal to three times the diameter of piles is considered negligible, since this portion of the pile length may have negligible overburden pressure or may be subjected to scouring. The length of pile from the depth of negligible shaft frictional force to a depth equal to 20 times the diameter of pile is considered as the zone in which shaft frictional force increases with depth. The shaft friction frictional force below this zone remains constant with increase in depth of pile.

The mobilized shaft frictional force, along the length of the pile also depends on the amount of relative axial movement between the pile and the soil. The modelling of

the shaft frictional force interaction with pile is carried out by computation of maximum mobilized skin friction (t_{max}) at various depth along the pile. The computation of maximum mobilized shaft frictional force (t_{max}) at various depth under consideration along the pile is computed using the following equations (FEMA 356, 2000)

$$t_{max} = \sum_{i=1}^{i-1} F_{di}\, P_i \tan(\delta_i) a_s L_i \tag{3.4}$$

$$P_i = \sum_{j=0}^{i} L_j \gamma \leq P_c \tag{3.5}$$

The modelling of the shaft frictional resistance is also carried out using load transfer curve known as $t - z$ curve which provides a relation between the axial movement of pile vs the skin frictional force mobilized along the perimeter of the pile shaft. Vijayvergiya (1977) observed that the mobilized shaft frictional force due to relative movement of soil and pile reaches certain peak value at a small movement and remain constant beyond that. The relation proposed by Vijayvergiya (1977) between the movement of pile and shaft frictional force mobilized is as

$$t = t_{max} \times \left[2 \times \sqrt{\frac{z}{z_c}} - \frac{z}{z_c} \right] \tag{3.6}$$

$$t = t_{max} \quad \text{for } z > z_c$$

The movement (z_c) required for mobilization of maximum shaft frictional forces (t_{max}) is given as 5.00 mm for sand. Mosher (1984) studied the available load transfer relation for shaft frictional force of axially loaded pile driven in sand and proposed a relation for $t - z$ curve. Further, API (2007) recommended a relation for t −z curve in bilinear form for cohesionless soil as shown in Table 3.1.

Table: 3.1 Shaft skin friction *vs* pile movement

Pile movement	t/t_{max}
0.00	0
2.54mm	1.00
∞	1.00

In the recommendation of API (2007), the mobilization of maximum shaft frictional force in the pile is assumed to commence at a pile movement of 2.54mm (0.1in). Amongst these, the $t-z$ curve proposed by Vijayvergiya (1977) and similar recommendation by API (2007) is commonly adopted by designers. The comparison of the curves recommended by API (2007) and Vijayvergiya (1977) is shown in Fig. 3.3.

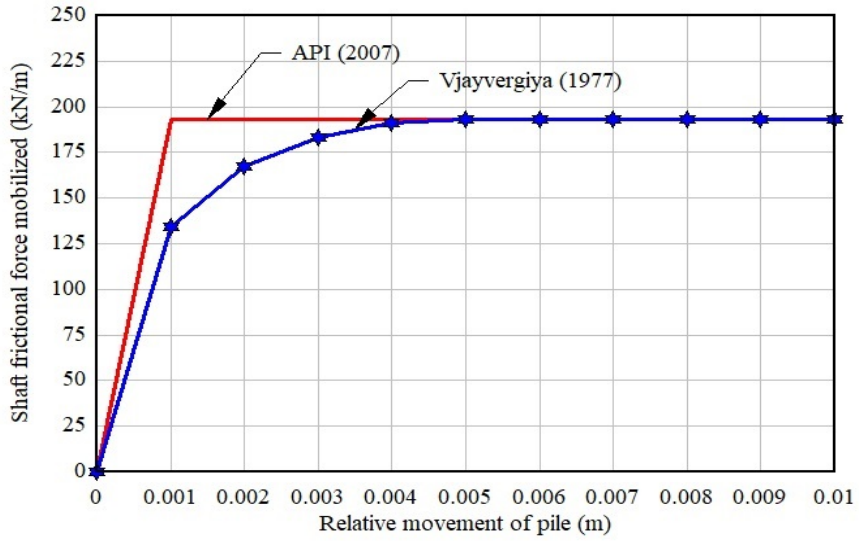

Fig. 3.3 Comparison of $t-z$ curve of API (2007) and Vjayvergiya (1977)

The $t-z$ curve recommended by API (2007) may be more conservative since the nonlinear behaviour of the soil has been approximated by bilinear curves. This would also simulate higher value of shaft frictional force with a small relative soil-pile movement. The behaviour of soil is inherently nonlinear and hence $t-z$ curve

relation given by Vijayvergiya (1977) is observed to be realistic for nonlinear behaviour shaft skin friction. This relation has also been adopted in a recommendation by Lam and Martin (1986). Hence, the $t-z$ curve given by Vijayvergiya (1977) has been adopted in present study.

3.3 Soil Pile Interaction in Axially loaded pile in Clay

In cohesive soil, where internal angle of friction $\emptyset = 0$, the standard relation for estimation of the tip bearing capacity of pile is calculated using the following equation was proposed by Prakash and Sharma (1990) as

$$Q_p = A_p c N_c \tag{3.7}$$

The recommended value of $N_c = 9$ in API (2007) is adopted in this study. Further, the $Q-z$ curve, which is recommended by API (2007) as shown in Fig 3.1 is adopted in the present study for modelling of tip bearing-settlement of pile interaction in soft and stiff clay.

In the computation of the axial resistance contributed by shaft friction force f_s mobilised in the pile shaft embedded in clay, the following relation is adopted as proposed by Prakash and Sharma (1990).

$$f_s = c + \sigma_v \tan\delta \tag{3.8}$$

where c is the cohesion in clay soil, σ_v is the vertical stress and δ is the angle of wall friction between pile and soil. Taking $\emptyset = 0$ for the cohesive soil and taking $c = c_a$, the Equation (3.8) reduces as

$$f_s = c_a \tag{3.9}$$

Hence the maximum shaft frictional force mobilised in pile embedded in the clay soil can be calculated as

$$t_{max} = \sum_{L=0}^{L=Le} c_a \, a_s \Delta L \tag{3.10}$$

where ΔL is the incremental length of pile. In the computation of frictional force, the upper portion of the pile for an embedded length equal to four times the diameter of pile is ignored as recommended by FEMA 356 (2000). A constant adhesion in the pile shaft is considered remaining part of the pile shaft. The axial movement of pile versus the mobilised shaft skin frictional force mobilised is modelled by adopting the $t - z$ curve as recommended by API (2007). The values normalised $t - z$ curve as recommended by API (2007) for clay are shown in Table 3.2.

Table: 3.2 The value of $t - z$ curve recommended by API (2007) for clay soil

z/D	t/t_{max}
0.0016	0.30
0.0031	0.50
0.0057	0.75
0.0080	0.90
0.01	1.00
0.02	0.70 to 0.90
∞	0.70 to 0.90

3.4 Soil Pile Interaction in Laterally Loaded Piles

Heteny (1964) derived the differential equation taking it as a beam column element for laterally loaded pile with axial load. The derivation was based on the assumption that a bar on elastic foundation is subjected to a horizontal load and a pair of compressive forces acting at the centre of the gravity of the end cross section of the bar. The following differential equation is proposed by Prakash and Sharma (1990) for a laterally loaded pile assuming that the pile is a linearly elastic beam.

$$E_p I_p \frac{d^4y}{dx^4} + P_x \frac{d^2y}{dx^2} - p = 0 \tag{3.11}$$

The soil reaction per unit length in Equation (3.11) is expressed as $p = ky$. This differential equation can be solved by classical method of the beam theory or by finite difference formulation. Further, the solution of Equation (3.11) can also be obtained if the soil modulus k can be expressed as a function of x, the point on the pile along its depth and y, the lateral deflection of pile. The numerical description of the soil modulus is accomplished by a family of curves that show soil reaction p as a function of deflection y (Reese and Welch, 1975). From this analysis, the information on the initial slope in the plot of p *vs* y and the magnitude of ultimate soil resistance p_u that develops with relative large deflection of pile are gathered, leading to the concept of $p - y$ presented as shown in Fig. 3.4. These curves as shown in Fig. 3.4 have the following assumed characteristics:

1. A set of $p - y$ curves represent the lateral deformation of soil under the horizontally applied pressure on a discrete vertical segment of pile at any depth.
2. The curve is independent of the shape and stiffness of the pile and is not affected by loading above or below the discrete vertical segment of soil at that depth. While the assumption is not strictly true, Reese (1977) stated that the experimental results indicates that the assumption is sufficiently accurate for practical purpose

Thus, from this stated concept, the soil can be replaced by a numerical model represented by discrete $p - y$ characteristics as shown in Fig. 3.4. A series of $p - y$ curves would represent the deformation of soil with depth for a range of lateral pressure varying from zero to the yield strength of soil.

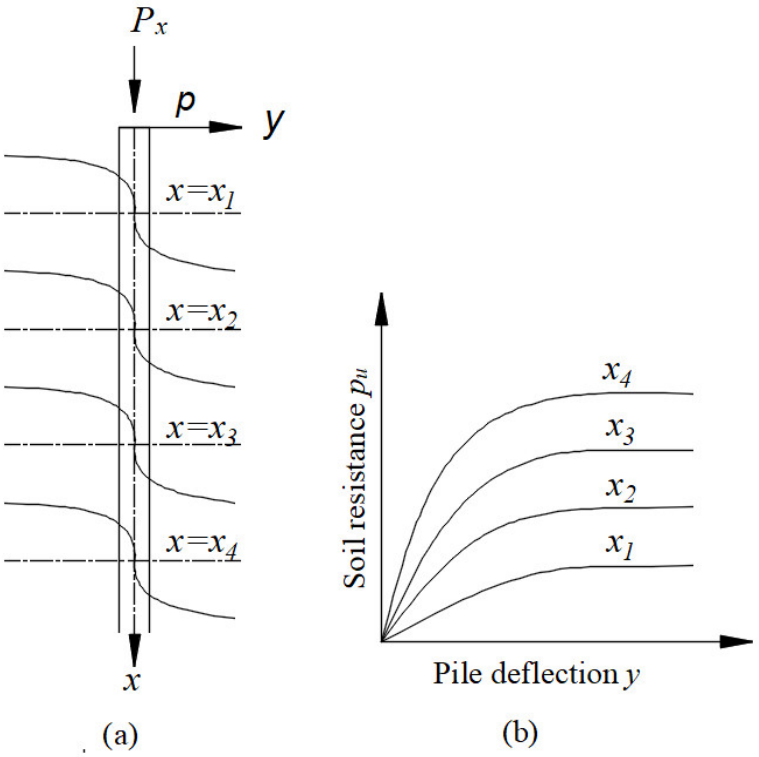

Fig. 3.4 (a) Shape of $p-y$ curves at various depth x below the ground surface, (b)Typical $p-y$ plot (Prakash and Sharma, 1990).

3.4.1 Lateral Soil Resistance for Pile in Sand

The lateral resistance of soil to pile deflection was derived by Reese (1962) in which pile was idealized as rigid cylinder moving laterally in a cohesionless soil. The cylinder was considered to be translating into the soil without rotation and the resulting resisting forces were computed. In the formulation of relation for the lateral resistance of soil, two failure models were considered. The assumed first model of failure is shown in Fig. 3.5. The first model is related to the resistance near the ground surface, considers a passive wedge failure, while the second model consider the resistance of soil at some depth below the ground level, assuming a flow failure of soil around the pile. In the first model considering the passive wedge model of failure, the computation of lateral resistance of soil near the ground surface

to the deflection of pile was carried out considering the geometry of passive wedge as shown in Fig 3.5.

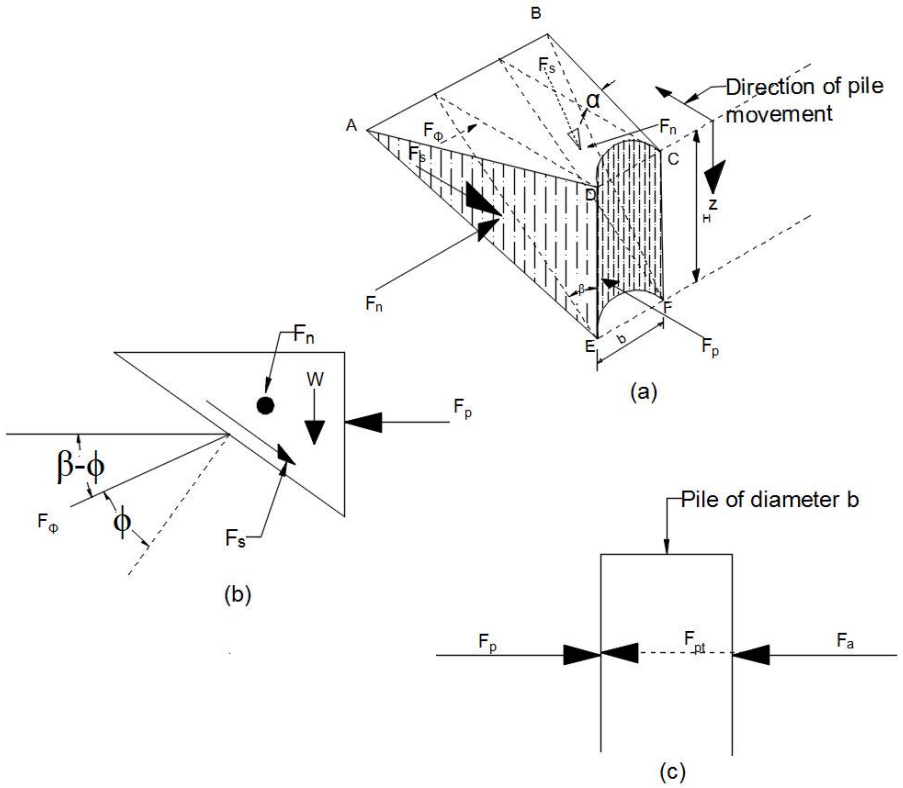

Fig. 3.5 Assumed Passive Wedge type failure of a pile in sand (a) general shape of wedge, (b) forces on wedge, (c) forces on pile (Reese et al. 2006)

The total ultimate lateral resistance F_{pt} of the pile is equal to the passive force F_p minus the active force F_a. The active force F_a was computed using Rankine's theory, using minimum coefficient of active earth pressure and the passive force F_p was computed from the geometry assuming the Mohr-Coulomb failure was satisfied in planes ADE, BCE and ABFE. It was assumed that there is no frictional resistance on the base of the pile and therefore there was no tangential force on the surface CDEF. Computing the forces in the sides of passive wedge the ultimate soil

resistance near the ground surface per unit length of the pile was derived as (Reese et al. 1974):

$$P_{us} = \gamma H \left[\frac{K_0 H \tan \emptyset \sin \beta}{\tan(\beta - \emptyset) \cos \alpha_s} + \frac{\tan \beta}{\tan(\beta - \emptyset)} + (D + H \tan \beta \tan \alpha_s) + K_0 H \tan \beta (\tan \emptyset \sin \beta - \tan \alpha_s) - K_a D \right] \quad (3.12)$$

The value of α_s is taken between $\phi/3$ to $\phi/2$ for loose sand and up to $\emptyset$ for dense sand. The value of β is taken as $45 + \frac{\phi}{2}$. The coefficient of passive pressure and active pressure is calculated from Rankine's theory as

$$K_p = \tan^2\left(45 + \frac{\phi}{2}\right) \quad (3.13)$$

$$K_a = \tan^2\left(45 - \frac{\phi}{2}\right) \quad (3.14)$$

In the second model, it is assumed that the failure at some depth below the ground is due to the mechanism of flow failure. The soil is assumed to move horizontally around the pile rather than move outward or upward (Reese 1962). Fig. 3.6 shows a section of pile subjected to lateral movement and the crosshatched area is used for the analysis. Assuming the mechanism of flow failure in the free body diagram of blocks shown in Fig. 3.6, block 1 fails by shearing, block 2 fails by shearing, block 3 keeps shape but gets displaced relative to pile and block 4 and block 5 fail in shearing. Under this state of stress, the ultimate soil resistance for the horizontal movement of the soil is given as (Reese et al. 2006):

$$p_{ud} = K_a \gamma D H (\tan^8 \beta - 1) + K_0 D \gamma H \tan \phi \tan^4 \beta \quad (3.15)$$

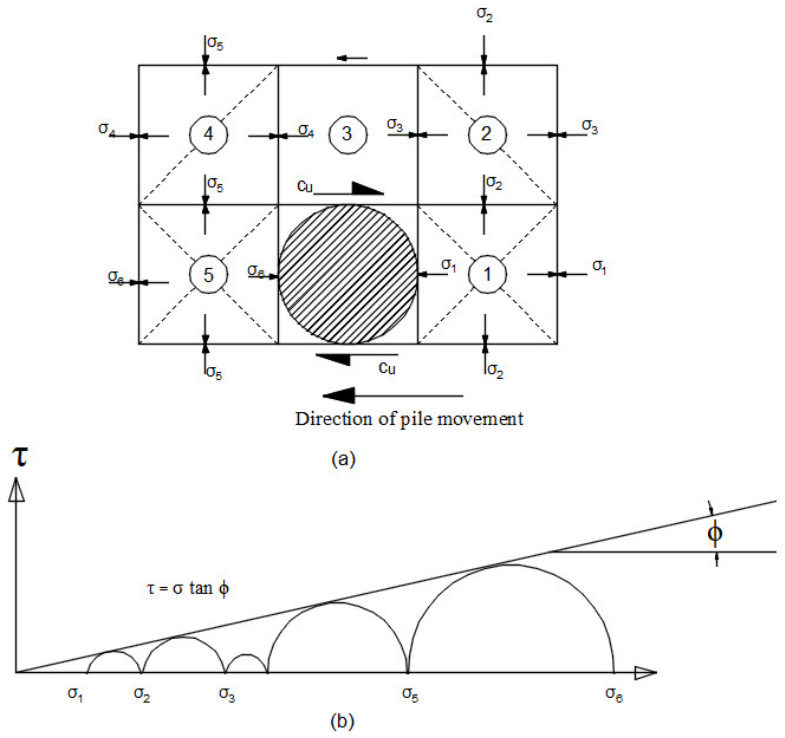

Fig. 3.6 Assumed model of soil failure by lateral flow around a pile in sand: (a) section through the pile, (b) Mohr-Coulomb diagram (Reese et al. 2006)

Bogard and Matlock (1980) modified some terms of the Reese's formulation resulting in the simplification of Reese's method. The ultimate soil resistance is calculated by grouping terms to form constant, which vary with ϕ . The equation for calculation of ultimate resistance of soil at depth z for a pile of diameter D is derived by Bogard and Matlock (1980) as

$$P_{us} = (C_1 \times z + C_2 \times D)\gamma z \tag{3.16}$$

$$P_{ud} = (C_3 \times D)\gamma z \tag{3.17}$$

The value of coefficient C_1, C_2, C_3 can be determined from the relations (O'Neill and Murchison 1983) as

$$C_1 = \frac{K_0 \tan \emptyset \sin \beta}{\tan(\beta - \emptyset)\cos \alpha} + \frac{\tan^2 \beta \tan \alpha}{\tan(\beta - \emptyset)} + K_0 \tan \beta \ (\tan \emptyset \sin \beta - \tan \alpha) \tag{3.18}$$

$$C_2 = \frac{\tan\beta}{\tan(\beta - \emptyset)} - \tan^2(45 - \alpha) \tag{3.19}$$

$$C_3 = 0.4\tan\emptyset\tan^4\beta + \tan^2(45 - \alpha)(\tan^8(\beta - 1) \tag{3.20}$$

and $$\alpha = \frac{\emptyset}{2}, \quad \beta = 45 + \frac{\emptyset}{2} \tag{3.21}$$

3.4.1.1 Formulation of $p - y$ Curve for Sand

Parker and Reese (1970) conducted test on 2-inch diameter and 104-inch length pipe pile under axial load and 2-inch diameter and 92-inch length pipe pile under lateral load. Both the tests were conducted in sand bed. In the installation process the sand was placed around the test pile. The test was conducted under static load only. The comparison between measured and theoretically defined curves of soil resistance versus lateral deflection of pile indicated that two straight line was fairly good approximation to represent the behavior test pile under lateral loading. Considering this approximate representation of results, a relationship has been developed for transition between the two straight lines to allow the curve to be described analytically as continuous function without greatly altering the values of the curve. Taking inference from the hyperbolic stress-strain curve of soil transition type hyperbolic equation has been developed as (Parker and Reese, 1970):

$$p = p_u \times \tanh\left[\frac{k_s \times y}{p_u}\right] \tag{3.22}$$

The value of the ultimate lateral resistance of the sand was calculated from the Equations (3.12 and (3.15) proposed by Reese (1962). The $p - y$ curve computed using Equation (3.22) which was developed based on the results of test on 2-inch pile was found to be in good agreement with the field test of other three sites conducted by other researchers (Parker and Reese, 1970).

Reese et al. (1974) presented formulation of $p - y$ for sand based on the field test performed at Mustang Island, Texas in 1967. Pipe piles of diameter 24.0 inch and 69 feet length were loaded laterally in a medium dense sand. The applied lateral load was both monotonic and cyclic. A mathematical expression for $p - y$ curve was formulated by Reese (1974) so that the predicted pile movement and deflection would match measured values. The curves presented by Reese consisted of 3 segments comprising of two straight lines with a parabola in between as shown in Fig.3.7.

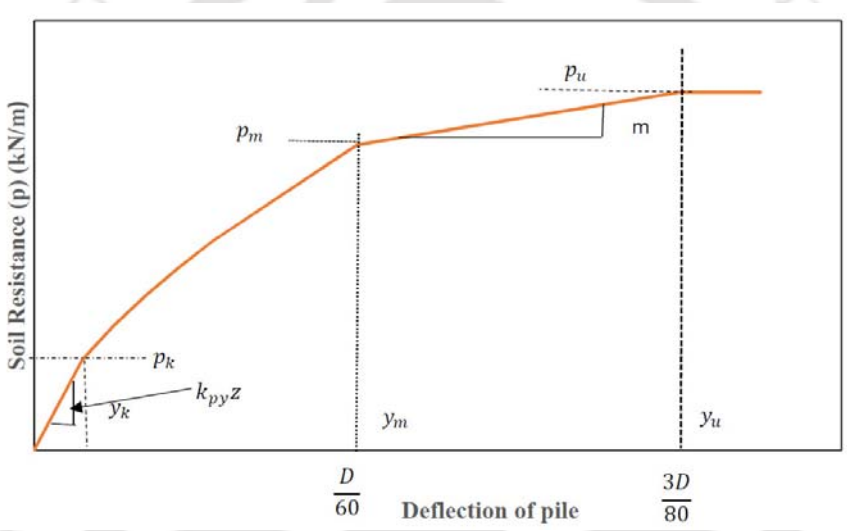

Fig. 3.7 Characteristics of $p - y$ curve for static and cyclic loading in Sand (Reese, 1974)

The ultimate soil resistance is determined by taking the minimum value computed from Equation (3.12) and Equation (3.15). Empirical factors are used to modify the ultimate resistance p_u for static and cyclic loading. The value p_m as shown in Fig. 3.7 is expressed percentage of p_u while the value of y_m and y_u are expressed in ratios of pile diameter. The point (y_k, p_k) is determined from an empirical relation involving y_m, y_u, p_m and p_u. The initial slope of the curve is related to the

coefficient of subgrade modulus. The formulation was the recommended one in API prior to its 20th Edition.

O'Neill and Murchison (1983) compiled the data of fourteen field tests of laterally loaded pile where the soil condition differed, and the load included static and cyclic loading. All of these test piles were analyzed using the four $p - y$ criteria: (1) by segmented method by Reese et al. (1974), (2) A modification of the method by Reese et al. (1974) in which simplified expression of p_u given by Bogard and Matlock, (1980) were used (3) Bilinear method proposed by Scott (1980) and (4) Continuous hyperbolic tangent curve proposed by Parker and Reese (1970). A comparison of different criteria was done, which were then evaluated individually. The predicted versus measured pile head deflection, predicted versus measured maximum moment and the distance to maximum moment for the static and cyclic load cases for each site were evaluated. The error for each criterion was computed for each site for all the methods. The continuous hyperbolic method gave least error amongst all methods that have been formulated for cyclic load. The continuous hyperbolic method was also observed to have the best fit with the experimental results. Thus, the hyperbolic method is recommended in API (2007) with further simplification in the theoretical expression of lateral load resistance and correction factor for tapered and H shaped pile. The detailed recommendation of API (2007) for computation of $p - y$ relation based on the hyperbolic formulation is written as

$$p = A \times p_u \times \tanh\left[\frac{k \times H}{A \times p_u} \times y\right] \tag{3.23}$$

where A empirical adjustment factors for p_u are simplified as $A = 0.9$ for cyclic loading and $A = 33 - 0.8z/D \geq 0.9$ for static loading. The ultimate lateral resistance of the soil for the shallow depth location and deep location shall be computed from the simplified Equation (3.16) and (3.17) proposed by Bogard and

Matlock (1980). A comparison of the segmented $p-y$ curve formulated by Reese (1974) and the hyperbolic curve formulated by Parker and Reese (1970) which is further adopted by API 2007 for the soil of $\phi = 35^0$ and $k = 33930kN/m^3$ at depth of 12m below the ground level is shown in Fig. 3.8.

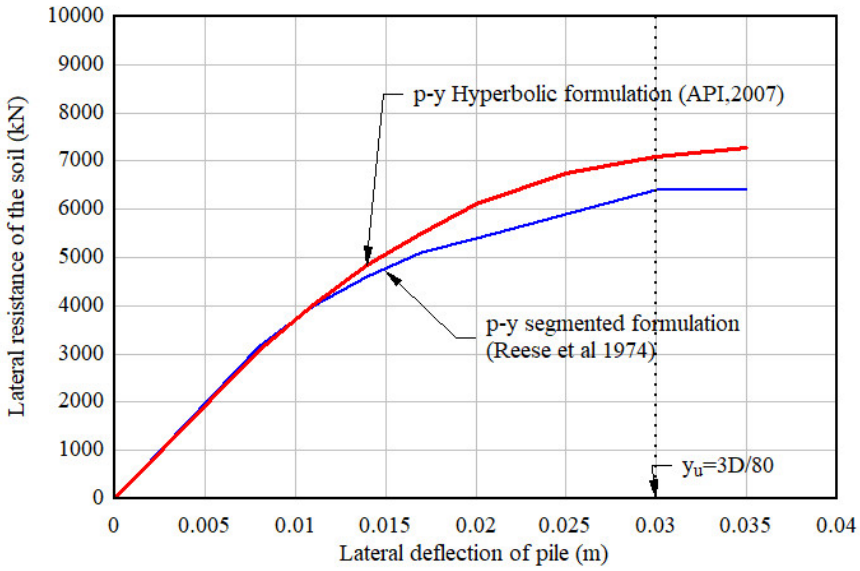

Fig. 3.8 Comparison of segmented $p-y$ curve (Reese (1974) and hyperbolic $p-y$ curve of API (2007)

The comparison of the curves indicates that both curves give the same initial stiffness of the soil and the segmental method gives a lesser resistance at higher displacement of pile. The hyperbolic formulation is found to provide the best fit with the experimental results (O'Neill and Murchison, 1983) and hence, the hyperbolic method as recommended by API (2007) is adopted in the calculation of $p-y$ curve for the sand following the Equation at (3.23) in this study.

3.4.2 Lateral Load Resistance for Piles in Soft Clay

The lateral resistance for soft clay is computed by assuming that the clay is confined so that plastic flow around the piles occurs only in the horizontal plane. The ultimate

lateral resistance per unit length of the pile diameter D under this condition is expressed as (Matlock, 1970):

$$P_u = N_p \times c \times D \tag{3.24}$$

The variation of the lateral resistance of the soft clay from the ground surface to the depth below the ground is accounted for by the variation of the value of non-dimensional coefficient of the ultimate resistance N_p. Matlock (1970) indicated that the consensus value of the coefficient (N_p) given by various investigators for soft clay soil flowing around the cylindrical pile at the considerable depth below the surface is 9. Near to the ground surface, the front soil will fail by shearing forward and the corresponding value of N_p reduces in the range of 2 to 4 depending on whether the pile segment is considered as a plate with only frontal resistance or square cross section with soil shear acting along the sides. For a cylindrical shape near the surface, a value of 3 is approximated for very near the surface (Matlock H., 1970) for estimating the lateral resistance of the soft clay. The coefficient of the lateral resistance of the soft clay should therefore be expected to vary from this proportionate value of 3 at near the surface to a maximum of 9 at depth X_R, which is termed as depth of reduced resistance. Within the upper zone, the resistance to vertical movement of clay is provided by an overburden pressure σ_x from the soil itself and by resistance developed by deformation within the surrounding soil mass. This resistance to vertical movement increases with distance from the free-soil surface. The following relation was given for the variation of non-dimensional coefficient of ultimate lateral resistance by Matlock, (1970) as

$$N_p = 3 + \frac{\sigma_z}{c} + J\frac{z}{D} \tag{3.25}$$

In the Equation (3.25), J is a constant coefficient. Matlock (1970) stated that first term of Equation (3.25) expresses the resistance at the free surface, second term

gives increase in resistance with depth due to overburden pressure, and the third term provides geometric related restrain that even a weightless soil around the pile provides against upward flow. The value of $J = 0.5$ was suggested by Matlock (1970) based on the Sabine test. The value of the depth at which the value of N_p becomes equal to the maximum value of 9 is given as

$$X_R = \frac{6D}{\frac{\gamma D}{c} + J} \tag{3.26}$$

3.4.2.1 Formulation of $p - y$ for Soft Clay

Matlock (1970), based on the field test followed by laboratory test of pile made the following observations as a basis for the formulation of the $p - y$ curve for soft clay which is reproduced for complete understanding of the background of the $p - y$ relation provided by him.

1. Resistance deflection $(p - y)$ characteristic of the soils is highly nonlinear and inelastic.
2. Within the practical range, the fundamental resistance-deflection characteristics of the soil appear to be independent of degree of pile head restraint.
3. A principal effect of the cyclic loading appears to be the permanent displacement of the soil away from the pile in the direction of loading.
4. Permanent displacement of soil created a slack zone in the resistance-deflection characteristics. On reloading the pile with forces lesser than that previously attained value, greater bending moment was observed as compared to the bending moment obtained with similar loading during initial cyclic loading, indicating effect of slack zone.

5. Although significant changes occurred with the continued repetition of load cycle, at any given magnitude of lateral load (except the highest) the behaviour of the pile soil system tended to be stabilized. Such equilibrium response was usually attained to a practical degree in less than 100 cycles.

It was also observed by Matlock (1970) that subsequent deposition of clay or slurry in the cavity formed due to permanent displacement under cyclic loading is not followed by any significant gains in strength, unless it is filled with granular materials. Matlock (1970) gave the formulation for the $p-y$ curve based on his study and observation on field test. The Sabine Test is stated to be the prime basis for the formulation of the $p-y$ for soft clay. The $p-y$ curve given by Matlock (1970) for soft clay is given in Fig.3.9

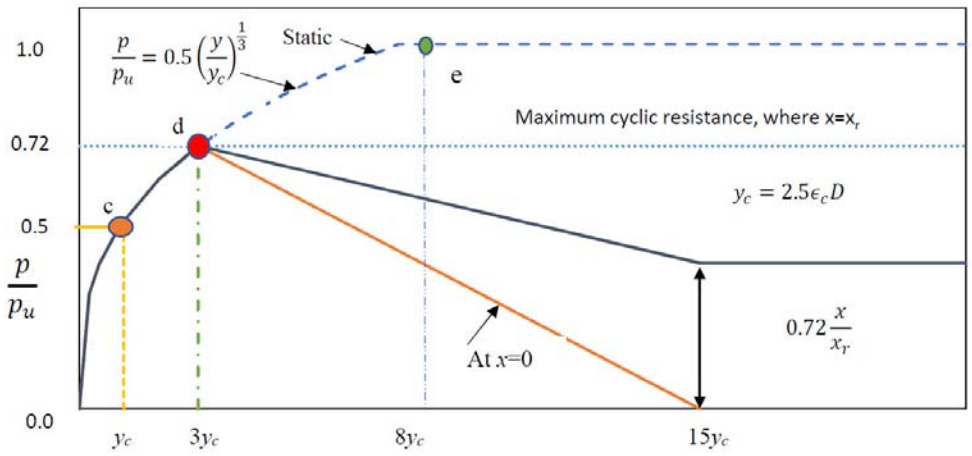

Fig.3.9 $p-y$ curve for soft clay (Matlock 1970)

API (2007) prescribed the procedure for computation of $p-y$ curve in the line with formulation by Matlock (1970). For static lateral load, API (2007) provides a variation of ultimate lateral load between $8c$ to $12c$ except in shallow depth where failure occurs in different modes due to minimum overburden pressure. API (2007) also recommends a range of lateral bearing capacity of the soil from $3c$ to $9c$ to

take into account for determination in the lateral bearing capacity below static load level under cyclic loading. The lateral load bearing capacity for $p-y$ curve for soft clay is recommended to be computed from Equations (3.27) and (3.28) as

$$P_u = 3c + \gamma X + J\frac{cX}{D} \tag{3.27}$$

and

$$P_u = 9c \quad \text{for X} \geq X_R \tag{3.28}$$

The value of c is taken as the undrained shear strength of undisturbed clay and the value of dimensionless empirical constant J is taken in ranges of 0.25 to 0.5. The X_R is the depth below soil surface to the bottom of reduced resistance zone in metre which is defined in Equation (3.29) as

$$X_R = \frac{6D}{\frac{\gamma D}{c} + J} \tag{3.29}$$

API (2007) also states that the lateral soil resistance-deflection relationship for pile is generally nonlinear. For the case where the equilibrium has been reached under cyclic loading, the $p-y$ curve is recommended to be generated from the Table:3.3

Table:3.3 The value of $p-y$ relation for soft clay under cyclic loading

$X > X_R$		$X < X_R$	
P/P_U	y/y_c	P/P_U	y/y_c
0.00	0.0	0.00	0.0
0.23	0.1	0.23	0.1
0.33	0.3	0.00	0.3
0.5	1.0	0.5	1.0
0.72	3.0	0.72	3.0
0.72	∞	$0.72X/X_R$	15.0
		$0.72X/X_R$	∞

The value of y_c is calculated using ϵ_c which is ts the strain which occurs at one half of the maximum stress on laboratory unconsolidated undrained compression

test of undisturbed soil sample. The tabulated data of $p - y$ curve as recommended by API as shown in Table 3.3 is adopted in the present study in modelling of soil structure interaction of pile under lateral loading since these recommendations are based on the formulation by Matlock (1970)

3.4.3 Lateral Load Resistance for Piles in Stiff Clay

Two models are used for computing the ultimate lateral load resistance of stiff clay. The first model assumes that the stiff clay is likely to move up and down and eventually coming out of the ground surface and the second model takes over below the first and assumes the horizontal movement of stiff clay (Reese et al. 2006). The resistance of the stiff clay in the first model is computed by assuming a passive wedge failure sliding in front of the cylinder translating into the soil without rotation as shown in the Fig. 3.10.

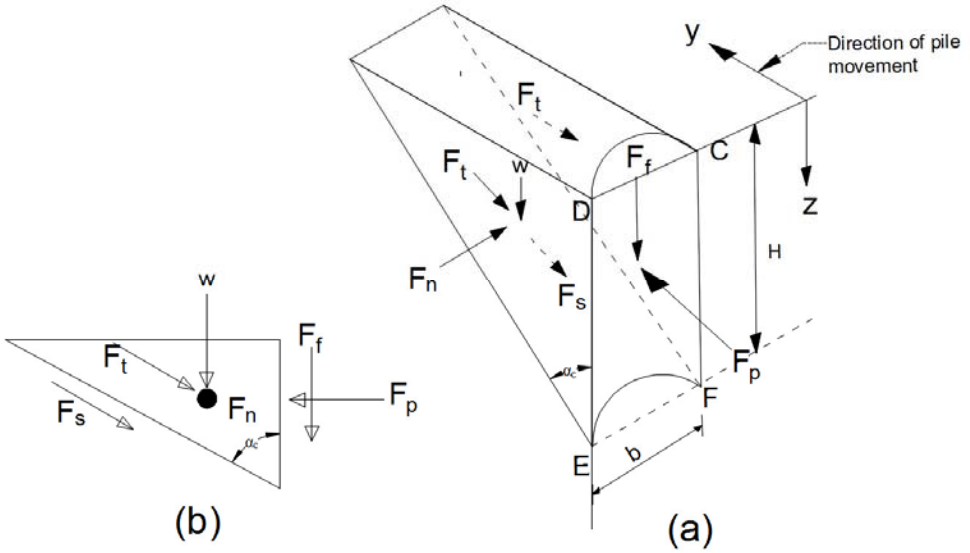

Fig. 3.10 Assumed passive wedge type of failure for clay (a) Shape of wedge (b) force acting on wedge (Reese et al. 2006).

In the derivation of the ultimate resistance of clay to pile deflection, the shear strength of the clay is assumed as constant over depth H. The vertical force in the interface between the upward moving soil and the pile is assumed to be zero. Considering the weight of the wedge and taking sliding force F_s and F_t into account the lateral resistance of clay F_p has been calculated. Further, differentiating F_p with respect to cylinder height H and solving for p_{u1}, the relation for ultimate resistance near the surface is derived by Reese et al. (2006) as

$$P_{uc1} = c_a D[\tan\alpha_c + (1+\kappa)\cot\alpha_c] + \gamma DH + 2c_a H(\tan\alpha_c \sin\alpha_c + \cos\alpha_c) \tag{3.30}$$

The value of c_a is taken as average undrained shear strength in Equation (3.30). The reduction factor for the shearing resistance along the face of the pile κ is set equal to zero since undrained shear strength is assumed to be fully developed which is logical for case of cyclic loading and, and α_c is set at 45^0, then Equation (3.30) reduces to

$$P_{uc1} = 2c_a D + \gamma' Dz + 2.83c_a z \tag{3.31}$$

The second model adopted for computing ultimate resistance p_{uc2} is shown in Fig. 3.11 (Reese et al. 2006) indicating horizontal movement of the pile. At some point below the ground level maximum resistance to soil moving horizontally encountered. Considering that the Block 5 moves laterally, a stress of sufficient magnitude is generated in that block to cause failure. The stress is transmitted to Block 4 and finally to Block 1 with assumed movement indicated by the dotted lines. Block 3 is assumed to have not distorted, but failure stress develops on the side of the block as it slides.

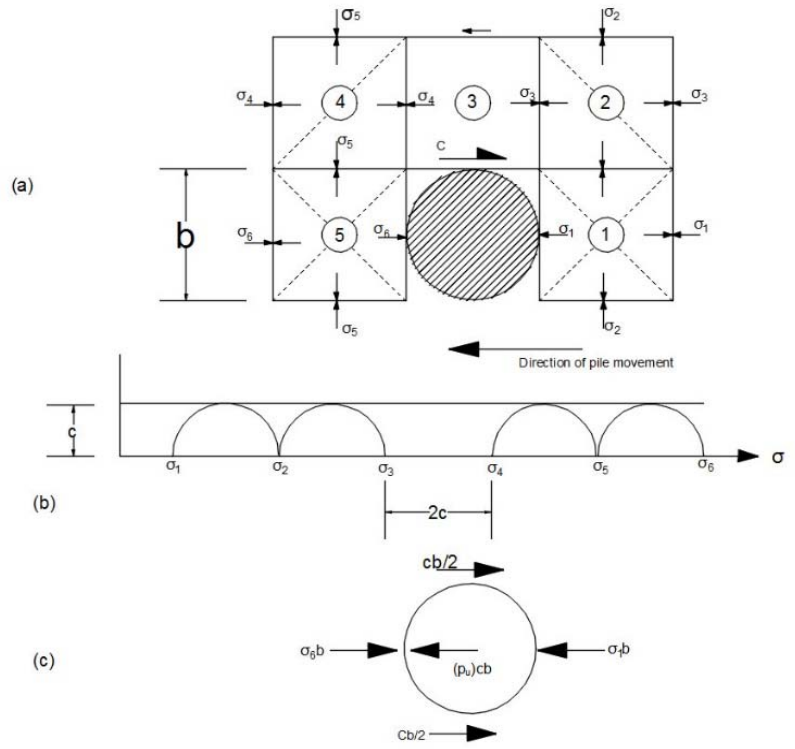

Fig.3.11 Assumed soil failure by lateral flow around a pile in clay; (a) Section through pile; (b) Mohr-column Diagram; (c) Force acting on a section of pile (Reese et al. 2006)

Considering the Mohr-coulomb diagram in shown in Fig.3.11(b) and free body diagram shown in Fig. 3.11(c), it has been assumed that the ultimate resistance p_{uc2} as independent of σ_1 because the difference in the stress on the front of σ_6 and back of σ_1 is equal to $10c$. The shape of cross section of pile was also considered to have some influence in the magnitude of p_{cu2}. It was assumed that the resistance developed on each side of the pile is equal to $cD/2$ the relation for ultimate resistance for flow failure is given as (Reese et al. 2006):

$$p_{uc2} = \big((\sigma_6 - \sigma_1) + c\big)b = 11cb \tag{3.32}$$

The ultimate lateral resistance of the stiff clay is computed from Equation (3.31) and (3.32) is adopted in the generation of $p - y$ curve of stiff clay.

3.4.3.1 Formulation of $p - y$ curve for stiff Clay

Reese et al. (1975) performed lateral load tests with steel pipes that were 641mm (24 in.) in diameter and embedded for a depth of 15.2m (50 ft) long. The piles were driven into stiff clay at a site near Manor, Texas. Static and cyclic load tests were conducted in the presence of free water. The $p - y$ curve was derived for static and cyclic load test on the piles. It was observed that there was an excellent agreement between the experimental and computed results. Based on the characteristics of $p - y$ curve from the results of test under static and cyclic loading, the following observation were made by Reese et al. (1975).

1. In the $p - y$ curves, initial slope and ultimate resistance increases with the increase in depth.
2. Comparison of $p - y$ curve for short term static loading with the $p - y$ curve for the cyclic loading shows that the soil resistance decreases as a result of cyclic loading.
3. For any particular depth, the initial slope of $p - y$ curve is relatively steep. At a particular deflection, the ultimate soil resistance is developed and beyond this point there is a reduction in soil resistance with continued deflection.
4. The $p - y$ curve from cyclic loading test shows that the shape of initial part is similar to that of curve obtained for static loading. The value of ultimate resistance for cyclic curves are significantly lesser than the values for static counterparts. Further, for curves under cyclic load, ultimate resistance was obtained with lesser deflection than the curves under static load.

The characteristic shape of $p - y$ curve proposed for cyclic loading in presence of free water is shown in Fig.3.12

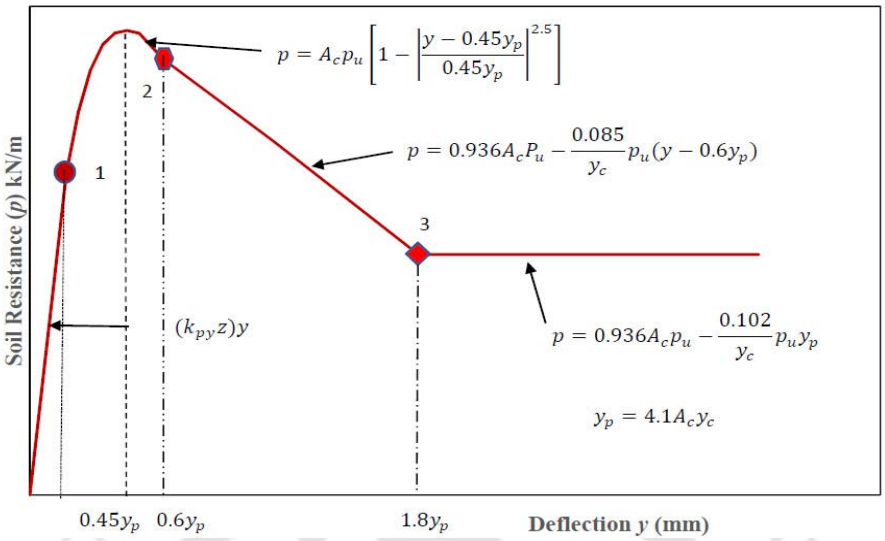

Fig. 3.12 Characteristic of $p - y$ curve for cyclic loading in stiff clay in the presence of free water (Reese et al. 1975)

As shown in Fig 3.12 the $p - y$ curve for cyclic loading consists of an initial straight-line portion from origin to point 1, a parabolic section from point 1 to point 2 and a straight line from point 2 to point 3 and a horizontal line from point 3. Further, it has also been observed that the computed lateral load resistance from Equation (3.31) and (3.32) are higher than the values obtained experimentally. This has been adjusted adopting an empirical factor A_s for static loading and A_c for cyclic loading which is computed from the ratio of experimental ultimate lateral load resistance to computed ultimate lateral load resistance. The $p - y$ curve formulated by Reese et al. (1975) for cyclic loading has been adopted in modelling the lateral soil structure interaction of pile in stiff clay in present study.

3.5 Group Effect on $p - y$ Curve

The group effect in lateral capacity of the pile shows softening of the lateral stiffness of the piles. Full size and model test by numerous researchers show that in general the lateral capacity of pile in a pile group versus that of a single pile is reduced as

the pile spacing is reduced (Lam et al. 1998). The group effect in the $p - y$ curve is accounted for by adopting a *p*-multiplier which modifies the lateral soil resistance at various depth for taking the group effect in the model. The *p*-multiplier suggested by various researchers are given in Table: 3.4.

Table: 3.4 Value of cycle 1 *p*-multiplier from various experiment on 3x3 pile group with centre to centre spacing equal to $3D$ (Lam et al. 1998)

Pile Test, soil description, References	p-multiplier on single pile $p - y$ curve		
	Front row	Middle row	Back row
Free-Head, Medium dense sand, relative density Dr = 50% Brown et al. (1998)	0.8	0.4	0.3
Fixed-Head, Medium dense sand, Dr = 55% McVay (1995)	0.8	0.46	0.3
Free-Head, Soft to Medium Clay and Silt, Rollins et al. (1997)	0.60	0.38	0.45

Lam and Martin (1986) also observed that the group effect that was estimated from the theoretical consideration of elastic continuum did not account for the fact that more rigid members are present in the soil medium in the presence of pile group that would act as reinforcing element in the soil mass. Furthermore, the elastic continuum also could not account for the compaction of soil mass caused by pile driving process around the piles in the group. The compaction of soil medium during the piling process was observed to be significant for sandy soils for piles with closer spacing. Considering these facts Lam et al. (1998) suggested that *p*-multiplier factor of 0.5 that might represent the average adjustment factor to develop average condition to fit the overall group effect. Such simplification has been suggested for practical design considering the cyclic earthquake loading condition. This is because, the front pile row will become the rear pile row when

the loading is reversed, making it difficult to maintain a different p-multiplier specific to the row.

3.6 Calculation of Linear Stiffness of Soil

To carry out free vibration analysis of the bridge linear properties of the soil like modulus of elasticity of soil and elastic modulus of horizontal reaction for the soil are modelled. The modulus of the horizontal reaction for the sand has been modelled as recommended by Tarzaghi (1955). The magnitude of support spring constant is assumed to be independent of the pile diameter and varies linearly with depth (Lam and Martin,1986) as

$$k_s = k_1 z \tag{3.33}$$

In Equation (3.33), k_s is taken as stiffness support spring in force per unit length per unit deflection. The value of k_1, the coefficient of subgrade modulus can be computed based on either density or internal angle of friction of soil and z is the depth from the grade level. The value of k_1 are adopted from the initial tangent modulus value recommended by Reese (1974) (Lam and Martin, 1986).

Lam and Martin (1986) suggested that in case of clay, the equivalent linear spring constant to account for the soil support on piles can be developed based on the nonlinear $p - y$ procedure for soft clay. This recommendation was based on the consideration that under normal design load levels, the pile response is largely affected by the support characteristics at shallow depth. Therefore, the deep seated horizontal plastic flow failure mechanism can be ignored. The equation to calculate the ultimate resistance for the shallower failure mechanism given by Matlock (1970) can be used to develop a further simplified linear procedure. Further, the secant stiffness at one-half of peak load level on $p - y$ curve can be used to develop the equivalent linear stiffness. With these consideration, the equivalent linear secant

stiffness of clay is calculated as per the relation proposed by Lam and Martin (1986) for analysis of piles in clay as

$$k_s = k_0 + k_1 z \tag{3.34}$$

The initial value of stiffness of clay k_0 is calculated from the relation

$$k_0 = \frac{0.6c}{\varepsilon_c} \tag{3.35}$$

The coefficient of modulus of subgrade reaction for clay is calculated from relation

$$k_1 = \frac{0.2}{\epsilon_c} + \left(\gamma + \frac{Jc}{D}\right) \tag{3.36}$$

The value of c is taken as the undrained shear strength of the clay. The value of ϵ_c in recommended as 0.01 in absence of laboratory data (Lam and Martin, 1986)

3.7 Modelling of Far Field Soil Effect

The approach with the *p-y* curve for dynamic analysis of pile foundation is further extended by adding dashpot in series in order to account for radiation damping of soil. The soil around the pile and in the zone of strong nonlinear response called as near field soil, modelling of soil response is carried out with nonlinear $(p - y)$ curve which accounts for the nonlinear behaviour of the soil. The soil in vicinity of the pile but away from the zone of strong nonlinear behaviour called as far field soil, responds elastically to the lateral forces generated by the pile. This far field soil effects are modelled with elastic element. The arrangement enables the model to logically reproduce the nonlinear effect in the dynamic response by transferring the motion through the areas of strong nonlinear behaviour to the far field linear behaviour. In the nonlinear zone, the energy dissipation is achieved through the hysteretic behaviour of the soil and in the far field area the energy is dissipated through radiation damping. The far field reaction in each layer of soil are modelled by a set of springs and dashpots representing the dynamic stiffness and damping

properties of far field soil. The overall dashpot representing damping of far field soil consist of two dashpots. One related to the radiation damping denoted as c_r that representing the radiation of energy per unit length of pile by waves spreading geometrically away from the pile soil interface. The other dashpot denoted as c_m , simulating the material dissipation of energy per unit length of pile. Therefore, the total damping coefficient per unit length of pile is the sum of both the radiation and material damping and can be represented as

$$c_x = c_r + c_m \tag{3.39}$$

The computation of radiation damping is done based on formulation given by various researchers with the 1-D and 2-D idealization of wave propagation problem. In the one-dimensional radiation damping the damping coefficient is computed by considering analogy between the one-dimensional wave propagation in a space or cylinder of infinite length and a viscous dashpot as schematically shown in Fig. 3.13.

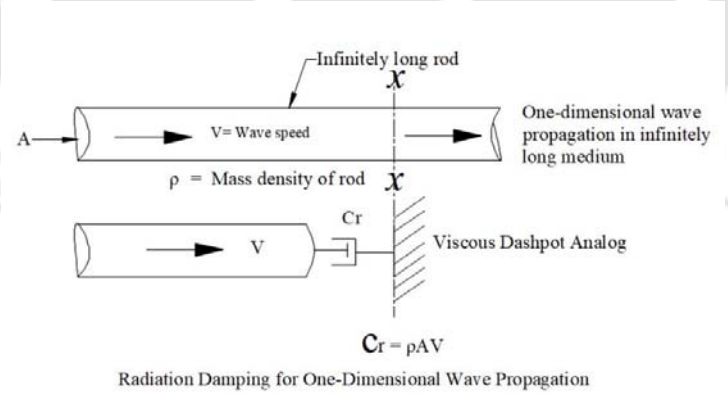

Fig. 3.13 One Dimensional model of wave propagation (Gazetas and Dobry, 1984a)

Considering a harmonic (P or S) wave form as

$$u = u_0 . exp\left[i\omega\left(t - \frac{x}{V}\right)\right] \tag{3.38}$$

where u_0 is the wave amplitude ω is the circular frequency, t is the time and V is the corresponding wave velocity (V_p or V_s).

The total force induced by the wave on a perpendicular area surface A at location of $x - x$ can be expressed as:

$$F = \rho V A_r \dot{u} \tag{3.39}$$

Therefore, the semi-infinite portion of the space or the cylinder located at the right of x can be replaced by a viscous dashpot having a constant coefficient which is defined as coefficient of radiation damping as (Gazetas and Dobry, 1984a)

$$c_r = \rho V A_r \tag{3.40}$$

Berger et al (1977) adopted the 1-D analogy to estimate radiation damping coefficient along a laterally oscillating laterally pile. It was assumed that the horizontally moving pile section with effective width $b = 2r_0$ would solely generate 1-D P-wave traveling in the direction of shaking and SH-wave travelling in the direction perpendicular to the direction of shaking as shown in Fig. 3.14.

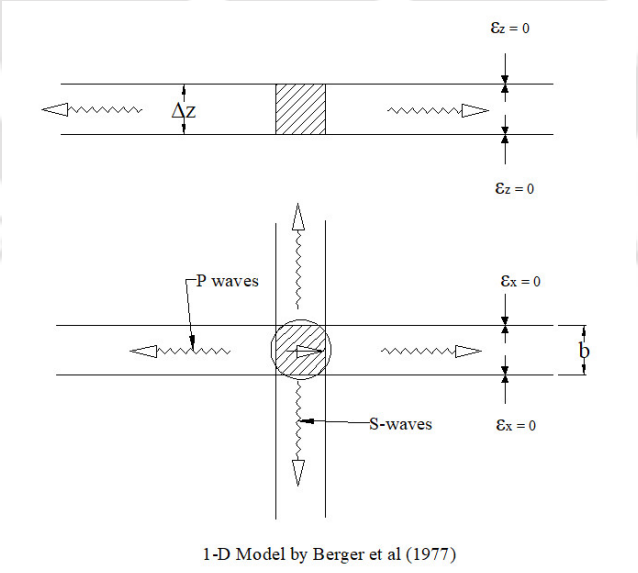

Fig. 3.14 One Dimensional model of wave propagation (Berger et al. 1977)

Thus, using this analogy, a relation has been proposed to compute of constant coefficient of viscous dashpot which will fully absorb the energy of all waves originating at the pile soil interface as

$$c_r = 4r_0\rho_s V_s\left[1 + \frac{V_P}{V_s}\right] \tag{3.41}$$

The V_p and V_s in the Equation (3.41) stand for P-waves and S-waves velocities of the soil at depth of the interest. The V_p and V_s are related through the poison's ratio ν of soil as

$$V_p = V_s\left[\frac{2(1-\nu)}{(1-2\nu)}\right] \tag{3.42}$$

Gazetas and Dobry (1984) developed a plain strain model for computation of radiation damping coefficient. In this approach, a plain strain model has been approximated based on the assumption that compression and extension wave propagate in two quarter planes along the direction of loading, while the shear waves are generated in two quarter planes perpendicular to the direction of loading as shown in Fig. 3.15.

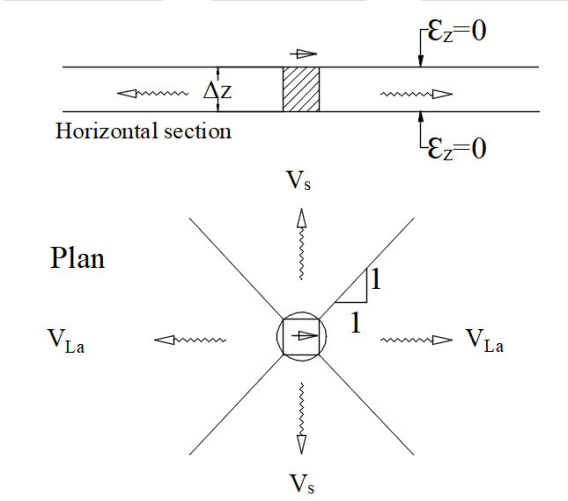

Fig. 3.15 Plain strain 2-D Wave propagation model (Gazetas and Dobry,1984)

Only horizontal shear deformation has been allowed within each quarter and all the straight line originally normal to the corresponding direction of waves has been assumed to remain normal during the oscillation. Each quarter plane has been assumed to vibrate independent of the other three quarters. The circular section of pile is replaced by square having same perimeter $2\pi r_0$. It is also assumed that the shear wave propagates with velocity V_s in two quarter planes and that compression and extension propagates in the other two quarter planes with Lysmers Analog Velocity V_{La} defined as

$$V_{La} = \frac{3.4V_s}{\pi(1-\nu)} \tag{3.43}$$

By adding up the energy radiated away in four quarter planes, the expression of radiation dashpot coefficient for circular cross section is obtained as

$$c_r = 4r_0\rho_s V_s \left\{1 + \left[\frac{3.4}{\pi(1-\nu)}\right]^{\frac{5}{4}}\right\} \left(\frac{\pi}{4}\right)^{3/4} a_0^{-1/4} \tag{3.44}$$

Where a_0 is non-dimensional frequency given by the relation, $a_0 = 2\pi f r_0/V_s$. To account for the material hysteretic damping, Gazetas and Dobry (1984) also observed that the relation for calculation of the material dashpot can be approximated as

$$c_m = 2k_{sec}\frac{\beta_s}{\omega} \tag{3.45}$$

where k_{sec} is secant lateral stiffness of pile, β_s is the hysteretic damping coefficient of soil and ω is the frequency of excitation. The hysteretic damping coefficient β_s for a given soil is the function of induced strain. Seed et al. (1984) suggested a correlation between the hysteretic damping coefficient of sandy soil and strain which could be adopted for the estimation of hysteretic damping coefficient. Similarly Seed and Idriss (1970), provided a correlation between strain

and the hysteretic damping coefficient β_s for the clay soil, which could be adopted for the estimation of hysteretic damping coefficient for clay soil.

Further, Gazetas and Dobry (1984) proposed that the value of the stiffness in lateral direction k_{sec} can be approximated as frequency independent and expressed as multiple of local soil Young's modulus E_s as

$$k_{sec} \cong k_L(z) = \delta E_s \tag{3.46}$$

The coefficient δ is independent of depth z. Selected value of δ is required to ensure that the top deflection of pile supported by independent elastic spring modulus $\delta E_s(z)$ per unit length is the same as true deflection of pile embedded in an elastic continuous with young's modulus $E_s(z)$. The value of δ suggested was in the range of 1 to 1.2 for fixed head pile by Gazetas and Dobry (1984). Therefore, the expression of the stiffness k_L at depth z is obtained as

$$k_L(z) = 1.2E_s(z) \tag{3.47}$$

Furthermore, the stress strain behaviour of the soil is nonlinear in nature as the elastic components are relatively smaller than the plastic strain component. The modulus of elasticity of the soil also vary with the confining pressure and the percentage of strength mobilised (Duncan et al. 1980). Konder et al. (1963) showed that the nonlinear stress strain curve for a soil could be approximated reasonably by hyperbolic the equation of the form

$$(\sigma_1 - \sigma_3) = \frac{\epsilon}{\frac{1}{E_i} + \frac{\varepsilon}{(\sigma_1 - \sigma_3)_{ult}}} \tag{3.48}$$

The parameters E_i is the initial tangent modulus of the stress strain curve, σ_1 and σ_3 are the major and minor principal stress respectively. The $(\sigma_1 - \sigma_3)_{ult}$ is the asymptotic value of the stress difference which is related to the strength of the soil.

Duncan et al. (1980) showed that the tangent modulus can be calculated using the relation as

$$E_t = \left[1 - \frac{R_f \sin\emptyset(\sigma_1 - \sigma_3)}{2c\cos\emptyset + 2\sigma_3 \sin\emptyset}\right]^2 KP_a \left(\frac{\sigma_3}{P_a}\right)^n \quad (3.49)$$

where R_f is the failure ratio with a value varying from 0.5 to 0.90 for most of the soil type, c is cohesion of soil, $\emptyset$ is frictional angle of the soil, the parameter K is the dimensionless modulus number, n is the dimensionless modulus exponent and P_a is atmospheric pressure introduced into the equation to make the conversion from one system of unit to another system. The P_a will have the same unit at that of E_t and σ_3.

The values of tangent modulus computed from Equation (3.49) is adopted as the modulus of elasticity of the soil in calculation of stiffness of pile which include the effect of confining pressure at various depths. The minor principal stress is computed as $\sigma_3 = K_0\sigma_1$, where value of K_0 is taken equal to $(1 - \sin\emptyset)$ for sand and $(0.95 - \sin\emptyset)$ for clay (Lambe and Whitman, 1963). The stiffness of the pile for far field soil can be finally calculated taking the tangent modulus of soil with confining effect as

$$k_L(z) = 1.2E_t \quad (3.50)$$

The shear modulus of the soil at various depths of the pile has been calculated using the relation as

$$G_S(z) = \frac{E_t\,(z)}{2(1+\nu)} \quad (3.51)$$

The value of shear wave velocity varying at various depth can be computed from the standard relation as

$$V_s(z) = \sqrt{\frac{G_s(z)}{\rho}} \tag{3.52}$$

Thus, the overall dashpot coefficient of the pile for far field per unit length of pile in lateral direction at depth z can be written as

$$C_L(z) = 2D\rho_s V_s \left\{1 + \left[\frac{3.4}{\pi(1-\nu)}\right]^{\frac{5}{4}}\right\} \left(\frac{\pi}{4}\right)^{\frac{3}{4}} a_0^{-\frac{1}{4}} + 2k_L(z)\frac{\beta_s}{\omega} \tag{3.53}$$

3.8 Abutment Backfill Interaction

In any bridge under normal operation, the backfill soil behind the abutment gets compacted by vibration caused by the traffic load and also gets consolidated because of the weight of the approach slab cast at the bridge approach. Further, in case of the IAB, because of cyclic loading on the backfill due to expansion and contraction of the bridge superstructure on account of the temperature changes, densification of the soil takes place. Therefore, backfill soil behind the bridge abutment is considered to be dense compacted sand, representing actual condition at site. No variation in properties of backfill soil is considered in this study. In addition, when abutment is displaced towards the backfill, additional supports are provided by the backfill behind the abutment. As the wall moved towards the backfill, passive pressure condition is developed and as the wall moves away from the backfill active earth pressure condition developed.

Clough and Duncan (1991) studied the relation between earth pressure and wall movement through experiment as well as using finite element analysis as shown in Fig. 3.16. From the result of the study it was observed that after a sufficiently large movement towards the backfill, limiting passive pressure is developed. If the movement towards the backfill is continued even after maximum pressure is reached, the passive earth pressure would remain constant. It was also concluded

that the same was true for active pressure generated when the wall moved away from the backfill.

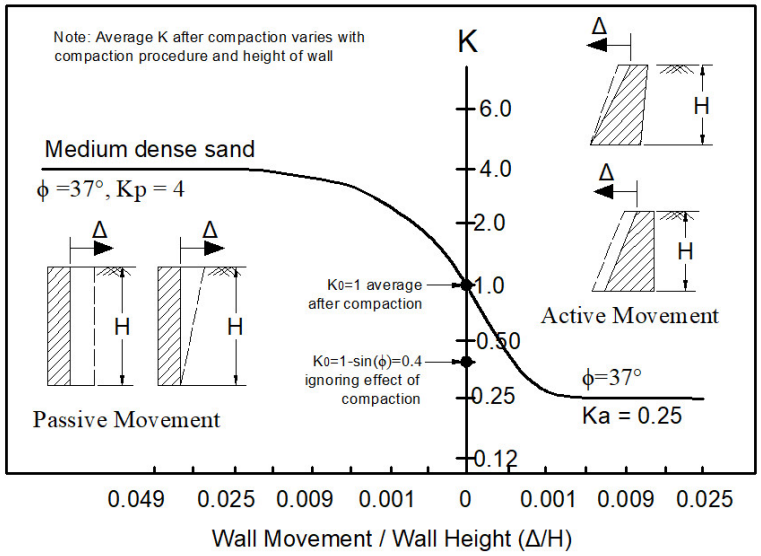

Fig. 3.16 Relationship between wall movement and passive pressure

England et al. (2000) carried out an experiment on influence of cyclic loading of on retaining wall simulating the thermal loading on the wall followed by theoretical investigation. The retaining wall detailed to simulate stiff concrete abutment wall pinned as base. Following the recommendation of England et al. (2000) a relationship between passive pressure and wall movement was adopted in BA 42 (2003). This relationship is expressed as

$$K^* = K_0 + \left[\frac{d}{0.03H}\right]^{0.6} K_p \tag{3.54}$$

Duncan and Makwa (2001) carried out analysis of the passive earth pressure on retaining structures using Log Spiral theory. In the analysis, the 3-D mechanism of failure was also taken in to account. The relationship between passive resistance and deflection was approximated by a hyperbolic relation as

$$p_p = \frac{y}{\left[\frac{1}{k_{max}} + R_f \frac{y}{p_{ult}}\right]} \tag{3.55}$$

The value of k_{max} is calculated using the elastic solution for horizontal displacement of uniformly loaded vertical rectangular area in the half space as proposed by Duglas and Devis (1964). In addition, an experimental study was also carried out in Virginia Polytechnic Institute to observe the relationship between the passive pressure and wall movement. The experimental study was conducted by applying lateral load on anchor block. The anchor block was bearing against natural soil in one set up while in another set up the block was bearing against dense crusher run backfill. A fairly good agreement between the theoretical and experimental results were observed.

University of Massachusetts Transportation Centre conducted study for evaluation of behavior of passive earth pressure behind IAB (Thompson and Lutenagger,1998). Passive loading test was conducted on rigid concrete wall to study the effect of wing wall orientation and lateral earth pressure developed in abutment wall. Based on the results of study a relation between wall movement and lateral passive pressure was proposed which is incorporated in the MassHighway Manual (2005) as

$$K^* = 0.43 + 5.7\left(1 - e^{-190\left(\frac{d}{H}\right)}\right) \tag{3.56}$$

Duncan and Makwa (2001) indicated that the computation of the passive earth pressure using Rankine's theory provides a very conservative value as the theory does not consider the wall soil interface friction. On the other hand, the Coulomb's theory provides erroneous value when the wall friction angle δ is more than 0.40 times the angle of internal friction ϕ of the backfill soil. The Logarithmic Spiral theory was found to be reasonable for accurate estimation of passive pressure

coefficient, when the wall friction angle is greater than 0.40. However, Equation (3.56) considers a constant coefficient of 5.7 for passive pressure, but it may vary as per the angle of internal friction, wall friction angle and the theory of earth pressure adopted. Further, Lemitzer et al. (2008) observed a high value of passive earth pressure coefficient from the full-scale test on abutment. These studies suggested that the passive earth pressure coefficient can be as high as 15.10 to 16.30. Therefore, the value of 5.7 is required to be replaced by coefficient of passive earth pressure that is variable with backfill soil properties. Hence, the modified relationship between the passive pressure and wall movement as recommended in MassHighway manual (2005) is adopted for this study. The modified relationship is expressed as

$$K^* = \mathrm{k_0} + \mathrm{K_p}\left(1 - e^{-190\left(\frac{d}{H}\right)}\right) \tag{3.57}$$

A comparison of coefficient of passive earth pressure from Equation (3.54) and (3.57) for 5.50m height of abutment taking $k_0 = 0.43$ and $k_p = 6.20$ is shown in Fig 3.17.

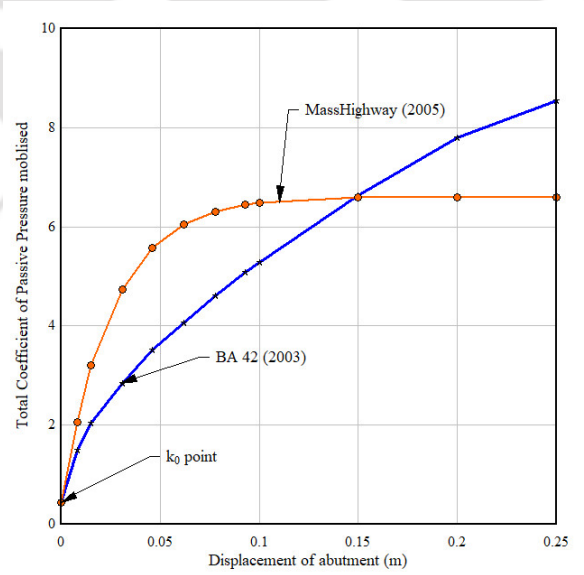

Fig. 3.17 Coefficient of passive pressure generated versus displacement of wall

As per the full-scale test by researchers, it is indicated that the maximum passive pressure shall be generated only if the wall is displaced to the range of value as given in Table 3.5.

Table 3.5 Maximum displacement required for full mobilization of passive pressure.

Type of soil	Maximum wall displacement required for mobilization maximum passive pressure		
	Clough and Duncan (1991)	Canadian Geotechnical Society (2006)	Rollins and Cole (2006)
Dense sand backfills	55mm	110mm	192mm

The comparative studies show that the maximum passive pressure expected from the Equation (3.57) as recommended in MassHighway manual (2005) is observed to be in agreement with the required displacement. However, expected passive pressure from Equation (3.54) recommended in BA42 (2003) is lower for lower displacement level and increases continuously with increase of displacement. This tendency of increasing passive pressure with increase in deflection contradicts observations from experimental results (Clough and Duncan, 1991 and Duncan and Makwa, 2000) that after exceeding certain level of displacement the passive pressure tends to remain constant. Thus, the recommendation of MassHighway manual (2005) is observed to give reasonable prediction of passive pressure coefficient.

3.9 Implementation of Soil Pile Interaction

In the implementation of the soil pile interaction, the piles are discretized into smaller elements first. The deformation of the pile under lateral load is maximum near the ground surface. Hence the pile is discretized to smaller elements in the

region up to 10 times the diameter of the pile from the ground level, to capture the response of the pile to lateral load as accurately as possible. The nonlinear $p - y$ curve for lateral load deflection and $t - z$ curve for the axial load-transfer are developed for each node located at different depth below the ground surface. The nonlinear springs representing these load deflection and load transfer relations are attached to each node. The lateral load resistance calculated for each node are modified by *p*-multiplier to account for the group effect. The value of *p*-multiplier for the lateral soil resistance is taken as 0.50 as discussed in section 3.9. The tip load displacement curve for tip bearing interaction is attached at the bottom end of the pile. The schematic diagram of modelling process of the pile under lateral and vertical without incorporation of far field soil element is shown in Fig. 3.18

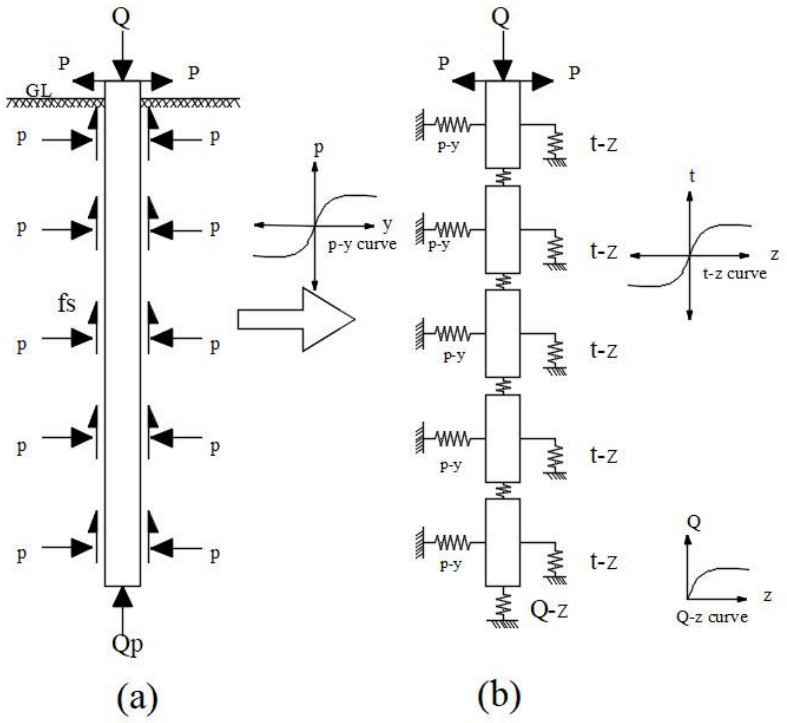

Fig.3.18 Schematic representation of soil pile interaction modelling of pile of without far field soil element (a) free body diagram of forces acting on pile (b) mathematical representation of pile soil interaction

The incorporation of far field soil element is further carried out by attaching the far field soil spring in series with the nonlinear $p - y$ spring as shown in Fig. 3.19.

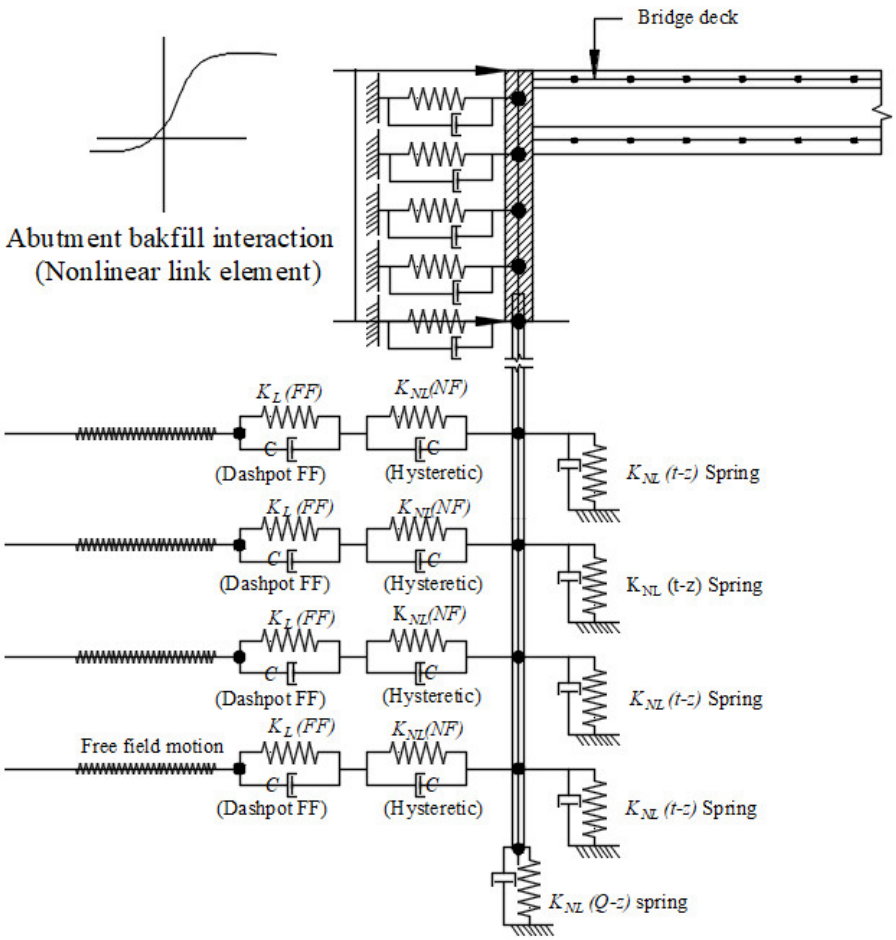

Fig. 3.19 Schematic diagram of abutment backfill interaction and far field soil element along with near field soil in abutment pile.

During nonlinear dynamic analysis the damping associated with near field soil model C_{NL} is generated from the hysteresis model of the material adopted for the modelling of the nonlinear spring. The far field soil contribution is modelled with linear spring K_L representing the linear response of soil. The stiffness and damping representing the far field soil is attached in series with the near field modelled using $p - y$ curve (Naggar and Novak, 1995, Kornkasem et al.,2001). The vertical

radiation damping has not been considered as the lateral deformation of the bridge is the prime objective of the present study.

The modelling of abutment backfill interaction is done by calculating the hyperbolic force displacement relation for each node in abutment considering the tributary area under the influence of the node. The soil spring representing the force displacement relation for abutment backfill interaction is attached to the respective node on abutment wall.

3.10 Concluding Remarks

In this chapter different approaches to modelling of soil pile interaction under axial and lateral load have been studied. Important methods adopted in modelling tip bearing interaction, shaft skin frictional force interaction and lateral load displacement interaction for piles in sand, soft clay and stiff clay have been critically reviewed. In addition, the modelling approach for far field soil reaction in lateral soil pile interaction have also been studied. For the abutment backfill interaction, different nonlinear relation formulated based on theoretical as well as experimental results have been considered in the study. Based on the analysis of the different approaches to consider soil-pile interaction it is observed that:

1. Modelling of soil pile interaction with discrete nonlinear springs representing the nonlinear behavior of soil is found to be quite effective to implement for analysis of IAB. In the modelling of soil pile interaction of piles in sand the $p-y$ curve formulated by Parker and Reese (1970) and recommended for modelling lateral soil pile interaction in API (2007) for piles in sand is adopted in this study. In the modelling of lateral soil pile interaction of piles in soft clay, the $p-y$ curve formulated by recommended in API (2007) as per the formulation given by Matlock (1970) is found to be adequate. The

formulation also takes into account the strength degradation of clay under cyclic loading due to formation of gaps. Similarly, the $p-y$ curve formulated by Reese for stiff clay is also observed to be adequate for modelling lateral soil pile interaction for piles in stiff clay.

2. In the modelling of axial tip bearing interaction for pile in sand, clay and stiff clay the load settlement $Q-z$ curve recommended in API (2007) is found to be adequate. In the modelling of skin shaft friction interaction for pile in sand the load transfer $t-z$ curve recommended by Vijayvergiya (1977) is observed to be reasonable. In the case of soft and stiff clay the load transfer $t-z$ curve recommended in API (2007) is found to be adequate.
3. In the case of far field soil reaction modelling the formulation proposed by Gazetas and Dobry (1984) is simple and can be implemented easily in the analysis of IAB.
4. For modelling of abutment backfill interaction relationship between the passive pressure and wall displacement adopted in MassHighway manual (2005) is observed to produce reasonably accurate passive pressure with movement of abutment wall consistent with experimentally predicted results.

Chapter 4

Finite Element Modelling and Analysis of Integral Abutment Bridge

4.1 Introduction

The integral abutment bridge has a rigid continuous superstructure integrated to the abutment and piers, if any. The abutments are restrained at both ends by backfill. Due to such configuration of the of bridge, the external load due to seismic excitation and vehicular load on the bridge deck spreads throughout the supports which are rigidly connected to the deck. In addition, the internal deformation due to thermal expansion and contraction, shrinkage and creep in the deck induces stress in the supports. The simple idealization with single degree of freedom (SDOF) lumped mass model for estimation of design forces for the substructure, as carried out in conventional bridge, may be erroneous. Therefore, it is imperative to construct three-dimensional model of IAB taking into account the soil pile interaction and abutment backfill interaction for simulating geometric domain and accurate evaluation of response characteristics of the prototype bridge under the action of possible primary and secondary forces.

This chapter presents details steps of constructing three-dimensional finite element model of IAB. The principal objective of the modelling and analysis is the quantification of seismic and thermal response of the bridge in terms of member displacement and forces. Therefore, priority is assigned to accurate representation of different components at its global position, accurate simulations of connections between substructure and superstructure and representation of mass at sufficiently discretized location to capture the nonlinear behavior of the bridge structure. The

nonlinear properties of the bridge components are included in the modelling of the materials.

The soil pile interactions of the piles supporting the abutment and pier are modelled by $p - y$ curve to represent lateral soil resistance versus pile deflection, $Q - z$ curve for the axial load versus settlement at the pile bottom tip and $t - z$ curve to accommodate the frictional forces developed in the pile shaft due to relative displacement between soil and pile. For modelling the far field soil reaction, linear stiffness and dashpot is adopted for simulating the linear response and dissipation of energy into the soil. Further, to observe the effect of the properties of soil in the foundation, different properties of soil classified as soft clay, stiff clay, loose sand, medium dense sand (Medium sand) and dense sand are considered in the modelling of soil pile interaction with distinguishing values of stiffness of each type, as recommended in standard literatures and specification.

Response spectrum analyses of the bridge models with different types of soil in foundation are carried out to record the vibrational characteristics of the bridge and comparison thereof. Nonlinear time history analyses of the bridge are also carried out to identify the effect of soil properties in foundation to the seismic response of the bridge and to appreciate the effect of incorporating far field soil reaction in soil pile interaction modelling.

In addition to the above, the nonlinear static analysis is carried out on the models of the bridge for observing the effect of thermal expansion and contraction load on the bridge deck, pier, abutment and on piles supporting abutments and piers. Concluding observations are made based on the results of the analysis for further guidance in configuration, modelling analysis and design of integral abutment bridge.

4.2 Description of the Bridge

The bridge under consideration for the study is an IAB with a total length of 120 m. It has two end spans of 37.50 m and one central span of 45 m. The general arrangement drawing of the bridge is shown in Fig. 4.1. The deck of the bridge consists of a concrete deck slab of 250 mm thickness supported by four numbers of steel plate girders. The connection between the deck slab and steel girders is achieved through shear connectors. Diagonal bracing of the girder is provided at 5000 mm intervals along the span. The abutment wall at both ends of the bridge is 1000 mm thick with overall height of 5000 m. Circular pier with diameter of 1500 mm with clear height of 4000 mm up to the bottom level of pier cap are provided. Rigid connection of the girder end and abutment is ensured by encasing the end of girder into the abutment wall. The rigid connection between the pier and the girder is achieved through hold down bolts encased in the pier cap. The abutment is supported by pile foundation with five numbers of concrete pile of 900 mm diameter arranged in single row. The piers are also supported by pile foundation with eight piles of 900 mm diameter each arranged in two rows with a pile cap of a 1500 mm thick slab. Upstream and downstream face of the pile has been provided with circular shape to reduce the hydraulic forces due to obstruction of flow of flood water. The connection between abutment wall and the pile supporting the abutment is enlarged to 1500 mm for a depth of 1500mm for providing enough cover to reinforcement of the pile embedded in the wall. The sectional details of deck and detailing of reinforcement for abutment, pier and pile is shown in Fig. 4.2.

Fig. 4.1 General arrangement of the bridge

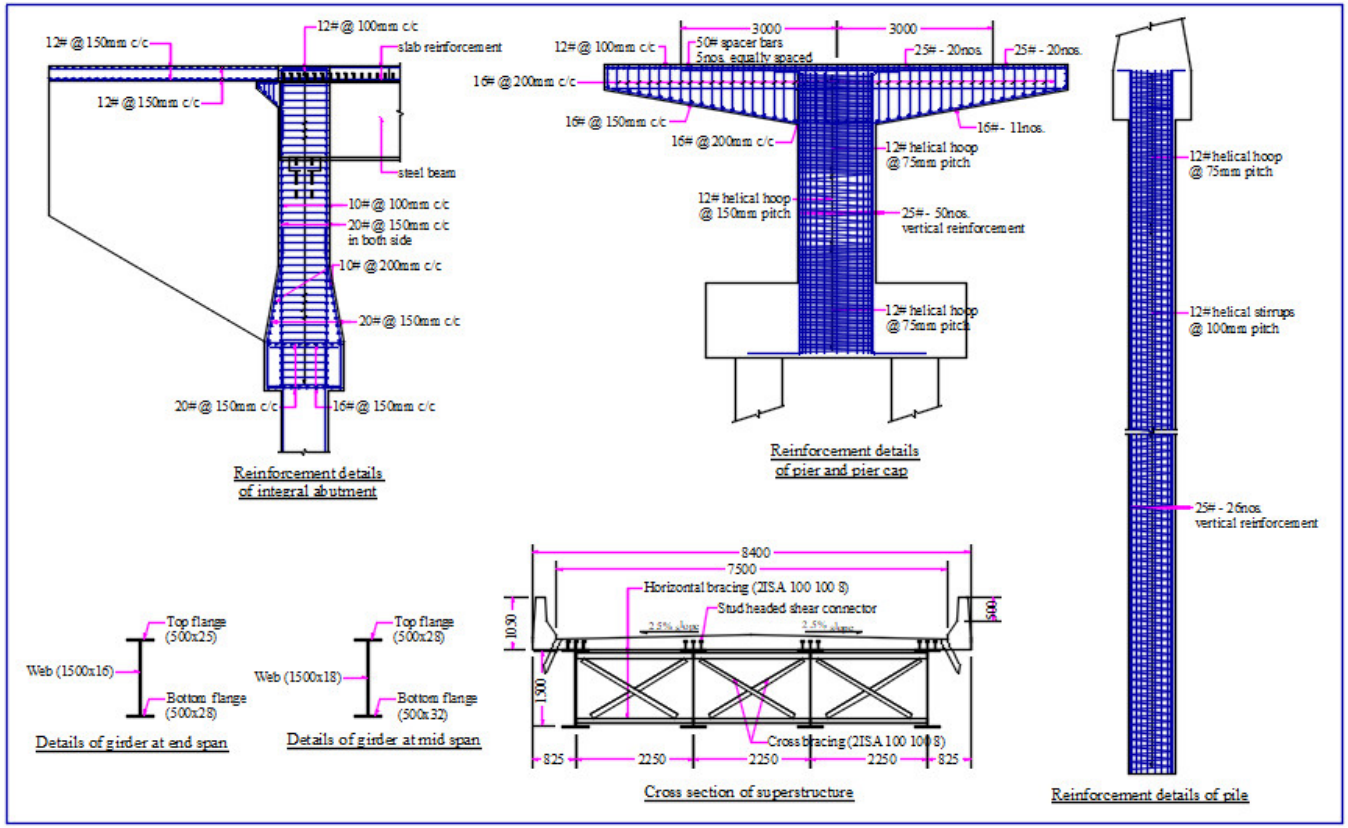

Fig. 4.2 Sectional details of deck and reinforcement detailing of abutment, pier and pile

The ratio of area of reinforcement to the cross-sectional area of abutment wall pier and pile along with grade of concrete provided is given in Table 4.1:

Table 4.1: Details of reinforcement and grade of steel in substructure of bridge

SL No	Description of component	Grade of concrete	Main rebar	Confining rebar
1.	Abutment wall,	M30	0.8%	0.5%
2.	Pier,	M35	1.4%	0.3%
3.	Abutment and pier pile	M35	2.0%	0.3%

4.3 Finite Element Modelling of Bridge

It is observed from the review of literature on finite element modelling of IAB under the action of thermal load that the modelling of pile, pier and abutment are done with beam element while modelling of the deck of bridge is also done using beam element with equivalent properties of the deck system for concrete as well as for steel composite deck. In addition, the CALTRANS Bridge Design Practice (CALTRANS, 2015) recommends adopting grillage models for modelling steel composite deck superstructure, where superstructure cannot be considered as rigid, particularly for very long and narrow bridges and interconnection. Therefore, the superstructure of the bridge considered for present study is modelled using grillage model since the deck width of the bridge is quite narrow as compared to the length of the bridge. The deck of the bridge is thus idealized as a series of longitudinal and transverse beam elements interconnected at the nodes. The longitudinal steel composite girder is modelled with longitudinal grillage beam with the stiffness properties of the composite section taking the effective width of the reinforced concrete deck slab into account. The reinforced concrete deck slab of the bridge is modelled by transverse grillage beam with the depth of the beam equal to the thickness of the deck and width of the beam equal to the spacing of the transverse

beam. The portion of the effective width of the reinforced concrete deck slab modelled along with the steel girder in the longitudinal direction is transformed to an equivalent steel section through the modular ratio of steel and concrete and is assigned a massless material since the seismic weight or mass of the portion of the effective width of the reinforced concrete deck slab is considered in the modelling of the deck slab using transverse grillage beam. The bracing of the girders in the deck is modelled as truss element by considering the effective axial stiffness of bracing in transverse direction. The schematic diagram of grillage modelling of deck is shown in Fig. 4.3.

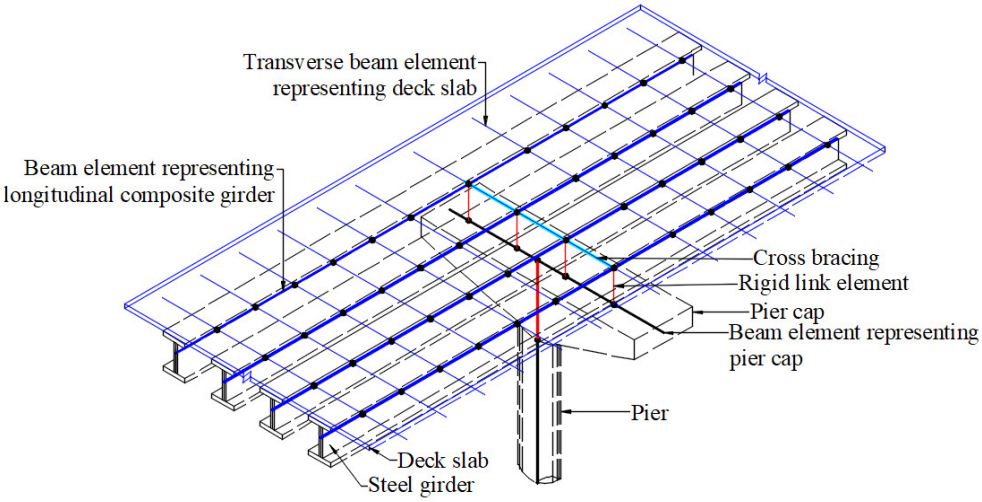

Fig. 4.3 Schematic diagram for grillage model of the bridge deck

The grillage modelling is stated to be not suitable for the design of deck slab as it does not provide the three-dimensional response of deck slab (Vayas and Iliopulos, 2014). However, it is considered adequate for modelling the deck of IAB to be analyzed under seismic and thermal load. Further, in the simulation of deck using grillage model, discrete frame elements are used leading to overall simplification and significant reduction in the degrees of freedom as compared to the modelling

of the deck slab with shell element. Thus, substantial computational advantages are derived through such grillage modelling of deck slab.

The superstructure of the bridge is long compared to the width and depth of the girder and is assumed to respond elastically under lateral seismic loading (Priestley et al., 1996). Hence, the structural component of the superstructure is modelled with elastic properties of the materials.

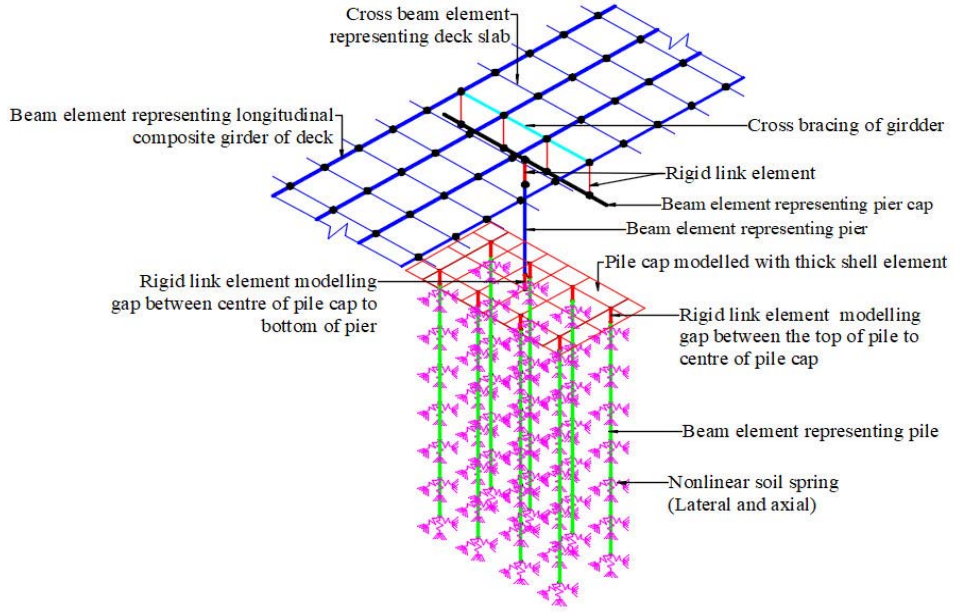

Fig. 4.4 Finite element model of a part of sample bridge

As shown in the schematic diagram for strategies in finite element modelling of the bridge with pile foundation in Fig. 4.4, the total deck assembly is placed at the centroid of the composite deck in its location in elevation in the model. In addition, the pier cap is modelled with beam element and placed at the centroid of the section in location of the element in elevation. The gaps that created between the centroid of the girder to the centroid of the pier cap and centroid of the pier cap to the end of the pier is connected by adopting rigid link element. The connection through these gaps are established by adopting rigid link elements, enabling each structural

element to be positioned at their corresponding centroidal location in elevation. The abutment wall is modelled with thick shell element and the ends of the girders are connected to the abutment wall. The pier, pier cap and piles are modelled using beam element. The pile cap in pier foundation is modelled using thick shell element. The abutment wall is modelled with thick shell element so that the transverse shear deformation is accounted for at the location of bending stress concentration such as base of the abutment and the location of connection with girder. Similarly, the pile cap is also modelled with thick shell to account for the shear deformation at such locations. In the detailed reinforcement design, the main vertical bars in the abutment wall is provided with rectangular links and lateral cross ties for confining the core concrete of the wall. Similarly, the main vertical bars of the piers and piles are provided with spiral hoops for confinement of the core concrete. Therefore, the modelling of the behaviour of the confined core concrete in pier and pile of the bridge foundation are done by adopting the stress-strain model given by Mander (1988) as shown in Fig. 4.5. The cover concrete is however modelled using the stress strain model of unconfined concrete (Priestley et al., 2007).

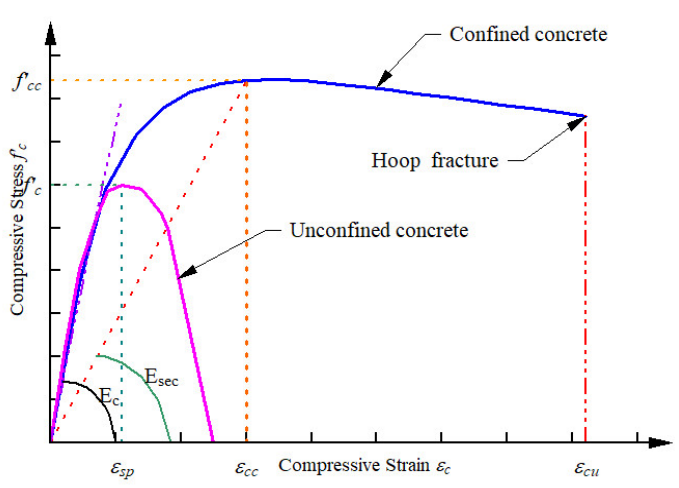

Fig. 4.5 Stress Strain curve of concrete (Mander 1988)

The stress strain curve of rebar adopted in the modelling of pier is shown in Fig 4.6. The stress strain relation of the rebar consists of an elastic portion, a yield plateau and strain hardening range in which the stress increases with strain. The value of ultimate strain ϵ_{su} is taken as 0.12 and the strain harding is assumed to start at strain of 0.02. The value of the reduced ultimate tensile strain ε_{su}^{R} is taken as 0.090 for the reinforcing bar of 32mm diameter or less (CALTRANS, 2010)

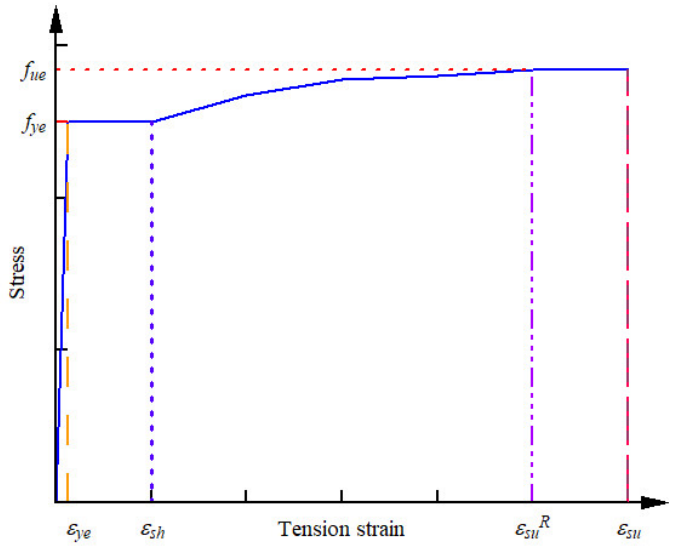

Fig. 4.6 Stress strain curve of rebar (CALTRANS, 2010)

The inelastic behaviour of the reinforced concrete piers and piles of the bridge is modelled by adopting the moment curvature relationship of confined concrete. The plastic moment capacity and the yield moment capacity of the piles and pier are calculated considering the idealized moment curvature as recommended in CALTRANS Seismic Design Criteria (2010), as shown in Fig.4.7. The corresponding axial load considered in the moment curvature analysis of pier and pile is evaluated from the dead load on the bridge to be on the conservative side. To accommodate the fluctuation in the axial load during seismic action, maximum range of $-0.05P_n$ in tension and $+0.15P_n$ in compression is adopted in the

moment curvature analysis (Aviram et al. 2008) where P_n is the axial load on the pile/pier from superimposed dead load. In the moment curvature analysis for modelling of plastic hinges using the idealized moment curvature curve as shown in Fig. 4.7 the failure of the cross section is defined as fracture of steel rebar when its strain reaches the value of ϵ_{su} or crushing of confined concrete at strain ϵ_{cu} whichever is earlier. The plastic moment capacity M_p is defined by balancing the areas between the actual and idealized moment curvature curve beyond the yield point.

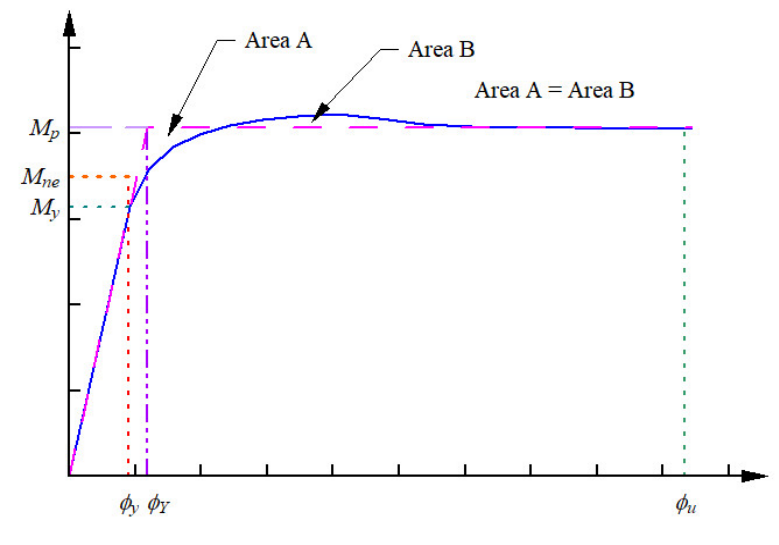

Fig.4.7 Idealized Moment curvature diagram CALTRANS (2010)

The expected nominal moment capacity M_{ne} for the piers and piles are defined based on the expected concrete and steel strength when either concrete strain reaches 0.003 or the reinforcing steel strain reaches reduced ultimate tensile strain ϵ_{su}^{R} whichever is earlier. The modelling of plastic hinges in this study is carried out using idealized moment curvature adopted as shown at Fig. 4.8 (SAP2000, Aviram et al., 2008). The value of expected nominal yield moment capacity M_{ne} and corresponding nominal yield curvature $\emptyset_Y$ is used to define the yield point of the

hinge. The plastic moment capacity M_p and the corresponding plastic curvature $\emptyset_p$ is used to define the ultimate capacity point in the hinge. The plastic curvature is as $\emptyset_p = \emptyset_u - \emptyset_Y$. The implementation of modelling of the plastic hinge is carried out by defining the moment curvature capacity points shown in Fig. 4.8 as

1. Point A = 0.0, 0.0 (no load)
2. Point B = $M_{ne}, \emptyset_Y$ (Yield point)
3. Point C = $M_P, \emptyset_P$ (Ultimate capacity)
4. Point D = $0.2M_P, \emptyset_P$ (Degraded capacity taken as 20% of plastic moment
5. Point E = Failure point taken just higher than point D with positive slope

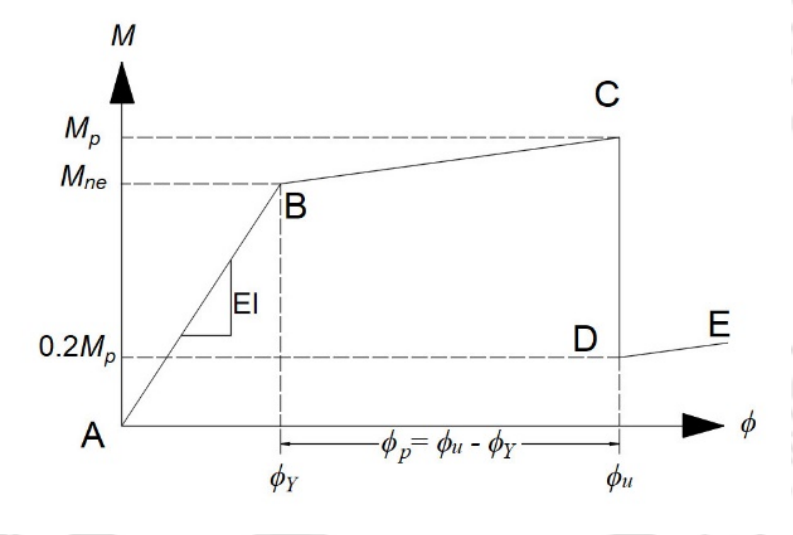

Fig. 4.8 Idealized moment curvature relation for modelling plastic hinge

The pile and pier are having circular cross section with uniform reinforcement in circumferential area and thus have uniform capacity in all direction. Hence, the modelled hinge is taken to be symmetric about all axes. The plastic hinge length L_p is adopted in the estimation of plastic rotation at the location of plastic hinge. Further, the curvature shall not drop to zero at the base of the column as the strains of the tension reinforcement will only drop at a depth equal to the true development

length of the reinforcement. Simultaneously, on the other side of the column, the compression strain of the concrete shall also not immediately drop to zero at the base but will gradually dissipate with depth (Priestley et al. 2007). Thus, the plastic hinge length also includes a component of strain penetration length L_{sp}, which takes into account the effect of tensile reinforcement in anchorage deformation. The curvature over the strain penetration length is considered equal to the curvature at the base of column. The plastic hinge length is calculated using the relation proposed by Priestley et al., (2007) as

$$L_p = k_{pl} L_c + L_{sp} \geq 2L_{sp} \quad (4.1\text{ a})$$

where k_{pl} is a constant, L_c is the length from the critical section to the point of contraflexure and L_{sp} is the length of strain penetration. The constant k_{pl} is calculated from the relation as;

$$k_{pl} = 0.2\left(\frac{f_u}{f_y} - 1\right) \leq 0.08 \quad (4.1\text{b})$$

The relation for computation of length of strain penetration is given as (Priestley et al. (2007) as

$$L_{sp} = 0.022\, f_{ye} d_{bl} \quad (4.1\text{c})$$

The stiffness degradation and the hysteretic energy dissipation of the reinforced concrete members is modelled by adopting the Takeda model. The Takeda model was developed by Takeda et al. (1970), which was based on the experimental observation on behaviour of a number of medium sized concrete members tested under lateral load reversal with light to medium axial load. The model is considered appropriate for the study as it simulates the phenomenon of continuous degradation of stiffness with increasing displacement amplitude beyond the point of yielding.

In order to ensure accuracy in the response of the structure from the finite element analysis of the bridge, successive mesh refinement is considered in the analysis of the bridge model till convergence in the solution is obtained. More refinements are carried out in the upper portion (up to 10 times the diameter) of the pile using beam elements for better prediction of the deformed configuration. Relatively coarser discretization is adopted for the remaining parts of the piles. Uniform discretization is adopted for the pier represented using beam elements. In the modelling of abutment wall with thick shell elements, uniform size of elements are used in the meshing of the domain. The density of the mesh is increased successively such that the responses of the structural components converge with finer mesh. However, it has also been observed that with the increase in the mesh density of the element, the computational time for nonlinear analysis of the bridge increase significantly. In view of this, the mesh density has been kept to the optimum level limiting the variation of results with finer mesh to a reasonable margin.

4.4 Modelling of Nonlinear Soil Pile Interactions

Goel (1997), Spyrakos and Loannidis (2003) and Farahani et al. (2010) reported significant influence of the properties of soil in the seismic response of a bridge. The literatures on thermal analysis of IAB also revealed that the stiffness of the soil in the foundation significantly affects the response of a bridge to thermal loads. Thus, the present study is focussed on understanding the response of the IAB founded on different types of soil namely, Loose Sand, Medium Dense Sand (Medium Sand), Dense Sand, Soft Clay and Stiff Clay under seismic excitation. The distinction amongst different types of soils are based on the range of engineering properties attributed to the type of soil in standard literature which is based on the field and laboratory tests. The engineering properties of each type of

soil adopted in the present study are shown in Table 4.2 and 4.3. The modulus of elasticity of the soil considered in Table 4.3 is within the range of value prescribed in AAHSTO (2012) for each type of soil. The initial modulus of subgrade reaction of sand adopted in the modelling of soil stiffness has been taken from the value recommended by O'Neill and Murchison (1983). The modulus of subgrade of clay has been adopted from the value as recommended by Reese et. al. (2006).

Table 4.2 Properties of different types soil [Tarzaghi et. al (1996)]

Type of soil	Range of SPT-N value	Average N value	Angle of internal friction (ϕ)	Unit weight of soil (γ) kN/m^3
Loose Sand	4-10	7	30^0	16
Medium Sand	10-30	20	35^0	18
Dense Sand	30-50	40	40^0	20
Soft clay	2-4	3	0	17
Stiff Clay	8-15	12	0	19

Table 4.3 Strength parameters of different types of soil [O'Neill and Murchison (1983), AASHTO (2012)]

Type of soil	Modulus of elasticity (kPa)	Initial Modulus of subgrade reaction kN/m^2/m	Poisson's Ratio (ν)
Loose Sand	8750	10000	0.30
Medium Sand	15000	21000	0.32
Dense Sand	22500	35000	0.35
Soft clay	8700	55000	0.45
Stiff Clay	32500	110000	0.50

The soft and stiff clay considered in this study is assumed to be normally consolidated. The strength parameters of stiff and soft clay adopted in this study are taken from ASCE/SEI-41 (2006) as shown in Table 4.4.

Table 4.4 Range of strength parameter of clay and value adopted in this study

Type of soil	Range of value of cohesion c (KPa) (ASCE/SEI-41-2006)	Value of cohesion c adopted (KPa)	Value of adhesion c_a adopted (KPa)	ϵ_c adopted (Reese et al. (2006)
Soft Clay	12-24	24	23	0.02
Stiff Clay	48-96	72	41	0.006

Further, the pile capacity parameters i.e. bearing capacity factor for computing the bearing capacity of sand is adopted as shown in Table 4.5, based on the recommendation in API (2007).

Table:4.5 Bearing capacity factor and parameters for cohesionless soil (API,2007)

Type of soil	End Bearing Factor (N_q)	Limiting unit end bearing value (MPa)
Loose Sand	12	3
Medium Sand	20	5
Dense Sand	40	10

The pile capacity parameters i.e. the value of effective horizontal stress factor and angle of wall friction for calculation of shaft skin frictional force are adopted as shown in Table 4.6. based on recommended in FEMA 356 (2000).

Table: 4.6 Effective horizontal stress factor and friction angle (FEMA 356, 2000)

Type of pile/pier	F_{di} downward	F_{di} upward	Angle of friction
Drilled pier	0.70	0.40	0.75ϕ

Adopting the properties and parameters of different types of soil, as presented in Table 4.2 - 4.6, along with the strategy of modelling discussed in Chapter 3, numerical model of IAB with soil pile interaction is developed. Further, uniform strata of soil are assumed along the foundation depth in all the models considered with different types of soils.

4.4.1 Modelling of Soil Pile Interaction of Axially Loaded Pile in Sand

The ultimate tip bearing capacity of pile in sand is calculated using the Equation (3.2). This pile tip bearing interaction with soil is modelled using load settlement $(Q - z)$ curve as recommended in API (2007) which is shown in Fig. 3.1. The $Q - z$ curve for pile in sand with ultimate bearing capacity computed by taking the adopted parameters as shown in Table 4.5 for sand is shown in Fig. 4.9.

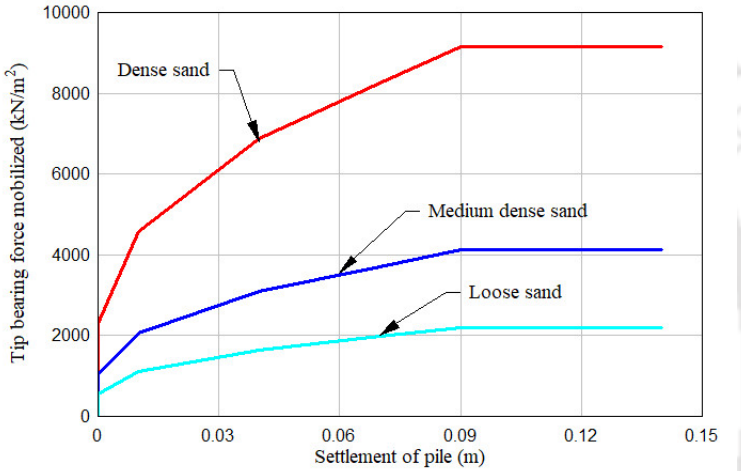

Fig. 4.9 $Q - z$ curve of sand adopted in the modelling

The computation of the shaft frictional force mobilized in the pile shaft due to relative displacement of pile and sand is computed using Equation (3.4) and (3.6). The representative $t - z$ curve adopted in modelling of the shaft frictional force for different location along the depth of the pile in dense sand is shown in Fig. 4.10. The horizontal stress factor and wall friction angle recommended for drilled pier in FEMA356 (2000) is adopted for the large diameter bored cast-in-situ concrete piles of the bridge under consideration.

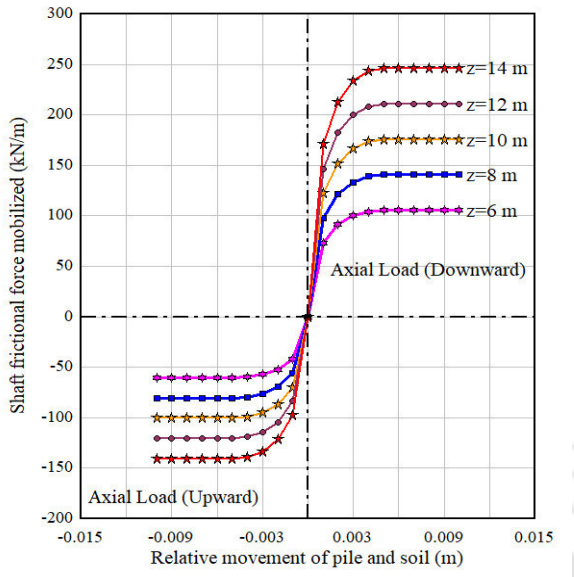

Fig. 4.10 Representative $t - z$ curve of pier pile in Dense sand

4.4.2 Modelling of Soil Pile Interaction of Axially Loaded Pile in Clay

The tip bearing capacity of the piles in clay is calculated using Equation (3.7) and considering properties of clay as shown in Table 4.4. The dimensionless bearing capacity factor is taken as 9 ($N_c = 9$). The computed $Q - z$ curve adopted in the modelling of the soil pile interaction for pile in soft and stiff clay is shown in Fig. 4.11.

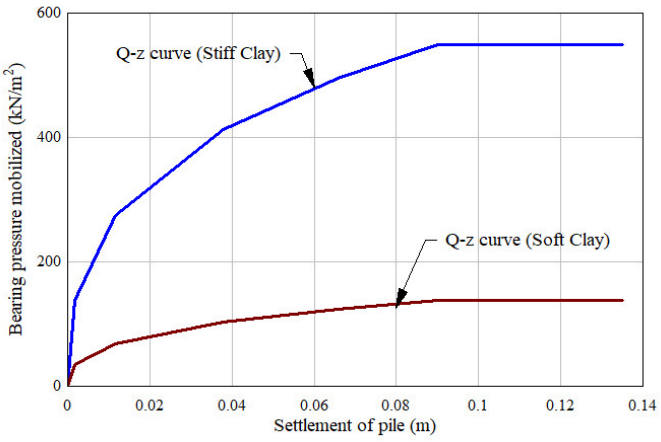

Fig. 4.11 $Q - z$ curve of soft and stiff clay

The computation of maximum shaft frictional force for the piles in clay is done using Equation (3.10). The modelling of the shaft frictional force experienced by the pile in clay is carried out adopting the $t-z$ curve as recommended in API (2007). The $t-z$ curve obtained for soft clay and stiff clay based on adopted strength and parameters, shown in Table 4.4, is depicted in Fig 4.12.

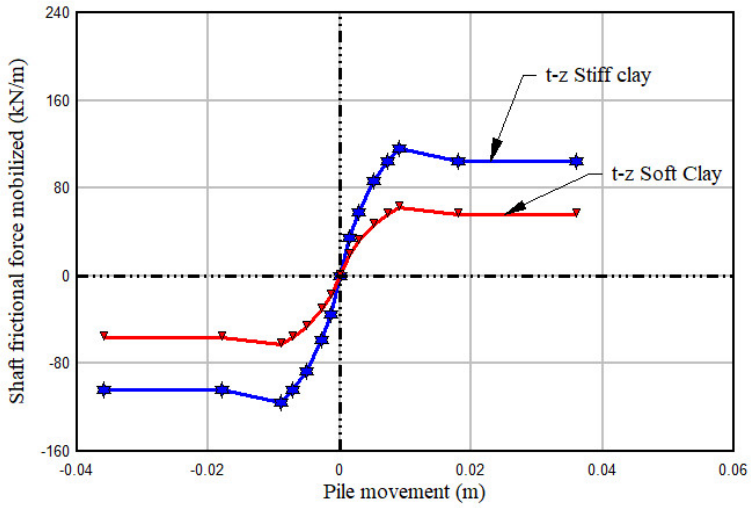

Fig.4.12 $t-z$ curve of pier in stiff and soft clay

4.4.3 Modelling of Soil Pile Interaction of Laterally Loaded Pile in Sand

The modelling of the soil pile interaction of the laterally loaded pile is carried out by adopting the hyperbolic formulation as per Equation (3.23). The ultimate lateral resistance of sand is calculated using the Equation (3.16) and (3.17). The values of coefficient C_1,C_2 and C_3 adopted in the calculation of ultimate lateral resistance of sand is computed using Equation (3.18) to (3.20) which are as shown in Table 4.7.

Table 4.7 Coefficient for ultimate lateral resistance of soil for pile in sand (O'Neill and Murchison, 1983)

Type of sand	Angle of internal friction	`Coefficient for ultimate lateral resistance of soil		
		C_1	C_2	C_3
Loose sand	30^0	2.04	2.67	28.75
Medium sand	35^0	3.02	3.42	53.79
Dense sand	40^0	4.51	4.38	104.15

The $p-y$ curves for piles in loose sand, medium sand and dense sand is computed at different selected depth along the pile. The value of the ultimate lateral resistance of sand at a depth is adopted by taking the minimum value out of the ultimate lateral resistance of sand calculated from Equation (3.16) and (3.17). The factor to account for the cyclic loading condition is taken as 0.90 (API, 2007) for the computation of $p-y$ curves at different depth along the pile. The representative $p-y$ curve calculated for selected depth for dense sand adopted in the model are shown in Fig.4.13.

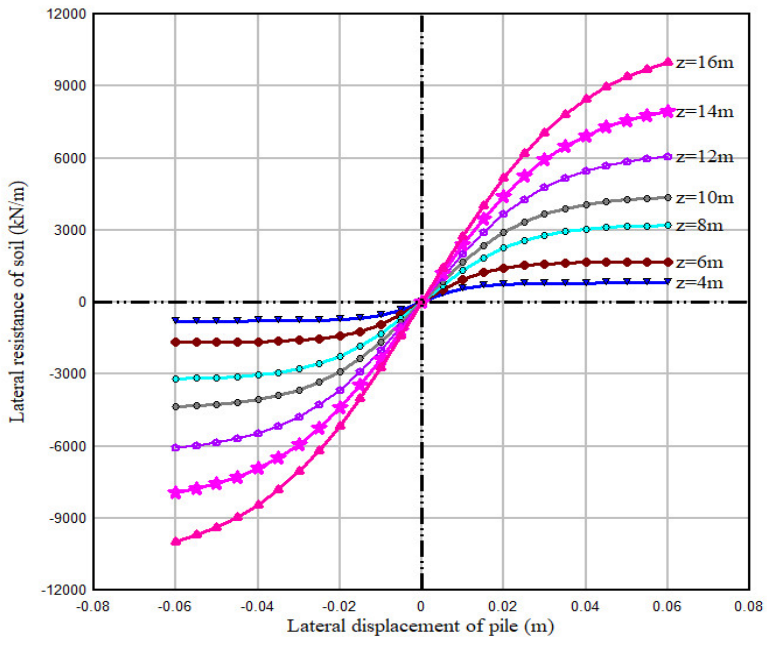

Fig. 4.13 Representative $p-y$ curve of pier pile in Dense sand

4.4.4 Modelling of Soil Pile Interaction of Laterally Loaded Pile in clay

The modelling of the lateral load resistance of pile in soft clay is done as per the recommendation of the API (2007) shown in Table 3.3. The ultimate lateral load resistance of soft clay which is used for computation of the $p - y$ curves for piles in soft clay is calculated using Equation (3.27) and (3.28). After attaining the depth of increasing lateral resistance, the ultimate lateral resistance of soft clay remains constant. Therefore, the values $p - y$ curves for piles in soft clay after the depth of increasing resistance remain constant. The representative $p - y$ curves for soft clay which is adopted in the modelling of the soil pile interaction of bridge in clay is shown in Fig. 4.14.

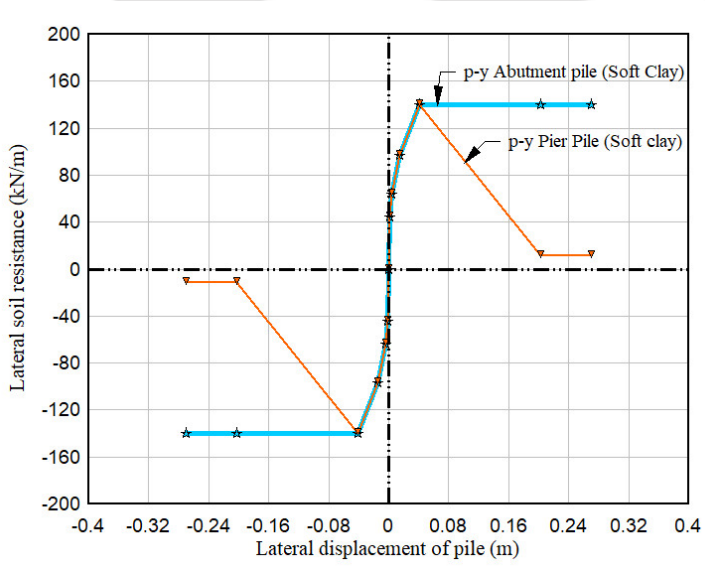

Fig. 4.14 Representative $p - y$ curve for pile in soft clay under cyclic loading.

In case of abutment piles, the abutment backfill surcharge exert additional pressure at the pile cap level. This additional pressure is expected to increase the lateral resistance of soft clay to pile deflection and restrain the formation of gaps between pile and soft clay under lateral cyclic loading on the pile. The calculation of non-

dimensional coefficient for ultimate lateral resistance of soft clay using the Equation (3.25) takes this phenomenon into account in the form of additional equivalent surcharge height. Therefore, no degradation in lateral resistance of the soft clay under cyclic loading is indicated in the pile supporting abutment. But on the other hand, the piles supporting the pier foundation do not have additional confining pressure at pile cap level and therefore, it experiences degradation in strength after a certain amount of lateral deflection under cyclic loading.

Further, for modelling of soil pile interaction for laterally loaded pile in stiff clay, the formulation given by Reese et al. (1975) is adopted. The computation of the lateral soil resistance per unit length of the pile is done using minimum of the values obtained from Equations (3.31) and (3.32) corresponding to the depth of the pile segment under consideration. The $p - y$ curve, calculated for piles supporting the abutment and pier adopted in the modelling of the IAB in stiff clay is shown in Fig. 4.15.

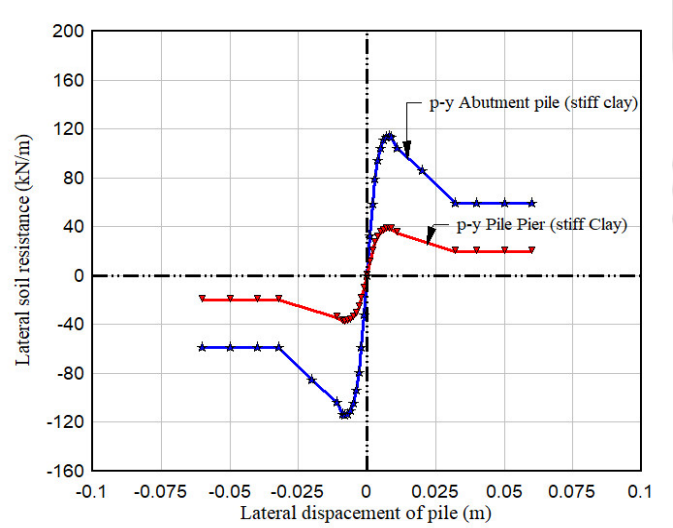

Fig. 4.15 $p - y$ curve for pile in stiff clay for abutment and pier foundation under cyclic loading.

In the formulation for the $p - y$ curve for stiff clay, there is degradation of lateral soil resistance of pile in abutment and pier foundation under cyclic loading after certain amount of deflection of pile. However, the lateral resistance of pile of abutment in stiff clay is appreciably high due to surcharge load from abutment backfill.

4.5 Modelling of Far Field Soil Reaction

Modelling of far field soil reaction for soil pile interaction is carried out as per the formulation proposed by Gazetta and Dobry (1984) assuming uniform soil strata. This formulation is found to be adequate for modelling the far field soil effect. This method has also been adopted by Kornkasem et al. (2001) in modelling of pile supported bridge for seismic analysis. The hysteretic damping as well as overall radiation damping coefficient of the pile is calculated from Equation (3.53). Seed et al. (1984) indicated that the hysteretic damping coefficient of the soil is a function of the strain induced in the soil by the seismic wave propagating through the soil. The far field soil, responding to the wave radiated from the interface of soil and pile, is considered to deform within the range of linear strain limit. Kramer (1996) observed that a strain limit up to 0.001% in soil is not large enough to induce nonlinearity in the stress-strain behavior of soil. Thus, adopting this range of strain, the damping ratio of sand is taken as 2% from the chart given by Seed et al. (1984) as shown in Fig. 4.16.

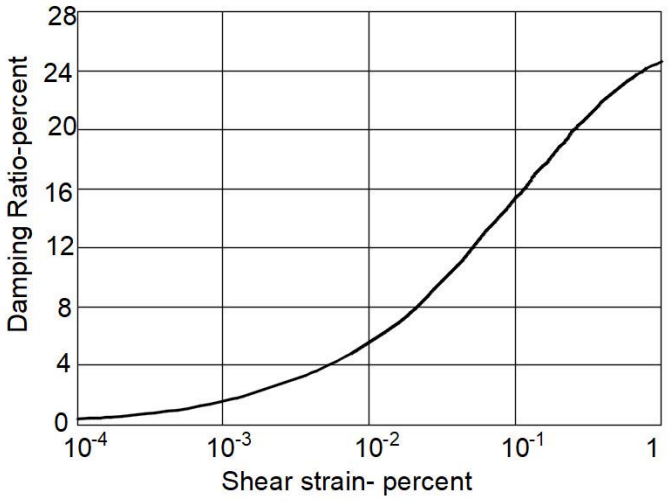

Fig. 4.16 Damping ratio for sand (Seed et al. 1984)

Similarly, the deformation of clay in far field area is also considered to remain within the elastic strain range of 0.001%. Thus, the damping ratio of the clay soil is taken as 2.5%, from the chart given by Seed and Idriss (1970), in the form of damping ratio of clay as a function of strain induced by seismic wave propagating through the soil, shown in Fig. 4.17.

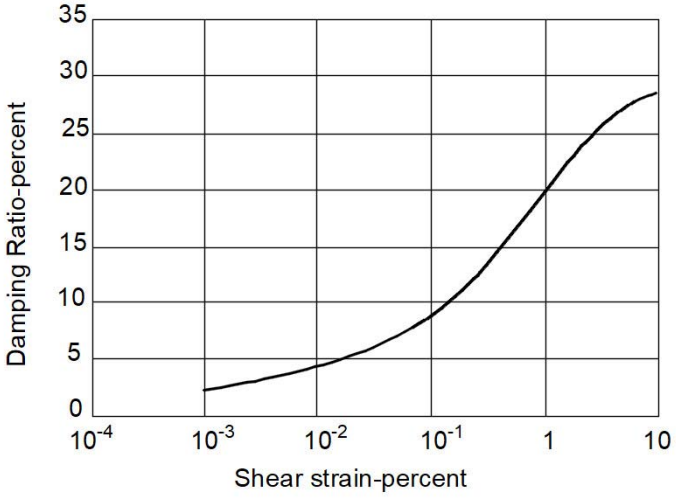

Fig. 4.17 Damping ratio for saturated clay (Seed and Idriss, 1970)

In the time response history analysis of the IAB models, time history of two typical earthquakes are selected for the analysis of the bridge. The selected earthquake time histories are matched with the response spectrum (RS) of IRC: 6 (2014) for soft soil, medium soil and hard soil. The predominant frequency of the matched ground motion is as shown in Table 4.8. These excitation frequencies are used in the calculation of the non-dimensional frequency a_0 and hysteretic damping of the soil.

Table:4.8 Excitation frequency in scaled ground motion to RS of IRC:6 (2014)

Earthquake time history	Circular Frequency (ω) of scaled excitation (radian/sec)		
	Soft soil	Medium soil	Hard soil
El Centro (1940)	15.14	16.23	16.6
Koyna (1967)	13.99	14.57	15.59

The tangent modulus of elasticity of soil including the effect of confining pressure is computed using Equation (3.51), which is adopted in the evaluation of stiffness of pile. The parameters like modulus number, modulus exponent and failure ratio adopted in the calculation of the tangent modulus of elasticity of the soil are adopted from the values given by Duncan et al. (1980) and are shown in Table 4.9:

Table:4.9 Parameters for calculation of confining effect on soil Modulus

Type of soil	Modulus Number (K)	Modulus exponent (n)	Failure factor (R_f)
Loose sand	300	0.25	0.7
Medium sand	450	0.25	0.7
Dense sand	600	0.25	0.7
Soft clay	90	0.45	0.7
Stiff Clay	120	0.45	0.7

The variation of representative values of modulus of elasticity of soil along the depth of the pile foundation calculated using Equation (3.51) and adopted in the modeling of the stiffness of pile is shown in Fig. 4.18.

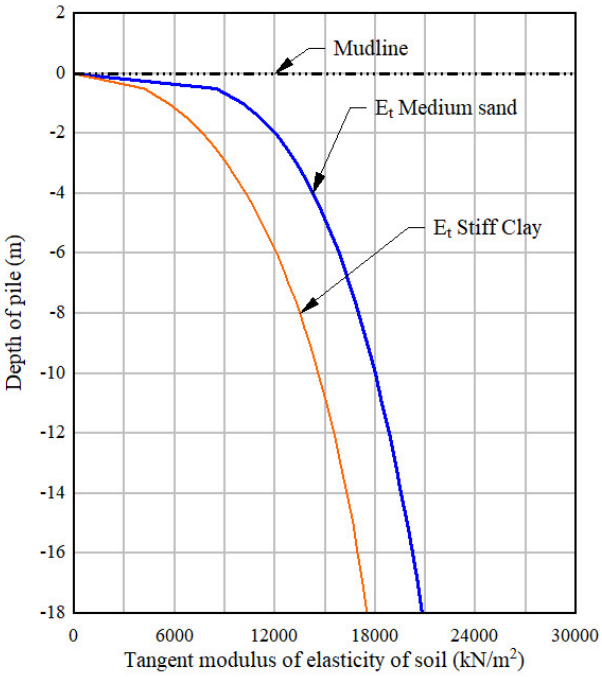

Fig. 4.18 Variation of tangent modulus of elasticity of soil along the depth of pile

These adopted vales are observed to be within the range of the modulus of elasticity for similar types of soil provided by AASHTO (2012).In order to estimate the shear wave velocity to be used in the calculation of damping coefficient, the shear modulus of soil at various depth is calculated using the Equation (3.51) and the corresponding shear wave velocity is calculated using Equation (3.52) for every increment in depth of pile. The representative coefficient of damping computed from Equation (3.53) is for piles in loose sand, medium dense sand and dense sand corresponding to the El Centro ground motion shown in Fig. 4.19.

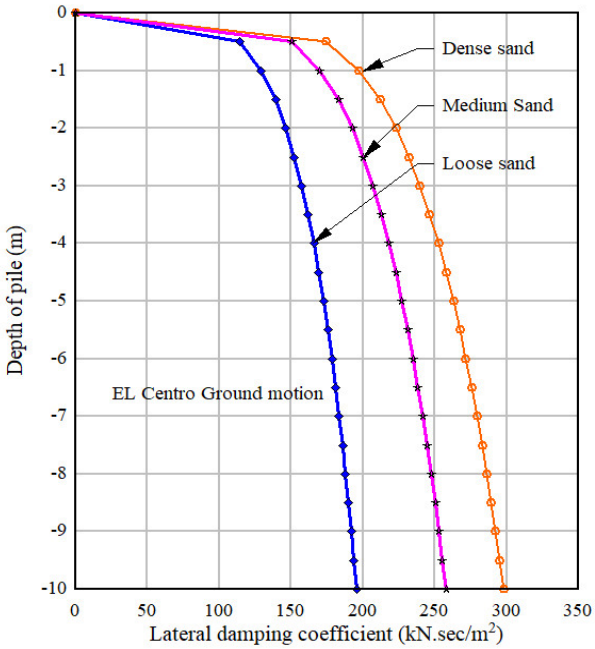

Fig. 4.19 Coefficient of damping for different soil types corresponding to El Centro Ground motion

4.6 Modelling of Abutment Backfill Interaction

The interaction between the abutment wall and backfill earth pressure is modelled by using Equation (3.57). The densification of the backfill fill materials take place during the operation of the bridge as discussed in Section 3.12 therefore, to simulate the behavior of the dense backfill during the service life of the bridge the properties of dense sand is adopted for the backfill materials. The properties of dense sand adopted in modelling of backfill are taken as shown in Table 4.10.

Table 4.10 Properties of backfill soil behind the abutment

Soil type	Unit weight of soil (γ)	Angle of internal friction (ϕ)	Poisson's Ratio (ν)	Initial Modulus of subgrade reaction (k)	Angle of wall friction (φ)
Dense Sand	20 kN/m^3	40^o	0.34	35000 kN/m^3	17^0

The coefficient of earth pressure at rest, k_0 is taken as 1.0 based on the recommendation of Clough and Duncan (1991) for compacted backfill. The computed nonlinear curve for abutment backfill interaction is adopted in the modelling and some representative curves at depth 3.0 m and at 4.75 m from the top of abutment are as shown in Fig 4.20.

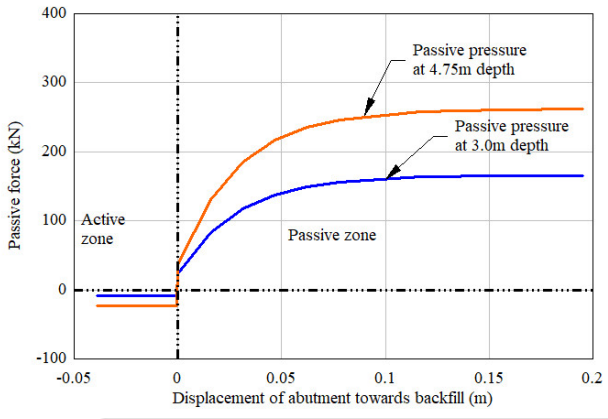

Fig. 4.20 Representative curves showing passive resistance versus displacement of the wall in abutment backfill interaction

4.7 Effect of Different Lateral Soil-Structure Interaction Modelling Approach on Dynamic Characteristics of IAB

The effect of near field and far field soil reaction modelling on the dynamic characteristics of IAB is studied through the modal analysis for two categories of models. First category accommodates modelling of lateral soil pile interaction using nonlinear $p - y$ curve only representing near field soil and is termed as NF model. The other model considers far field soil reaction element along with the near field soil in the modelling of the lateral soil pile interaction and is termed as NF+FF model. The schematic representation of first category of the model is as shown in Fig. 4.21. These models can represent the nonlinear response of soil close to the

pile under action of lateral load as discussed in Section 3.7. The far field soil springs adopted in the (NF+FF) consist of a linear spring representing the elastic response of soil of an infinite medium and a dashpot representing the radiation damping. The linear stiffness of the soil is computed as detailed in Section 3.6 which is adopted for linear analysis of the model. The schematic representation of second category of model is shown in Fig. 4.22. It may be noted that in the both NF and NF+FF model, the soil springs are only shown which is actually a combination of spring and dashpot as shown in Fig. 3.19. In both the models, the tip pile bearing interaction is modelled using nonlinear springs of $Q-z$ (load-settlement) curve and the shaft skin friction mobilized by the differential movement of soil and pile is modelled using nonlinear springs of $t-z$ (load-movement) curve.

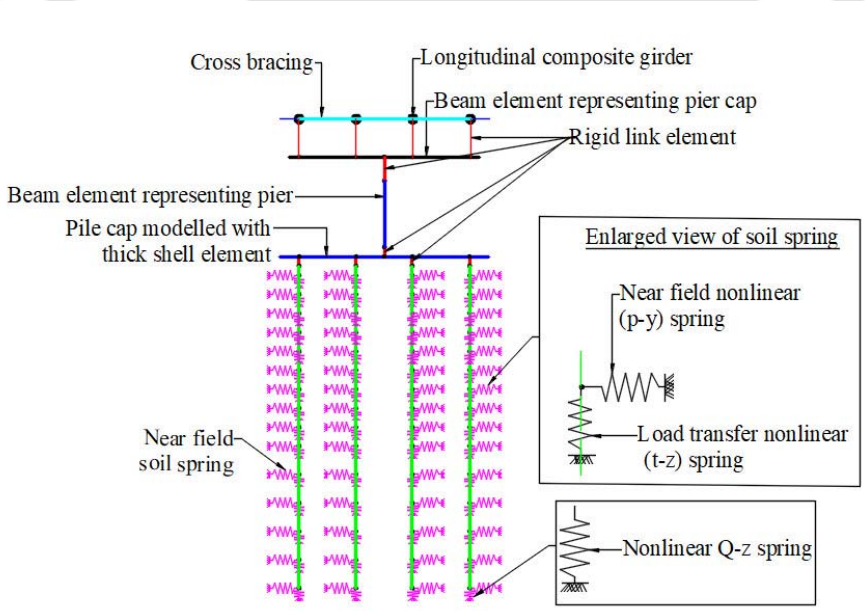

Fig. 4.21 Schematic diagram of NF model of bridge

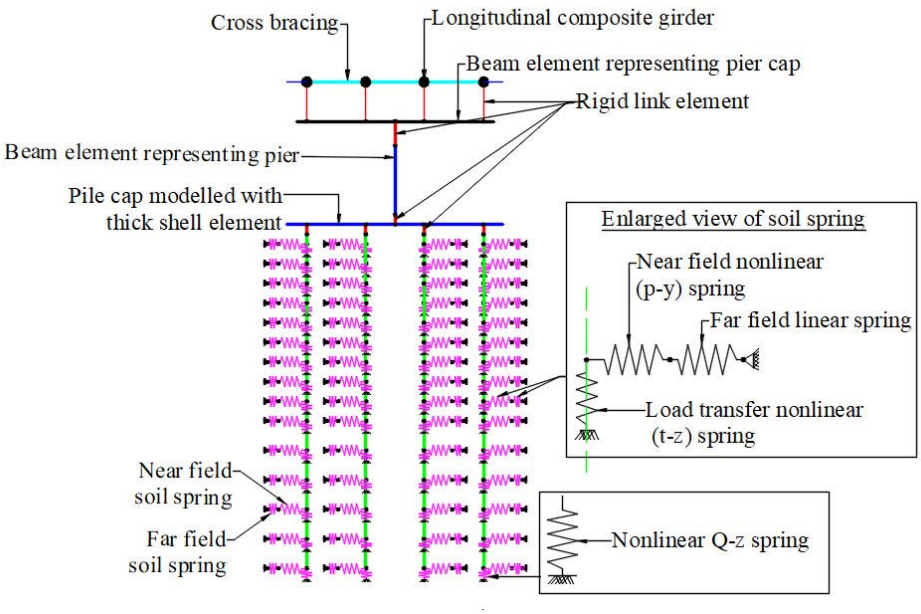

Fig. 4.22 Schematic diagram NF+FF model of bridge

The three- dimensional model of NF+FF developed in SAP2000 is shown in Fig. 4.23.

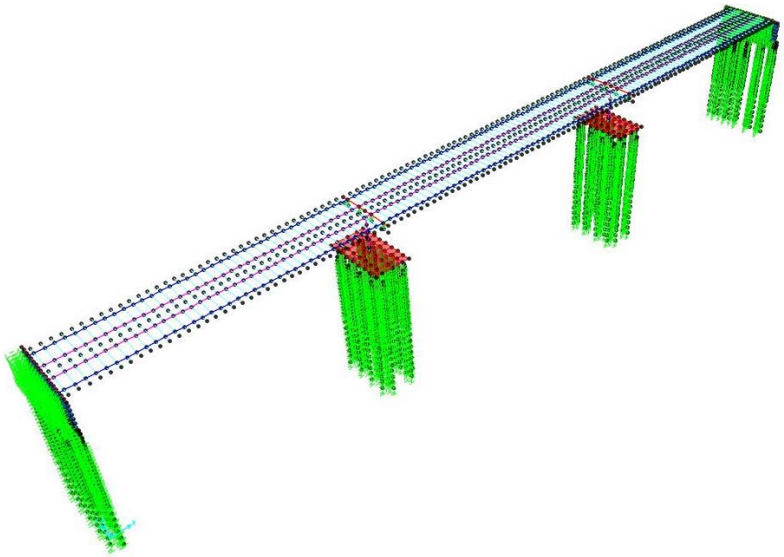

Fig. 4.23 NF+FF model of bridge developed in SAP2000

The free vibration analysis of both the categories of models are carried out in SAP2000. The modal vibration period of the first three modes of each category of bridge model on different types of foundation soil is shown in Table 4.11.

Table: 4.11 Modal Period of vibration of IAB with NF and NF+FF model of IAB

Foundation soil	Modal period of NF model			Modal period of NF+FF model		
	Mode1 (sec)	Mode 2 (sec)	Mode 3 (sec)	Mode1 (sec)	Mode2 (sec)	Mode3 (sec)
Soft Clay	0.614	0.445	0.323	0.680	0.494	0.451
Stiff Clay	0.527	0.427	0.30	0.571	0.441	0.442
Loose Sand	0.460	0.423	0.290	0.510	0.435	0.381
Medium Sand	0.437	0.417	0.280	0.467	0.430	0.310
Dense Sand	0.432	0.414	0.280	0.458	0.427	0.302

It can be observed from Table 4.11 that the modal periods of the IAB decreases with the increase in the stiffness of the soil in the foundation. Furthermore, it is also observed that modal vibration period of the NF+FF models are longer than that of NF model in the IAB under study. This signifies that NF+FF models are more flexible. The increase in the modal period of vibration in the NF+FF model from the NF model is 10.74% for bridge in soft clay, 8.34% for bridge in stiff clay, 10.86% for bridge in loose sand, 6.8% for bridge in medium sand and 6.1% for the bridge in dense sand. Similar increase in the modal period of vibrations were recorded by Kornkasem et al. (2001) in parametric study conducted on pile supported bridge, considering the effect of far field soil reaction. Mazon et al. (2014) observed that the modal period of vibration and mode shapes are altered by

connection properties of girder with the abutment. In the present study, the connection properties of both categories of model viz. NF and NF+FF are equal. Hence, the vibration period is affected due to incorporation of far field soil reaction in the soil pile interaction modelling. Table 4.12 shows the mode shapes and participating mass ratio of the first mode of integral abutment bridge model with NF model founded on different types of soil.

Table: 4.12 Characteristics of first mode of NF model of IAB

Foundation soil	1st Mode Period (sec)	Participating mass ratio			Mode shape
		Ux	Uy	Rx	
Soft Clay	0.614	≈ 0	51.0%	24.9%	Transverse with rotation @ x-axis
Stiff Clay	0.527	≈ 0	44.10%	25.41%	Transverse with rotation @ x-axis
Loose sand	0.460	≈ 0	35.50%	23.6%	Transverse with rotation @ x-axis
Medium sand	0.437	≈ 0	30.55%	22.65%	Transverse with rotation @ x-axis
Dense sand	0.432	≈ 0	28.34%	22.19%	Transverse with rotation @ x-axis

As observed from Table 4.12, the participating mass ratio of first mode of NF model of the IAB in the longitudinal direction is almost zero. The significant longitudinal mode of the model also appears at higher modes. This is because of the stiff response of the bridge in the longitudinal direction due to the restraining effect of abutment with its backfill. The participating mass in transverse direction is also observed to be decreasing with the increase in the stiffness of soil in the foundation. This indicates that the soil properties in the foundation influences the seismic force on the IAB and signifies the importance of considering soil structure interaction in the modelling of foundation. Table 4.13 shows the mode shape and participating mass ratio of the first mode of the NF+FF model of IAB.

Table: 4.13 Characteristics of first mode of NF+FF model of IAB

Foundation soil	1st Mode Period (sec)	Participating mass ratio			Mode shape
		Ux	Uy	Rx	
Soft Clay	0.680	≈ 0	56.60%	24.47%	Transverse with rotation @ x-axis
Stiff Clay	0.571	≈ 0	50.70%	24.07%	Transverse with rotation @ x-axis
Loose sand	0.510	≈ 0	47.48%	23.74%	Transverse with rotation @ x-axis
Medium sand	0.467	≈ 0	39.66%	23.11%	Transverse with rotation @ x-axis
Dense sand	0.458	≈ 0	35.79%	22.80%	Transverse with rotation @ x-axis

The Table 4.13 indicates that the properties of the first mode in NF+FF models are also similar to that of NF models except for the variation in the magnitude of vibration period and participating mass ratio. The comparison of the participating mass ratio of first mode of NF model in Table 4.12 and NF+FF model in Table 4.13 indicates that the participating mass ratio in transverse direction in NF+FF model is higher than that of NF model. Minimum increase of participating ratio of 5.6% in soft clay and maximum increase of 11.98% in loose sand is observed. Hence, the incorporation of the far field soil reaction in soil pile interaction modelling affects the dynamic characteristics and seismic response in the IAB. Fig. 4.24 shows the first mode shape of the NF+FF model in SAP2000.

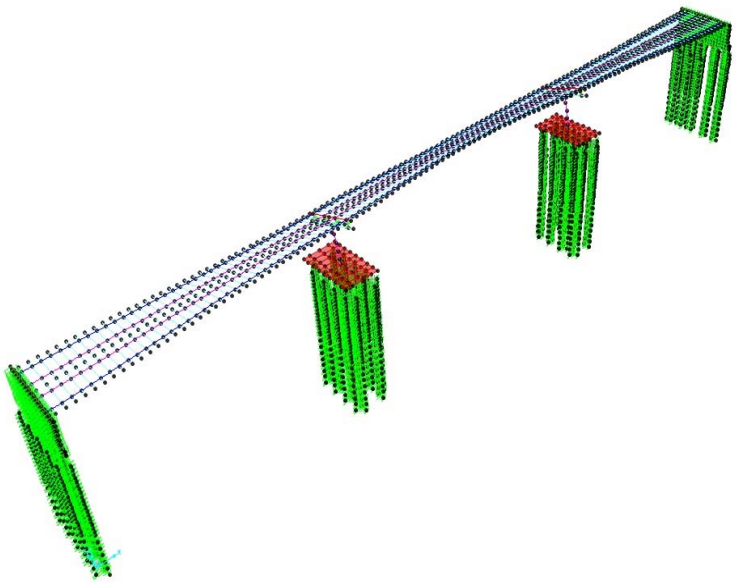

Fig. 4.24 First mode shape of NF+FF model

Table: 4.14 shows the Characteristics of the dominant longitudinal mode of NF and NF+FF model of IAB. Any other mode prior to predominant mode does not have significant participating mass ratio in the longitudinal direction. As may be seen from Table 4.14, significant longitudinal modes are at higher modes with very short modal period of vibration. This signifies stiff character of IAB in the longitudinal direction due to an increase in the stiffness in the longitudinal direction from the restraining effect of abutment, backfill and pile.

Table:4.14 Characteristics of dominant longitudinal modes of NF and NF+FF model of IAB

Type of soil	NF model of IAB			NF+FF model of IAB		
	Prominent Longitudinal Mode			Prominent Longitudinal Mode		
	Mode No	Period (sec)	Participating mass ratio	Mode No	Period (sec)	Participation mass ratio
Soft Clay	17	0.150	36.02%	17	0.163	28.88%
Stiff Clay	16	0.128	33.95%	17	0.141	36.9%
Loose sand	17	0.119	57.08%	17	0.134	42.3%
Medium sand	15	0.107	35.48%	17	0.127	56.0%
Dense sand	14	0.11	42.09%	17	0.122	59.4%

The modal properties of the bridge as observed from the free vibration analysis and as shown in Table 4.12 - 4.14 signifies that the shape of the first fundamental mode of the bridge is transverse with rotation having a large value of participating mass ratio. Hence, the elastic seismic forces in the longitudinal direction is comparatively lower than that in the transverse direction. These will also result in a lower seismic displacement of the bridge in the longitudinal direction, rendering the response of bridge in transverse direction only as critical and governing for design.

Table 4.15 shows the elastic design moment for the pier of the bridge considered in this study using NF and NF+FF model of IAB. The forces are calculated by carrying out response spectrum analysis by adopting the response spectrum for zone V as per IRC:6 (2014) for various types of soil and the seismic moment in two orthogonal directions is calculated. The design moment (M_D) is calculated from the combination rule $M_D = \pm M_2 \pm 0.3M_3$ (IRC: 6:2014), where M_2 is the moment in transverse direction and M_3 is the moment in longitudinal direction. The observation from Table 4.15 indicates that the elastic seismic design force increases in the NF+FF model of the bridge in loose sand, medium sand and dense sand. This is because of the fact that although the modal vibration period of the first mode of NF+FF models of IAB in different types of soil increases from that of corresponding NF models, the modal vibration periods of both categories of models remains in the zone of constant acceleration of the design spectrum due to small variations of the periods. Therefore, the effect of increase in the participating mass ratio is manifested in the form of increase in seismic forces.

Table 4.15 Comparison of elastic design force of NF and NF+FF model

Type of soil	Moment in NF model of IAB (kN-m)			Moment in NF+FF model of IAB (kN-m)			Reduction (+) /increase (-) (%)
	M_2	M_3	M_D	M_2	M_3	M_D	
Soft Clay	6850	1418	7294	6720	1214	7084	2.88
Stiff Clay	7656	1466	8055	7556	1308	7930	1.55
Loose sand	7796	1007	8098	8175	1339	8576	-6.0
Medium sand	7312	609	7493	7886	1065	8205	-9.49
Dense sand	6611	192	6668	6919	827	7176	-7.49

However, in the IAB in soft and stiff clay, the increase in the period reaches the zone of monotonous decrease of acceleration of design response spectrum. Hence, despite an increase in the participating mass ratio of the first mode of NF+FF model, there is simultaneous decrease in the acceleration to the bridge. This results into a trend of reduction in the seismic forces in NF+FF models of IAB in soft and stiff clay.

4.8 Seismic Analysis of Integral Abutment bridge

In order to observe seismic performance of IAB, a nonlinear dynamic time history analysis is carried out using NF and NF+FF models. Nonlinear analyses is considered as most of the soil springs are nonlinear and the structure may also encounter nonlinearity under the action of seismic excitation. The main objective of the analysis is to appreciate the behavior of IAB more thoroughly from the computed displacement of deck, abutment, pile supporting the substructure and drift of the pier. The analysis is also focussed on observing the effect of incorporating far field soil reaction in the soil pile interaction modelling in the response of the bridge under seismic excitation. Therefore, two different earthquake ground motions having variable source characteristics are selected for use in the nonlinear time history analysis of the bridge models. The Characteristics of selected

earthquake ground motion is shown in Table 4.16. Two ground motions representative of source characteristics of medium and hard soil representing possible variation of seismic conditions at site of the bridge in the analysis is considered adequate for the present study.

Table 4.16 Characteristics of considered Earthquake ground motion

Earthquake acceleration	PGA (g)	Predominant period (sec)	Represented source characteristics
EL Centro (N-S) (1940)	0.318	0.309	Medium Soil
Koyna (Trans) (1967)	0.488	0.47	Rock

Seismic analysis is carried on the bridge for computing the peak response using different bridge models for hazard level as per design response spectrum. Thus, the ground motion selected is matched to the target response spectrum (RS) given in IRC:6 (2014) for different types of soil in the foundation. The selected target response spectrum for different type of soil is shown in Fig. 4.25.

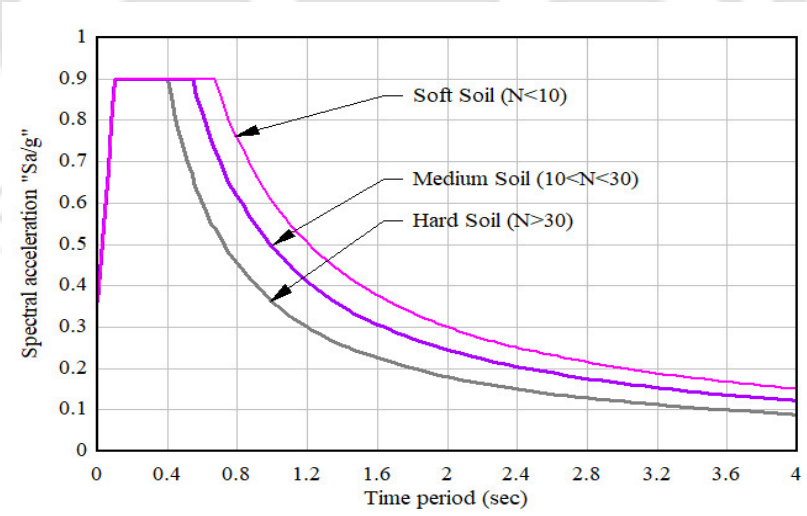

Fig. 4.25 Response spectrum adopted in the analysis of bridges (IRC:6,2014)

The matching of the ground motion has been carried out using the software SeismoMatch (version 2.1.0) from SeismoSoft, Pavia, Italy. The comparison of

ground motion before matching and after matching with response spectrum indicates that the characteristics of the time series are not dramatically altered by the matching process. The comparative plot of original ground motion and matched ground motion for a particular soil in foundation is shown in Fig. 4.26 and Fig. 4.27.

(a)

(b)

(c)

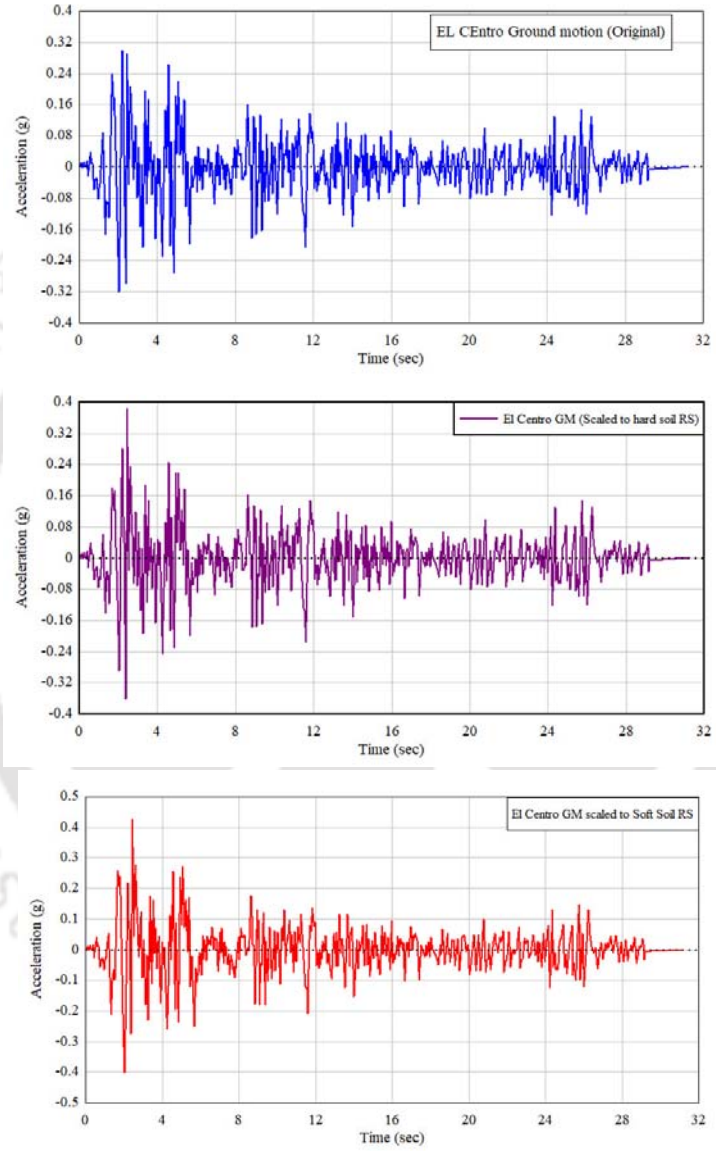

Fig. 4.26 El Centro ground motion (a) original and (b) scaled to RS Hard soil (c) scaled to RS soft soil

(a)

(b)

(c)

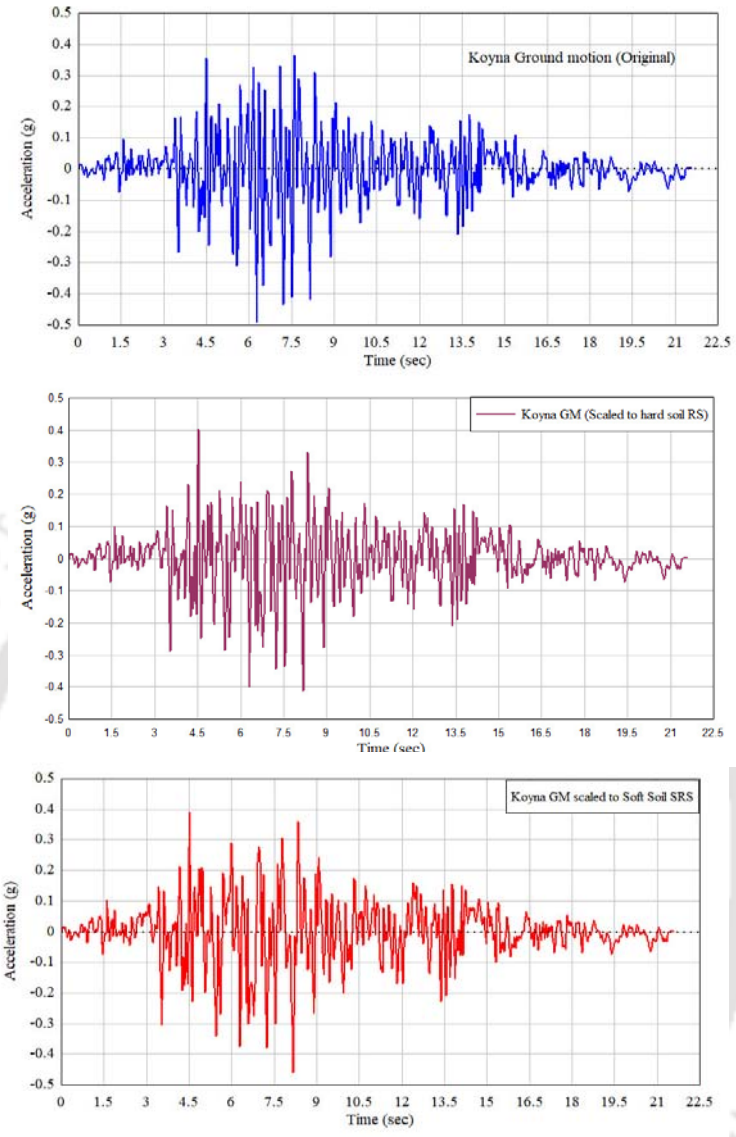

Fig. 4.27 Koyna ground motion (a) original (b) scaled to RS hard soil and (c) scaled to RS soft soil.

However, the peak ground acceleration of scaled El Centro ground motion increased in all types of soil as compared to the original peak ground acceleration. The peak ground motion of Koyna remains almost the same for all types of soil even after scaling. Table 4.17 shows the modified peak ground acceleration of the considered ground motion after scaling to the target response spectrum.

Table: 4.17 Comparison of PGA of original ground motion and scaled ground motion

Earthquake ground motion	Original PGA (g)	PGA after scaling (g)		
		Hard soil	Medium soil	Soft soil
El Centro	0.318	0.383	0.396	0.425
Koyna (trans)	0.488	0.413	0.441	0.459

Fig. 4.28 shows the 5% damped response spectrum of original El Centro and Koyna Earthquake ground motion. It can be observed that the peak spectral acceleration of the ground motions is almost normalized along the peak spectral acceleration of target design spectrum for medium soil. The extent of period of amplification effect of soil is also extended to the period corresponding to the target spectrum.

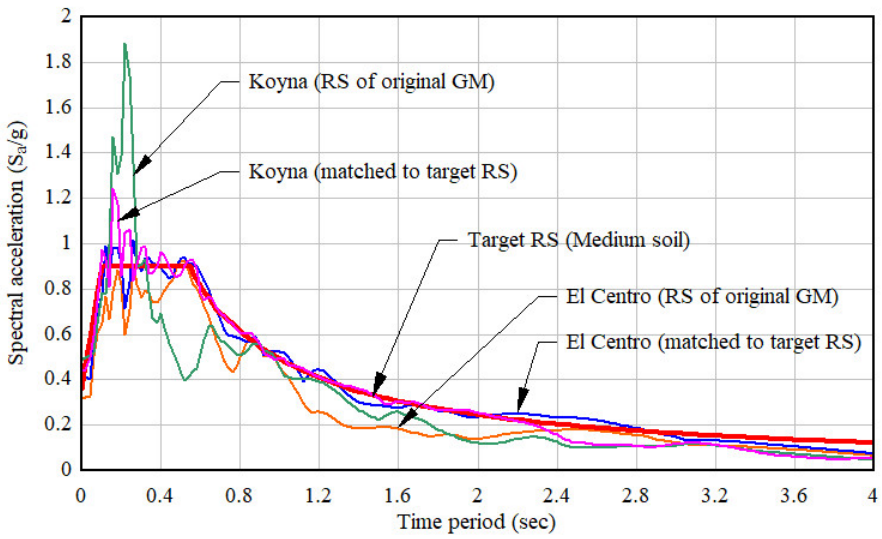

Fig. 4.28 Spectrum compatible El Centro and Koyna ground motion for medium soil

Further, the predominant frequency of input ground excitation after matching to target RS for the nonlinear time response history analysis of the bridge is shown in Table 4.18.

Table 4.18 Properties of scaled input ground motion

Ground motion	Soil type as per IRC:6 (2014)	Predominant frequency of ground motion (rad/sec)	Adopted as input ground motion for soil type in foundation
El Centro	Soft Soil	15.02	Loose sand /soft clay
	Medium Soil	16.23	Medium sand / stiff clay
	Hard Soil	16.60	Dense sand
Koyna	Soft Soil	13.99	Loose sand /soft clay
	Medium Soil	14.57	Medium sand / stiff clay
	Hard Soil	15.59	Dense sand

The nonlinear time history analysis of the bridge has been carried out in SAP2000. The vertical component of the excitation is not considered in the analysis. Further, for the case of damping of integral bridge, Goel (1997) identified the damping ratio of Painter Street Overpass (PSO) in the range 6-15% for first transverse mode from the ground motion recorded during the earthquake event on the bridge. Sungchil et al. (2011) also computed the equivalent modal damping ratio of the PSO and observed that the current 5% damping ratio used in the response spectrum based seismic analysis and design underestimates the system damping of a short span bridge. AASHTO Guide specification for LRFD Seismic Design of Bridge (AASHTO, 2009) specifies that higher damping ratio may be adopted if the bridge has the following characteristics: (1) abutment are designed for sustained soil mobilization, (2) superstructure is continuous without hinge or join and (3) the length of the bridge is less than 300ft. Thus, the approximating damping ratio for the present IAB with steel composite deck considered in this study with a value of 5% is reasonable. In view of these, the damping of the bridge is approximated using Rayleigh damping where parameters are computed by assuming 5% modal

damping ratio for the first two modes of the bridge. The ground acceleration is applied in two orthogonal directions.

Fig. 4.29 to 4.33 show the deflection of the pier pile in the transverse direction for NF and NF+FF models of the IAB under ground motion adopted in the analysis. It is observed that the transverse deflection of the pile NF+FF model is larger than the transverse deflection of the pile in NF model. This is attributed to the effect of far field soil pile interaction modelling in which the pile foundation system becomes relatively more flexible. Berger et al. (1977) also observed that the detailed analysis including dashpot representing the radiation damping produces slightly larger displacement in pile. Erhan and Dicleli (2014) also observed that the deflection of H-pile supporting abutment of IAB modelled with detailed soil structure interaction including radiation damping was more than that of simplified model under the action of high intensity seismic excitation.

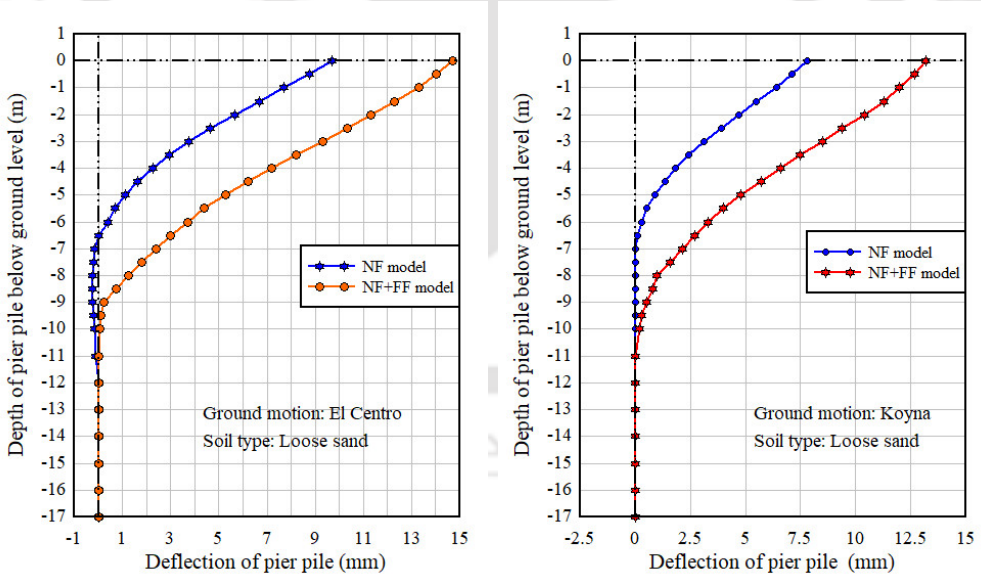

Fig. 4.29 Deflection of pier pile of NF and NF+FF model in loose sand under El Centro and Koyna ground motion excitation.

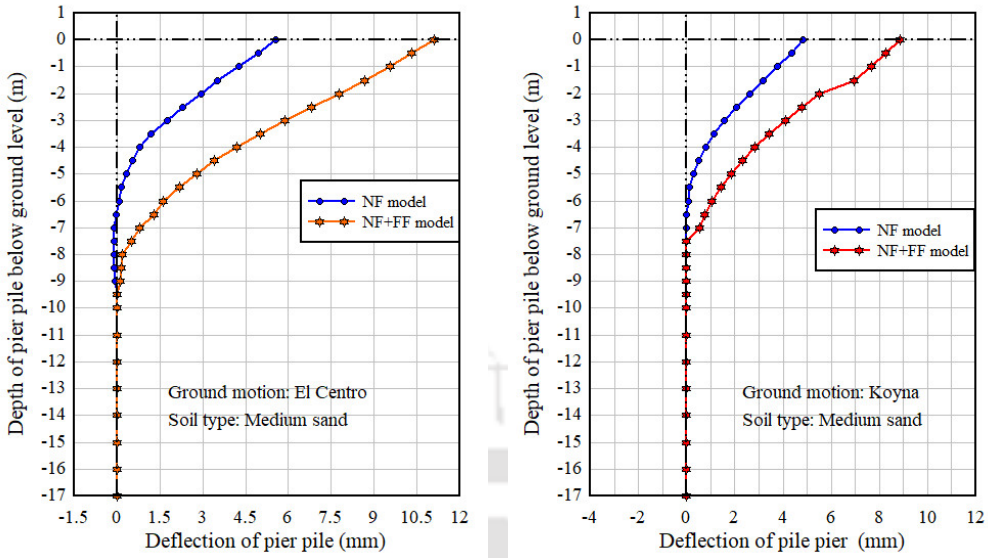

Fig. 4.30 Deflection of pier pile of NF and NF+FF model in medium sand under El Centro GM and Koyna Ground motion excitation.

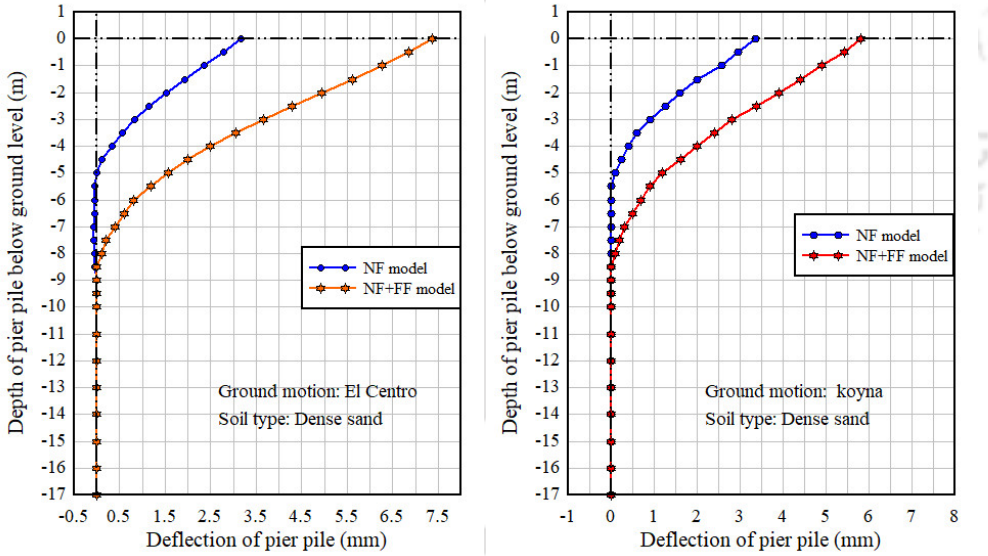

Fig. 4.31 Deflection of pier pile of NF and NF+FF model in dense sand under El Centro and Koyna ground motion excitation.

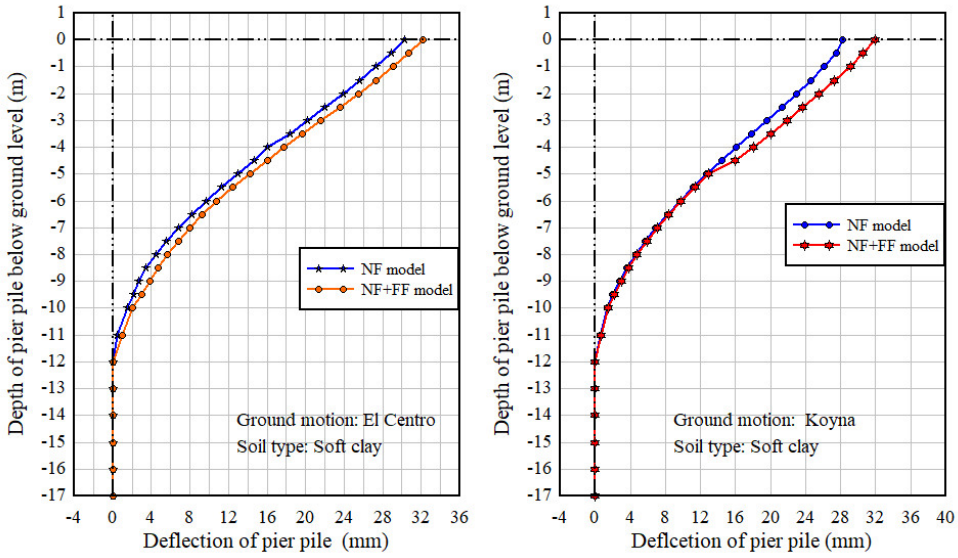

Fig. 4.32 Deflection of pier pile of NF and NF+FF model in soft clay under El Centro and Koyna ground motion excitation.

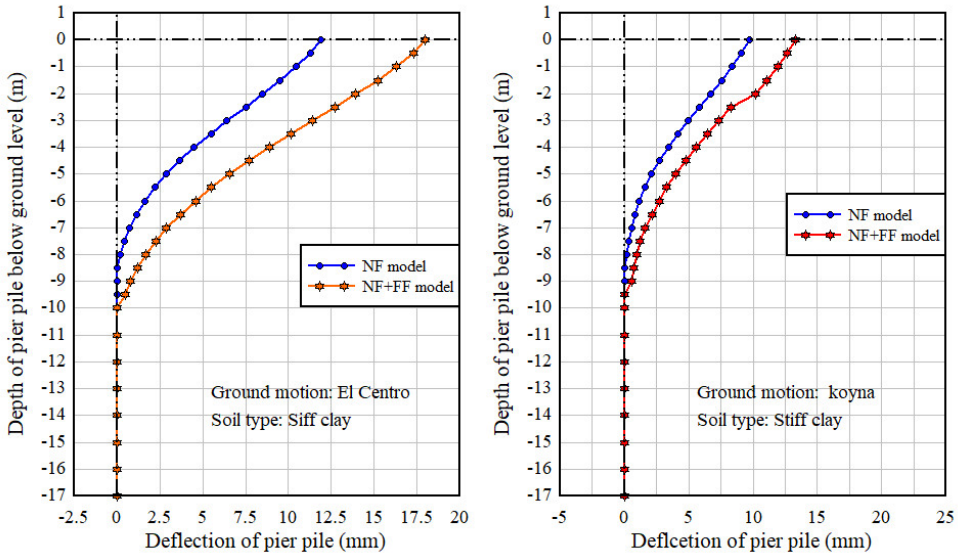

Fig. 4.33 Deflection of pier pile of NF and NF+FF model in stiff clay under El Centro and Koyna ground motion excitation.

It is also observed that in the NF model founded in loose sand, medium sand, dense sand and stiff clay, the lateral deflection of pile becomes negligible at a depth around seven times the diameter of the pile from the ground. However, in soft clay, depth at which the lateral deflection becomes negligible extends to around 10 times

the diameter of the pile. Further, in the case of NF+FF model, the depth at which the lateral deflection of pile becomes negligible is deeper as compared to the NF model due to the added flexibility in the pile foundation which in turn is due to the inclusion of far field soil modelling. However, for the bridge in soft clay, the difference in lateral deflection of pile in NF model and NF+FF model is very negligible indicating that the effect of incorporating far field soil modelling in soil piles interaction has no significant effect in the seismic response of IAB in soft clay. Table 4.19 shows the variation in transverse deflection of pile top corresponding to NF and NF+FF model.

Table 4.19 Peak transverse deflection of pile top supporting pier of NF and NF+FF model

Type of Foundation soil	Transverse deflection of at top of pier pile under different ground motion (mm)			
	El Centro GM		Koyna GM	
	NF	NF+FF	NF	NF+FF
Soft Clay	30.22	32.20	28.20	31.90
Stiff clay	11.90	18.00	9.74	13.27
Loose Sand	9.70	14.71	7.80	13.17
Medium sand	5.40	11.12	4.48	8.85
Dense sand	3.16	7.36	3.55	5.80

The data presented in Table 4.19 indicates larger transverse displacement of the top of the pile supporting pier in the NF+FF model as compared to the displacement of corresponding NF model. Under the excitation of El Centro ground motion, the observed lowest increase in deflection of NF+FF model is 6.5% for the model of IAB in soft clay, while the highest increase is 133% for the model of bridge founded in dense sand. In the case of excitation under Koyna ground motion, the observed lowest increase in the deflection in NF+FF model is 13.12% for the model in soft clay and the highest increase is 97.69% in medium sand. This primarily signifies

the impact of the modelling of the far field soil reaction in soil pile interaction in addition to the effect of excitation frequency of ground motion in the response of the pile foundation of IAB.

Fig. 4.34 to 4.38 shows the seismic moment in transverse direction induced in the pile supporting the pier in NF and NF+FF model founded on various types of foundation soil. The seismic moments are corresponding to the level of excitation of ground motion matched to the design response spectrum for different types of soil having PGA as shown in Table 4.17. These seismic moments are plotted taking absolute maximum value of moment induced by seismic excitation at the locations along the depth of pile.

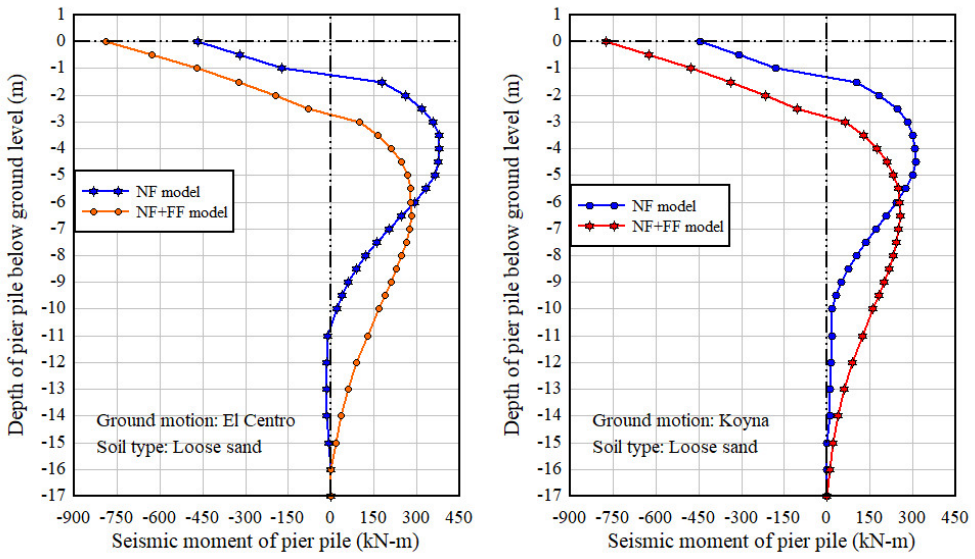

Fig. 4.34 Seismic moment of pier pile of NF and NF+FF model in loose sand under El Centro and Koyna ground motion excitation.

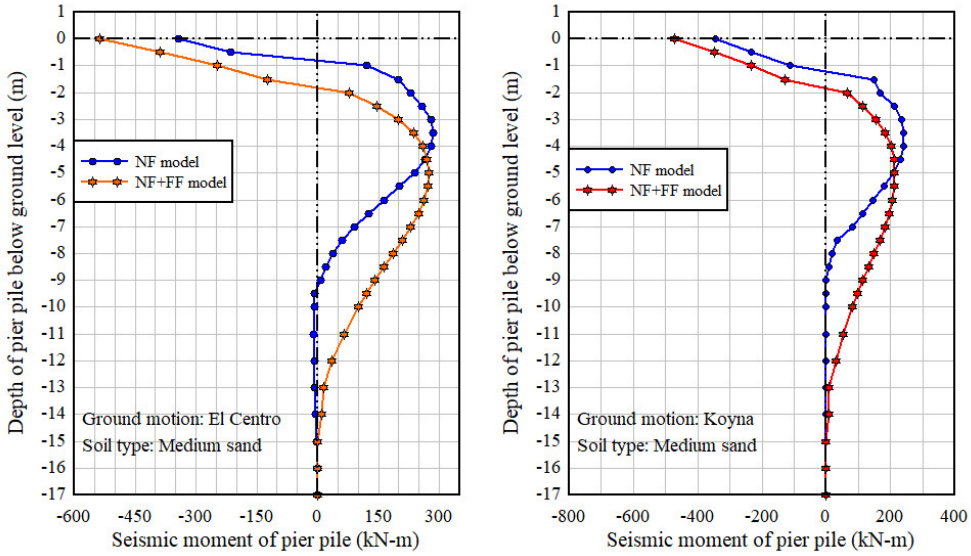

Fig. 4.35 Seismic moment of pier pile of NF and NF+FF model in medium sand under El Centro and Koyna ground motion excitation.

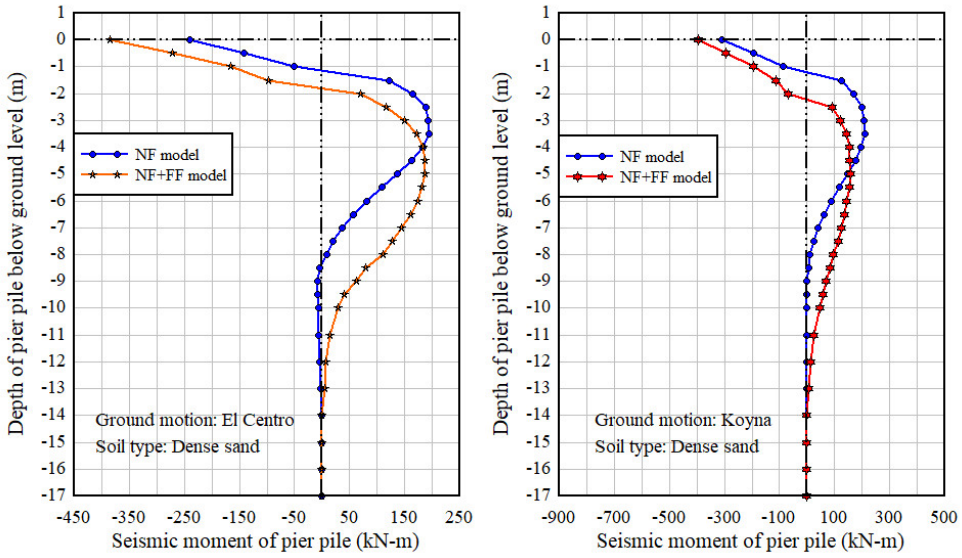

Fig. 4.36 Seismic moment of pier pile of NF and NF+FF model in dense sand under El Centro and Koyna ground motion excitation.

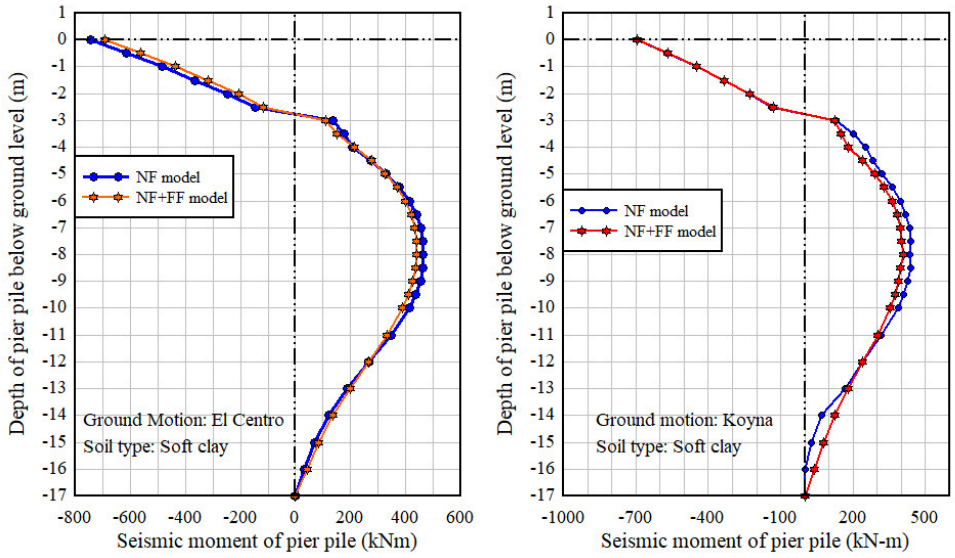

Fig. 4.37 Seismic moment of pier pile of NF and NF+FF model in soft clay under El Centro and Koyna ground motion excitation.

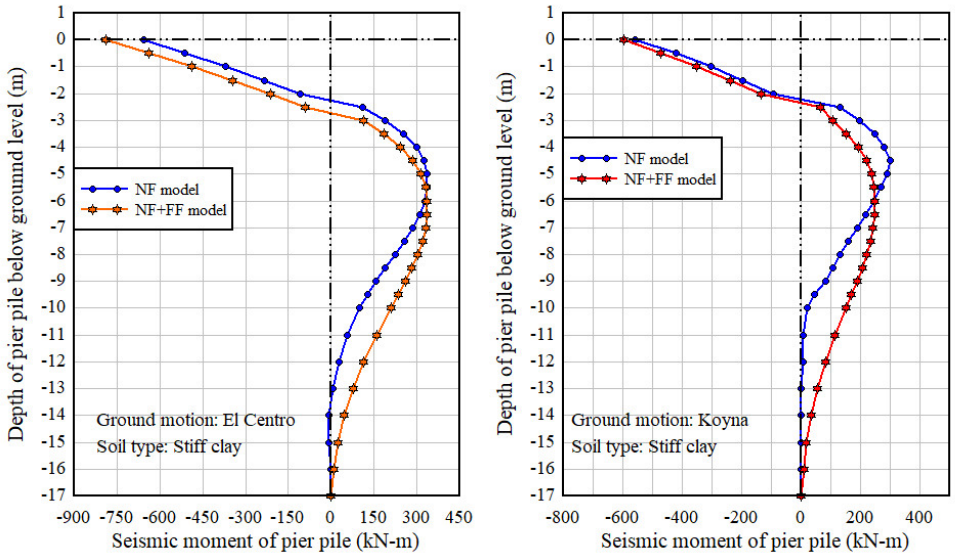

Fig. 4.38 Seismic moment of pier pile of NF and NF+FF model in stiff clay under El Centro and Koyna ground motion excitation.

The maximum seismic moment induced at the top of the pile is observed to be larger in NF+FF models, as compared to that of NF model which is in line with the larger deflection of pier pile in NF+FF model as observed earlier. However, it is found that in the pier piles in soft clay and stiff clay, there is insignificant difference

between the results from the models. Further, due to higher flexibility, the point of first inflection point from the top of the pile is also observed to be deeper in NF+FF model as compared to the corresponding NF models. Table 4.20 gives the comparative data of maximum transverse seismic moment induced in the pile under selected ground motion.

Table 4.20 Maximum seismic moment in pile supporting pier for NF and NF+FF model

Type of Foundation soil	Maximum transverse seismic moment in pier pile under ground motion (kN-m)			
	El Centro GM		Koyna GM	
	NF	NF+FF	NF	NF+FF
Soft Clay	695	648	695	693
Stiff clay	689	790	558	598
Loose Sand	467	789	444	775
Medium sand	343	538	345	473
Dense sand	241	385	311	395

From Table 4.20, it is observed that there is no significant difference in the seismic moment in the pile of the pier of NF+FF model with that of NF models of IAB in soft clay under seismic excitation of El Centro and Koyna ground motion. This is due to insignificant effects of the far field soil modelling in dynamic characteristics of IAB in soft clay, as observed in the case of pile deflection as well. An average increase in the range of 26%-74% in seismic moment of pier pile is recorded for the pile in loose, medium and dense sand under excitation of El Centro and Koyna ground motion. The highest increase recorded amongst the models is 74% in the NF+FF model of bridge in loose sand under excitation of both the ground motions. This increase is due to a combination of increased deformation and higher

participating mass ratio in NF+FF in first mode in the transverse direction as shown in Table 4.14.

Fig. 4.39 to 4.48 show the overall displacement time response histories of the bridge deck under action of selected ground motions. The excitations are applied in the transverse direction of the bridge founded on different type of soils.

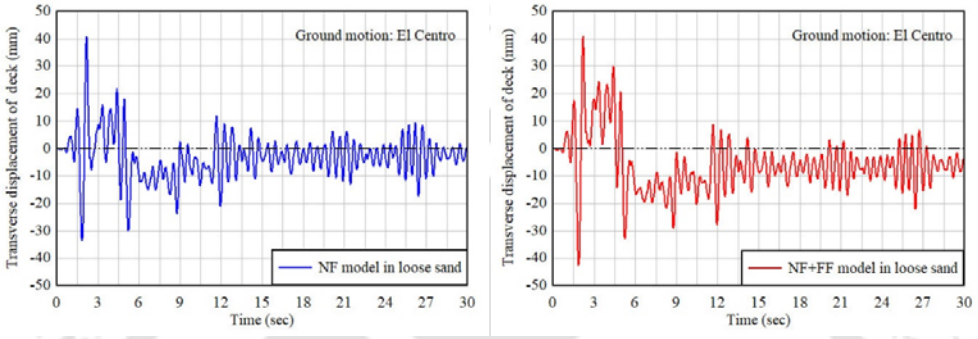

Fig.4.39 Response history at of bridge top of pier of NF and NF+FF model in loose sand under excitation of El Centro Ground motion

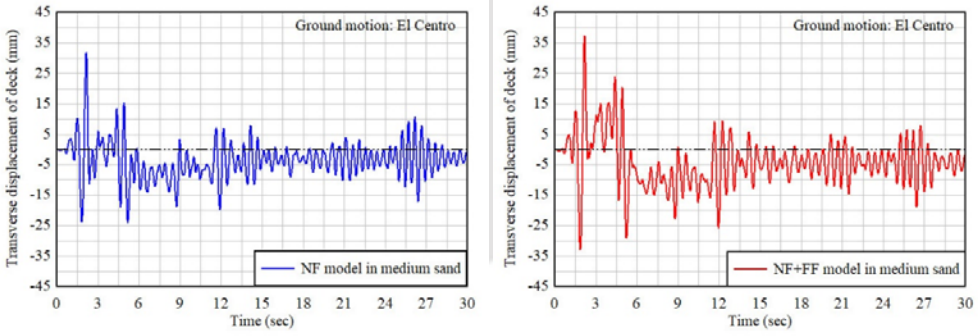

Fig.4.40 Response history at of bridge top of pier of NF and NF+FF model in medium sand under excitation of El Centro Ground motion

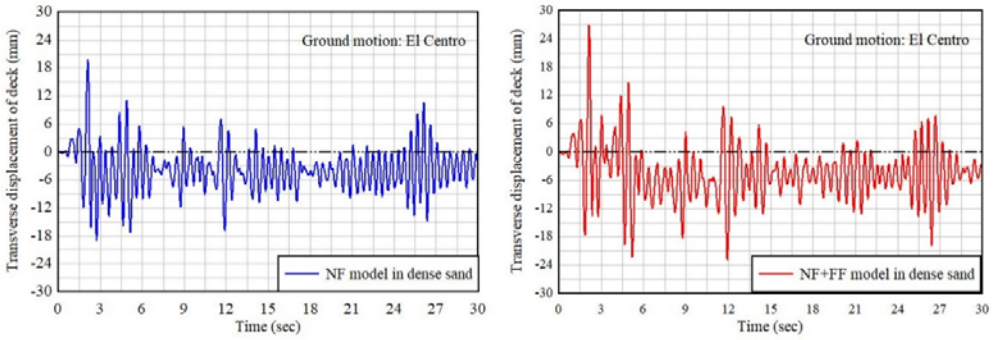

Fig.4.41 Response history at top of bridge pier of NF and NF+FF model in dense sand under excitation of El Centro Ground motion

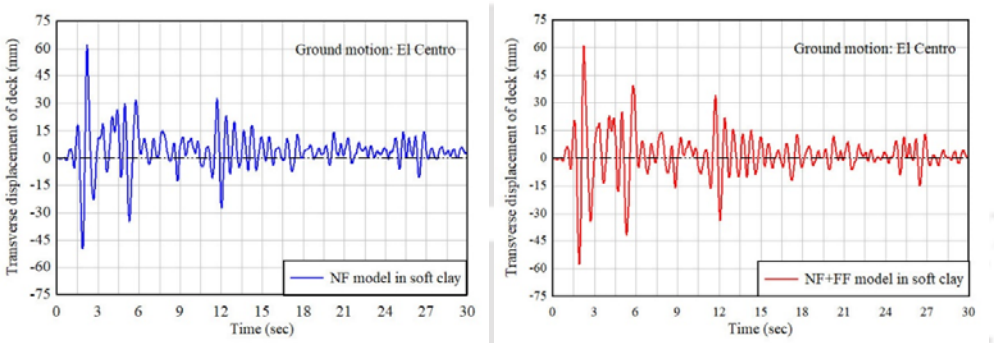

Fig.4.42 Response history at top of bridge pier of NF and NF+FF model in soft clay under excitation of El Centro Ground motion

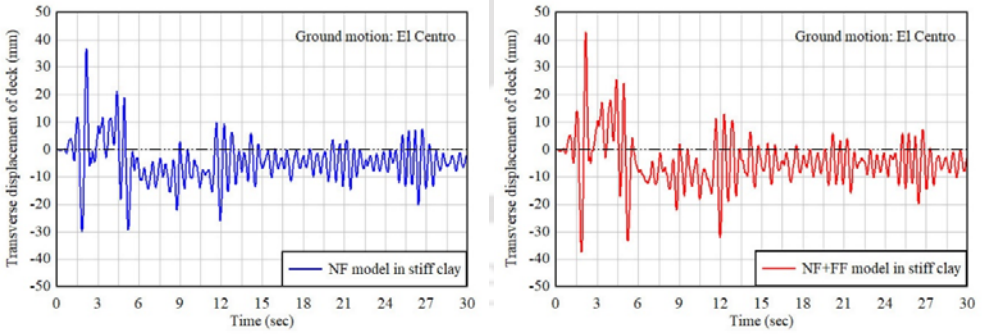

Fig.4.43 Response history at top of bridge pier NF and NF+FF model in stiff clay under excitation of El Centro Ground motion

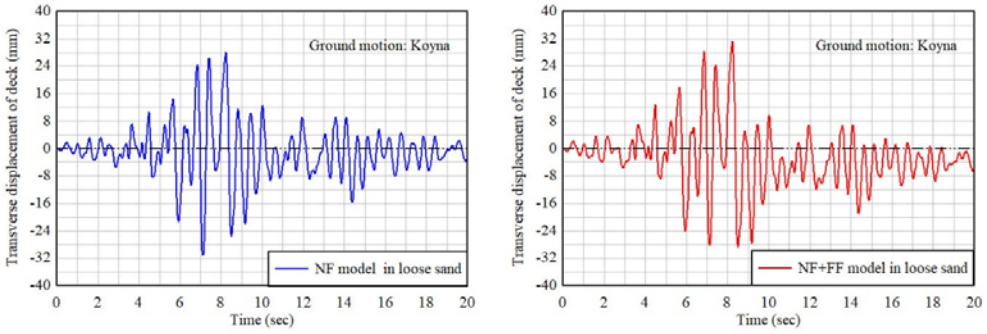

Fig.4.44 Response history at top of bridge pier of NF and NF+FF model in loose sand under excitation of Koyna Ground motion

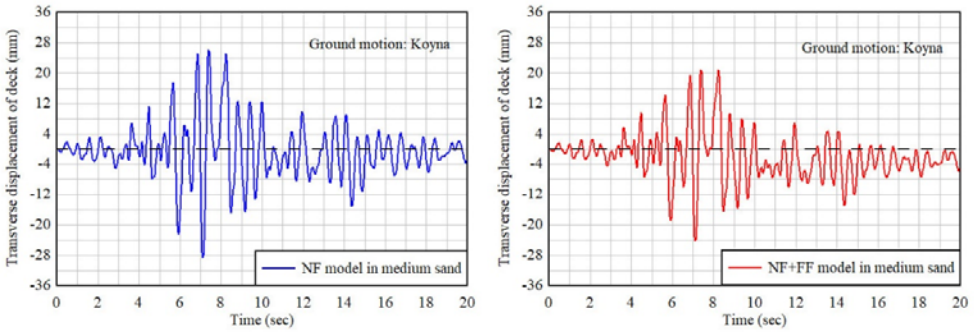

Fig.4.45 Response history at top of bridge pier of NF and NF+FF model in medium sand under excitation of Koyna Ground motion

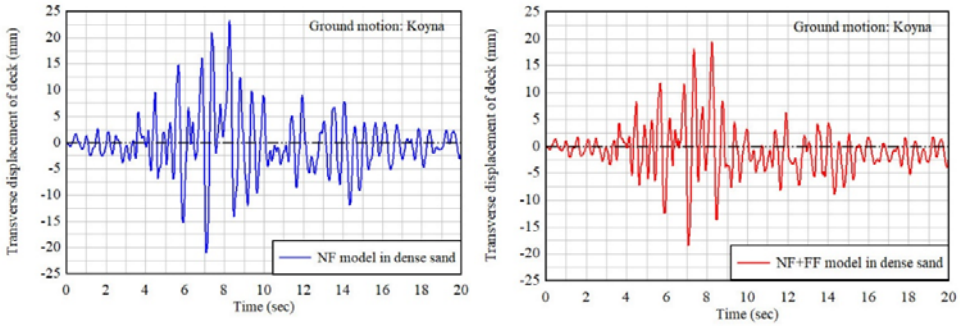

Fig.4.46 Response history at top of bridge pier of NF and NF+FF model in dense sand under excitation of Koyna Ground motion

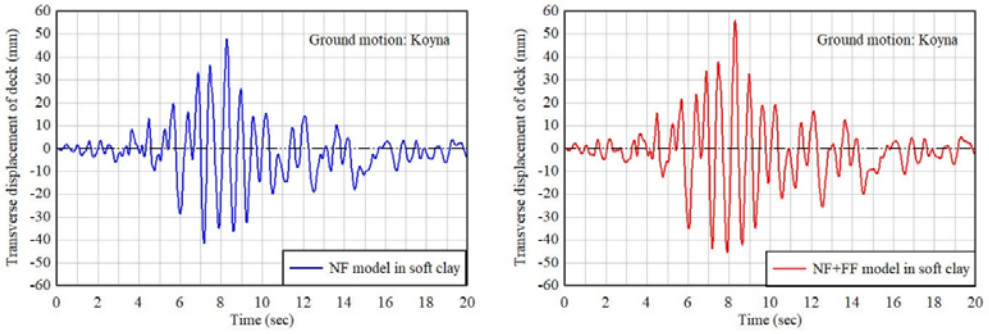

Fig.4.47 Response history at top of bridge pier of NF and NF+FF model in soft clay under excitation of Koyna Ground motion

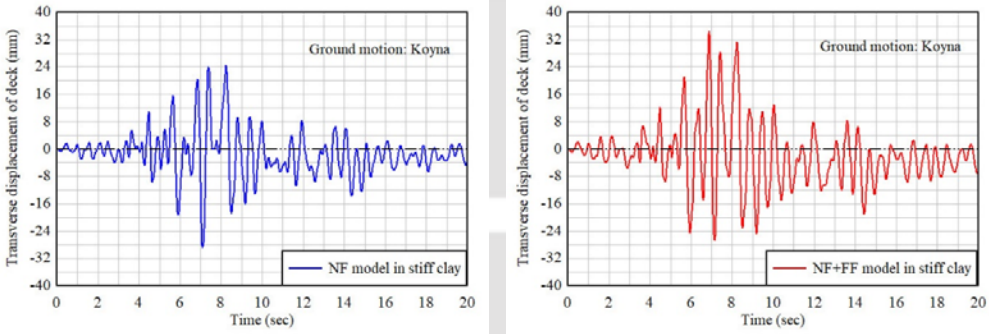

Fig.4.48 Response history at top of bridge pier of NF and NF+FF model in stiff clay under excitation of Koyna Ground motion

The displacement time history of pier from Fig. 4.38 to 4.48 indicates that at the level of excitation by the selected ground motion with PGA indicated at Table 4.17, the model of IAB founded on different types of soil yields, resulting in permanent deformation. This is manifested by the shifting of initial equilibrium of oscillation of the model during the course of ground excitation. It is observed that there is a trend of larger transverse deformation of pier in NF+FF models than that of the NF model in all types soils considered at the foundation level. Table 4.21 shows the maximum transverse displacement of the top of bridge pier of NF and NF+FF model.

Table 4.21 Peak transverse seismic displacement at pier top of NF and NF+FF model

Type of Foundation soil	Transverse seismic displacement at pier top under ground motion (mm)			
	El Centro GM		Koyna GM	
	NF	NF+FF	NF	NF+FF
Soft Clay	61.56	62.10	47.87	55.00
Stiff clay	37.94	41.97	28.17	34.55
Loose Sand	40.83	42.54	30.56	34.15
Medium sand	29.92	39.20	24.06	28.58
Dense sand	19.86	26.00	18.23	23.41

The displacement of the bridge pier is observed to be decreasing with the increase in the stiffness of the soil in foundation in both NF and NF+FF model. It is also observed that the transverse displacement in NF+ FF models are generally larger than that in the NF model.

The increased displacement of pier in NF+FF model is due to added increase in the flexibility of the bridge from the modelling of far field soil reaction in pile soil interaction. Maghaddasi et al. (2010) observed that the foundation flexibility causes total displacement of the structure to be more than that of the fixed based model. Table 4.22 shows the drift of pier of IAB founded on different types of soil under excitation of ground motion considered in transverse direction. The value of drift in NF+FF models of IAB under excitation of both the ground motion considered are observed to be higher than that of corresponding NF model irrespective of soil type in foundation. One of the reasons for the increase in drift of NF+FF model of can be attributed to the fact that although the increase in time period of NF+FF model is within the time period with constant acceleration, this increase in time period increases the spectral displacement of the pier. The increase in drift of pier in NF+FF model signifies potential of higher damage in the pier. This clearly

indicates that in the case of IAB in loose sand, medium and dense sand, ignoring far field soil reaction may provide erroneous results leading to under design of the bridge pier. The larger drift of model in loose sand is partly attributed to the higher PGA of ground motion in loose soil due to scaling which is adopted in the analysis of the model.

Table 4.22 Drift of pier of NF and NF+FF model under selected ground motion.

Type of Foundation soil	Drift of pier under ground motion (%)			
	El Centro GM		Koyna GM	
	NF	NF+FF	NF	NF+FF
Soft Clay	1.54	1.55	1.20	1.38
Stiff clay	0.90	1.05	0.70	0.86
Loose Sand	1.02	1.06	0.76	0.85
Medium sand	0.75	0.98	0.60	0.71
Dense sand	0.50	0.65	0.46	0.59

Further, the longitudinal displacements of the abutment are observed too small due to the restraining effect provided by abutment, abutment pile and backfill pressure. This restraining effect also reduces the deformation of the piers along the bridge axis as the deck is continuous along the length of bridge. Such reduction of deformation results in lesser vulnerability of the bridge to seismic damage along the bridge axis.

4.9 Thermal Load Analysis

The piles supporting the abutment and pier foundations are subjected to cyclic loading due to expansion and contraction of the superstructure under thermal variation. In the summer, the superstructure expands and pushes the abutment and pile towards the backfill and in winter, the superstructure pulls the pile of the abutment and pier in opposite directions. Consequently, the pile may be subjected

to one dominant cycle of displacement in each year due to seasonal (summer and winter) temperature changes. Additionally, the piles may also be subjected to numerous smaller cycles of displacement due to daily and weekly variation of the temperature. Dicleli (2003) recorded that, the amount of such daily and weekly cyclic displacement is around 20 to 40% of the yearly displacement. The daily and yearly variation of temperature in the locality, where the designed bridge is expected to be located, is shown in Fig. 4.49.

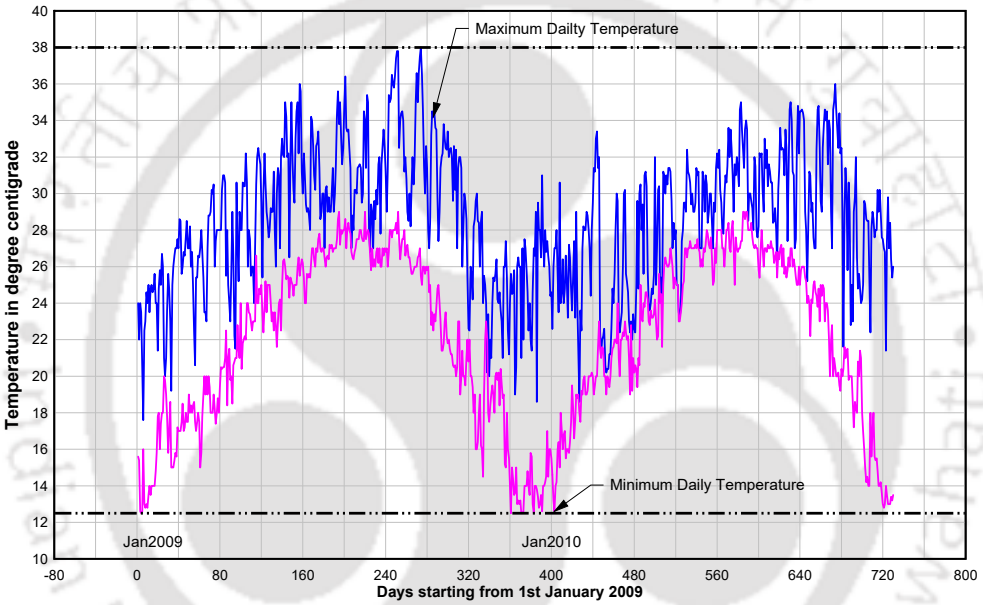

Fig. 4.49 Amplitude of yearly and daily variation of temperature at considered bridge site

The upper curve shows the maximum daily temperature recorded and the lower curve shows the minimum daily temperature recorded in the town. As may be seen from Fig. 4.49, the value of maximum temperature recorded at the place is 38 degrees centigrade and the minimum temperature recorded is 12.5^0 C. The daily variation of recorded temperature ranges from 2% to 50% of daily maximum value. The specification of the Indian Road Congress IRC:6 (2014) recommends a maximum and minimum bridge temperature of 37.5^0 C and 2.5^0 C respectively for the area. Thus, the maximum temperature recorded at the place almost matches

maximum temperature in the specification, but it somewhat deviates in case of minimum temperature where it is observed to be 12.0^0C. This is because the specification covers a wide range of areas adjoining the place of recording station of temperature. Therefore, for the present study, the value of seasonal variation of maximum bridge temperature of 37.5^0 C and a minimum temperature of 2.5^0 C as per IRC:6 (2014) is taken for the bridge. Dicleli (2003) and Kim and Laman (2010) adopted the yearly variation in estimating the thermal variation in their analysis on integral abutment bridge as daily analysis of variation is not easily manageable. Due to a long rainy season, the major construction activities of the bridge are carried out during the dry days of winter in the locality where the bridge is proposed. Further, concreting work in cold temperature below 10^0 C is avoided if no specific arrangement for curing is adopted. Thus, in the present study, for the generalization of the results of study, the temperature at which the superstructure is constructed is assumed arbitrarily as 20^0 C. With this value of temperature for construction of superstructure, the amplitude temperature variation affecting longitudinal expansion and contraction of deck is estimated as 17.5^0 C.

Furthermore, the bridge considered for analysis under thermal load has a composite deck (steel girder with the reinforced concrete slab) and they have different coefficient of thermal expansion. Therefore, to model the composite deck of the bridge for thermal load, an average coefficient for thermal expansion of the composite section is calculated adopting Equation (4.2) (Girton et al., 1991).

$$\alpha_{ave} = \frac{A_d E_d \alpha_d + A_g E_g \alpha_g}{A_d E_d + A_{sg} E_g} \tag{4.2}$$

where A_d is the area of concrete deck, A_{sg} is the area of steel girder, E_d is the modulus of elasticity of concrete deck, E_g is the modulus of elasticity of the steel girder, α_d is the coefficient of thermal expansion of the concrete deck materials and

α_g is coefficient of thermal expansion of steel girder. Taking the value of thermal expansion of the concrete, $\alpha_d = 10\times10^{-6}$ mm/mm/ ^{0}C, and the coefficient of thermal expansion of steel girder $\alpha_g = 1.2\times10^{-6}$mm/mm/^{0} C, the average thermal expansion coefficient of the bridge works out to be 1.08 $\times10^{-5}$ mm/mm/^{0} C. This average coefficient of thermal expansion has been adopted in the modelling of thermal load on the bridge and in computation of unrestrained theoretical expansion of the bridge.

The deck of the bridge considered in this study is also integrated with the pier. Thus, the thermal expansion or contraction load shall induce deformation on the abutment and pier, the value of which will depend on the length of the deck from the centre of the bridge to pier and abutment respectively. The thermal load on the bridge is applied on the longitudinal girder modelled with an average coefficient of thermal expansion, as calculated from Equation (4.2). Thippeswamy et al. (2002) observed that in the case of IAB with pile foundation or with spread footing hinged at the base of abutment, the stresses induced in the foundation due to creep and shrinkage of deck as well as thermal gradient across the depth of the deck is negligible. Hence, only the component of uniform effective temperature of the girder is considered in the analysis. The nonlinear static (Pushover) method is adopted in the analysis considering the deformed condition of the bridge under dead load. The additional axial force on the pier and abutment due to transient live load on the bridge is also not considered during the pushover analysis, to be on the conservative side, while evaluating displacement capacity of the pier and abutment. The unrestrained theoretical expansion of the bridge under the maximum temperature amplitude of 17.5^0 C expected to be loaded to each abutment is obtained from the relation as:

$$\Delta L = \alpha_{ave} \Delta T \frac{L}{2} \tag{4.3}$$

While working out the unrestrained theoretical expansion of the deck, the long-term effect of the girder, like creep and shrinkage and the effect of the girder deflection due to external load in the longitudinal expansion of the deck is not considered. The displaced shape of the bridge under thermal expansion of 17.5^0C is shown in Fig. 4.50

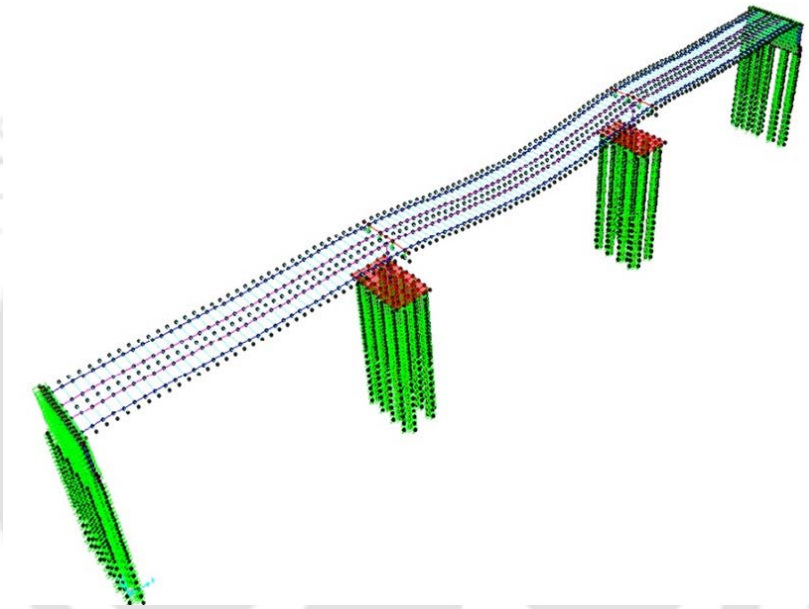

Fig. 4.50 Deformed shape of bridge under thermal expansion loading

The comparison of theoretical deck expansion with the computed displacement of abutment and pier due to rise of temperature of deck by 17.50^0 C is shown in Table 4.23 and Table 4.24. The displacement of abutment and pier of the bridge do not vary significantly with different type of soil in the foundation as may be observed from Table 4.23 and 4.24. This is because, the displacement of abutment is affected by the stiffness of backfill materials (Faraji et al. 2001, Dicleli and Albhaisi, 2003, Dicleli and Albhaisi, 2004, Kim and Laman, 2010) and all the bridges with different soil types in the foundation have the same dense sand backfill behind the abutment.

Table: 4.23 Displacement of abutment top from analysis under thermal loading

Unrestrained theoretical Expansion of deck	Displacement of abutment due to rise of temperature of deck17.5^0 C				
	Loose sand	Medium sand	Dense sand	Soft clay	Stiff clay
11.47 mm	6.38 mm	7.08 mm	7.75 mm	6.39 mm	6.35 mm

Table: 4.24 Displacement of pier top from analysis under thermal loading

Unrestrained theoretical expansion of deck up to location of pier	Displacement of pier top due to rise of temperature of deck 17.5^0 C				
	Loose sand	Medium sand	Dense sand	Soft clay	Stiff clay
6.27 mm	3.10 mm	3.30 mm	4.10 mm	3.9 mm	3.87mm

The properties of the soil surrounding the pile do not have a significant effect on the displacement of abutment in this study and similar results were also been observed by Faraji et al. (2001).

Table 4.23 and Table 4.24 indicate that the actual displacement of the abutment and pier is lower than the theoretical expansion of deck at the location of pier and abutment location. This lower displacement is due to the restraining effect of the abutment, backfill, pier integrated with the deck. Concrete piles in supporting the abutment and the combination abutment with backfill provides high lateral stiffness on account of which the displacement of the abutment along longitudinal axis reduces (Kim and Laman, 2010). Fennema et al. (2005) has also observed a displacement of 4.80mm in the abutment of an instrumented IAB against theoretically calculated thermal movement of 20.0 mm. The abutment considered was instrumented and had an average height of 4390 mm supported by H-piles. Further, the displacement of pier is restrained through strut action of deck in between the abutments. In the field performance evaluation of Orange-Wendell

bridge in Massachusetts, USA, Breña et al. (2007) also observed displacement of abutment that ranged between 30% to 60% of the theoretical displacement.

Fig. 4.51 (a) shows the displacement of the abutment along with the pile supporting abutment under thermal expansion due to variation of temperature by 17.5^0 C. The primary mode of movement of abutment is observed to be by rotation about the base of the abutment which is consistent with the observation of Fennama et al. (2005). The variation of deflection of the pile founded on different types of soil is observed to be not significant. The deflection of the pile below the abutment is affected by lateral stiffness of pile as well as the amount of movement of abutment in the form rotation about its base. Since the deflection of the abutment is restrained by backfill pressure, the amount of deflection induced in the pile on account of rotational movement of abutment is insignificant to cause damage to the concrete pile supporting the abutment. The amount of deflection in the abutment pile at about 6.0 m below the base of abutment can be ignored since the amount is too small to cause significant stress in the pile. Fig. 4.51(b) shows the simultaneous deflection of pier pile during the expansion of the bridge under the variation of temperature by 17.5^0 C. The amount of deflection of the pier pile is observed to be too small to cause significant stress in the pile. Further, Fig 4.52 (a) and 4.52 (b) shows the moment induced in the abutment and pier pile by thermal expansion due to rise of temperature by 17.5^0 C respectively. The moment induced in the abutment pile in different type of soil do not vary significantly in the present study. However, moment in the pile in stiffer soil tends to be higher than the pile in softer soil. The maximum moment in the pile is observed to occur at the top of pile i.e. the point of connection with the abutment. The point of inflection of the moment is located at a depth of around 7.00 m, which is eight times the diameter of the pile. Similarly, the

moment induced in the pier pile also tends to be higher in the pile in stiffer soil. The maximum moment of the pile occurs at the top as well as at a depth of around 4.0 m from the top. However, the maximum moment in the pier pile is too small to cause structural damage to pile considering the flexural capacity of the pier pile.

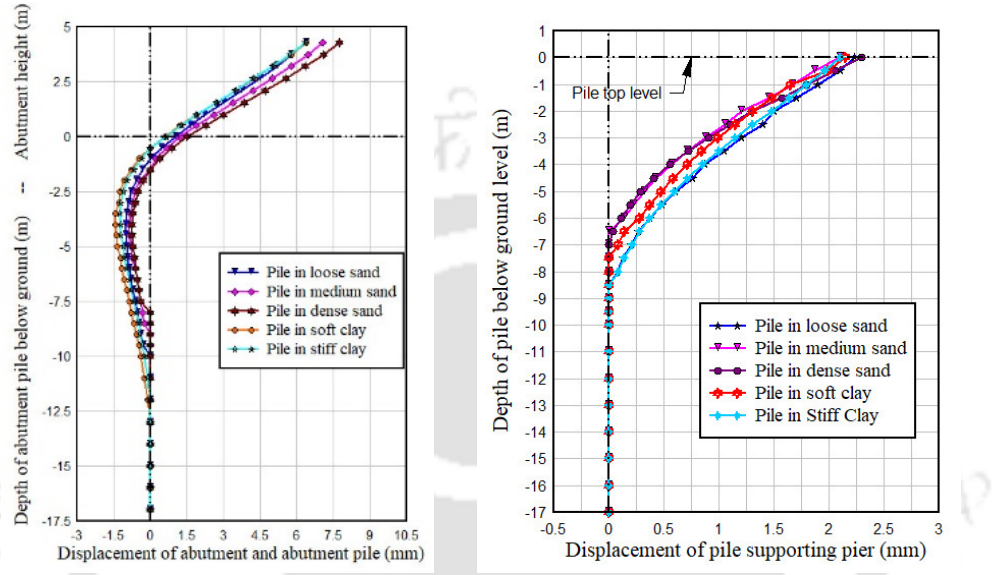

(a) (b)

Fig. 4.51 Displacement of (a) abutment and abutment pile (b) pier pile under thermal expansion for rise of temperature by 17.5^0 C

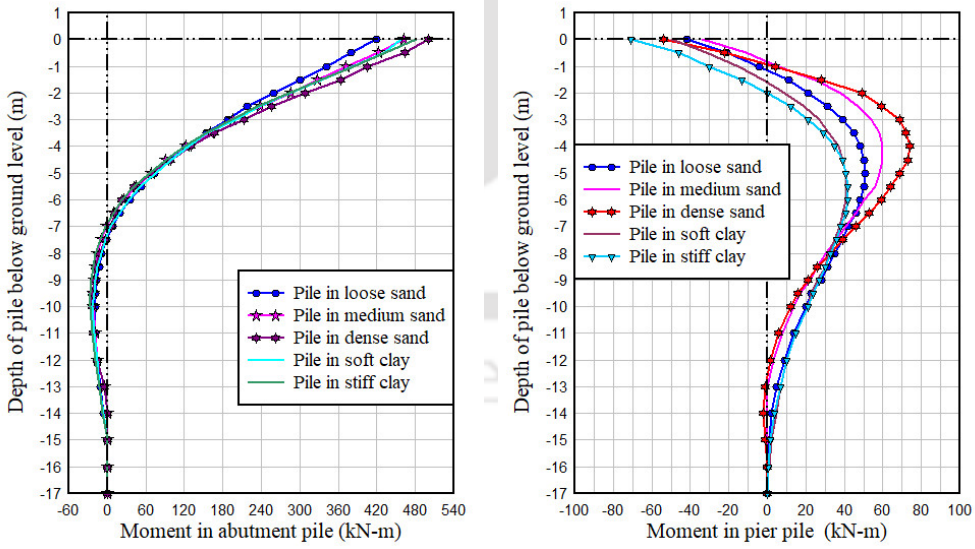

(a) (b)

Fig. 4.52 Moment in (a) Abutment pile and (b) Pier pile under thermal expansion due to rise temperature by 17.5^0 C

Fig. 4.53 shows the moment induced in the abutment wall by thermal expansion of deck due to rise of temperature considered. There is a marginal increase in the moment in abutment with increase in the stiffness of the soil surrounding the pile. This is attributed to the larger restraint provided at the base of the abutment while its top moves with the expanding deck. Similar results were also observed by Dicleli (2003), during the parametric study carried out to evaluate the effect of soil modulus in abutment displacement and moment.

Further, exercises are carried out to assess how the computed moment induced by thermal expansion compares with the capacity of pier and abutment. The cyclic strains induced in the in abutment and abutment pile are desired to be limited within elastic limit to avoid damage due to of low cycle fatigue. Therefore, the approach of assessment is carried out with a target elastic strain limit in rebar of concrete.

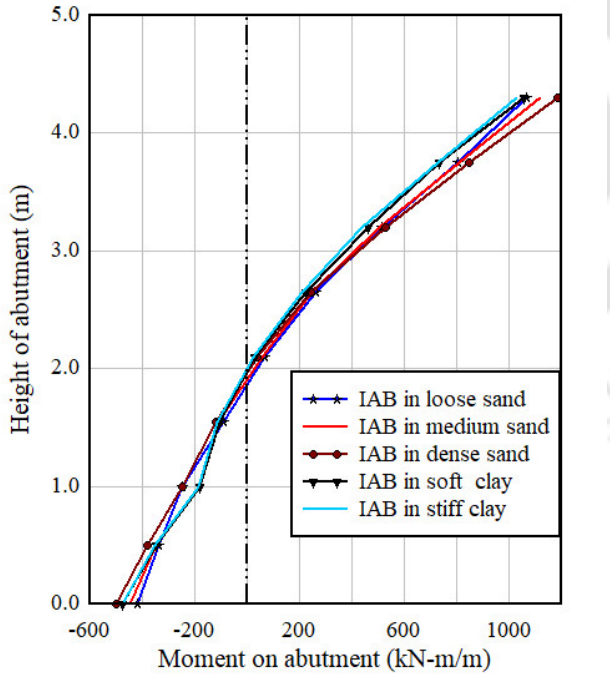

Fig. 4.53 Moment induced in abutment wall by thermal expansion of deck due to rise of temperature by 17.5^0 C.

Priestley et al. (2007) indicated that the structural element with compression gravity load (Wall and column), a maximum tensile strain of 0.015 during seismic response corresponds to the residual cracks of 1.00 mm which should not need any remedial action under normal condition. In addition, in the bilinear idealization of moment curvature for design purpose Priestley et al. (2007) defined the point of first yield point as the point on the moment curvature when the extreme tension reinforcement attains the yield strains, or the extreme concrete compression fiber attains a strain of 0.002, whichever occurs first. Thus, limiting the compressive strains of concrete to 0.002 and tensile strains to yield strains of rebar ($\epsilon_y = f_y/E_s$), the minimum curvature out of the two conditions is computed for the concrete pile and the abutment wall as the first yield curvature ($\emptyset_{y1}$). The neutral axis is computed for computation of curvature is done by using the relation derived by Dutta and Mander (1998), which is also recommended in "Seismic Retrofitting Manual for Highway Structure - part 1" (Buckle et al. 2006) as

For circular section:

$$\frac{c}{D} = \frac{1}{\beta_c}\left[\frac{\frac{P_e}{f_c' A_g} + 0.5\rho_t \frac{f_y}{f_c'}\left(\frac{1-\frac{2c}{D}}{1-\frac{2d'}{D}}\right)}{1.32\alpha_c}\right]^{0.725} \tag{4.4}$$

For Rectangular section:

$$\frac{c}{D} = \frac{\left(\frac{P_e}{f_c' A_g}\right) + \left(\frac{\gamma\rho_t \frac{f_y}{f_c'}}{1-\frac{2d'}{D}}\right)}{\alpha_c\beta_c + \frac{2\gamma\rho_t \frac{f_y}{f_c'}}{1-\frac{2d'}{D}}} \tag{4.5}$$

The c and γ in this equation represent depth of neutral axis and reinforcement configuration factor respectively. The value $\gamma = 0.0$ is adopted for wall section bending about the weak axis. The corresponding moment capacity at the first yield curvature is computed taking the gross section properties of the component and the effective elastic modulus of the concrete $E_{c,eff}$ allowing creep effect using the relation as:

$$M = E_{c,eff} I_g \emptyset_{y1} \tag{4.6}$$

For the present calculation, the value of secant modulus (E_{cm}) of M30 and M35 grade of concrete is adopted as 31GPa and 32GPa respectively (IRC:112, 2011). The creep coefficient (φ_t) calculated using recommendation in IRC:112 (2012) works out to 1.0 for abutment as well as for the concrete pile. The resultant value of effective modulus of elasticity of the concrete is calculated as 15.5GPa and 16.0GPa for M30 and M35 respectively. The computed moment capacity of the abutment and concrete pile corresponding to the first yield curvature are shown in Table 4.25.

Table 4.25 Thermal moment and Moment capacity corresponding to first yield curvature in abutment and pier

Component of IAB	Maximum moment induced by thermal expansion	First yield curvature ($\emptyset_{y1}$)	Moment capacity corresponding the $\emptyset_{y1}$
Abutment	1185 kN-m/m	0.0028/m	3615 kN-m/m
Pile	500 kN-m	0.0042/m	2156 kN-m

On examination of the values Table 4.25 it is clearly evident that the moment induced due to thermal load are much below the corresponding moment capacity at first yield curvature. Therefore, strain in the concrete pile, abutment wall and pier are expected to be within the elastic limit and not vulnerable to low cycle fatigue

due to cyclic thermal deformation. This is because the low cycle fatigue failure in a material is due to a relatively small number of load or deformation cycle and typically involves large deformation that exceeds elastic limit (Brown and Kunnath, 2000), whereas in the present case the stresses are quiet expected within the elastic limit.

Furthermore, the safe deflection of the abutment is also estimated by using the first yield curvature of the pile. The deflection pattern of the abutment with pile as shown in Fig. 4.51(a) indicates that the abutment rotates about its base while deflecting under thermal expansion of deck. The bottom of the abutment is connected to a pile in the form of a pile cap with detailing for rigid behavior. Hence, the plastic hinges are expected to form at the top portion of the concrete pile below the cap under excessive deflection of abutment, if any. Therefore, the allowable safe deflection at the top of abutment is estimated by substituting the value of first yield curvature of concrete pile in the relation for computation of yield displacement of pier using curvature as (Priestley et al. (2007):

$$\Delta_{y1} = \emptyset_{y1} \frac{\left(H + L_{sp}\right)^2}{3} \tag{4.7}$$

The height of abutment (H) up to the centroid of the deck is 4.30 m and the strain penetration is estimated using the relation $L_{sp} = 0.022 f_y d_{bl}$ (Priestley et al.,2007). The allowable safe deflection of the abutment at near elastic response computed using Equation (4.7) works out to 29.12 mm, which is higher than the actual deflection recorded and also higher than the theoretical unrestrained expansion of the deck. The allowable length of IAB with the present configuration of bridge is estimated by rearranging Equation (4.3) and adopting average coefficient of thermal expansion of deck ($\alpha_{ave} = 1.08 \times 10^{-5}$ mm/mm/degree C), a rise of temperature (ΔT) by 17.5^0 C and an allowable deflection (ΔL) equal to 29.12mm.

The allowable length of IAB estimated with these data works out to be 308 m, whereas the length of bridge constructed is 120.00 m. It is observed that the allowable length of IAB considering the expansion of the deck due to the rise of bridge temperature depends on the height of abutment, flexibility of the pile supporting the abutment, amount of thermal variation and backfill pressure. As reported by Burke Jr. (2009), IAB of length 152.4 m to 243.8 m were constructed in Kansas, California, Colorado and Tennessee. Tennessee DOT also constructed Happy Hollow Creek Bridge of seven span prestressed concrete curved IAB of total length of 358m using tall flexible pier and abutment supported on single row of H Piles. In order to have an approximate basis for estimating length of IAB with concrete pile foundation in abutment before detailed analysis and design, the yield curvature relation provided by Priestley et al. (2007) is adopted. The yield curvature for circular column is computed as (Priestley et al.,2007)

$$\emptyset_y = \frac{2.25\,\epsilon_y}{D} \tag{4.8}$$

The ratio of first yield and yield curvature ($\emptyset_{y1}/\emptyset_y$) computed with the data of sectional properties of pile foundation in abutment for the present configuration works out to 0.669. Rounding up this value arbitrarily to a lower value of 0.50, to be on the conservative side, the value of first yield curvature is taken as half of the yield curvature ($\emptyset_{y1} = 0.5\emptyset_y$). The approximate relation for estimating the allowable length of IAB, by rearranging the Equation (4.3) and calculating allowable safe deflection of abutment based on the first yield curvature of the concrete pile, is derived as:

$$L_{IAB} = \frac{\emptyset_y H^2}{3\alpha_t \Delta T} \tag{4.9}$$

In the Equation (4.9) the length of strain penetration is ignored. The allowable length computed using Equation (4.8) with $\alpha_{ave} = 1.08 \times 10^{-5}$ mm/mm/^{0} C and $\Delta T = 17.5^0\ C$ for the present configuration of composite deck is 203 m. The allowable length with concrete deck having $\alpha_t = 10 \times 10^{-6} mm/mm/^0$ C the present configuration of substructure works out to 220 m. However, in order to use the Equation (4.8) for estimation of allowable length of IAB, the minimum grade of concrete in the pile shall be M35 and the average volumetric ratio of main reinforcement shall not be less than 2% as the neutral axis of section for calculation of first yield curvature are based on these parameters. Further, the abutment should be configured to have more flexural stiffness than those of piles.

4.10 Concluding Remarks

In this chapter, 3-D finite element of model of IAB is developed incorporating soil pile interaction and abutment backfill interaction. Two categories of model, viz. NF and NF+FF models were developed to study the effects of incorporation of far field soil reaction on dynamic characteristics of IAB. Based on the results of modal analysis, nonlinear time history analysis and thermal load analysis of these models of IAB, the following observations are recorded:

1. The incorporation of far field soil reaction in the modelling of soil pile interaction (NF+FF models) increases the flexibility of the foundation and bridge as a whole, resulting in a longer period of vibration. The overall transverse displacement of pier of IAB in NF+FF models is higher than that in the NF model irrespective of type of soil in the foundation.
2. The variation of seismic forces on pile in soft clay and stiff clay are less sensitive to the incorporation of far field soil reaction modelling in soil pile interaction. However, in the case of NF+FF models of IAB in loose, medium

and dense sand, the seismic design moment in the pile is observed to increase by a significant amount as compared to that of the NF model. In addition, the drift of pier in transverse direction also increases significantly in the NF+FF models. Hence, the estimation of design forces from NF model of IAB for design may lead to unsafe design of piles and pier of IAB.

3. The abutment with backfill exhibits stiff response to longitudinal seismic excitation, thereby reducing longitudinal seismic displacement. Therefore, the seismic forces in longitudinal direction are observed to be not critical for design of pier and pile of IAB.

4. For the thermal variation of 17.5^0 C considered in the analysis, the displacement in pier and abutment due to the thermal expansion of deck under study is lower than the theoretical unrestrained expansion. The thermal moment induced in the pile and abutment are much below the elastic moment capacity of abutment wall and pile. The strain induced by thermal load on piles and abutment are therefore, expected to be well within elastic range. The resulting strain fatigue life of the rebars are expected to be higher than the design life of the bridge.

5. In the IAB with present configuration of abutment supported with concrete pile, the displacement of the abutment wall under the thermal load is observed to be primarily in the form of rotation of abutment about its base. The allowable deflection of the abutment, which is one of the primary factors affecting the allowable length of IAB, depends on the height of abutment and flexibility of the supporting pile foundation. The approximate allowable length of IAB for a particular configuration can be estimated by computing

the allowable safe deflection of abutment using section curvature analysis of pile with a specified target strain.

Chapter 5

Structural Response Control of Integral Abutment Bridge using Sleeved Pile

5.1 Introduction

The principle of lengthening the period of vibration of structure by increasing its flexibility concepts for reduction of transmissibility of ground motion to the structure is well accepted concept in the earthquake response control of structure. Therefore, the concept of increasing the time period of vibration and enhancement of energy dissipation capacity of a structure are regarded as a very attractive way of improving the seismic resistance. In the case of IAB the deck of the bridge is integrated to abutment and hence the traditional method of dissipation of energy by installing isolation in between the abutment and superstructure may not be feasible, while keeping the typical configuration of the bridge type. Therefore, one of the strategies for lengthening the vibration period of IAB is to introduce added flexibility in the foundation. This can be achieved by using the concept of sleeved pile which would provide flexibility at the base of foundation. The sleeved pile is comprised of a pile within a sleeve having inner diameter substantially larger than the outer diameter of the pile to allow free lateral movement of the pile within the sleeve. The pile inside the sleeve is supported either by embedding it in the concrete fill in the sleeve up to some depth below the grade level or by pile to sleeve connection at discrete points along the elevation. Alternatively, the sleeved pile is also constructed by wrapping the pile with compressible sheet so that it does not experience the restrain or transfer lateral force to the surrounding soil. The principal function of the sleeve is to provide a pile of unsupported length, thereby achieving flexible and low stiffness response to horizontal loading. The sleeved pile also

permits transfer of horizontal reaction from the pile to the soil well below the ground surface where the soil resistance to the lateral forces are substantially higher than those near the ground level.

In this chapter introduction of sleeved pile is explored with the objective of enhancing the performance of the bridge under seismic excitation. The influence of sleeved pile in dynamic characteristics of the IAB is studied by developing models of IAB with different installation process of sleeved pile in abutment and pier foundation. In addition, the effect of sleeved length and founding soil types on the dynamic characteristics of the IAB is also studied. Based on the results of parametric studies on the dynamic characteristics of IAB with sleeved pile, a design methodology is proposed for sleeved pile foundation of the bridge. Further, linear and nonlinear dynamic analyses are carried out for computation of the seismic response of IAB with sleeved pile founded on different founding soil type for comparison with those of IAB without sleeved pile. The response of IAB with sleeved pile subjected to thermal loading is also studied for observing the beneficial effect of sleeved pile in the overall performance of the bridge under thermal load.

5.2 Structural Arrangement of Sleeved Pile Foundation

Holley, Jr. et al. (1973) presented a concept for the sleeved pile for adoption in offshore structures with an objective to achieve bending flexibility of the pile to minimize shear and bending stresses. This was also intended to accommodate lateral displacement of the superstructure due to thermal expansion or contraction. The structural arrangement of sleeved pile presented by Holley, Jr. et al. (1973) is shown in Fig. 5.1.

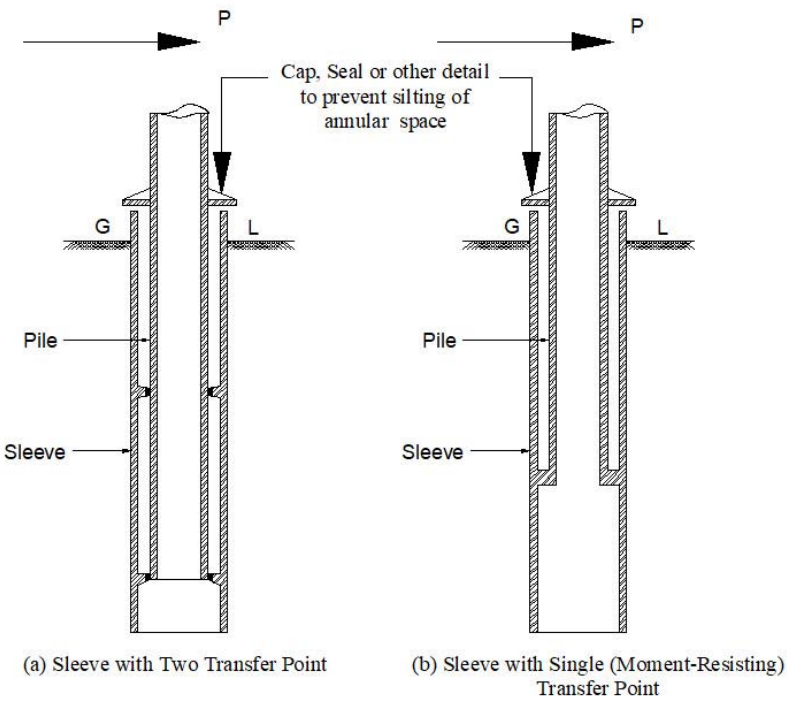

Fig. 5.1 Sleeved pile construction in offshore structure (Holley Jr, et al. 1973)

The sleeve has an inner diameter sufficiently in excess of the outer diameter of the pile enclosed by the sleeve to prevent contact between the two, except at the designed force transfer point. Two options for design of force transfer points were suggested. In the first option as shown in Fig 5.1(a), the transfer of force from pile to sleeve and to the soil is affected at two points located at different elevations by placing a diaphragm between the pile and the sleeve. In the second option as shown in Fig.5.1(b), the transfer of force from the pile to the sleeve and in turn to the soil is at only one point located at an elevation above the bottom of end of sleeve and the connection is designed to transfer both the lateral and bending forces at these points.

Raupach et al. (1981) proposed a concept of sleeved pile for providing flexible subsurface foundation of building as shown in Fig. 5.2 for aseismic design of building.

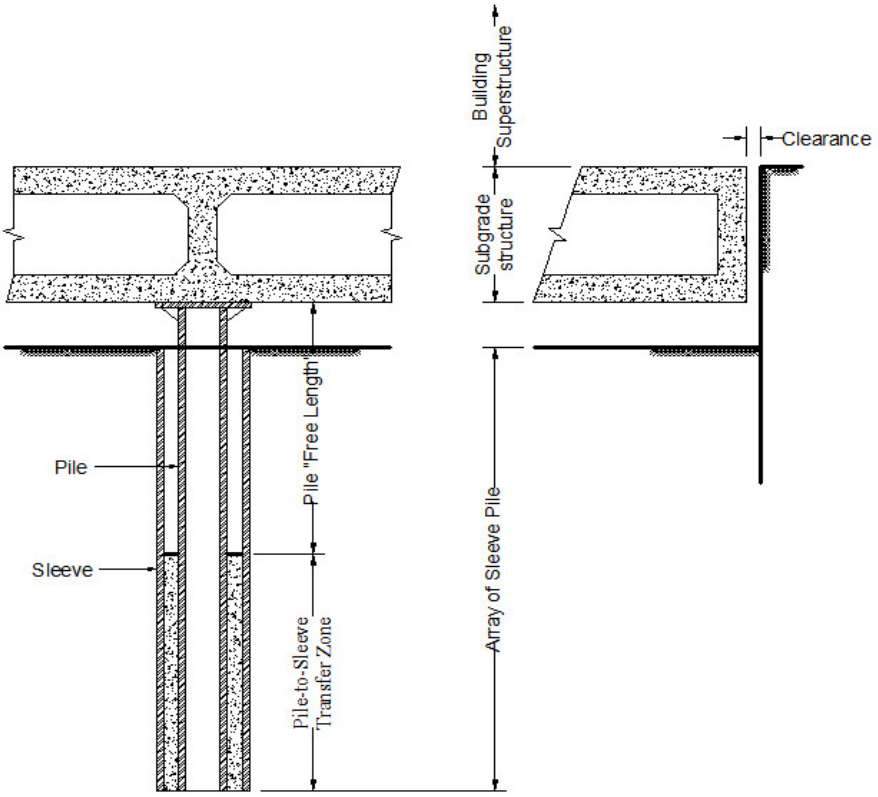

Fig. 5.2 Schematic diagram of building on sleeved pile (Raupach et al., 1981)

The arrangement of a sleeve substantially of larger diameter is arranged to permit large bending deformation in the pile without excessive stresses and strains. The steel pile in the sleeve is extended up to the required depth. Thereafter, the gap between the pile and casing is filled up with concrete up to the bottom level of free length of the steel pile. The load transfer from the steel pile to the casing and in turn to the soil takes place in the embedment portion of the steel pile in the concrete. The sleeved pile was assumed to be fixed at the top level of concrete infill for the purpose of analysis and design.

Boardman et al. (1983) developed a concept of the sleeved pile as shown in Fig. 5.3 which was implemented in the construction of the Union House, New Zealand in 1983. The building was designed to minimize ductility demand of each individual member in the superstructure by providing energy dissipators and bracings within the structures. To allow the dissipators to function, the base of the superstructure had to be free to move, which was achieved by the use of long sleeved pile pinned as shown in Fig. 5.3.

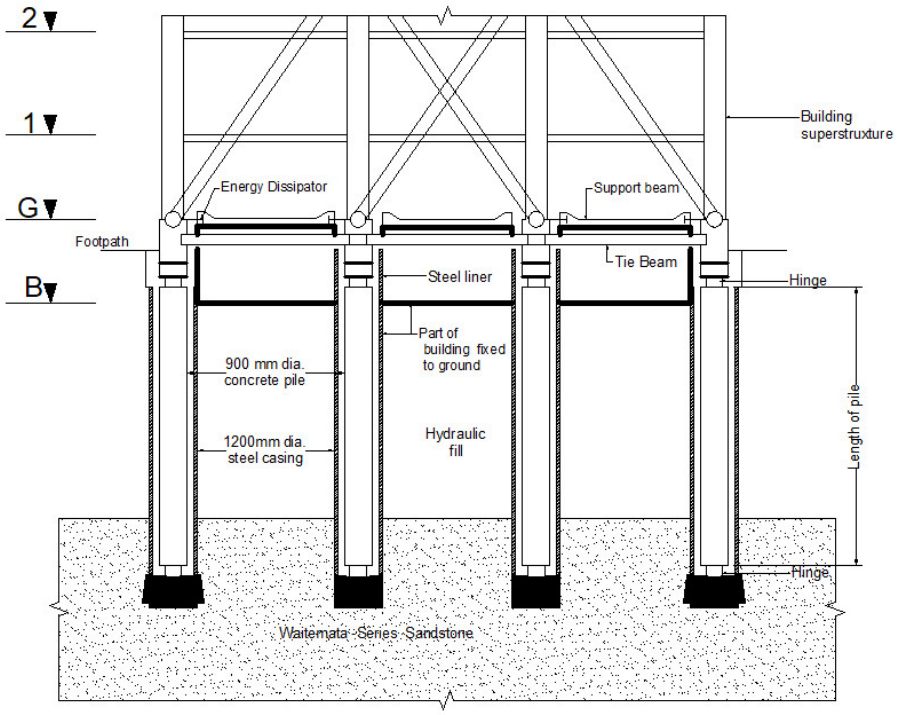

Fig. 5.3 Arrangement of sleeved pile in Union House in Auckland, New Zealand (Boardman et al.1983)

In the construction, the steel casing was provided for the full depth of pile so that the piles behaved like flexible energy dissipators under seismic forces. It was reported that during the design process of the building, the analysis had been carried out by removing the dissipators and supporting the building laterally only with the

flexible sleeved piles. The results of the analysis indicated an almost perfectly isolated state of the building with virtually no lateral load. However, the relative deflection between the ground and the structure was too large to be accommodated in the design (Boardman e al.1983).

The proposed arrangement of the sleeved pile to be adopted in the present study in the foundation of the bridge pier and abutment is shown in Fig. 5.4.

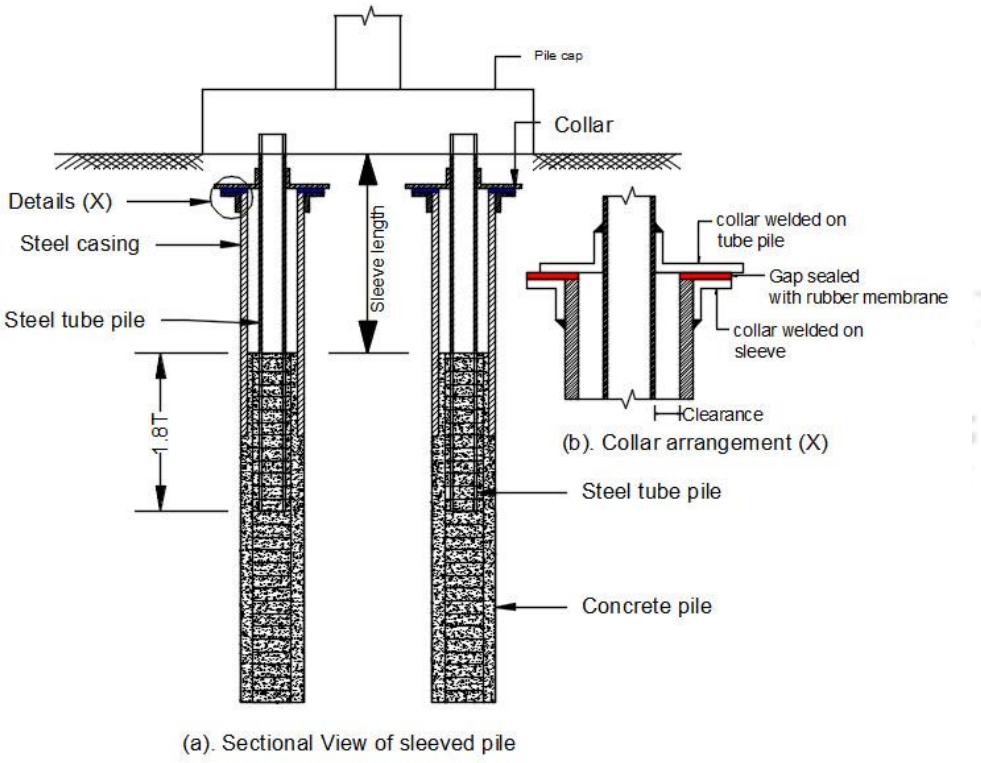

Fig.5.4 Proposed of arrangement of sleeved pile for bridge in the present study

In the proposed arrangement of sleeved pile assembly, the bottom portion of the pile shall be of concrete and the top portion shall be of steel tube pile. The diameter of the concrete pile shall be substantially larger than that of the outer diameter of the steel tube pile. The bottom end of the steel tube pile shall be embedded in to the bottom concrete pile up to a designed depth and the top end shall be embedded into

the pile cap. The portion of steel tube pile from the top of concrete pile to the bottom level of pile cap shall be sleeved inside a steel casing as shown in Fig. 5.4. The casing will prevent the interaction of steel tube pile with surrounding soil enabling the same to behave as free-standing pile. The free-standing length of pile sleeved inside the casing is denoted as sleeve length. The theoretical depth of fixity of the pile embedded in soil is taken as $1.8T$, where T is the characteristics length of pile (Barker et al., 1991). Hence, in the present arrangement, the bottom end of the steel tube pile is proposed to be embedded for a length equal to 1.8 times the characteristics length of concrete pile. Further, apart from the requirement from structural capacity, the diameter of the bottom concrete pile shall also be adjusted to allow the steel tube pile to be inserted within the core concrete without interfering with the main longitudinal reinforcement and circular lateral reinforcement. The clearance provided should also be adequate to facilitate concreting with appropriate compaction.

The construction of the sleeved pile shall be done by boring hole for the pile with designed diameter of concrete pile. After the completion of boring up to the designed depth, the reinforcement of the pile shall be inserted in the hole and concreting of the pile shall be initiated. When the concreting reaches the designed bottom level of embedment of the steel tube pile, the same shall be inserted inside the reinforcement and concreting shall be continued. Further, when the concreting reaches the proposed bottom level of the casing, the same shall be inserted and concreting inside the casing shall be continued up to the bottom level of sleeved length. In order to prevent entry of silt and sand in the clearance between the casing and the pile, two collars, one to steel tube pile as top collar and other to the casing as bottom collar are welded as shown in Fig. 5.4 (b). A small gap between two

collars is maintained, which is filled with rubber membrane is provides so as to allow relative displacement under seismic excitation.

5.3 Dynamic Analysis of Integral Abutment Bridge with Sleeved Pile

Modelling of superstructure and substructure of IAB with sleeved pile is exactly the same as that of IAB with conventional pile as presented in Chapter 4. Modification is carried out in the modelling of soil pile interaction. In the IAB with sleeved pile, the portion of the sleeve length of the pile do not come in contact with soil and hence do not experience resistance from the soil stressed due to lateral deflection of pile. Therefore, soil springs modelled using $p - y$ curve representing the lateral soil pile interactions are removed from the sleeve length portion in the model. Further, with the objective of studying the influence of sleeved pile and its sleeve length on the dynamic characteristics of IAB two categories of models are developed. In the first category, the abutments at both end is supported on concrete pile and the piers are supported on sleeved pile. This first category of the model is classified as Model-1. Multiple models of this category are developed by increasing the sleeved length from initial length of 2.5m to 6.50m with increment of 0.50m in subsequent model. Further, to observe the influence of the soil type in foundation of IAB with sleeved piles different founding soil type is also considered varying from loose and dense sand for the models. Typical view of Model-1 developed using SAP2000 (Version18) is shown in Fig. 5.5. In the second category of model, the sleeved pile foundations are provided in both abutment and pier. This second category of model is classified as Model-2. Multiple models of this category are also developed by increasing the sleeved in foundation of abutment and pier from initial length of 2.50m to 6.50m with increment of 0.5m in subsequent model. The

founding soil type of Model-2 is also considered as loose sand and dense sand to study the influence of founding soil on the dynamic characteristics of the model. In both the models for the purpose of parametric study the steel tube pile of outer diameter of 400 mm with wall thickness of 32 mm is chosen as section of sleeved pile arbitrarily for parametric study.

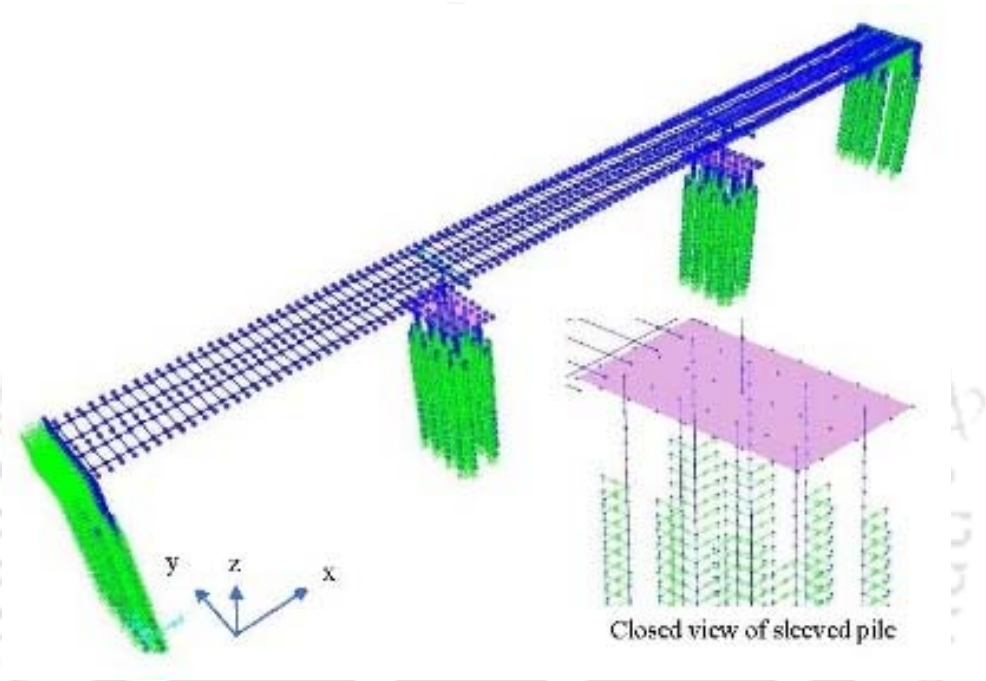

Fig. 5.5 Model-1 Concrete pile in abutment and sleeved pile in pier foundation

The Modal analyses of all the models under two categories of models are carried out and representative characteristics of a first mode of models are shown in Table 5.1. From Table 5.1, it is observed that there is a significant increase in the time period of vibration with the increase in sleeve length as compared to that of bridge without sleeved pile. The participating mass ratio of the IAB with sleeved pile in transverse direction are also observed to be increasing with the increase in the sleeve length in the foundation. This is attributed to increase in the flexibility of the bridge structure.

Table 5.1 Characteristics of first modes of model 1 and model 2

Type of founding soil	Categories of model with variation of sleeved pile in foundation of bridge	Sleeve length in pier pile	Modal Time period (sec)	Participating mass ratio	
				Ux	Uy
Loose sand	Without sleeved pile	0.0m	0.469	0.0	35.50%
	Model 1	2.5m	0.506	0.0	47.00%
		4.5m	0.572	0.0	53.40%
		6.5m	0.684	0.0	58.11%
	Model 2	2.5m	0.514	0.0	51.10%
		4.5m	0.644	0.0	69.70%
		6.5m	0.891	0.0	77.80%
Dense sand	Without sleeved pile	0.0m	0.442	0.0	28.35%
	Model 1	2.5m	0.469	0.0	38.60%
		4.5m	0.529	0.0	49.04%
		6.5m	0.656	0.0	55.26%
	Model 2	2.5m	0.475	0.0	41.95%
		4.5m	0.595	0.0	67.01%
		6.5m	0.743	0.0	77.64%

Similar pattern of increase in time period and the participating mass ratio with the increase in the sleeve length is observed in Model-2 as well. This increase in the participating mass ratio may have an adverse effect in the form of increase in seismic design force, if the shift of the period of the structure due to the introduction of the sleeved pile is not large enough to cross the threshold of maximum time period of constant acceleration zone in response spectrum. This implies that, a minimum length of sleeved length is required to be provided to increase the flexibility of the structure for increasing the structural vibration period to a value beyond the zone of constant acceleration. It is also observed that the model-2

manifest to be more flexible than model-1 indicating a preferable configuration of IAB with sleeved pile.

The response spectrum analysis of the IAB models with different sleeved length is carried out to study the variation of the elastic seismic forces induced in the pier of the bridge. The elastic response spectrum provided in IRC:6 (2014) and as shown in Fig. 4.23 for different types of soil is adopted in the analysis of the bridge. The design seismic moment in the pier and pile have been calculated by taking seismic moment in two orthogonal directions and combining the same as per following combination rules prescribed by IRC:6 (2014) as shown below:

$$M_{Edseis} = \pm M_{seisx} \pm 0.3M_{seisy} \quad (5.1a)$$

$$M_{Edseis} = \pm 0.3M_{seisx} \pm M_{seisy} \quad (5.1b)$$

The variation of design seismic moment in bridge pier as obtained from response spectrum analysis using the combination rules given in Equation (5.1), for loose and dense sand are shown in Fig. 5.6 and Fig. 5.7 respectively. It is observed from these two figures that in pier of both Model-1 and Model-2, the seismic moment decreases with increase in sleeved length of the foundations irrespective of founding soil type. This is attributed to the added flexibility as a result of incorporating sleeved pile in the foundation, thereby lengthening the period of vibration of the bridge resulting into decrease in the inertial forces. The appreciable reduction in seismic design moment in the pier occurs with sleeved length longer than 4.50 m in IAB in loose and dense sand. These calculated moments are based on arbitrary selection of section of sleeved pile for parametric study but indicates that a longer sleeve length than this threshold value for effective reduction of seismic forces in pier and abutment of IAB. Further, it implies that the required

length of sleeve for effective reduction in seismic force of pier of IAB is influenced by the founding soil types.

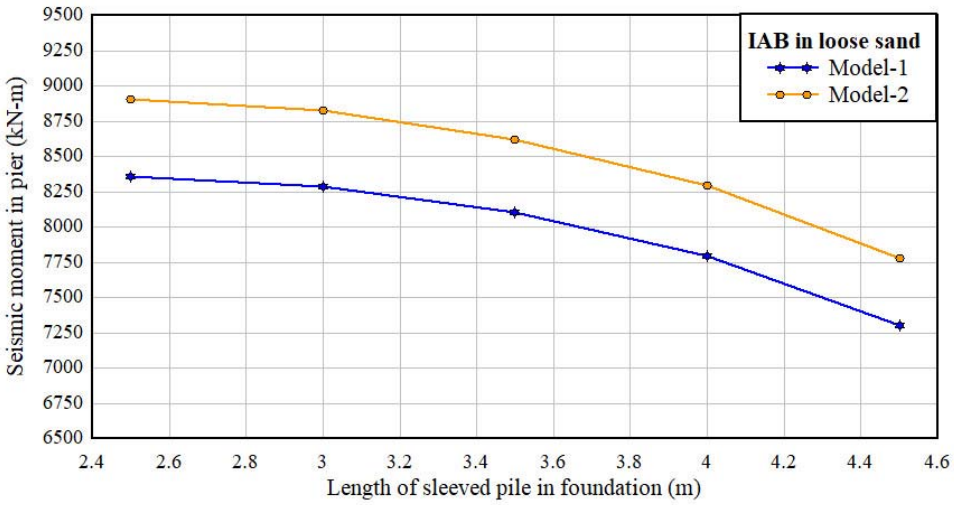

Fig. 5.6 Seismic design moment in piers *vs* sleeved length in sleeved pile of IAB in loose sand

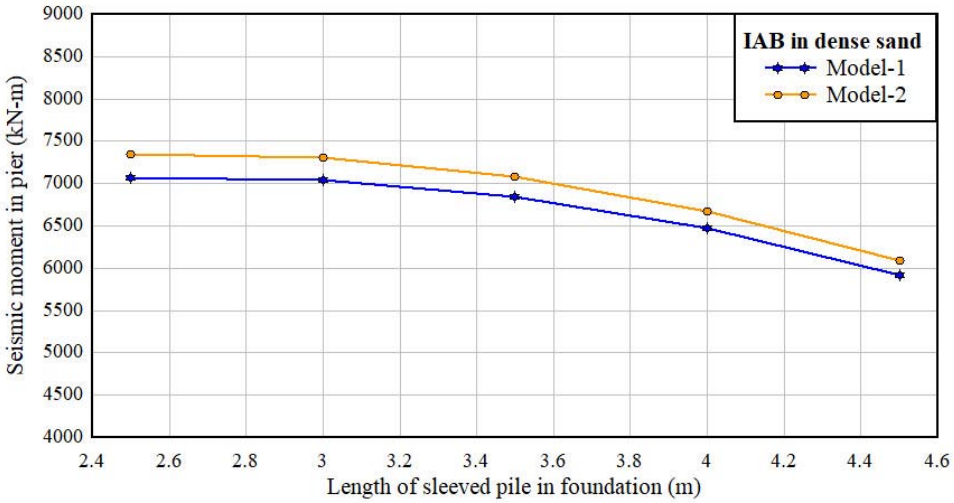

Fig. 5.7 Seismic design moment in piers *vs* sleeved length in sleeved pile of IAB in dense sand

Fig. 5.6 and Fig. 5.7 also displays that although model-2 is more flexible as evident from time period corresponding to first mode of vibration (Table 5.1) the seismic design moment in pier of Model-2 is higher than that of Model-1. This occurs

because of the fact that in the case of Model-1, the abutments are supported on concrete pile and the piers are supported on sleeved pile due to which the foundation of abutments becomes stiffer than that of pier. Further the flexibility of the pier foundation increases with the increase in sleeved length in subsequent model, while the stiffness of abutment foundation remains the same. Hence the pier of the Model-1 supported on comparatively more flexible foundation attracts lesser inertial forces. However, in the case of Model-2, both the abutments and piers are supported on sleeved piles with equal sleeve length and sectional properties. However, the number of piles in pier foundation is more than that of abutment and thus the pier foundation becomes stiffer than that of abutment in Model-2. Hence the seismic forces in pier are larger as compared to that of Model-1. Goel (1997) also observed that a flexible abutment may leads to more deformation in the other lateral load resisting elements in the bridge. This signifies a requirement for adjustment of the horizontal stiffness for foundation of lateral load resisting components of the IAB with sleeved pile for optimum uniform reduction of seismic force.

Furthermore, it is also observed that with the provisions of sleeved pile in the foundation of abutment and pier, the seismic moments in the piles of IAB are observed to increase. The amount of increase is found to be more in IAB in loose sand that that in dense sand. The rate of increase in seismic moment starts decreasing with the increase in sleeve length provided when the sleeve length provided is more than 5.50 m in both model-1 and model-2. However, since the pile supporting IAB is designed mainly for providing adequate load carrying capacity the increase in the seismic moment would not make any significant impact chosen size of pile. As may be seen Table 5.2, the increase value of seismic design moments would not require additional specific provision and rather would increase the safety

margin in seismic performance of the bridge. In addition, the seismic moment indicated in Table 5.2 is based on the arbitrary section and sleeve length considered for parametric study and thus the actual increase with designed section and sleeve length are expected to be on the lower side.

Table 5.2 Seismic moment *vs* length of sleeved pile in Model-1 and Model-2

Type of founding soil	Categories of model with variation of sleeved pile in foundation of bridge	Sleeve length in pier pile	Seismic moment in sleeved pile (kN-m)	
			Abutment pile	Pier pile
Loose sand	Without sleeved pile	0.0m	327	394
	Model 1	2.5m	470	396
		4.5m	561	543
		6.5m	694	647
	Model 2	2.5m	386	380
		4.5m	702	716
		6.5m	776	818
Dense sand	Without sleeved pile	0.0m	279	278
	Model 1	2.5m	295	280
		4.5m	312	397
		6.5m	350	416
	Model 2	2.5m	298	302
		4.5m	448	465
		6.5m	501	492

The variation of seismic design moments in pier and piles as observed from response spectrum analysis of modal-1 and model-2 also indicate that the sleeved pile foundation shall be more effective for IAB in dense sand. The Model-2 manifest more flexibility with longer time period corresponding to first model of vibration. The configuration also provides adequate scope to designer for manipulating the stiffness of sleeved pile both in pier and pile foundation.

5.4 Design Parameters for Sleeved Pile in IAB

It is observed from the modal analysis of IAB with sleeved pile that the installation of sleeved pile in bridge foundation makes the bridge structure more flexible resulting in a longer period of vibration. This increase in the period of vibration reduces the seismic forces on the components of the bridge substantially, if the increased period crosses the threshold value of maximum time period of constant acceleration zone in design spectrum and shifted to the zone where the acceleration decreases monotonically. The provision of sleeved pile in foundation of abutment and pier foundation is also found to be preferable since the arrangement leads to more flexible behavior of bridge. It is also observed that adjustment between the horizontal stiffnesses of the foundation of abutment and pier of IAB with sleeved piles is required to avoid excessive concentration of seismic forces in the components of bridge with stiffer foundation.

5.4.1 Horizontal Stiffness of the Sleeved Piles

Kaynia and Kausel (1980) derived the expression for equivalent horizontal dynamic stiffness of sleeved pile. For the derivation a simplified model of sleeved pile with superstructures was considered as shown in Fig. 5.8.

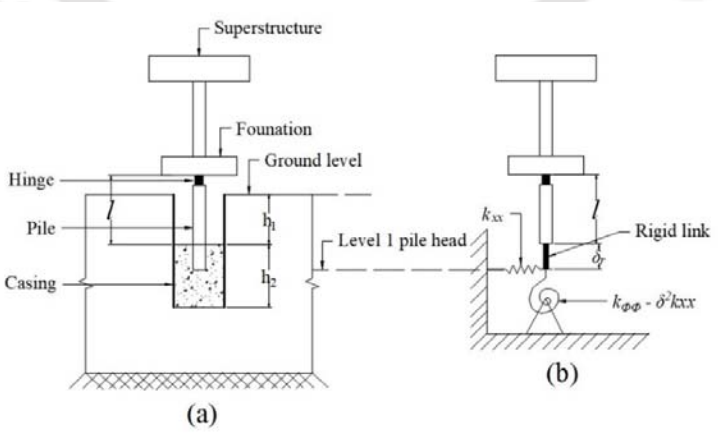

Fig. 5.8 Idealised model of sleeved pile (a) Simple SDOF model (b) mathematical model (Kaynia and Kausel (1980)

To account for the coupling effect at the pile head, a rigid link of length δ_r was added to the column and the new system was mounted on uncoupled swaying and rocking spring as shown in Fig. 5.8 (b). The expression for equivalent horizontal stiffness (k_{eq}) for sleeved pile with constant diameter which fixed at bottom and hinged at top and considering the coupling effect as

$$k_{eq} = \frac{3E_pI_p}{l^3} \times \frac{a^3}{3} \times \frac{1 - ab\left(a\frac{\delta_r}{l} + \tan a\right)}{\left[1 + \left(1 + \frac{\delta_r}{l}\right)a^2 b\right]\left(a\frac{\delta_r}{l} + \tan a\right) - a\left(1 + \frac{\delta_r}{l}\right)} \quad (5.2)$$

where the dimensionless parameters a and b are defined as

$$a = \sqrt{\frac{Pl^2}{E_pI_p}} \quad (5.3a)$$

$$b = \frac{E_pI_p}{l(k_{\emptyset\emptyset} - \delta_r^2 k_{xx})} \quad (5.3b)$$

$$\delta_r = -\frac{k_{x\emptyset}}{k_{xx}} \quad (5.3c)$$

where E_p is the modulus of elasticity of material of pile, I_p is the moment of inertia of pile and l is the sleeved length of the sleeved pile and P is the axial load on pile. Raupach et al. (1981) approximated the sleeved pile of building as a single degree of freedom (SDOF) model of vertical cantilever column with rigid superstructure on top for obtaining the horizontal stiffness of pile. The free-standing length of pile was taken from the bottom level of the encasement of sleeved pile to the bottom of the building. The horizontal and rotational stiffness of soil at the base of piles was ignored and the superstructure was considered rigid. Imposing these assumptions, the expression for the horizontal stiffness (k_p) of the sleeved pile fixed at the top and bottom ends was derived (Raupach et al.,1981) as

$$k_p = \frac{12E_pI_p}{l^3} \times \frac{a^3}{12} \times \frac{\sin a}{2 - 2\cos a - \mathrm{a}\sin a} \quad (5.4)$$

In the present study, the assumption of SDOF is adopted for computation of horizontal stiffness of the sleeved pile in IAB. The computation of the lateral stiffness of the sleeved pile for the IAB is carried out using Equation (5.4) taking the free length of the pile from the top of the concrete fill in the casing of sleeved pile to the bottom of the pile cap.

5.4.2 Design Displacement and Shear Force of Sleeved Pile

Design of sleeved pile is carried out based on the seismic acceleration, design displacement and shear forces obtained from the design response spectrum (IRC:6:2014). To reduce the transmission of ground acceleration to the bridge the time period of vibration is required to be lengthened by the introduction of sleeved pile in foundation to a value more than the maximum threshold period of constant acceleration in design spectrum which are 0.4 sec for IAB in hard soil, 0.55 sec for IAB in medium soil and 0.67 sec for IAB in soft soil. This will enable shifting of time period of vibration of IAB in the zone, where acceleration decreases with time period in the design spectrum. Therefore, the preliminary design is started by taking a value of target period of vibration of the IAB from the design spectrum where the acceleration decreases with period. In case of design of sleeved pile for building, Biggs (1982) suggested adoption of long design period in the range of 6 to 12 sec and high strength steel sleeved pile for maximum efficiency of the sleeved pile in the building. However, this range of design time period is not practicable for the types of bridge as the excessive flexibility will results in instability and excessive deflection of the bridge damaging the connected components affecting the functioning of the bridge. Thus, in this study the target vibration period of

fundamental mode of the bridge is taken in a range of 2 to 3 times the maximum threshold time period of constant acceleration design response spectrum for different types of soil in the foundation.

The designed displacement at the top of the sleeved pile is computed using the spectral acceleration (S_{pa}) in the considered design response spectrum. The design displacement is the drift of the sleeved pile which is directly related to the seismic force induced in the pile. The maximum design displacement D_{max} is computed using the relation as (Chopra, 2007)

$$\mathrm{D}_{max} = \frac{S_{pa}}{\omega_p^2} \tag{5.5}$$

where, ω_p, the target frequency of vibration of SDOF model of the pile which is calculated from the target time period of the bridge. The maximum shear force S_{max} is calculated by taking the mass M_t on the pile and spectral acceleration considering SDOF model of pile as

$$\mathrm{S_{max}} = \omega_p^2 \mathrm{D}_{max}\, \mathrm{M}_t \tag{5.6}$$

Two levels seismic design approach is adopted in which case the design basis earthquake acceleration is taken as half of the maximum ground acceleration. The design displacement is computed considering approximation with SDOF model. Hence, for design of sleeved pile of IAB, the iteration in design is initiated with half the displacement computed using design basis earthquake considering framed configuration of bridge to avoid over estimation of displacement and forces to begin with.

5.4.3 Sleeved Length of Sleeved Pile Foundation

The length of the sleeved pile for the IAB is calculated using equation for computation of length of sleeved length of pile for building which was derived from

the expression of equivalent horizontal stiffness of the pile proposed Raupach et al. (1981) as

$$l = \frac{g}{\omega_p^2 \, \pi^2 \, \frac{P}{P_E}} a'^3 \frac{\sin a'}{2 - 2\cos a' - a' \sin a'} \tag{5.7}$$

where P is the axial load on pile, P_E is the Euler's buckling load for column fixed against rotation at both top and bottom and free to displace at top, a' is a dimensionless parameter. The expression for dimensionless parameter a', in Equation (5.7) is given as

$$a' = \pi \sqrt{\frac{P}{P_E}} \tag{5.8}$$

The Euler's buckling load for a considered boundary condition in Equation (5.7) was computed using the expression given as

$$P_E = \frac{\pi^2 E_p I_p}{l_e^2} \tag{5.9}$$

The ratio of P/P_E is assumed initially anticipating large bending stress in addition to axial load on the sleeved pile. Raupach et al. (1981) had presented a plot of ratio P/P_E *vs* period of one degree of freedom model based on parametric studies on design of sleeved pile for building as shown in Fig. 5.9. The time period of considered bridge in this study is much lesser than that of building in the reference. The curve in Fig. 5.10 is taken as guiding data for assuming the value of P/P_E value only for the time period of the bridge.

The relation for calculating the length of sleeved pile given in Equation (5.8) do not take into account the effect of the stiffness of the founding soil. Hence iteration with

design sleeved length can also be initiated with a value lesser than the calculated if the bridge is founded on dense sand.

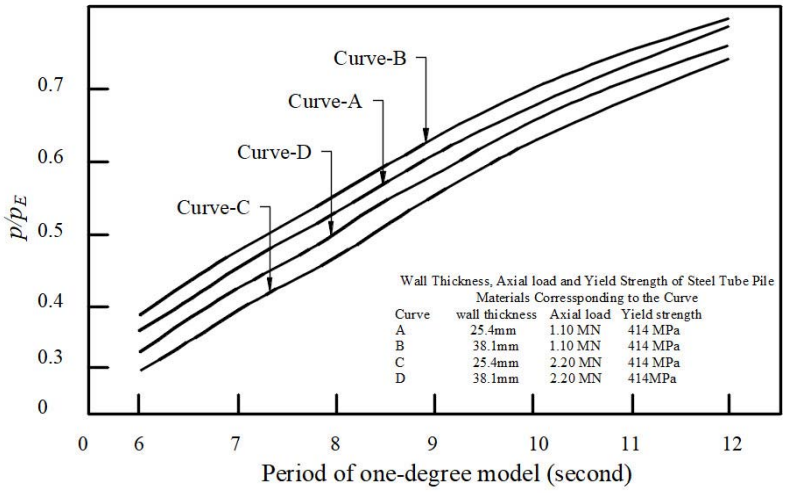

Fig. 5.9 P/P_E *vs* time period of structure (Rapach et al. 1981)

5.4.4 Section of Sleeved Pile

Rearranging the Euler's buckling Equation (5.9) and expressing Euler's buckling load in the form of load ratio, the moment of inertia of the sleeved pile is expressed as:

$$\mathrm{I_p} = \frac{P l_e^2}{\pi^2 E_p \left(\frac{P}{P_E}\right)} \tag{5.10}$$

The preliminary section of sleeved pile is derived from cross sectional moment of inertia of pile computed from Equation (5.10). For arriving at the final designed section of the pile, trial and error method is adopted by varying one dimension (e.g. wall thickness of pile) while keeping the other (e.g. diameter of pile) as constant. While adopting the final section of sleeved pile, it is ensured that the stress induced in the section is within the yield strength of the pile material.

5.4.5 Design Moment and Stress in Sleeved Pile

The bending moment for the preliminary design is computed by combining the moment generated at the base of the sleeved pile due to lateral force at the top of the pile and the $P-\Delta$ effect moment. The combination is adopted considering that the maximum displacement D_{max} and maximum shear force S_{max} will occur simultaneously. The maximum bending moment M due to the combined effect is calculated as (Raupach et al., 1981)

$$M = P\,D_{max} - S_{max}l \tag{5.11}$$

The stresses developed in the section of sleeved pile due to the combined effect of both axial compression and bending is calculated as

$$f_{bc} = \frac{P}{A_s} + \frac{M\,(D_s + t_s)}{2\,I_s} \tag{5.12}$$

where I_s is the moment of inertia of steel tube pile section, A_s is the area of steel tube pile section D_s is the average diameter of the steel tube section and t_s is the thickness of wall of the steel tube the Equation (5.12) is rearranged as

$$f_{bc} = \frac{P}{A_s} + \frac{P}{2\,I_s}(D_s + t)\left\{D_{max} - \frac{S_{max}}{M_t}\frac{l}{g}\right\} \tag{5.13}$$

The length and sectional properties of sleeved pile obtained from these design steps are adopted as the initial dimensions for starting the iterative analysis for arriving at the final section and length of the sleeved pile in pier.

5.4.6 Final Design of Section of Sleeved Pile

The final section of the sleeved pile supporting the abutments and piers is arrived at by adjusting the horizontal stiffness of their foundation to ensure an approximately uniform capacity. The comparison and adjustment of horizontal stiffness of the sleeved pile foundation is carried out by considering the sleeved pile supporting abutments at both ends as one unit and piles supporting the piers in

between abutment as another unit. The balance of lateral stiffness is carried out between these two lateral load resisting units. This consideration is adopted to ensure that the seismic forces in abutment and in its foundation and the seismic forces in pier and in its foundation are approximately uniform. The horizontal stiffness of sleeved piles is computed using Equation (5.4) for comparison.

In the present study, the horizontal stiffness of sleeved pile in pier foundation is more than that of abutment and in addition the mass on the pier from the tributary deck area is also more than that on abutment. Hence, in the first place the adjustment of the stiffness is carried out by increasing the sectional properties of the sleeved pile in abutment by a factor equal to the ratio of mass on pier to mass on abutment to keep the horizontal stiffness of sleeved pile in pier comparatively more flexible by the factor. This additional increase in the stiffness in foundation of abutment is made by modifying the dimensions of the steel tube of sleeved pile supporting the abutments. The ratio of horizontal stiffness of pier pile to the abutment pile is kept less than 1.0 to avoid concentration of seismic forces in the pier due to higher stiffness of its foundation since the pier is vulnerable lateral load resisting component of any bridge.

Furthermore, the three-dimensional model of the bridge is created by incorporating designed sleeved pile in the foundation of the abutment and the pier. Response spectrum analysis of the bridge is carried out to estimate the design seismic forces in the sleeved pile. The structural design of the sleeved pile is carried out considering it as beam column member subjected to design superimposed load combined with seismic forces. Iterative response spectrum analysis is carried out by modifying the sectional properties of the pile to keep the capacity of the sleeved pile within the required factor of safety. The final designed section of the sleeved

pile is considered for checking buckling capacity of the sleeved pile system under static axial load and finally nonlinear time history analysis is carried out for evaluation of seismic capacity.

5.4.7 Buckling Load of Sleeved Pile

Sleeved pile designed as per the procedure outlined in the previous sections and the same is checked for buckling load under load combination as per IRC:6: (2014) by considering sleeved pile system as similar to that of partially embedded pile. The free-standing length of the sleeved pile is analogous to the pile extending above ground level in partially embedded pile. Barker et al. (1991) stated that when such type of pile is subjected to axial load it may buckle, and the buckling capacity of the piles may control the failure. The evaluation of bucking load is carried out adopting the solution given by Davisson and Robinson (1965) for partially embedded piles in terms of idealized equivalent free-standing cantilever as shown in Fig. 5.13.

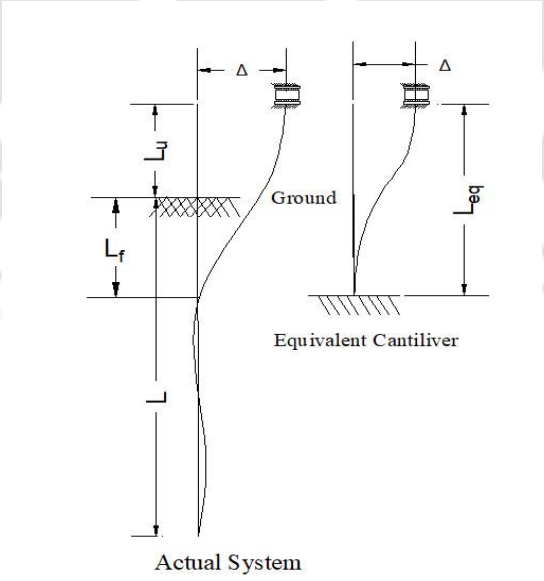

Fig. 5.10 Equivalent free-standing cantilever column for partially embedded pile (Davisson and Robinson, 1965)

Davisson and Robinson (1965) defined the equivalent free-standing cantilever length L_{eq} as the sum of unsupported pile length above the ground and additional length of fixity to the depth below the ground level and the equivalent system. The depth of fixity L_f of the equivalent cantilever is expressed as a function of flexural stiffness of pile (E_pI_p) and soil stiffness, expressed in terms of soil modulus. The length of fixity below the ground is calculated as:

$$L_f = 1.8T \tag{5.14}$$

where and T is the characteristic length of the pile calculated from the relation as proposed by Davission and Robinson, (1965);

$$\mathrm{T} = \left(\frac{E_pI_p}{n_h}\right)^{0.2} \tag{5.15}$$

The value of n_h is taken from the recommendation given by Tarzaghi (1955) as shown in Fig. 5.11. The equivalent free-standing cantilever length of the pile with sleeved pile is calculated as:

$$L_{eq} = L_u + L_f \tag{5.16}$$

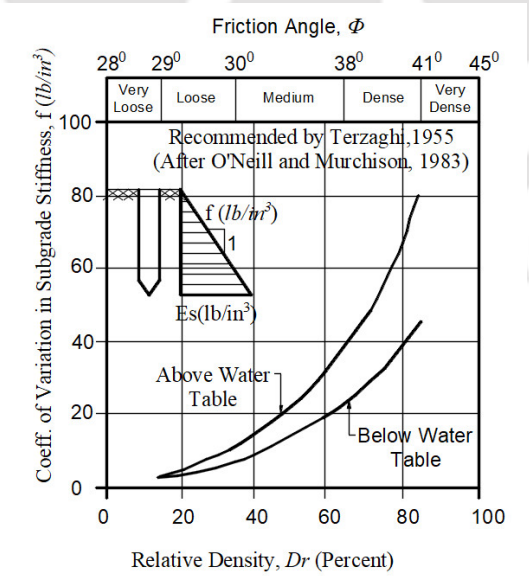

Fig. 5.11 Recommended coefficient of variation in the subgrade modulus with depth for sand and clay (Buckle et al. 2006).

The length of fixity L_f calculated using Equation (5.14) is considered as the depth below the ground level at which the pile can be assumed as fixed (Davisson and Robinson, (1965). However, in the present study it is considered as the depth below the bottom end of the sleeved length which have high confining pressure from the soil above the level. Hence, the actual depth of fixity (L_f) for the present condition may be lower than the calculated value using Equation (5.14). Therefore, the equivalent free-standing length of sleeved pile considered may be on conservative side.

Furthermore, this equivalent free-standing length of the sleeved pile consists of two segments with different materials. The top sleeve length portion is of steel pile and the bottom portion between the bottom of sleeve length up to the depth of fixity consists of composite steel concrete material. The analysis can be carried out using the properties of the composite section but for simplification in evaluation of the buckling load, the composite properties of pile in overlapping portion is ignored and considered as concrete pile. Thus, the properties of bottom concrete pile are transformed into those of steel pile using modular ratio. The equivalent circular diameter of the section and the sectional moment of inertia of the transformed section are calculated. The sleeved pile is thus finally transformed into stepped column with uniform material properties as shown in Fig. 5.12. In addition, the top of sleeved pile is embedded into the rigid pile cap having heavy axial load and hence, rotation of the top of the sleeved pile is practically restrained by the pile cap. The axial buckling capacity of the stepped column is thus computed by using the relation for stepped column fixed at bottom end and restrained against rotation but free to translation at top and using the following equation (Gambhir, 2005):

$$P_{cr} = \frac{\pi^2 E I_1}{L^2} \times \left[\left(\frac{L_1}{L}\right) + \left(\frac{I_2}{I_1}\right)\left(\frac{L_2}{L}\right) + \left(\frac{1}{2\pi}\right)\left(1 - \frac{I_2}{I_1}\right)\sin\left(\frac{2\pi L_1}{L}\right)\right] \quad (5.17)$$

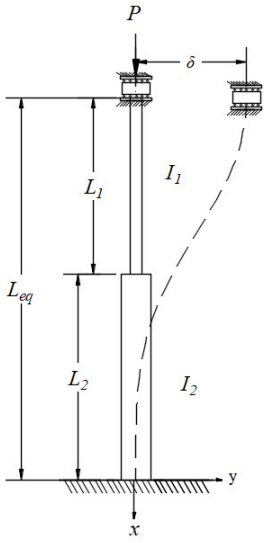

Fig. 5.12 Schematic Diagram of Column with Varying Section

The buckling load of the sleeved pile is also calculated by modelling the stepped column in finite element software SAP 2000 (Version 18). In the finite element model of the sleeved pile, the bottom portion is modelled as beam element with the properties of concrete and the top portion is modelled as beam element with properties of steel. The lateral and axial resistance of the soil to the concrete pile is accounted for by modelling with lateral load displacement $(p - y)$ curve, load transfer $(t - z)$ curve and load settlement $(Q - z)$ curve. A factor of safety of 3 for factored load on the sleeved pile is considered adequate for the buckling load.

5.5 Seismic Performance of IAB with Sleeved Pile

Result of dynamic analysis of IAB with sleeved pile in Section 5.3 indicates a reduction in the seismic moment induced in the pier. This shows improvement in the seismic performance of the IAB with sleeved pile. To study effectiveness of

sleeved pile in controlling seismic response of IAB, models of IAB with sleeved piles on different types of soil are developed. Linear and nonlinear dynamic analyses are carried out for comparing responses of IAB with and without sleeved piles. It is already observed in Chapter 4 that the added flexibility in foundation of bridge in soft clay and stiff clay by modelling the far field soil reaction do not have significant difference in seismic response of bridge. Hence any attempt like introduction of sleeved pile for effective reduction of seismic forces in IAB founded on soft and stiff clay may not be effective. Therefore, influence of sleeved pile in dynamic response of the IAB studied for loose, medium and dense sand only.

The sample design of sleeved pile for IAB is carried out considering the founding soil type as medium sand. The target time period of vibration is adopted as 1.37 s which is 2.5 times the maximum period of constant spectral acceleration zone in design response spectrum. The maximum design displacement is calculated by adopting the spectral acceleration of 0.9g as per the design response spectrum prescribed in IRC:6, (2014). The axial load on the sleeved pile is estimated as 614 kN. Structural steel grade E450 is adopted for the sleeved pile (IS: 2062, 2011). The step by step calculation in design of sleeved pile is shown in annexure A.

The designed section of sleeved pile for abutment foundation is of steel tube section having outer diameter of 500mm with wall thickness of 20mm. The designed section of sleeved pile for pier foundation is also of steel tube having outer diameter of 400mm with wall thickness of 20mm. Both the sleeved pile supporting abutment and pier is provided with a designed sleeved length of 8.0 m. The sleeved pile of the sample bridge as designed for medium sand is also considered for loose sand and dense sand for the comparative study of seismic performance IAB with sleeved pile.

5.5.1 Linear Dynamic Response of IAB with Sleeved Pile

The model of IAB with sleeved pile is developed incorporating the designed length as discussed in Section 5.3. The results of free vibration analysis of IAB with designed sleeved length is shown in Table 5.3.

Table 5.3 Vibration period of mode1 and mode 2 of IAB with sleeved pile

Soil type in foundation	Vibration period	
	Mode 1	Mode 2
Loose sand	1.14	0.57
Medium sand	1.11	0.56
Dense sand	1.08	0.47

The fundamental period of vibration of IAB with sleeved pile has increased substantially as compared to that of IAB without sleeved pile as shown in Table 4.11. The linear seismic response is obtained by response spectrum analysis of the IAB with sleeved pile. The seismic moment in the pier of IAB with sleeved pile is calculated using the response spectrum adopting the response spectrum prescribed in IRC: 6 (2014) for different type of founding soil in two orthogonal direction. The design moment in the pier of IAB with sleeved pile is calculated from the combination rule prescribed in IRC:6 (2014) and compared with the results obtained from the IAB without sleeved pile (NF +FF model) in Section 4.7. Table 5.4 shows the comparison of moment induced in the pier of IAB with and without sleeved pile computed from elastic response spectrum analysis. It is observed that the elastic seismic design moment in the pier decrease with introduction of sleeved pile as compared to the design moment in the pier without sleeved pile. Table 5.4 also indicates the seismic moment in the sleeved pile of pier foundation.

Table: 5.4 Elastic seismic forces in pier and pile of IAB without and with sleeved pile

Type of soil in foundation	Seismic moment in pier without sleeved pile (kN-m)	sleeved length of pile (m)	Seismic moment in pier with sleeved pile (kN-m)	Seismic moment in sleeved pile in pier (kN-m)
Loose sand	8090	8	4496	615
Medium sand	7493	8	3857	511
Dense sand	6668	8	3549	375

From Table 5.4, it is also observed that the seismic design moment in piers of IAB decreases with the increase in the stiffness of the founding soil. Similarly, the seismic design moment in the sleeved pile also decreases with the increase in the stiffness of soil in the foundation. It can also be noted that the design moment for pier pile as presented in Table 5.4 for medium and dense sand increase by around 30% as compared to the seismic moment in pier without sleeved pile as shown in Table 5.2. This increase demand in seismic moment however has no specific effect on the size of the pile designed primarily to take vertical load.

5.5.2 Nonlinear Dynamic Response of IAB with Sleeved Pile

For the purpose of studying the nonlinear dynamic response of IAB with sleeved pile the model of sleeved pile with designed sleeved length is provided in foundation as discussed in section 5.3. In the modelling of the pile, the bottom portion of the sleeved pile is modelled as a concrete pile, ignoring the steel concrete composite properties in the portion of concrete pile. The plastic hinges of concrete pier and piles are modelled as described in section 4.3. The hinges in the steel tube pile is modelled as per specification in FEMA 356 (2000) for steel structures. Further, IAB with sleeved pile is subjected to seismic excitation of El Centro (1940) N-S component and Koyna (1967) Trans component earthquakes ground motion.

The ground motion is matched to design response spectrum as detailed in Section 4.8. The response of the IAB with sleeved pile is compared with the IAB without sleeved pile (NF+FF model) for comparative study. The comparison of transverse acceleration time histories at the top of pier of IAB with and without sleeved pile on different founding soil are shown in Fig. 5.13 to 5.18.

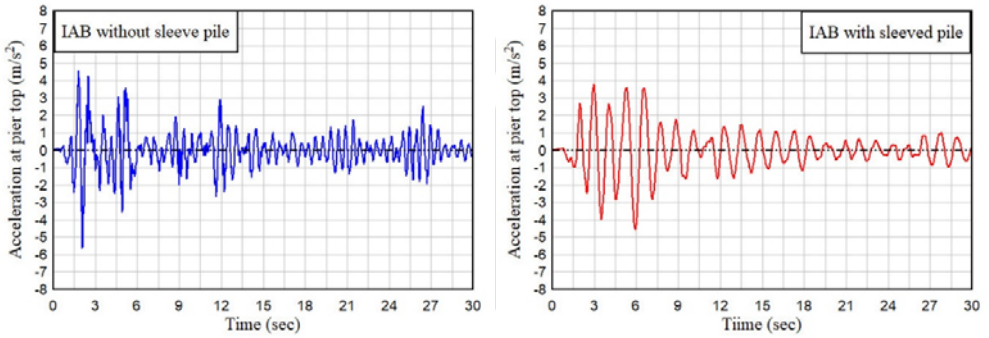

Fig. 5.13 Transverse acceleration at pier top of IAB with and without sleeved pile in loose sand under excitation of El Centro ground motion

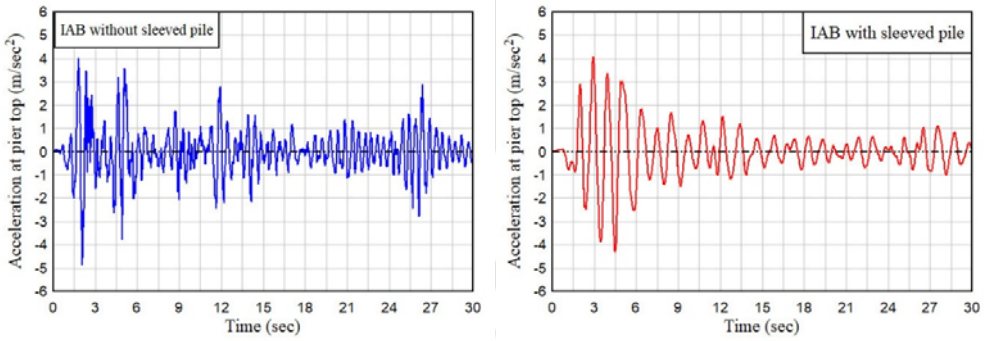

Fig. 5.14 Transverse acceleration at pier top of IAB with and without sleeved pile in medium sand under excitation of EL Centro ground motion

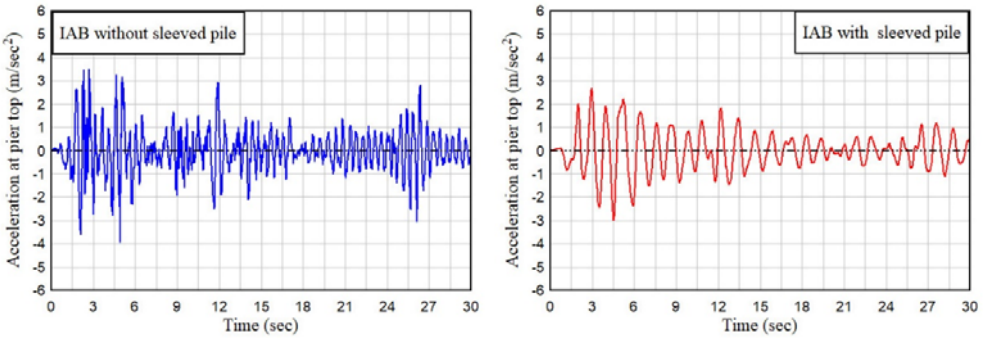

Fig. 5.15 Transverse acceleration at pier top of IAB with and without sleeved pile in dense sand under excitation of El Centro, ground motion

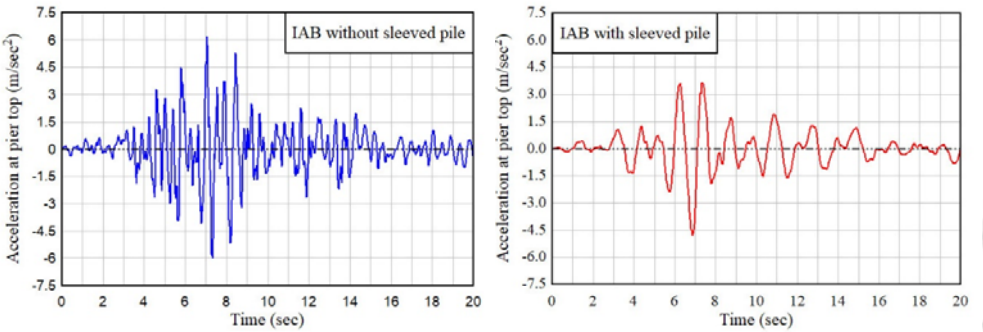

Fig. 5.16 Transverse acceleration at pier top of IAB with and without sleeved pile in loose sand under excitation of Koyna ground motion

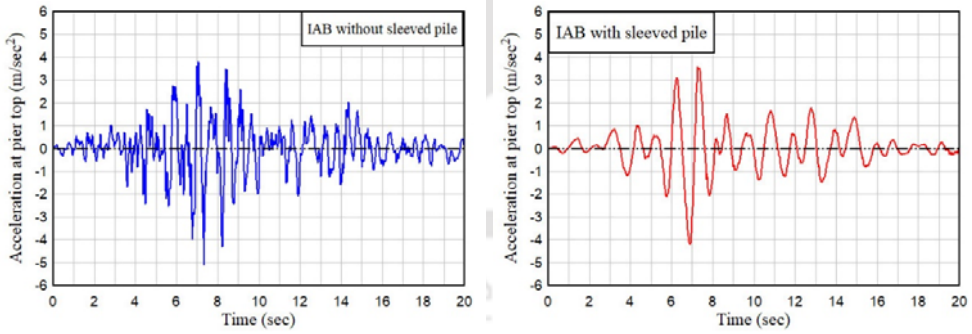

Fig. 5.17 Transverse acceleration at pier top of IAB with and without sleeved pile in medium sand under excitation of Koyna ground motion

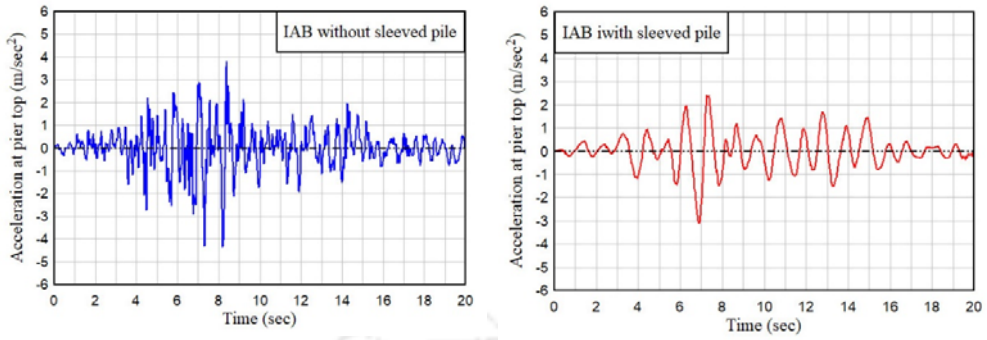

Fig. 5.18 Transverse acceleration at pier top of IAB with and without sleeved pile in dense sand under excitation of Koyna ground motion

The comparison response of IAB with and without sleeved pile as shown in Fig. 5.13 to 5.18, it may be observed that ground excitation transmitted to the top of pier of IAB with sleeved piles is lower than that in without sleeved pile. This reduction in transmitted ground acceleration is observed under both ground motions considered and irrespective of founding soil type. Table 5.5 shows the peak acceleration response at top of pier of IAB without and with sleeved pile on different founding soil types under the considered ground motions in transverse direction.

Table: 5.5 Peak acceleration response to pier top of IAB with and without sleeved pile in transverse direction

Ground motion	Type of soil in foundation	Peak acceleration at top of pier in transverse direction (m/sec^2)		Reduction in acceleration (%)
		Without sleeved pile	With sleeved pile	
El Centro	Loose sand	5.613	4.56	18.7%
	Medium sand	4.886	4.317	11.65%
	Dense sand	3.916	2.965	24.28%
Koyna	Loose sand	6.172	4.785	22.47%
	Medium sand	5.105	4.22	17.33%
	Dense sand	4.332	3.10	28.43%

The comparison of peak value of acceleration at pier top of IAB with and without sleeved pile as shown Table 5.5 indicates that maximum reduction in peak response is achieved in the IAB with sleeved pile founded in dense under both the ground motion.

Furthermore, Fig. 5.19 to 5.24 show the transverse displacement time history of the pier top of integral abutment bridge in different soil types without and with sleeved pile under excitation of two selected ground motions.

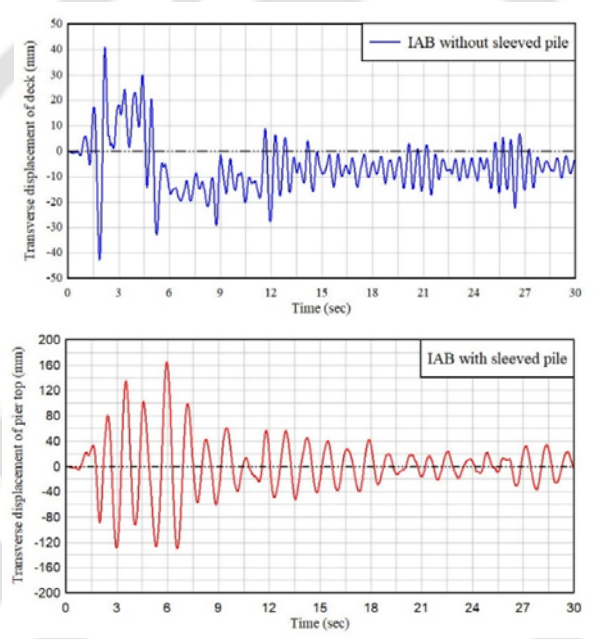

Fig. 5.19 Transverse displacement of pier top of IAB with and without sleeved pile in loose sand under excitation of EL Centro ground motion

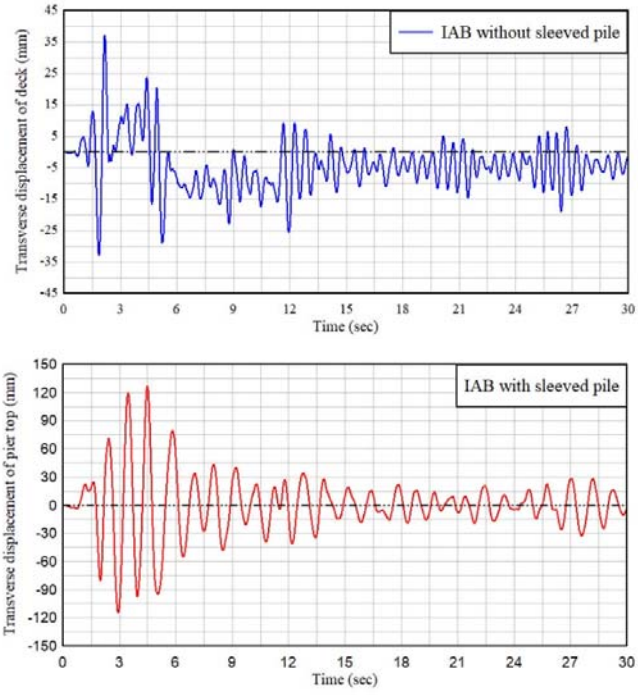

Fig. 5.20 Transverse displacement of pier top of IAB with and without sleeved pile in medium sand under excitation of EL Centro ground motion

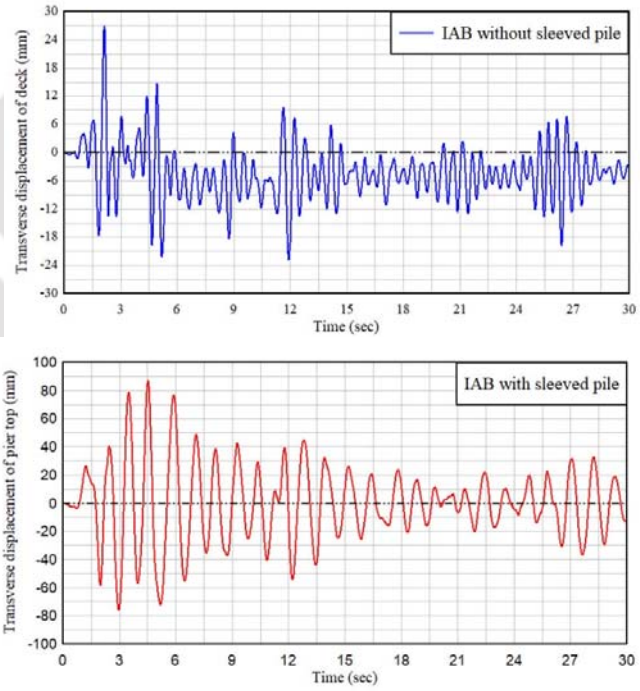

Fig. 5.21 Transverse displacement of pier top of IAB with and without sleeved pile in dense sand under excitation of El Centro Ground motion

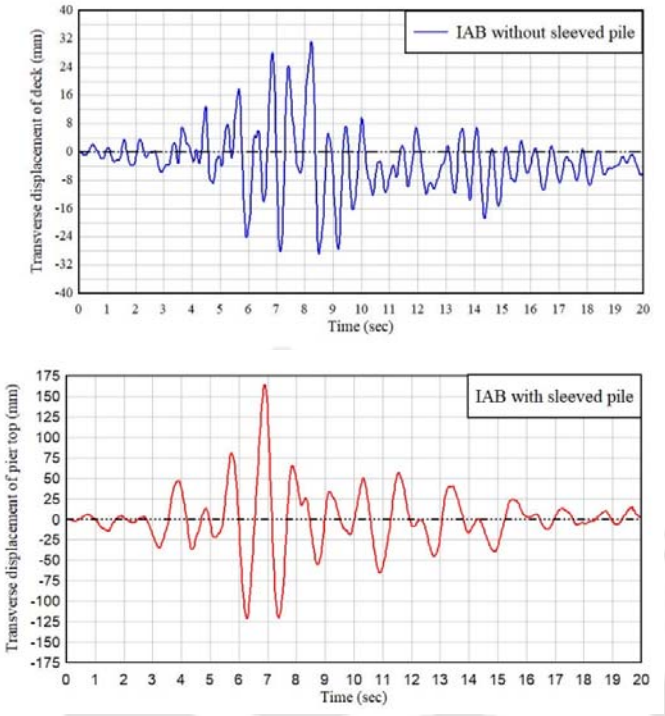

Fig. 5.22 Transverse displacement of pier top of IAB with and without sleeved pile in loose sand under excitation of Koyna ground motion

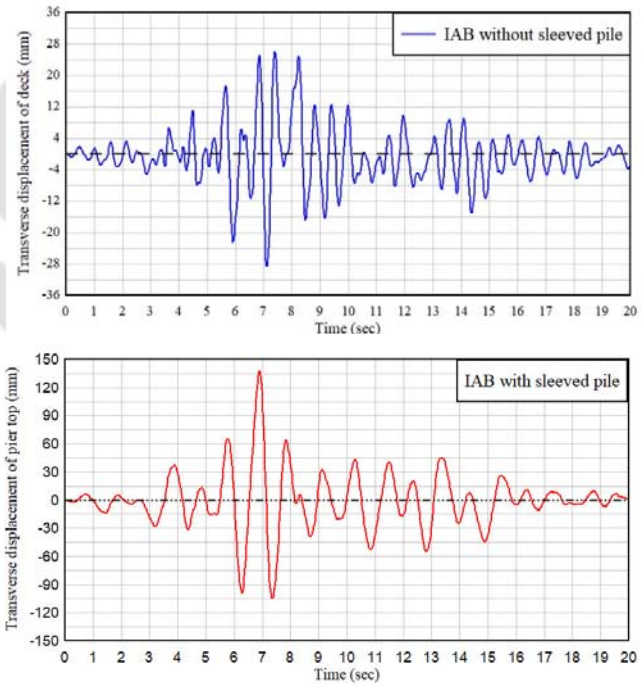

Fig. 5.23 Transverse displacement of pier top of IAB with and without sleeved pile in medium sand under excitation of Koyna ground motion

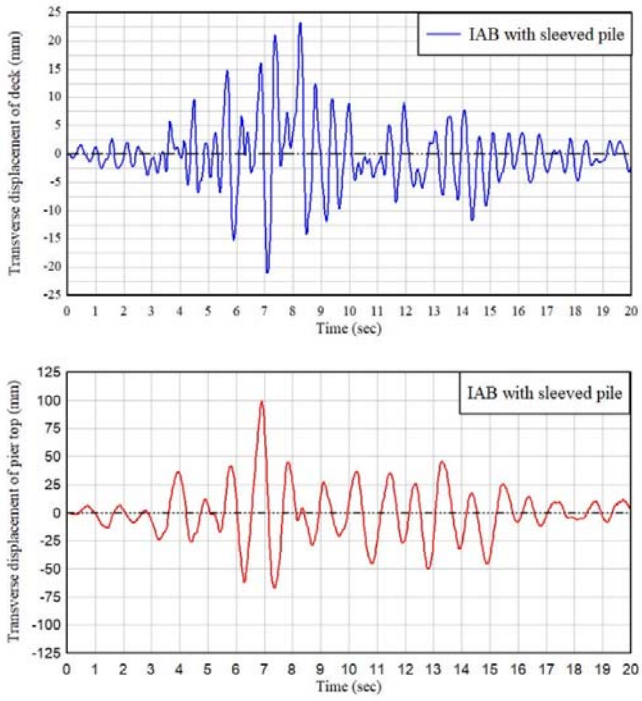

Fig. 5.24 Transvers displacement of pier top of IAB with and without sleeved pile in dense sand under excitation of Koyna ground motion

Examination of transverse displacement time histories of the pier top of IAB without sleeved pile in different types of soil in the foundation as shown in Fig. 5.19 to 5.24 indicates a sign of permanent deformation under the prescribed seismic ground excitations where shifting of axis of oscillation from the original equilibrium position is noted. On the other hand, the transverse displacement time history of the corresponding IAB with sleeved piles founded on different types of soil showed that the pier oscillates about the original equilibrium position throughout the period of ground excitation. This indicates that the response of the IAB with sleeved pile is in elastic state. The sleeved pile in the foundation of IAB is thus observed to enhance the seismic capacity of the bridge introducing appropriate flexibility into the system.

Table 5.6 shows the peak value of ground acceleration transmitted along bridge axis at the top of pier of IAB without and with sleeved pile on different founding soil types. The reduction in peak acceleration response may also be attributed to damping in soil pile and abutment backfill interaction.

Table: 5.6 Peak acceleration response at top of pier on IAB with and without sleeved pile along the bridge axis

Ground motion	Type of soil in the foundation	Peak acceleration at top of pier along the bridge axis (m/sec^2)		Reduction in acceleration (%)
		Without sleeved pile	With sleeved pile	
El Centro	Loose sand	7.57	4.99	34.08%
	Medium sand	7.22	4.96	31.30%
	Dense sand	7.49	4.82	35.64%
Koyna	Loose sand	4.86	4.48	4.05%
	Medium sand	6.44	5.21	19.09%
	Dense sand	7.35	5.18	29.52%

However, the record of displacement time history of IAB with sleeved pile shows substantial increase in overall displacement of the bridge pier as shown in Table 5.7.

Table 5.7 Peak transverse displacement of pier with and without sleeved pile

Type of soil in foundation of the IAB	Transverse displacement of pier top under ground motion (mm)			
	El Centro		Koyna	
	Without sleeved pile	With sleeved pile	Without sleeved pile	With sleeved pile
Loose sand	40.83	165.0	30.56	164.63
Medium sand	29.90	124.58	24.06	137.8
Dense sand	19.89	87.50	18.21	90.90

This maximum displacement recorded in IAB with sleeved is 304% to 438% above the displacement of IAB without sleeved pile. This recorded displacement is under excitation of considered ground motion having PGA as shown in Table 4.17. This increase in displacement is due to flexibility in foundation due provisions of sleeved pile. However, for the configuration of IAB considered, the deck of the bridge is integrated to pier and the scope of damage by unseating or damage of bearing is thus avoided. Further, as observed from the Fig. 5.19 - 5.24 that the pier of IAB with sleeved pile exhibits a stable state, where the piers are observed to oscillate about the initial equilibrium line throughout the period of excitation. The higher displacement is thus not considered as setback for design of IAB with sleeved pile. The longitudinal displacement of abutment along the bridge axis under excitation of both the ground motions are observed to be too small to cause any structural damage. This is due to the stiff behavior of IAB due to restrain in longitudinal direction derived from abutment, abutment pile and passive pressure mobilized in abutment backfill.

In addition, the sleeved pile is designed to displace freely under seismic excitation within the sleeve. Therefore, sufficient clearance between outer diameter of steel tube and inner diameter of casing is required for non-interference displacement of sleeved pile. Table 5.8 shows the maximum displacement of the top of sleeved pile in pier in foundation in transverse direction under considered ground motion. In the present study the internal diameter of the sleeve provided is 860 mm. Hence with the 400mm external diameter of sleeved pile the clearance available for free displacement of sleeved pile is 230mm. Thus, the clearance provided is adequate to accommodate the displacement of the sleeved pile in pier foundation under excitation of considered ground motion having PGA as shown in Table 4.17.

Table: 5.8 Maximum displacement of top of sleeved pile under seismic excitation

Type of soil in foundation of the IAB	Transverse displacement of top of sleeved pile under ground motion (mm)	
	El Centro	Koyna
Loose sand	142.8	143.00
Medium sand	109.00	121.40
Dense sand	78.20	89.00

5.6 Analysis of IAB with Sleeved Pile under Thermal Load

The area considered for the construction of the IAB with sleeved pile in the present study is expected to have a maximum uniform bridge temperature of 37.5^0C and minimum of 2.5^0C. The construction temperature of the deck is estimated to be 20^0C as discussed in section 4.9. The IAB with sleeved pile will also subjected to thermal expansion and contraction for temperature variation of 17.5^0C as that in IAB without sleeved pile considered in Section 4.9. The model considered for IAB is again considered for purpose of analysis of IAB with sleeved pile for thermal load. From the results of analysis, displacement in abutment in the longitudinal direction under thermal expansion loading is shown in Table 5.9.

Table: 5.9 Theoretical expansion and actual displacement of abutment bridge with sleeved pile in longitudinal direction.

Unrestrained theoretical expansion of deck	Recorded displacement of abutment at rise of 17.5^0 C		
	Loose sand	Medium sand	Dense sand
11.47 mm	7.38 mm	7.29 mm	7.40 mm

The values of displacement abutment of the IAB with sleeved pile as shown in Table 5.9 are almost the same as that of IAB without sleeved pile as shown earlier

in Table. 4.24. This indicates a dominance of the restraining force from the abutment and backfill passive pressure. Fig. 5.25 shows the deflected shape of the abutment with abutment pile for IAB with and without sleeved pile founded in loose sand and dense sand under thermal expansion of 17.5^0 C.

The deflected shapes of the abutment and abutment pile as shown in Fig. 5.25 indicate that in both cases, the abutment rotates about its base. The higher deflection of pile of IAB with sleeved pile signifies more flexibility in foundation of abutment. Similarly, Fig 5.26 shows the variation of moment in the abutment along height of abutment under thermal expansion of 17.5^0 C.

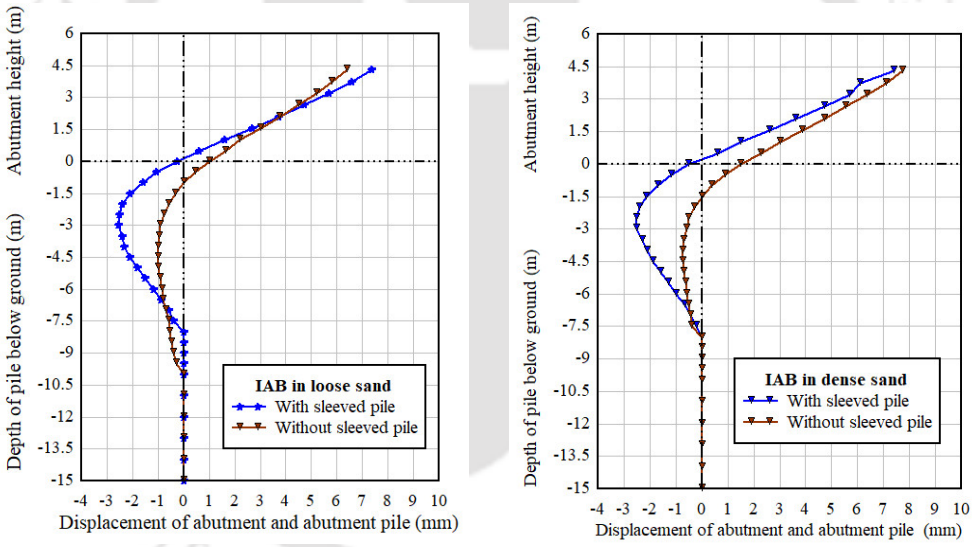

Fig. 5.25 Displacement of abutment and abutment pile of IAB with and without sleeved pile under thermal expansion of 17^0C

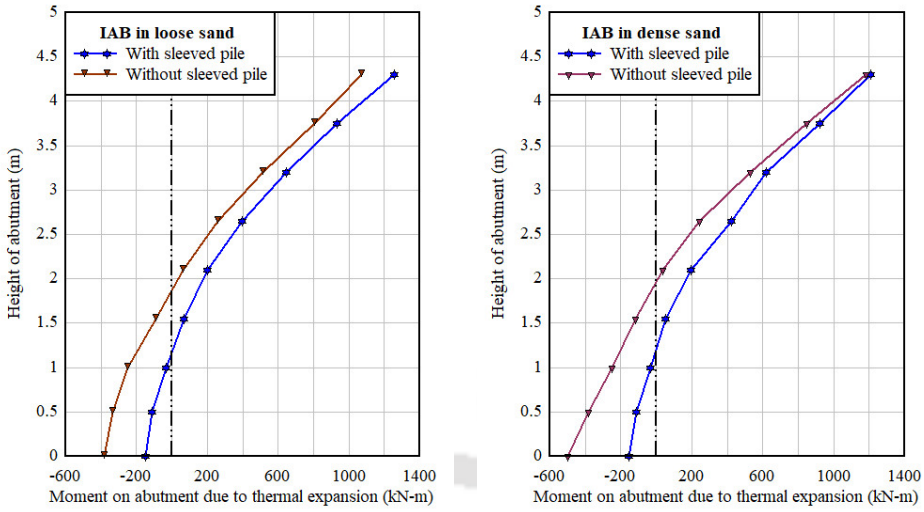

Fig. 5.26 Variation of moment in abutment with height of IAB with and without sleeved pile under thermal expansion of 17^0C

Comparison of the variation of moment in abutment along height from Fig. 5.26 displays a higher moment at the base of the abutment of IAB without sleeved pile, indicating stiffer response than that of IAB with sleeved pile. Therefore, the provision of sleeved pile in IAB have the advantage of enhancing the flexibility of the bridge under thermal loading and also in reducing the moment due to thermal expansion induced in the abutment wall.

5.7 Concluding Remarks

In this chapter, design of sleeved pile foundation for IAB carried out adopting the proposed method of design. The linear and nonlinear dynamic analyses are carried out using different models of IAB with and without sleeved pile for comparative study on their seismic performance. From the results of analyses the following observations are recorded.

1. The arrangement of sleeved pile is theoretically observed to be an effective means of controlling seismic response of IAB. The seismic performance of

the bridge improves with the adoption of sleeved pile in foundation IAB and also increase the overall safety margin of bridge. The sleeved pile will be a durable isolator for the IAB constructed in high seismic risk area.

2. The design method of sleeved pile developed by Raupach et al. (1981) for design of sleeved pile for building has a minor limitation, since the effect of soil stiffness below the sleeved pile were ignored in formulation of the relations, on account of which, requirement of number iteration in fixing length of pile in different type of soil increases. However, considering the complexity involved in the computation incorporating stiffness of soil, the simplified method with iteration in design has an advantage and observed to be suitable for practical design of sleeved pile for IAB.

3. In case of integral abutment bridge, due to the added flexibility by sleeved piles the flexural moment induced in the abutment by thermal expansion and contraction is lesser than that of corresponding IAB with concrete pile. The provision of sleeved pile in the foundation of IAB guarantees flexible response to thermal load thereby increasing performance of IAB.

Chapter 6

Seismic Vulnerability Assessment of IAB with and without Sleeved Pile

6.1 Introduction:

The seismic capacities of the bridge categories under study are assessed by adopting the incremental dynamic analysis (IDA) and the seismic vulnerability is estimated through fragility function. The IDA provides a parametric analysis method that has recently emerged in several forms to estimate more thoroughly the structural performance under seismic load (Vamvastikos and Cornell, 2001). It involves subjecting a structural model to one or more ground motion records, each scaled to multiple levels of intensity, thus producing one or more curves of response *vs* intensity level. The IDA procedure provides valuable information regarding the distribution of the damage at different seismic intensity level (Tehrani and Michelli, 2013). This also provides a thorough evaluation of the seismic response for a wide range of seismic intensity level corresponding to different damage states, from yielding up to collapse. The IDA results are presented using an intensity measure (IM) *vs* a damage measure (DM) of interest. The IM is a non-negative scalable quantity which is obtained from the accelerogram. The commonly adopted scalable IM quantity that includes peak ground acceleration (PGA), peak ground velocity (PGV) and the 5% damped spectral acceleration $S_a(T_1 5\%)$ at the first mode period of the structure (Tehrani and Michelli, 2013). The results of the IDA are used in the development of the fragility curve for prediction of the capacity of the bridge at different damage states under seismic excitation.

In this chapter, the incremental dynamic analysis of IAB with and without sleeved piles is carried out under a suite of 20 earthquake ground motions. The observed

IM *vs* DM for each step of analysis for different ground motion is recorded for the generation of the IDA curves. Different damage states of the bridge pier are computed in terms of the drift ratio of the pier. The analytical fragility curves of each bridge for each damage state is developed for the comparative study of the probabilistic seismic capacity of the bridge. The stepwise methodology adopted in the process of this study are as follows:

1. A suite of 20 ground motions fulfilling the characteristics of strong ground motions is selected for use in the IDA of the bridge categories.
2. IDA is carried out on the nonlinear model of the bridge categories and a pair of IM and DM are obtained from each analysis and IDA curves are developed.
3. The seismic capacities of the bridges considered are obtained by interpolation from the IDA results for comparative study.
4. Median seismic demand for different damage state is obtained by summarizing IDA results and fragility curves for each damage state of the bridges considered are developed for comparative study.

6.2 Selection of ground motion

The selection of ground motion is known to be an important consideration in the assessment of seismic capacity of structure, based on dynamic analysis. The primary objective of IDA is to study the relative capacity of the bridge categories under seismic excitation without considering site-specific seismic hazard. Baker and Cornell (2006) investigated the effect of different record-selection strategies by selecting records in the following methods:

1. AR method, in which the records are selected arbitrarily without any attempt to match any specific properties of the record.

2. MR-BR method, in which records are selected based on magnitude (M), and distance (R) values representative of the site hazard without attempting to match the ϵ value.
3. ϵ-BR method, in which the records are selected based on ϵ values representative of site hazard without attempting to match magnitude and distance value.
4. CMS-ϵ method, in which the records are selected based on spectral shape that matches the conditional mean spectra.

The records selected under the four strategies were used as input for nonlinear dynamic analysis of 7 storied reinforced concrete frame buildings. The records selected under selection strategies of AR and MR-BR method was observed to produce a slightly higher response and also a higher probability of collapse than the records selected under other strategies as ϵ-BR and CMS-ϵ method. Therefore, in the present study, for general comparison of the seismic capacity of the bridge, the AR method of selection of the ground motion is a reasonable strategy. In addition, Haselton and Deielerion (2007) observed that the ground motion selected without consideration of ϵ should consist of strong motions representing an extreme event that may cause the collapse of the structure. To ensure that the ground motion selected should represent strong motions, the minimum limits on event magnitude, distance from source to site, peak ground acceleration and peak ground velocity was suggested by Haselton and Deielerion (2007). Thus, the selected ground motion has magnitude (M) > 6.5, distance from source to site(R) >10 km, peak ground acceleration > 0.2g and peak ground velocity of 15cm/sec. The list of 20 ground motion records selected for the IDA in this study is as given in Table 6.1. These selected ground motions have been downloaded from the library of ground

motion on the website of Consortium of Organization for Strong Motion Observation Systems (COSMOS).

Table: 6.1 List of ground motion records selected for IDA

SL No	Earthquake ground motion	M	PGA (g)	R (km)
1	Cape Mendocino, USA,1992	7.2	0.492	49.10
2	Chamoli, India,1999	6.6	0.359	12.30
3	Chi Chi, Taiwan,1999	7.6	0.361	24.70
4	Imperial valley, USA,1979	6.5	0.242	10.60
5	Imperial Valley, USA,1978	6.5	0.273	10.40
6	Indian Burma Border,1998	7.2	0.224	189.90
7	Indian Burma Border,1998	7.2	0.282	210.10
8	Kobe, Japan,1998	6.9	0.344	22.50
9	Lander, (2217) USA,1992	7.3	0.284	10.00
10	Lander USA,1992	7.3	0.222	31.00
11	Limon, Costarica,1991	7.5	0.261	10.00
12	Loma Priesta, USA,1989	7.5	0.398	14.30
13	Manjil, Iran,1990	7.4	0.496	12.60
14	Northridge, USA,1971	6.6	0.325	12.20
15	Northridge, USA,1971	6.6	0.354	23.50
16	Sand Fernando, USA,1971	6.6	0.254	16.50
17	Sand Fernando, USA,1971	6.6	0.213	23.10
18	Sand Fernando, USA,1971	6.6	0.283	19.80
19	Superstition Hill,USA ,1987	6.6	0.255	18.20
20	Uttarkashi, India1991	7.0	0.359	34.00

6.3 Damage States Modelling of IAB

The literatures on assessment of seismic vulnerability of bridge using fragility function indicates a trend of component level approach in which the contribution of the major bridge components such as pier, abutment and bearing are considered in

the overall bridge system fragility. The component wise damage states are therefore defined for the vulnerability assessment of the bridge under study. HAZUS-MH (2003) defined the qualitative damage states for the bridge as shown in Table 6.2.

Table 6.2 Description of bridge damage states (HAZUS-MH, 2003)

SL No	Damage States	Description of damage details
1.	None (ds1)	No damage on any component of bridge
2.	Slight/minor damage (ds2)	Minor cracking and spalling to the abutment, cracks in shear keys at abutment, minor spalling and cracks in hinges, minor spalling at column (damage requires no more than cosmetic repair) or minor cracking to the deck.
3.	Moderate damage (ds3)	Column experiencing moderate cracking (shear cracks) and spalling (column structurally still sound), moderate movement of abutment (< 2"), extensive cracking and spalling of shear keys, any connection having cracked shear keys or bent bolts, keeper bar failure without unseating, rocker bearing failure or moderate settlement of approach.
4.	Extensive damage (ds4)	Column degrading without collapse - shear failure – (column structurally unsafe), significant residual movement at the connections, or major settlement of approach, vertical offset of abutment, differential settlement at connections, shear key failure at abutment.
5.	Complete damage (ds5)	Column collapsing and connection losing at all bearing support, which may lead to imminent deck collapse, tilting of substructure due to foundation failure.

Each of the damage state is also associated with the timeline for restoration of the bridge. Further, for implementation in the analysis, the qualitative damage states

are assigned a quantitative measure for each damage state. These quantitative values are derived from experiments as well as from the interpolation of behavior of the bridge components. In the present study, the IAB considered has deck integrated with the pier and abutment. There is no bearing in the support of deck on pier and abutment. In addition, the abutments are restrained in the longitudinal direction by backfill earth pressure. The backfill earth pressure restrains the longitudinal displacement of the pier and abutment under seismic excitation. In addition, due to large transverse stiffness of the abutment, a rigid support to deck is also simulated in the transverse direction of the IAB. Therefore, the piers resisting inertial forces under seismic excitation in transverse direction are most vulnerable in the bridge system. Therefore, the pier is the vulnerable component of the bridge system. The comparative study of the capacity is carried out considering the damage states of piers only.

The quantified damage state for the bridge piers can be described by section curvature analysis and transforming the results in the form of displacement at the top of the pier. Dutta and Mander (1998) carried out tests on real scaled bridge pier and based on the results, provided a set of five different damage (limit) states and corresponding drift for the pier as reproduced in Table 6.3.

Table 6.3 Description of damage states of pier (Dutta and Mander, 1998a)

Limit (damage) States	Description of damage	Drift ratio
Almost no damage	First yield	0.005
Slight damage	Cracking and spalling	0.007
Moderate damage	Loss of anchorage	0.015
Extensive damage	Incipient column collapse	0.025
Complete damage	Column collapse	0.05

The strain-curvature and curvature-displacement relationships for a column, presented by Priestley et al. (2007), are also adopted in the estimation of the quantitative value of different damage states of the pier. Tehrani and Mitchell (2013) considered four damage states in the seismic assessment of a bridge, such as yielding, cracking, cover spalling and bar buckling. In order to assess the first two damage states, the drift ratio was estimated using limit strain recommended by Priestley et al. (2007) while for the third and fourth damage state, the empirical relation of drift ratio proposed by Berry and Eberhard (2007) were used.

Stefanidou and Kappos (2017) carried out moment curvature analysis of the pier taking into account the stress-strain models for confined and unconfined concrete and the stress-strain curve of steel thereby producing a bilinear moment curvature for the pier. Based on the results of the analyses, the limit (damage) states threshold defined in terms of the curvatures are reproduced in Table 6.4.

Table 6.4 Limit state definition for pier (Stefanidou and Kappos, 2017)

Limit state	Threshold value of curvature (φ)	Quantitative performance description
LS – minor /slight damage	$\varphi_1: \varphi_y$	Quasi-elastic behaviour – cracks rarely visible.
LS2 – moderate damage	φ_2: min ($\varphi: \epsilon_c > 0.004$, $\varphi: \epsilon_s > 0.015$)	Spalling of cover concrete; strength may continue to increase – crack within 1-2 mm.
LS3 – major /extensive damage	φ_3: min ($\varphi: \epsilon_c \leq 0.004 + \frac{f_{yw}}{f_{cc}}$, $\varphi: \epsilon_s \geq 0.06$)	First hoop fracture, buckling of longitudinal reinforcement, initiation of crushing of concrete core – crack with > 2 mm.
LS4 – failure – collapse	φ_4: min $\varphi: M < 0.90\ M_{max}$, $\varphi: \geq 0.075$)	Loss of load carrying capacity

Barry and Eberhard (2007) developed an empirical equation for the estimation of drift ratio of column for the damage states like spalling of cover concrete, bar buckling and bar fracture. The equation for drift ratio on onset of cover concrete spalling was given as (Barry and Eberhard, 2007)

$$\frac{\Delta_{sp}^{calc}}{L}(\%) \cong 1.6\left(1-\frac{P}{A_g f_c'}\right)\left(1+\frac{L}{10D}\right) \tag{6.1}$$

Similarly, the equation for the drift ratio on the onset of the bar buckling was given as

$$\frac{\Delta_{bb}^{calc}}{L}(\%) = 3.25\left(1+k_e\rho_{eff}\frac{d_b}{D}\right)\left(1-\frac{P}{A_g f_c'}\right)\left(1+\frac{L}{10D}\right) \tag{6.2}$$

The value of k_e is stipulated as 150 for a circular column with spiral reinforcement and the ρ_{eff} is computed from the relation $\rho_{eff} = \rho_s \frac{f_{ys}}{f_c'}$. The accuracy statistics of the drift ratio equation was against the bridge column dataset used in the study, with 29 observations for cover spalling and 30 observations for bar buckling. Berry and Eberhard (2007) indicated that for the bridge column dataset, the measured displacement at cover spalling to calculated displacement with the proposed Equation (6.1) had a mean of 1.07 and a coefficient of variation of 35%. Further, the ratio of measured displacement at bar buckling to the calculated displacement using Equation (6.2) had a mean of 1.01 and a coefficient of variation of 25%. It was also added that the drift of pier computed from the drift ratio equations proposed were as accurate as the results from more complex methods. In the present study, three damage states are adopted in the comparative study of the seismic capacities of the bridges. The damage states are yielding, concrete cover spalling and bar buckling. The drift ratio on the onset of the yielding is computed from the yield curvature-displacement relationship given by Priestley et al. (2007). The drift

ratio on the onset of concrete cover spalling and bar buckling is calculated from Equation (6.1) and (6.2) as proposed by Berry and Eberhard (2007). The drift ratio computed at the damage state for the bridge pier in the present study with an effective height of 4.00 m and a diameter of 1.5 m with the details of reinforcement ratio given in Table 4.10 are as shown in Table 6.5.

Table: 6.5 Damage state for the IAB pier considered in present study

Damage state	Drift Ratio	Description of damages
Yielding (DS1)	0.57	Initiation of cracks in cover concrete
Concrete cover spalling (DS2)	1.88	Spalling of cover concrete; strength may continue to increase.
Bar buckling (DS3)	4.37	Hoop fracture, buckling of longitudinal bar degradation of strength by cracking core concrete

6.4. Performing Incremental Dynamic Analysis

In the comparative study, the seismic capacity of IAB with and without sleeved pile in medium sand is considered as the founding soil type for the IDA. Nonlinear models are constructed for the evaluation nonlinear time response using IDA. The modelling of nonlinear behavior of structural component is carried out following the strategies described in Section 4.3. The IDA for IAB is performed by applying the excitation of the selected ground motion along the transverse direction, which is the direction of fundamental mode with higher participating mass ratio as shown in Table 4.11. Each record is scaled to cover the entire range of the structural response from elasticity to the yielding and finally to the collapse of the bridge. From the literatures on bridge specific vulnerability assessment, it is observed that the PGA and drift of pier is adopted commonly to characterize IM and DM of earthquake excitation of bridge. Hence, in the present study, the PGA and drift of

pier is adopted as corresponding IM and DM. In the initial stage of analysis, one or two elastic runs are carried out by scaling the IM level of the ground motion in the range of 0.10g to 0.15g (Vamvatsikos and Cornell, 2004). In the subsequent run, the ground motion records are stepped up with 0.05g times the number of run up to the step under consideration. The analysis with stepping up of IM is stopped when collapse state is indicated with large displacement without much increase in the strength. In order to ensure that the IM at which the model collapses is the lowest IM at which the bridge pier collapses under the corresponding ground motion, a confirmatory analysis is carried. This confirmatory analysis is done by taking an IM value in between the maximum IM value at which the model has collapsed and its next lower value. In the event of collapse at lower IM during a confirmatory analysis, the lower value is considered as the IM at which the bridge pier shall collapse under the considered ground motion. The displacements of pier (DM) corresponding to PGA (IM) are obtained from the results of the analysis in every step. Using the set of IM and DM values from series of analyses on the bridge model, the IDA curve for the bridge is generated for ground motions as shown in Fig. 6.1 and 6.2.

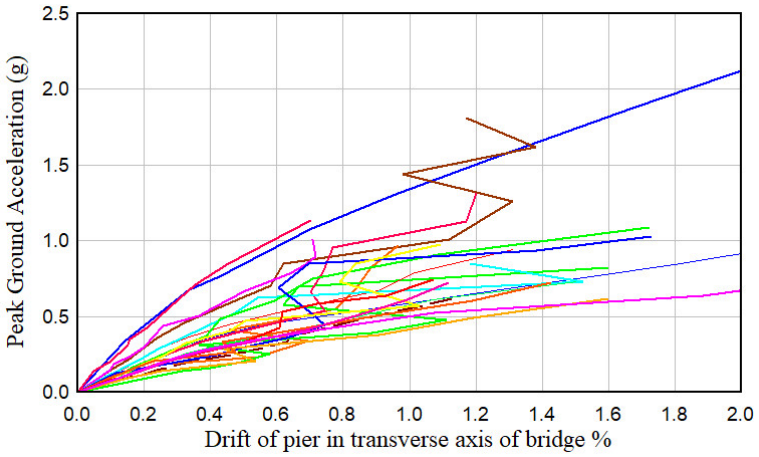

Fig. 6.1 IDA curve of IAB without sleeved pile

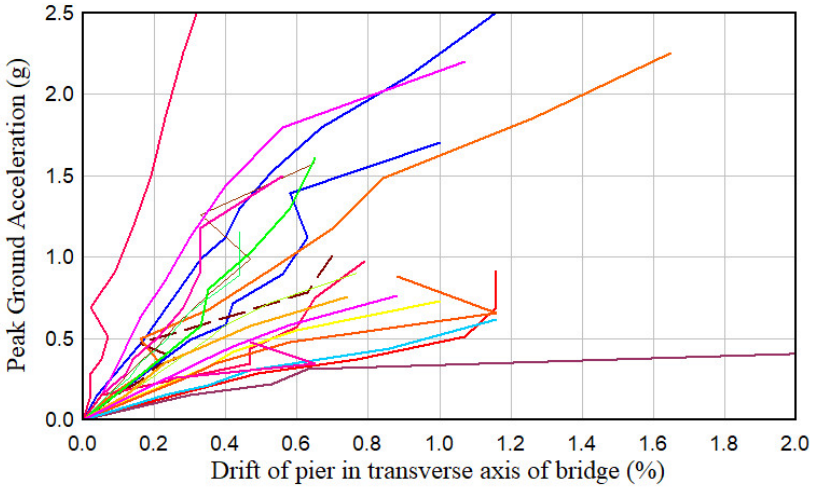

Fig. 6.2 IDA curve of IAB with sleeved pile

The IDA curves of IAB with and without sleeved pile as shown in Fig. 6.1 and Fig 6.2 indicate a distinct elastic linear region at lower IM. The linearity of different curves terminates at different IM and afterwards the majority of the curves soften. This depicts the behavior of the structure with initially linearly elastic elements. However, some of the IDA curves shown in Fig. 6.1 and Fig. 6.2 displays successive softening and hardening. The stiffness of some curves decreases with higher IM while that of some others increase. Such behavior is observed more in the IDA of the bridge with sleeved pile. Vamvatsikos and Cornell (2002) observed that it is the pattern and timing that also makes a difference in the response of the elastoplastic system rather than only by IM. As the accelerogram is scaled up, the weak response cycle in the early part of the time history response becomes strong enough to inflict damage and alter the properties of the structures subjected to the stronger cycles. The configuration of IAB with sleeved pile in foundation is different from the IAB without sleeved pile. Therefore, the presence of more curves with wavy character in the IDA curve of IAB with sleeved pile can be attributed to

the difference in the configuration of the foundation, thus modifying the dynamic characteristics of the bridge. By the interpolation of IDA curve pertaining to each ground motion record, the IDA results can be expressed in any IM. The extracted IM and DM values from each nonlinear dynamic analysis forming a set of discrete point for each record is interpolated for use in generating additional IM or DM values without additional analysis. Complex spline to simpler linear interpolation methods are adopted in the process. Mander et al. (2007) observed that interpolation using multiple spline function is cumbersome and not particularly useful for subsequent risk analysis. From the result of exploring several single functions for use in interpolation method, Mander et al. (2007) also observed the *Ramberg-Osgood* equation as the most suitable. Therefore, in the present analysis, the Ramberg – Osgood (R-O) equation is adopted for the interpolation of the IDA data which is given as (Mander et al. 2007)

$$\frac{EDP}{EDP_c} = \frac{IM}{IM_c} + \left(\frac{IM}{IM_c}\right)^r = \frac{IM}{K_e \times EDP_c}\left(1 + \left|\frac{IM}{IM_c}\right|^{r-1}\right) \tag{6.3}$$

where K_e is the initial slope of IDA curve in proportional range, IM_c is the critical intensity measure that occurs at the onset of large EDP that leads to subsequent collapse, EDP_c ($EDP_c = IM_c/K$) is the critical value of EDP and r is a constant. In the initial interpolation process, the value of r for each pair of the IM and DM in each step of the analysis for each ground motion is calculated. Further, using the median value of r for each ground motion, interpolation value of IM or DM for the ground motion is carried out. During the interpolation, it has been found that the value of r in R-O relation varies across the suite of IDA curve of ground motions. Mander et al. (2007) also observed the same variation in the seismic risk analysis of a bridge and hence adopted a fixed value of r , such as 12 for the New Zealand

code, 6 for the Japanese code and 6 for Caltrans in a seismic risk assessment analysis. In the present study also, the value of r is observed to be varying across the suit of IDA curve. Hence, the value of r adopted as 5 which is observed to be optimally fitting to the IDA curves generated in the analysis and adopted in the interpolation.

Furthermore, the scattered DM values in IDA curves are summarized to their 16%, 50% and 84% of DM values of given IM (Vamvatsikos and Cornell, 2004). To carry out the summarization of DM values, stripes of DM at arbitrary IM values are interpolated for each ground motion using R-O Equation (6.3). The value of K_e, IM_c and EDP_c for respective ground motion is adopted in the interpolation of DM values at a given IM. Therefore, each stripe of the DM for a given IM contains 20 DM values representing each ground motion. By summarizing the DM values for each stripe into their 16%, 50% and 84% fractiles, the DM values for given IM are interpolated for each fractiles to generate 16%, 50% and 84% of IDA curves. The summary of the IDA curve for IAB with and without sleeved pile for DM values given IM is shown in Fig. 6.3 and 6.4.

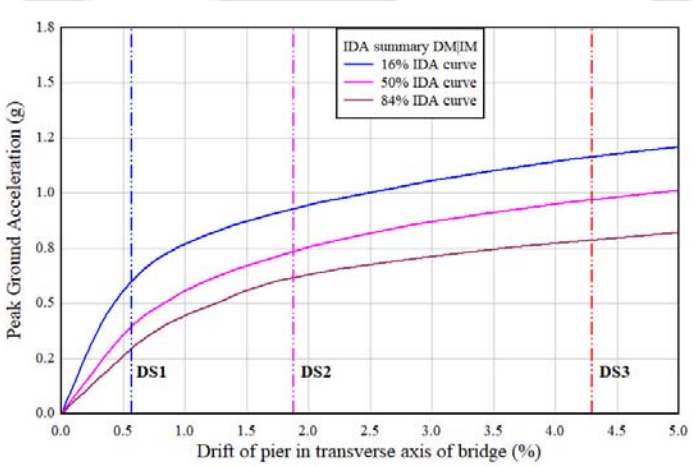

Fig. 6.3 The summary of IDA curve of IAB without sleeved pile into 16%, 50%. 84% fractiles of DM

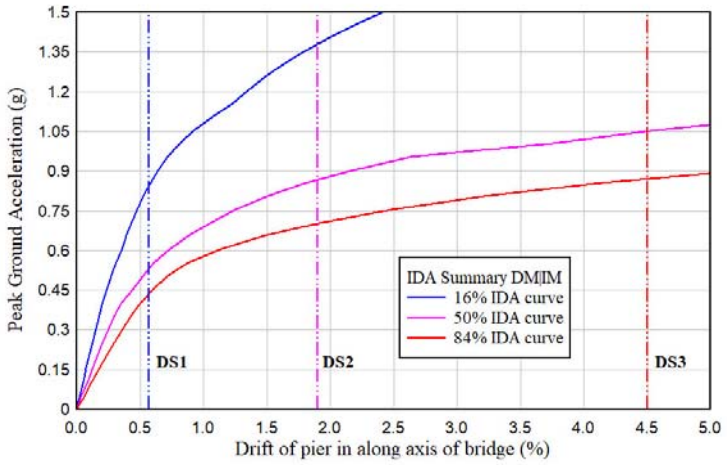

Fig. 6.4 The summary of IDA curve of IAB with sleeved pile into 16%, 50%. 84% fractiles of DM

Using the summary of IDA shown in Fig. 6.3 for IAB without sleeved pile, it is interpolated for the damage state DS1 the corresponding PGA for 16% fractiles of DM is 0.605g, 50% fractiles of DM is 0.40g and 84% fractiles of DM is 0.305g. Therefore, the demand for the damage state is interpolated as: for DS1, 84% of the records is to be scaled to PGA ≥ 0.305g or 50% of the records to PGA ≥ 0.40g or 16% of the records to PGA ≥ 0.605g (Vamvatsikos and Cornell (2002a). Thus, the median demand for DS1 works out to 0.4g which is the IM corresponding to $DM_{50\%}$. Table 6.6 shows the demand interpolated using summary of IDA curve as shown in Fig. 6.3 and 6.4.

Table 6.6 Demand interpolated for IAB with and without sleeved pile in terms of PGA against the fractiles of DM from IDA curve

Damage state	IAB without Sleeved Pile			IAB with Sleeved Pile		
	Corresponding PGA (g)			Corresponding PGA (g)		
	$IM_{16\%}$	$IM_{50\%}$	$IM_{84\%}$	$IM_{16\%}$	$IM_{50\%}$	$IM_{84\%}$
DS1	0.605	0.40	0.305	1.20	0.60	0.35
DS2	0.93	0.72	0.61	> 1.8	1.10	0.70
DS3	1.15	0.97	0.78	> 1.8	1.30	0.90

In addition, the median IDA curve of the bridge computed taking the median values of K_e, IM_c and EDP_c of 20 ground motions is adopted in the IDA. The interpolation of the IDA curve for arbitrary values of IM is done using R-O equation (Equation 6.3). Fig. 6.5 show the median IDA curve of IAB with and without sleeved pile. Fig. 6.5 displays that the seismic demand in the IAB with sleeved pile for the various damage state considered are much higher, implying superior performance from the bridge without sleeved pile. The median value indicated also almost corresponds to the median demand interpolated from the summary of IDA shown in Table 6.6. This also demonstrates that the sleeved pile in the foundation of the bridge is effective in improving the seismic performance of the bridge.

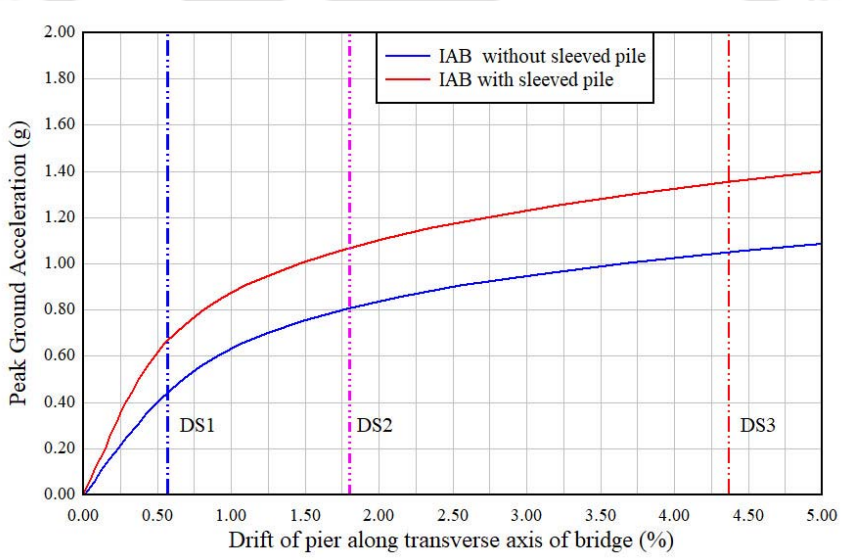

Fig. 6.5 Median IDA curve of the IAB with and without sleeved pile from R-O Equation

6.5 Seismic Fragility Analysis of IAB without and with Sleeved Pile

The fragility function describes the probability of exceedance as a function of ground motion intensity for multiple damage states. The seismic fragility curves have emerged as a powerful tool to quantify the probability of exceedance of a

certain level of damage for a given intensity level of ground motion. Broadly, three methods are adopted in the development of fragility curve, such as empirical, analytical and expert opinion based (ATC, Porter,2016). The empirical fragility function is one that is created by fitting a function to approximate observational data from the laboratory or real world. The observational data are one of the following:

(1) ordered pair of environmental excitation and a binary indicator of failure, like reaching or exceeding the specified limit states for each set of individual assets, or (2) ordered set of environmental excitations, number of assets exposed to that level of excitation and the number of assets that failed when subjected to the environmental excitation. The analytical fragility function is one derived for a class of assets by creating and analyzing a structural model of the asset class. The expert opinion fragility function is created by polling one or more experts who have experience with the asset in question, where the expert gives a guess of the failure probability as a function of environmental excitation. The empirical and expert opinion methods require a large amount of observed damage data and experience which is not within the reach of every engineer and hence the analytical method is observed to be more popular and extensively used in the study of seismic vulnerability of the bridge structures. In this current study also, the seismic fragility analysis of the bridge is carried out using the analytical method. The fragility curve of the bridge, which is the conditional probability state of the bridge's vulnerability as a function of ground motion, is a common tool for seismic assessment. The configuration of the bridge considered in the study indicates that the bridge will lose its function only if there is damage to the pier. Hence, the seismic fragility analysis is carried out considering the damage states of the pier.

The seismic fragility identifies the probability that the seismic demand on the structure (D) is greater than the capacity. The probability is conditioned on a chosen intensity measure (IM) which represents the level of seismic loading. The representation of this conditional probability is given as (Nielson and DesRoches, 2007):

$$Fragility = P[D \geq C|IM] = P[C - D \leq 0.0|IM] \tag{6.4}$$

The solution of the Equation (6.4) is accomplished through seismic demand obtained using IDA. Assuming that the demand and capacity of the structure to follow lognormal distribution, the fragility statement in Equation (6.4) takes the following form as (Nielson and DesRoches, 2007)

$$P[D > C|IM] = \phi\left(\frac{\ln(S_d/S_c))}{\sqrt{\beta_{D|IM}^2 + \beta_{cD}^2}}\right) \tag{6.5}$$

Taking the value of S_d(the median estimate of demand), S_c (median estimate of the capacity), $\beta_{D|IM}$ (the dispersion or logarithmic standard deviation of the demand conditioned on the intensity measure) and β_{cD} (the dispersion of the capacity), the fragility curve of the bridge is developed. In the estimation of uncertainty in the seismic demand $\beta_{D|IM}$ of bridge pier, Stefanidou and Kappos (2017) observed its value to be varying and increase with the higher level of intensity. It was also observed that uncertainty in seismic demand may be equal, greater, or even less than the value recommended in HAZUS. The HAZUS (2003) specifies a dispersion value of 0.60 for ground shaking algorithm of damage function of bridge. In the present study, for the purpose of comparative evaluation of the bridge type with and without sleeved pile, the value of $\beta_{D|IM}$ is taken as 0.6 in the line of dispersion value specified in HAZUS (2003). In addition, the value of dispersion of capacity is

adopted as 0.35 for pier in the line of representative value proposed by Stefanidou and Kappos (2017) in their studies of the development of bridge specific fragility curves.

Furthermore, the median demand for the different damage state is obtained from the summarized curve of IDA to various percentiles of DM. The PGA value corresponding to the damage state at 50% percentile of DM that is $IM_{50\%}$ is adopted as the median demand of the damage state. The value of median demand for various damage state adopted in the development of fragility curve for different damage state is shown in Table 6.7.

Table 6.7 Estimated median IM values from IDA summarization

Bridge type	Median IM for different damage states (g)		
	DS1	DS2	DS3
IAB without sleeved pile	0.4	0.72	0.97
IAB with sleeved pile	0.6	1.10	1.3

The comparative plot of the fragility curve developed for IAB with and without sleeved pile using the median demand is shown in Fig. 6.6 to 6.8.

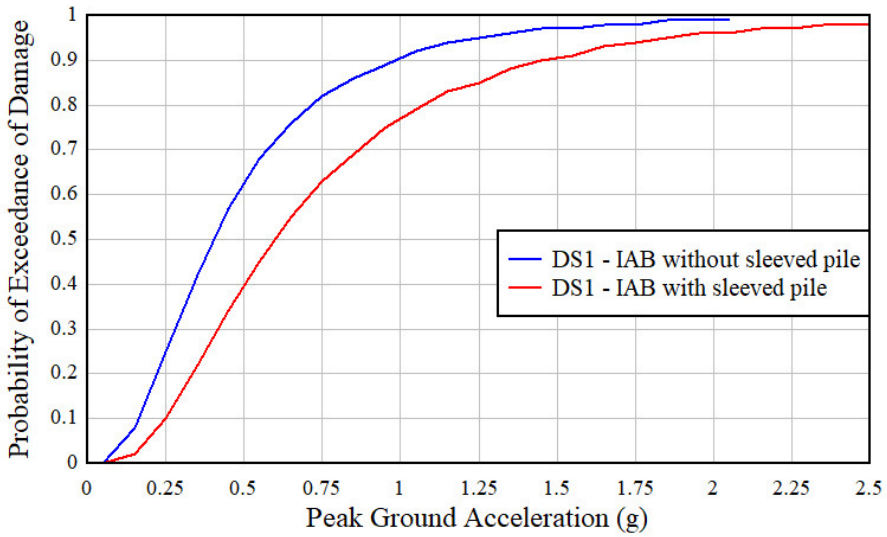

Fig. 6.6 Fragility curve of IAB with and without sleeved pile for damage state DS1

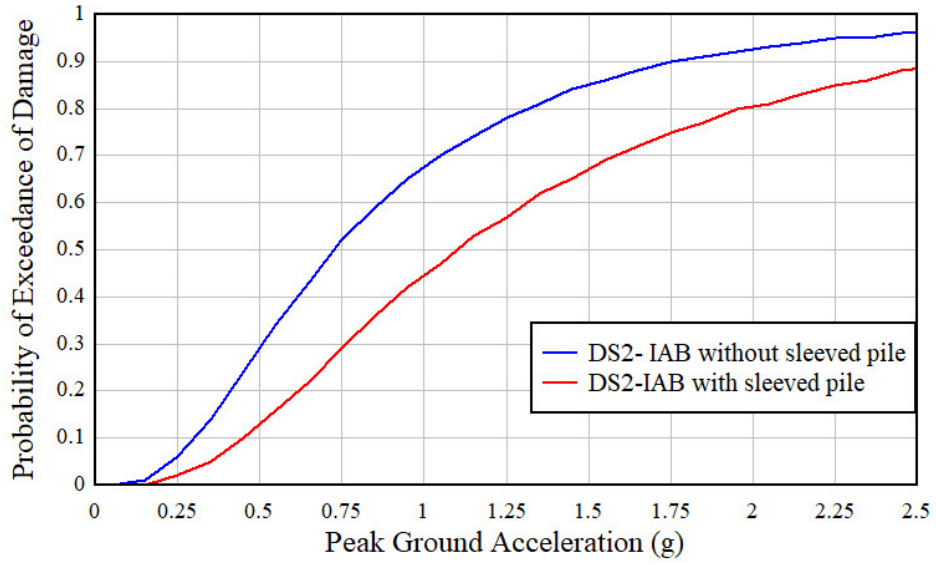

Fig. 6.7 Fragility curve of IAB with and without sleeved pile damage state DS2

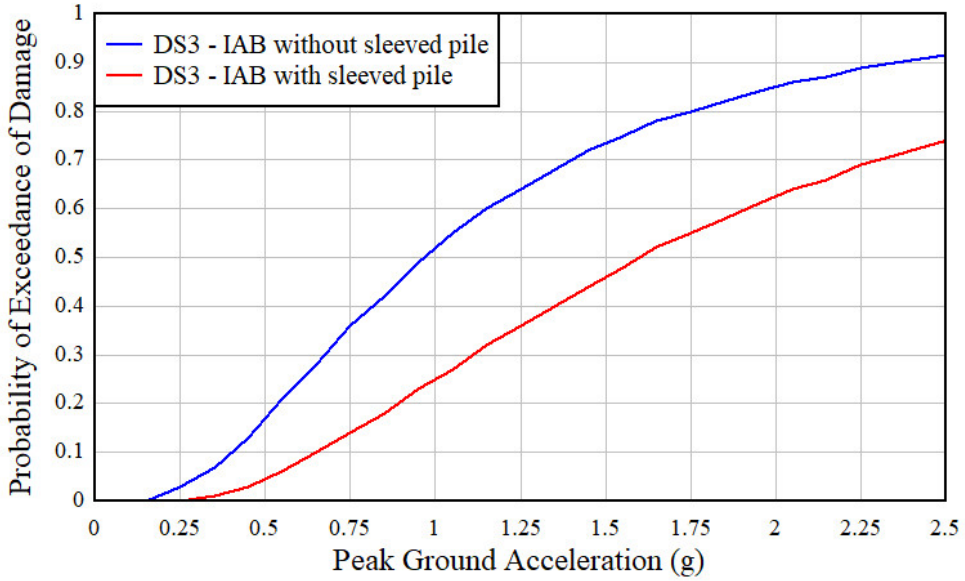

Fig. 6.8 Fragility curve of IAB with and without sleeved pile damage state DS3

The comparative study of the fragility curves of IAB with and without sleeved pile distinctively indicates that the bridge with sleeved pile is less vulnerable under different damage states considered. The ground acceleration required for initiating probability of exceedance of damage states in the bridge with sleeved pile is

observed to be marginally higher. This clearly signifies the improvement in seismic capacity of the bridge with sleeved pile.

6.6 Concluding Remarks

From the observation of the IDA results and analytical fragility curve developed for different categories of the bridges, the following conclusions are drawn:

1. A reasonable estimate of seismic capacity of IAB with and without sleeved pile can be made using IDA.
2. The IDA results and fragility curve of IAB with and without sleeved pile indicates that the bridge with sleeved pile in foundation is less vulnerable to seismic excitation.

Chapter 7

Summary and Conclusion

7.1 Summary

The Integral abutment bridges are designed without any movable deck joint at pier or at abutment and thus the construction practice of IAB is significantly different from the conventional method of construction of bridges where bearings are on pier and abutment to support the deck. In IAB, the deck of the bridge is cast monolithically with abutment wall and in the case of multiple span IAB, the deck is either integrated with pier designed for flexible behavior or supported on bearing on top of pier cap designed for rigid behavior. At present the major research activities are observed in the field of evaluation of performance of IAB under thermal load. The redundancy provided by the configuration of the bridge is observed to enhance the seismic performance of the bridge and hence, the bridge type is well suited for seismic resistant design of bridges with short to medium span, in areas classified as high seismic zone. However, the literature on seismic behavior of integral abutment bridges with soil structure interactions are scanty and thus, require additional studies for adoption of this type of bridge with confidence. In view of this, the objective of this study is aimed at developing a three-dimensional model of the bridge incorporating the soil structure interaction to observe the seismic characteristics and the response of IAB under seismic excitation. The implication of incorporating the soil structure interaction in evaluation of seismic response is also studied for the design of class of bridges for practical

implementation. In addition, a strategy for improving the seismic performance of the bridge under seismic event is also kept in view in this study.

Review of relevant literature indicates that piles are most commonly adopted for the foundation of IAB although spread foundations are also observed to be adopted for some short span IAB. Therefore, existing modelling approach in the soil pile interaction and abutment backfill interaction is studied in detail and most relevant strategies are identified for adopting in the modelling of soil pile interaction of IAB to be analyzed under seismic excitation. It has been observed that in modelling the axial capacity of pile, the load settlement $Q-z$ curve for modelling tip bearing interaction in pile and load transfer $t-z$ curve for modelling shaft skin frictional force interaction are adequate. Similarly, in the modelling of laterally loaded pile, the load deflection $p-y$ curve is observed to be commonly adopted and reasonably accurate for the simulation of soil pile interaction under cyclic loading. Therefore, these curves are adopted in the modelling of soil pile interaction in this study. In the modelling of far field soil reaction, the formulation based on the assumption of plain strain with two-dimensional wave propagation analogy is observed to be implementable in the modelling of lateral far field soil reaction for pile foundation in IAB. The studies on abutment backfill interaction indicates that the relation between the displacement of abutment wall towards backfill and the passive pressure mobilized is hyperbolic in nature.

The finite element model of the bridge considered in this study is developed in SAP 2000 (Version 18). The grillage model is adopted in the modelling of the deck. The abutment wall and the pier cap are modelled with shell element. The pier and piles are modelled with beam element. To compute the effect of the incorporation of far field soil model element, two categories of models are developed by changing the

soil pile interaction modelling. In the first model, the soil pile interaction is modelled with the soil spring of $p - y$ curve representing only the near field soil. In the second model, the far field soil elements are incorporated in the soil pile interaction modelling by attaching the far field soil element in series with the near field soil spring. Free vibration analyses of both the models are carried out to compute the dynamic characteristics of the models of IAB and the effect of far field soil reaction in the dynamic characteristic of the IAB. Further, nonlinear time response history of both the model were analyzed using design spectrum compatible ground motion record of El Centro and Koyna. The thermal load analysis is carried out using pushover analysis for thermal expansion and contraction of 17^0 C.

To enhance the seismic performance of IAB, the adoption of sleeved pile is observed to be beneficial in reducing the transmissibility of ground motion to superstructure of the bridge. The comparative evaluation of seismic capacity of bridge with and without sleeved pile using IDA exhibited a superior performance of bridge with sleeved pile under seismic event. Similarly, the fragility analysis of the bridge with and without sleeved pile also indicated that the bridge with sleeved pile is less vulnerable to seismic damages.

7.2 Major Findings

The major findings from the present study are summarized as:

1. The incorporation of far field soil reaction element in the modelling of soil pile interaction in IAB increases the flexibility of the bridge, resulting in a longer period of vibration of the bridge. The participating mass ratio in the fundamental mode of the vibration in transverse direction also increases with the incorporation of far field soil reaction modelling.

2. The seismic forces induced in IAB increase with the incorporation of far field soil element. This increase is observed to be significant in the seismic forces of piles supporting the abutment and pier. The drift in the pier of IAB in transverse direction is also observed to increase significantly with incorporation of far field soil reaction element enhancing the damage potential in pier.

3. High stiffness of IAB along the axis of the bridge due to the restraining effect of abutment and backfill is manifested in the appearance of first significant longitudinal mode as one of the higher modes with a short period of vibration. The seismic displacement along the axis of the bridge is observed to be minimal and therefore, IAB is observed to be less vulnerable to seismic excitation along the axis of bridge.

4. The thermal displacement of abutment along the axis of the bridge is lower than the computed value of unrestrained expansion for the thermal variation of 17.5^0 C. The abutment is found to rotate about its base while it deflects with expansion of deck at top.

5. The limiting length of IAB with concrete pile can be worked out by computing the allowable deflection of abutment. This is done by moment curvature analysis of pile section with target compressive or tensile strain under deformation due to the expansion of deck under maximum thermal variation.

6. The sleeved pile in IAB renders the bridge flexible as a whole by lengthening the vibration period of the bridge. The transmissibility of ground motion to superstructure in IAB with sleeved pile is reduced as compared to that of IAB without sleeved pile, thereby improving performance under seismic

excitation. The sleeved pile in bridge foundation is effective in controlling seismic response of bridge.

7. The proposed design strategy for sleeved pile is simple and implementable in the design office. Iteration may be required for the suitable adjustments in stiffness of pier and abutment foundations.
8. The comparative study on evaluation of seismic capacity of bridge using IDA indicates that the IAB with sleeved pile have higher seismic capacity than that without sleeved pile. The fragility analyses of both the bridge types also indicate that the IAB with sleeved pile is less vulnerable to seismic damage.
9. The concept of sleeved pile is an effective means of isolation of the bridge superstructure. Elastic response of the bridge under seismic ground motion can be ensured by adopting sleeved pile in the bridge foundation.

7.3 Recommendation for future works

The present research works can be further extended for developing more insight behavior of IAB as follows:

1. Experimental investigation of IAB without sleeved pile to observe the dynamic characteristics and seismic response of the bridge,
2. Experimental investigation of IAB with sleeved pile to observe the dynamic characteristics and seismic response of the bridge.
3. Field implementation of IAB with and without sleeved pile, and monitoring field performance of the bridge under thermal as well as seismic excitation using appropriate sensors.

Reference

[1] AASHTO [2012], "*AASHTO LRFD Bridge Design Specification 2012.*" Washington D.C.

[2] AASHTO [2009], "*AASHTO Guide Specification for LRFD Seismic Design of Bridge.*" Washington D.C.

[3] ASCE/SEI 41-06[2006], "*Seismic Rehabilitation of Existing Building*", ASCE, USA.

[4] Akbari R. [2010] "Seismic fragility analysis of reinforced concrete continuous span bridge with irregular configuration," *Structure and Infrastructure Engineering*, Volume 8, No. 9, November 2012. 873-889.

[5] Amde M., Tinsae W., Greimann L.F., Yang, P. S. [1988] "End Bearing Piles in Jointless Bridges, ASCE *Journal of Geotechnical and Geoenvironmental Engineering,* Vol.114, No. 8., pp 1870-1884.

[6] American Petroleum Institute [2007], "*Recommended practice For Planning, Designing and Constructing Fixed Offshore Platform – Working Stress Design,*" Transportation Research Board, API Publishing Services, Washington D.C USA,

[7] Applied Technology Council [1996], "*Seismic Evaluation and Retrofit of Concrete Buildings: Volume 1,"* Seismic Safety Commission, California,

[8] Arokiasamy M. Butreng N., Sivakumar M. [2004], "State-of- the- Art Integral Abutment Bridges: Design and Practice, *Journal of Bridge Engineering*, ASCE Vol. 9, No.5 pp 497-506.

[9] Aviram A., Mackie K.R. [2008], *"Guidelines for Non-linear Analysis of Bridge Structures in California, Berkeley"* PEER Report 2008/03.

[10] BA42 Highway Agency [1993], "*Design Manual for Integral Bridges: Design Manual for Road and Bridges, Vol. 1.*" The Stationary Office London,

[11] Barker R.M., Duncan J.M, Rojiani K.B., OOI P.S.K, Tan C.K, Kim S.G. [1991], "*NCHRP:* Manual for Design of Bridge Foundations"*, Transportation Research Board,* Washington D.C, USA,

[12] Berry M.P., Eberhard M.O. [2007]. "Performance Modelling Strategies for Modern Reinforced Concrete Bridge Columns." *Report No. PEER-2007/07*, Pacific Earthquake Engineering Research Centre, University of California, Berkeley, CA.

[13] Berger E., Dames & Moore, Mahim S.A. [1977], "Simplified method for evaluating soil-pile-structure interaction effects," *Offshore Technology Conference*, May 2-5, Hutson, Texas.

[14] Biggs J.M. [1982] "Flexible Sub-Surface Building Foundation Interface for Aseismic Design (Final Report)" *Report No R81-8*, School of Civil Engineering Massachusetts Institute of Technology Cambridge, Massachusetts.

[15] Boardman P.R., Wood B.J. [1983], "Union House-A Crossed Braced Structure with Energy Dissipators". *Bulletin of the New Zealand National Society for Earthquake Engineering Vol. 16 No.2 June 1983.* 83-97

[16] Boragrd D., Matlock H. [1980], "Simplified Calculation of $p - y$ Curves for Laterally Loaded Piles in Sand", Unpublished Report, Ertec, Inc.

[17] Breña S.F., Bonczar C.H., Civjan, S.A., Dejong J.T. Crovo D. [2007], "Evaluation of Seasonal and Yearly Behavior of an Integral Abutment Bridge." *ASCE Journal of Bridge Engineering*, Vol. 12, No.1 pp 64-71.

[18] Brown J. Kunnath S.K. [2000], "*Low Cycle Fatigue Behavior of Longitudinal Reinforcement in Reinforced Concrete Columns.*" Technical Report MCEER-00-0007, July 23, 2000.

[19] Buckle I.G., Friedland I., Mander J., Martin G., Nutt R. Power M. [2006]. "*Seismic Retrofitting and Manual for Highway Structures: Part-I Bridges*", Technical Report MCEER-06-SP10, Federal Highway Administration, USA.

[20] CALTRANS [2010], "*CALTRANS Seismic Design Criteria*, *Version 1.6"* www.dot.ca.gov/des/techpubs/bdp.html

[21] CALTRANS [2015], "*Bridge Design Practice",* Chapter 4 Department of Transportation, California, www.dot.ca.gov/des/techpubs/bdp.html

[22] COSMOS (Consortium of Organization for Strong Motion Observation Systems)Virtual Data Center - Strong Motion Center, www.cosmos-eq.org

[23] Coyle H.M., Sulaiman, I.H. [1967], "Load Transfer of Axially Loaded Piles in Clay," *Journal of Soil Mechanics and Foundation Engineering Division*, ASCE, Vol. 92, SM2, Paper No 2079, pp. 459-472.

[24] Charles W.W.Ng, Zang L.M. [2001], "Three-Dimensional Analysis of Performance of Laterally Loaded Sleeved Piles in Sloping Ground". *Journal of Geotechnical and Geoenvironmental Engineering*, Vol.127 ASCE June 2001, 499-509.

[25] Claugh G.M., Duncan D.W. [1991], "*Foundation Engineering Handbook.*" Edited By H.Y.Fang Indian Edition, CBS publishers, New Delhi,

[26] Chopra A.K. [2008], "*Dynamic of Structures, Theory and Application to Earthquake Engineering (Third Edition)*" Prentice-Hall of India Pvt. Ltd New Delhi.

[27] Civjan S.A., Bonczar C.H., Breña S.F, Dejong J.T., Crovo D. [2007]. "Integral Abutment Bridge Behavior: Parametric Analysis of Massachussetts Bridge." *Journal of Bridge Engineering*, ASCE Vol. 12, No.1 pp 64-71.

[28] Davisson M.T., Robinson, K.E., [1965] "Bending and Buckling of Partially Embedded Piles." *Proceeding of 6th International conference on Soil Mechanics and Foundation Engineering,* Montreal, Canada, 1965.

[29] Dicleli M., Albhaisi S.M. [2003], "Maximum length of integral Abutment bridges supported on steel H-piles driven in sand." *Engineering Structures*, Elsevier Vol.25 pp 1491-1504.

[30] Dicleli M., Albhaisi S.M. [2004], "Performance of abutment-backfill system under thermal variation in integral abutment bridges built in clay," *Engineering Structures*, Elsevier Vol.26 pp 949-962.

[31] Dicleli M. [2005], "Integral Abutment-Backfill Behavior on Sand Soil-Pushover Analysis Approach," *Journal of Bridge Engineering*, ASCE Vol. 10, No.3, pp 354-364.

[32] Dunker K.F., Liu, D. [2007], "Foundation for Integral Abutments," *"Practice Periodical on Design and Construction,* ASCE Vol. 12 No.1 pp 22-30.

[33] Duncan J.M., Byrne P., Wong K. S., Mabry P. [1980] "Strength, stress strain and bulk modulus of parameters for finite element analyses of stress and movement in soil masses." *Report No UCB/GT/80-01,* College of Engineering, University of California, Berkeley, California

[34] Duncan J.M., Mokwa R. L. [2001], "Passive Earth Pressure: Theories and Tests," *ASCE Journal of Geotechnical and Environmental Engineering,* Vol. 127; No. 3. pp 248-257.

[35] Dutta A. and Mander J.B. [1998], "*Capacity Design and Fatigue Analysis of Confined Concrete Column*", Technical Report MCEER-98-0007.

[36] Dutta A. and Mander J.B. [1998a], "Seismic Fragility Analysis of Highway Bridges", In. H. Kameda and L. Friedland, eds. *Centre-to-centre project workshop on earthquake engineering frontiers in transportation system* (International Center for Disaster-Mitigation Engineering (INCEDE)) 22-23 June 1998, Tokyo, Japan, Kyoto University, INCEDE report 1999-05, 1-36.

[37] Elnashai A.S., Sarno L.D., Kwon O.S [2015], "*Fundamentals of Earthquake Engineering form source to Fragility*," Second Edition. John Wiley and Sons Ltd, U.K.

[38] Erhan S., Dicleli, D. [2014], "Effect of dynamic soil-bridge interaction modelling assumption on the calculated seismic response of integral bridge." *Soil Dynamics and Earthquake Engineering,* Vol. 66 pp 42-55.

[39] Faraji S., Tim, J.M., Crovo, D. S., Erust H. [2001], "Nonlinear Analysis of Integral Bridge: Finite Element Model." *Journal of Geotechnical and Geoenvironmental Engineering*, ASCE Vol. 127; No.5., pp 454-461.

[40] Farahani R.V., Zhao, Q., Burdette, E.G. [2010], "Seismic Analysis of Integral Abutment Bridge in Tennessee, including Soil-Structure interaction." *Journal of Transportation Research Board* No 220, Washington D.C. pp 70-79.

[41] FEMA-356 [2000], *Pre-standard and Commentary for the Seismic Rehabilitation of Building*, FEMA, Washington D.C.

[42] Fennema J.L., Jeffrey A, L., Linzell, D.G [2005], "Predicted and Measured Response of an Integral Abutment Bridge," *Journal of Bridge Engineering,* ASCE Vol. 10, No. 6 pp 666-677.

[43] Gambhir M.L. [2005], "*Stability Analysis and Design of Structures*" Springer (India) Pvt. Limited, New Delhi.

[44] Gazetas G., Dobry R. [1984]. "Horizontal Response of Piles in Layered Soils," *Journal of Geotechnical and Geoenvironmental Engineering*, ASCE Vol. 110; No.1., pp 20-40.

[45] Gazetas G., Dobry R. [1984a], "Simple Radiation Damping Model for Piles and," *Journal of Engineering Mechanics*, ASCE Vol. 110; No.6., pp 937-756.

[46] Girton D. D., Hawkinson T. R. Greimann L. F. [1991], "Validation of Design Recommendation for Integral-Abutment Piles." *Journal of Structural Engineering,* ASCE Vol. 117, pp 2117-2134

[47] Goel R.K. [1997] "Earthquake Characteristics of Bridge with Integral Abutment," *Journal of Structural Engineering,* ASCE Vol. 123 pp 1435-1443

[48] Haselton C.B., Deierlein G.G. [2007], "Assessing seismic collapse safety of modern reinforced concrete moment-resisting frame building." *Report No PEER-2007/08*, Pacific Earthquake Engineering Research Centre, University of California, Berkeley, CA.

[49] HAZUS-MH MR4 [2003]. "*Multi-hazard Loss Estimation Methodology Earthquake Mode (FEMA-2003),*" National Institute of Building Sciences, Washington D.C.

[50] Holley Jr M.J., Holley H., Biggs J.M. & Kray C.J. [1973] "Sleeved Pile for Offshore Structure Under Lateral Loading." *Fifth Offshore Technology Conference, Huston, 29th April to May 2,1973.*

[51] IRC:6 [2014], "*Standard Specification and Code of Practice for Road Bridges, Section: II Load and Stresses*," Indian Road Congress, IRC Bhawan, New Delhi,

[52] IRC:112 [2011], "*Code of Practice for Concrete Bridges,*" Indian Road Congress, IRC Bhawan, New Delhi,

[53] IS: 800 [2007], "*Indian Standard Code for General Construction of Steel,*" 3rd revision, BIS New Delhi.

[54] IS: 2062[2011], "*Hot Rolled Medium and High Tensile Structural Steel - Specification (Seventh Revision)*" BIS New Delhi.

[55] Khodir Y.A., Hassiotis S. [2005], "Analysis of soil pile interaction in Integral abutment bridge," *Computers and Geotechnics,* Vol 32, pp 201-209.

[56] Kim W., Laman J.A. (2010), "Numerical analysis method for long-term behavior of integral abutment bridges," *Engineering Structures,* Elsevier Vol. 32, pp 2247-2257.

[57] Kim W., Laman J.A. [2010a], "Integral abutment bridge response under thermal loading," *Engineering Structures,* Elsevier Vol. 32, pp 1495-1508.

[58] Kim W., Laman J.A. [2011], "5-year Field Monitoring of Integral abutment bridges." *Journal of performance of constructed facilities,* ASCE, CF June 16, 2011, doi.10.1061/(ASCE)CF1943-5509 0000250.

[59] Kornkasem W., Foutch D., Long J. H. [2001], "Seismic Behavior of Pile-Supported Bridges." *PhD Thesis,* University of Illinois, Urbana-Champaign.

[60] Kramer S.L. [2003], "*Geotechnical Earthquake Engineering,"* Pearson Education (Singapore) Pte. Ltd.

[61] Kwon O.S., Elnashai A.S. [2010], "Fragility analysis of highway over-crossing bridge with consideration of soil structure interaction," *Structural and Infrastructural Engineering,* Vol. 6, No.1 pp 159-178.

[62] Kumar P.T.V. [2008], "Behavior of integral abutment bridges under temperature effect and seismic excitation," *PhD Thesis,* Indian Institute of Technology, Roorkee.

[63] Mander J.B., Priestley M.J.N., Park R., [1988], "Theoretical Stress-Strain Model for Confined Concrete," *Journal of Structural Engineering,* ASCE Vol. 114 No.8 pp 1084-1826

[64] Mander J.B., Dhakal R. P. Mashiko N., Solberg K.M. [2007], "Incremental dynamic analysis applied to seismic financial risk assessment of bridges." *Engineering Structures* Vol. 29, 2662-2672.

[65] *"MassHighway Bridge Manual Part I,"* [2005]", Massachusetts Department of Transportation.

[66] Matlock H. [1970] "Correlation for Design of Laterally Loaded Pile in Soft Clay." *Offshore Technology Conference*, April 22-24, Huston, Texas.

[67] Mauri R.F., Petro S.H. [2005], "Integral Abutment and Jointless Bridges (IAJB) 2004 Survey Summary", *The 2005- FHWA Conference, Integral Abutment and Jointless Bridges (IAJB 2005)*, March 16-18, 2005, Beltimore, Maryland.

[68] Meyer B.J., Reese L.C. [1979], "Analysis of Single Pile Under Lateral Loading," *Research Report No. 244-1,* Centre for Highway Research, The University of Texas, Austin, Texas, December 1979.

[69] Monzon E.V., Itani A.M., Pekcan G. [2014], "Seismic behavior and design of steel girder bridge with integral abutment," *Engineering Structures,* Vol. 10, 117-128, IOS Press.

[70] Mosher R.L. [1984], "*Load Transfer Criteria for Numerical Analysis of Axially Loaded Piles in Sand*," U.S. Army Engineering Waterways Experimental Station Automatic Data Processing Center, Vicksburg, M.S.

[71] Mistry V.C., [2005)], "Integral Abutment and Jointless Bridges", *The 2005- FHWA Conference, Integral Abutment and Jointless Bridges* (IAJB 2005), March 16-18, 2005, Beltimore, Maryland.

[72] Naggar M. H. El, Navak M. [1995], "Nonlinear lateral interaction in pile dynamics." *Soil Dynamics and Earthquake Engineering;* Vol. 14(1995) pp 141-157

[73] Nelson B.G., DesRoches R. [2007], "Seismic fragility methodology for highway bridges using component level approach." *Journal of Earthquake Engineering & Structural Dynamics; 2007* Vol. 36, pp 823-839.

[74] Ooi P.S.K., Lin, X., Hamada H.S. [2010],"Field Behavior of an Integral Abutment Bridge Supported on Drilled Shafts," *Journal of Bridge Engineering*, ASCE Vol. 15, No.1, pp 4-18.

[75] Oesterli, R.G, Volz, J.S. [2005], "Effective Temperature and Longitudinal Movement in Integral Abutment Bridges", *The 2005-FHWA Conference, Integral Abutment and Jointless Bridges* (IAJB 2005), March 16-18, 2005, Beltimore, Maryland.

[76] O'Neill M.W., Murchison J.M. [1983], "An Evaluation of P-Y Relationships in Sands". *A Report to the American Petroleum Institute (PRAC 82-41-1)*.

[77] Park R. and Paulay T. [1975], "*Reinforced Concrete Structures*", John Wiley and Sons, New York.

[78] Parkar F. Jr., Reese L.C., [1970], "Experimental and Analytical Studies of Behavior of Single Pile in Sand under Lateral and Axial Loading," *Research Report No 177-2*, Texas Highway Department in Collaboration with U.S. Department of Highway and Federal Administration.

[79] Porter K. [2016], "*A Beginner's Guide to Fragility, Vulnerability and Risk,*" University of Colarado Bulder 92, USA.

[80] Porter K., Kennedy R., Bachman R. [2007], "Creating Fragility Functions for Performance- Based Earthquake Engineering." *Earthquake Spectra,* Vol. 23*, No. 2* 471-489, May 2007. Earthquake Engineering Research Institute.

[81] Prakash S., Sharma H.S. [1990], "*Pile Foundations in Engineering Practice*" Wiley India Pvt. Limited, Noida.

[82] Priestley M.J.N., Calvi G.M., [1996], "*Seismic Design and Retrofit of Bridges,*" John Wiley & Son Inc, New York.

[83] Priestley M.J.N., Calvi G.M., Kowalsky M.J. [2007], "*Displacement-Based SeismicDesign of Structures,*" IUSS Press, Pavia, Italy.

[84] Pugasap K., Kim, W. Laman J.A. [2009], "Long-Term Response Prediction of Integral Abutment Bridges." *Journal of Bridge Engineering*, ASCE Vol. 14, No.2, pp 129-139.

[85] Raupach E., Schumacker B., Biggs J.M. [1981], "Flexible Sub-Surface Building Foundation Interface for Aseismic Design (Preliminary Studies)" *Report No R81-8*, School of Civil Engineering Massachusetts Institute of Technology Cambridge, Massachusetts.

[86] Reese L. C. [1962], "Ultimate Resistance Against a Rigid Cylinder Moving Laterally in a Cohesionless Soil" *SPE Production Research Symposium,* Tulsa, Okla, April 12-13, 1962

[87] Reese L.C., Cox, W.R., Koop, F.D. [1974], "Analysis of Laterally Loaded Pile in Sand," *Sixth Annual Offshore Technology Conference,* Dallas Texas, May 6-8, 1974.

[88] Reese L.C., Cox, W.R., Koop, F.D. [1975], "Field Testing and Analysis of Laterally Loaded Pile in Stiff Clay," *Seventh Annual Offshore Technology Conference,* Dallas Texas, May 5-8, 1975.

[89] Reese L.C., Welch R.C. [1975] "Lateral Loading of Deep Foundation in Stiff Clay." *Journal of Geotech Engineering Division,* ASCE Vol.101 No GT. 7 July 1975 pp 633-649.

[90] Reese L.C., Isenhower W.M., Wang, S.T. [2006] "*Analysis and Design of Shallow and Deep Foundation,*" John Wiley and Sons Inc. New Jersey

[91] SAP 2000 [Version 18] "*CSI Analysis Reference Manual*" Computers and Structure Inc. Berkeley, California USA.

[92] Seed H.B. Idriss I.M. [1970], "Soil Moduli and damping factors for Dynamic response analyses." *Research Report No. UCB/EERC-70-10,* University of California, Berkeley, California, USA.

[93] Seed H.B. Wong R.T., Idriss I.M. Tokimatsu [1984], "Moduli and Damping factor for dynamic analyses of cohesionless soil." *Research Report No. UCB/EERC-84/14,* University of California, Berkeley, California, USA.

[94] "SeismoMatch" version 2.1.0 SeismoSoft, Italy: www.seismosoft.com

[95] Shamsabadi A., Rollins K.M., Kapuskar M. [2007], "Nonlinear Soils-Abutment-Bridge Structure Interaction for Seismic Performance-Based Design," *Journal of Geotechnical and Geoenvironmental Engineering,* ASCE Vol.133; No. 6., pp 707-720.

[96] Shome N., Cornell, C.A. (1999). "Probabilistic Seismic Demand Analysis of Non-linear Structures." *Report No RMS-35*, RMS Program, Stanford university, Stanford C.A.

[97] Spyrakos C., Loannidis G. [2003], "Seismic behavior of a post-tensioned integral bridge including soil-structure interaction (SSI)." *Soil Dynamic and Earthquake Engineering,* Vol.23, pp 53-63.

[98] Stefanidou S.P., Kappos A.J. [2016], "Methodology for the development of bridge specific fragility curves," *Earthquake Engineering & Structural dynamics,* Vol. 46 pp 73-93.

[99] Sungchil L., Feng M.O., Kwon S.J., Hong S.H. [2011], "Equivalent Modal Damping of Short-Span Bridges Subjected to Strong Motion." *Journal of Bridge Engineering*, ASCE Vol. 16, No. 2 pp 316-323.

[100] Takeda T., Sozen M.A., Nielsen N.N. [1970], "Reinforced Concrete Response to Simulated Earthquake", *Journal of Structural Engineering,* ASCE Vol. 96, No 12, pp 2257-2273.

[101] Terzaghi K. [1955], "*Evaluation of Coefficient of Subgrade Reaction*", Geotechnique, ICE, Vol.5 No 4. pp 297-325.

[102] Terzaghi K., Peck R.B., Mesri G. [1996], "*Soil Mechanics in Engineering Practice, Third Edition*", John Wiley & Sons Inc, UK

[103] Tehrani P., Mitchell D. [2012], "Seismic Performance Assessment of Bridges in Montreal Using Incremental Dynamic Analysis," *Proceeding on World Conference on Earthquake Engineering*. Lipson, Portugal.

[104] Tehrani P., Mitchell D. [2013] "Seismic Risk Assessment of Four-Span Bridge in Montreal Designed Using the Canadian Bridge Design Code" *Journal of Bridge Engineering*, ASCE Vol. 19(8) pp A4014002-1 -9.

[105] Thippeswamy, H.K., GangaRao, H.V.S., Franco J.M. [2002] "Performance Evaluation of jointless Bridge," *Journal of Bridge Engineering,* ASCE Vol. 7, No.5, pp 276-289.

[106] Tinsae A.M.W., Greimann L. [1988], "End Bearing Piles in Jointless Bridges." *Journal of Structural Engineering,* ASCE Vol. 114, No 8, pp 1870-1884.

[107] Vamvastsiko D., Conell C.A. [2002], "Incremental Dynamic Analysis." *Earthquake Engineering and Structural Dynamic*, Vol.31 491-514.

[108] Vamvastsiko D., Conell C.A. [2002a], "Incremental Dynamic Analysis and its Application to Performance-Based Earthquake Egnineering." *12th European Conference in Earthquake Engineering*, Paper No 479.

[109] Vamvastsiko D., Conell C.A. [2004], "Applied Incremental Dynamic Analysis." *Earthquake Spectra*, Vol. 20 No.2 523-553. Earthquake Engineering Research Institute.

[108] Vijayavergiya V.N. [1977], "Load Movement Characteristics of Piles," *4th Symposium of Waterways, Port, Coastal and Ocean Division*, American Society of Civil Engineers, Long Beach, C.A. Vol.2 pp. 561-584.

[109] Weakley K. [2005], "VDOT Bridges Design Guidelines", *The 2005-FHWA Conference, Integral Abutment and Jointless Bridges* (IAJB 2005), March 16-18, 2005, Beltimore, Maryland.

[110] White ll, H. Pètursson, H. Collins P. [2007], "Integral Abutment Bridge: The European Way," *Practice Periodical on Design and Construction,* ASCE Vol. 15 No. pp 201-208.

[111] Yang P. S., Amde, M., Tinsae, W., Greimann L.F. [1985] "Effect of Predrilling and Layered Soil on Piles, *Journal of Geotechnical and Geoenvironmental Engineering,* ASCE Vol.111; No. 1., pp 001-018

[112] Zakeri B., Padgett, J.E., Amin G.G. [2014], Fragility Analysis of Skewed Single-Frame Concrete Box Girder Bridges." *Journal of Performance of constructed Facilities,* ASCE, Vol. 28, No. 3, pp 571-582.

Appendix A

Design Steps for Design of Sleeved Pile for IAB

Step 1: Finalization of Design Data

The design data as given in Table A.1 is collected from the geometry and design layout of the bridge and preliminary analysis of dead load and live load on the bridge as

Table A.1 Design date of sleeved pile foundation for integral abutment bridge

Type of soil in the foundation	Medium sand
Total length of the bridge	$L_{bridge} = 120m$
Length of end span	$L_{end} = 37.5m$
Length of central span	$L_{centre} = 45m$
Total number of piles in abutment	$n_{ap} = 2 \times 5 = 10$ nos
Total numbers of pile in pier	$n_{pp} = 2 \times 8 = 16$ nos
Axial load on piles in pier	$P_p = 614.00\ kN$
Axial load on abutment pile	$P_a = 512.00\ kN$
Target time period	$T_p = 1.375s$
Grade of steel to adopted	E 450
Yield strength of the steel	$f_y = 450\ MPa$
Modulus of Elasticity of the steel	$E_s = 200GPa$

The target time period of the bridge is taken as 2.5 times the highest threshold period of vibration in constant acceleration zone of response spectrum for the medium sand (IRC:6:2014).

Step 2: Ratio of mass in abutment and pier

Ratio of mass on pier to abutment

$$r_m = \frac{M_{pier}}{M_{abut}} = 2.2$$

Step 3: Design deflection and shear force

(a). Maximum spectral acceleration from 5% damped design response spectrum is taken as

$$S_{pa} = 0.90g$$

For design basis earthquake the spectral acceleration is obtained as

$$A_{DBE} = \frac{S_{pa}}{2} = 0.45g$$

(b). Target frequency of pile from target time period

$$\omega_p = \frac{2\pi}{T_p} = 4.57\ rad/s$$

(c). Design Basis ground displacement for single degree of freedom model from Equation (5.5) is

$$D_{DBE} = \frac{A_{DBE}}{\omega_p^2} = 211.339mm$$

(d). Displacement for piles in IAB for initial iteration

$$D_1 = \frac{D_{max}}{2} = 105.669mm$$

(e) Maximum shear force from Equation (5.6) is

$$S_{max} = \omega_p^2 D_1 M_t = 138.15\ kN$$

Step 4: Length of sleeved pile

(a). Assume the ratio of axial force and Euler's buckling capacity of sleeved pile as

$$r_p = \frac{P}{P_E} = 0.2$$

(b). Dimensionless parameter from Equation (5.8) is;

$$\mathrm{a}' = \pi \sqrt{\frac{p}{P_E}} = 1.405$$

(c). The length of sleeved pile from Equation (5.7) is;

$$l = \frac{g}{\omega_p^2 \, \pi^2 \, \frac{p}{P_E}} a'^3 \frac{\sin a'}{2 - 2\cos a' - a \sin a'} = 7.195 \, m$$

Provide the length of sleeved pile in pier pile by rounding up as:

$$l_p = 8.0 \, m$$

Length of sleeved pile in abutment is taken as the same as that of pier. Hence the length of sleeved pile for abutment is;

$$l_a = l_p = 8.0 \, m$$

Step 5: Section Properties of Sleeved Pile

(d). The required moment of inertia of the sleeved pile from Equation (5.10) is:

$$I = \frac{P_p l^3}{\pi^2 E \left(\frac{P_p}{P_E}\right)} = 99537930.81 \, mm^4$$

For assumed external diameter of the sleeved pile $D_{sp} = 400mm$, the theoretical wall thickness of steel tube of sleeved pile is

$$t_{cal} = \frac{8I}{\pi {D_{sp}}^3} = 3.96\mathrm{mm}$$

The minimum thickness required to be provided as per API (2007) is;

$$t_{min} = 6.35mm + \frac{D_{sp}}{100} = 10.35mm$$

Trial value of wall thickness of the steel tube pile section is $t_{sp} = 20mm$.

Accordingly, the other sectional parameters are

(i). Internal diameter of sleeved pile $d_{sp} = D_{sp} - t_{sp} = 380mm$

(ii). Average diameter of the steel tube sleeved pile

$$D_s = D_{sp} - \frac{t_{sp}}{2} = 390mm$$

(iii). Moment of inertial of sleeved pile as provided

$$I_{sp} = \frac{\pi D_s^3 t}{8} = 465890336.546mm^4$$

(vi) Area of the sleeved pile in pier $A_s = \pi D_s t = 24504.423mm^2$

Step 6: Moment and Stress in sleeved pile

(vi) Preliminary design moment from Equation (5.11) is

$$M = P_p D_{DBE} - S_{max} l_p = -1040.319\ kNm$$

(v) Stress in the pile from Equation (5.18) is;

$$f_{bc} = \frac{p}{A_s} + \frac{p}{2\,I}(D + t)\left\{D_{max} - \frac{S_{max}}{M_t}\frac{l}{g}\right\} = -404.163\ MPa$$

Step 7: Final Section of Sleeved Pile

The sectional properties of the sleeved pile in abutment is increased to make it comparatively stiffer so that inertial force in in abutment and the pier are more less the in the similar range.

(i) Theoretical increased moment of inertia of sleeved pile in abutment is

$$I_{sa\_cal} = r_m I_{sp} = 1024958740.40mm^4$$

Assume the external diameter of the sleeved pile in the abutment $D_{sa} = 500mm$

Theoretical wall thickness of the sleeved pile in abutment;

$$t_{sa\_cal} = \frac{8I_{sacal}}{\pi D_{sa}^2} = 20.55mm$$

Provide the thickness of the wall of sleeved pile in abutment $t_{sa} = 20mm$

(ii) Average thickness of the sleeved pile in abutment

$$D_a = D_{sa} - \frac{t_{sa}}{2} = 490mm$$

(iii) Moment of inertia of the sleeved pile in abutment calculated as

$$I_{sa} = \frac{\pi D_a^3 t_{sa}}{8} = 924013085.25mm^4$$

(iv). Non-dimensional term for the sleeved pile in pier foundation from Equation (5.3a)

$$a_p = \sqrt{\frac{P_p l_p^2}{E_s I_{sp}}} = 0.649$$

(v). Non-dimensional term for the sleeved pile in abutment foundation from Equation (5.3a)

$$a_a = \sqrt{\frac{P_a l_a^2}{E_s I_{sa}}} = 0.593$$

(vi). Total horizontal stiffness of the pier pile from Equation (5.4)

$$k_{pp} = \frac{12E_p I_p}{l_p^3} \times \frac{a^3}{12} \times \frac{\sin a}{2 - 2\cos a - \mathrm{a}\sin a} \times n_{pp} = 334673.43\ kN/m$$

(vii). Total horizontal stiffness of the sleeved pile as in abutment from Equation (5.4)

$$k_{ap} = \frac{12EI}{l_{ap}^3} \times \frac{a^3}{12} \times \frac{\sin a}{2 - 2\cos a - \mathrm{a}\sin a} \times n_{ap} = 41789.278\ kN/m$$

(viii) The ratio of stiffness of sleeved pile in pier to the sleeved pile in abutment foundation is computed as;

$$r_{stiff} = \frac{k_{pp}}{k_{ap}} = 0.801 < 1.0$$

The abstract of design parameters of sleeved pile are:

(1). Outer diameter of sleeved pile in the abutment $D_{sa} = 500mm$

(2) Thickness of wall of sleeved pile in the abutment t_{sa} =20mm

(3) Length of sleeved pile in the abutment $l_a = 8000mm$

(4) Outer diameter of sleeved pile in the pier $D_{sp} = 400mm$

(5) Thickness of wall of sleeved pile in the pier t_{sp} =20mm

(6) Length of sleeved pile in the pier $l_p = 8000mm$

Step 8: Structural Design of Sleeved pile

Design load on sleeved pile is calculated from the 3D model.

(1) Factored axial load due the dead load of superstructure, weight of wearing course, pier and pile cap $P_u = 1219kN$

(2) Factored design moment due to dead load, and seismic acceleration

$M_{Ed} = 778.0\ kNm$

The structural design of the sleeved pile is carried out taking the pile section as a beam column member. Both checks for section strength and overall member strength as per IS: 800: 2007 is carried out.

(a) Section strength

$$\frac{P_u}{P_{dz}} + \frac{M_z}{M_{dz}} = 0.78 < 1.0$$

(b) Member strength

$$\frac{P_u}{P_{dz}} + \frac{M_z}{M_{dz}} = 0.78 < 1.0$$

$$\frac{P_u}{P_{dz}} + C_{mz}\frac{M_z}{M_{dz}} = 0.82 < 1.0$$

Step 9: Checking of Load Capacity of Sleeved Pile

The evaluation of the overall capacity of the pile is carried out assuming the sleeved pile arrangement as a partially embedded pile (section 5.4.7).

A. Properties of bottom concrete filled tube pile:

(i) Overall diameter of bottom concrete filled tube pile $D_p = 900mm$

(ii) Grade of concrete adopted for filling tube pile: M35

(iii) Characteristic strength of concrete: $f_{ck} = 35MPa$

(iv) Modulus of elasticity of concrete $E_c = 5000\sqrt{f_{ck}} = 29580.399MPa$

(v) Gross moment of inertia of the bottom concrete filled tube pile

$$I_p = \frac{\pi}{64} D_p^4 = 0.032\ m^4$$

(vi) Gross area of bottom pile $A_p = \frac{\pi}{4} D_p^2 = 0.636\ \text{m}^2$

(vii) Grade of steel of steel tube pile $E450$

(viii) Yield strength of steel tube pile $f_y = 450MP_a$

B. Buckling capacity of the equivalent cantilever of sleeved pile

(i) Coefficient of subgrade reaction modulus for medium dense sand;

$$n_h = 4071 \frac{kN}{m^3}$$

(ii) Characteristic length of the flexible pile for sand,

$$\text{T} = \left(\frac{E_c \times I_p}{n_h}\right)^{0.2} = 2.977m$$

(iii) The depth of fixity from the bottom of sleeved pile,

$$L_f = 1.8T = 5.933m$$

(iv) Total length of pile $L_p = 18.0m$

(v) Length of pile below the sleeved pile $L_b = L_p - l_p = 10.00m$

(vi) The equivalent cantilever length of sleeved pile $L_{eq} = L_f + l_p = 13.933m$

(vii) Modular ratio of the steel and concrete $m = \frac{E_s}{E_c} = 6.761$

(viii) Transformed axial area of concrete pile to steel pile $A_{tr} = \frac{A_p}{m} = 0.094m^2$

(ix) Transformed diameter of the column $d_{tr} = \sqrt{\frac{A_{tr}4}{\pi}} = 346.122\ mm$

(x) Moment of inertia of transformed portion of column

$$I_{tr} = \frac{\pi}{64} d_{tr}^4 = 0.001\ m^4$$

(xi) Moment of inertia and length of steel tube sleeved pile in top portion of the sleeved pile (stepped column) $I_1 = I_{sp} = 32206233437.817mm^2$

(xii) Length of column in the top portion of stepped column

$$L_1 = l_p = 8000mm$$

(xiii) Moment of inertia of transformed steel pile in the bottom of sleeved pile

$$\mathrm{I}_2 = I_{tr} = 704511356.452mm^2$$

(xiv) Length of the bottom portion of the sleeved pile (stepped column)

$$L_2 = L_f = 5359mm$$

(xv) Buckling load of the sleeved pile

$$P_{cr} = \frac{\pi^2 E I_1}{L_{eq}^2} \times \left[\left(\frac{L_1}{L_{eq}}\right) + \left(\frac{I_2}{I_1}\right)\left(\frac{L_2}{L_{eq}}\right) + \left(\frac{1}{2\pi}\right)\left(1 - \frac{I_2}{I_1}\right)\sin\left(\frac{2\pi L_1}{L_{eq}}\right)\right] = 6455.83\ kN$$

It is observed that the overall factor of safety of sleeved piles section is 4.21.